AD 697 661

EXTINGUISHMENT OF SOLID PROPELLANTS BY RAPID DEPRESSURIZATION

C. L. Merkle, et al

Princeton University
Princeton, New Jersey

July 1969

CLEARINGHOUSE
FOR FEDERAL SCIENTIFIC AND TECHNICAL INFORMATION

Distributed . . . 'to foster, serve and promote the nation's economic development and technological advancement.'

U.S. DEPARTMENT OF COMMERCE/National Bureau of Standards

This document has been approved for public release and sale.

EXTINGUISHMENT OF SOLID PROPELLANTS BY RAPID DEPRESSURIZATION

Aerospace and Mechanical Sciences Report
No. 880

by

C. L. Merkle, S. L. Turk, and M. Summerfield

ONR CONTRACT Nonr 1858(32)

July, 1969

Transmitted by:

Martin Summerfield
Principal Investigator

1. Distribution of this document is unlimited.

Qualified requestors may obtain additional copies from the Defense Documentation Center. All others should apply to the clearinghouse for Federal Scientific and Technical information.

Guggenheim Laboratories for the Aerospace Propulsion Sciences
Department of Aerospace and Mechanical Sciences
PRINCETON UNIVERSITY
Princeton, New Jersey

ACKNOWLEDGEMENTS

This research under Contract Nonr 1858(32) was sponsored by the Power Branch, Office of Naval Research, Department of the Navy.

Dr. R. Roberts, Head, Power Branch, was the Technical Supervisor for this project. Mr. R. D. Jackel, also of the Power Branch, was the Project Monitor.

We are indebted to Mr. Peter L. Stang for handling most of the administrative tasks of this research project, for his help with many technical problems, and for his contributions in many intangible ways as well.

The practical know-how and experience of both Mr. Chris Felsheim and Mr. Samuel Morris has been a very important asset in this research program. We are very grateful to them for their help in developing the experimental apparatus and for their many suggestions and valuable advice. Our thanks also go to Mr. Roy Crosby for the considerable photographic work and many slides he made for us, and to Mr. John Batson who processed most of the propellant that was used in the experimental tests. The contributions by Mr. Mario Jackson are also appreciated.

Our thanks also go to the Design Group, under the direction of Mr. Tony Poli for many of the final curves in this report and other reports, and for their aid in the reproduction of this and other documents.

ABSTRACT

An extensive series of experimental rocket motor test firings has been conducted in a systematic manner to determine the rate of pressure decrease which is required to just extinguish a burning solid propellant. The results of these experimental tests have been used to determine the boundary between extinction and non-extinction for each of several propellant formulations. These boundaries are presented in terms of the initial pressure derivative, $(dp/dt)_o$, and the initial chamber pressure, p_o.

In these experimental firings, extinction was said to occur if, and when, the luminosity of the flame went to zero, regardless of whether the propellant re-ignited later. Specific results of the experimental testing indicate that increasing the oxidizer loading, or decreasing the oxidizer particle size, makes a propellant more difficult to extinguish. The addition of finely divided aluminum powder (at constant oxidizer to fuel binder ratio) leaves the extinction characteristics of a propellant nearly unchanged. In addition, our experimental results have also shown that there is little difference between the extinction characteristics of propellants containing PBAA, PBCT, or PU fuel binders, although other researchers have shown that some binders can have a strong effect on propellant extinction characteristics.

A companion theory which describes extinction by depressurization of AP composite propellants is developed based on the granular diffusion flame theory of steady state burning. The theoretical model takes advantage of the short relaxation time in the gas phase (compared to the characteristic times of both the solid phase and the depressurization process itself) to make a quasi-steady approximation in the gas phase. All other theories of non-steady burning in solid propellants have likewise included a quasi-steady gas phase approximation, but many have applied it incorrectly. The proper meaning of "quasi-steady" in this situation is that the characteristic reaction time in the gas phase has the same functional dependence on pressure and temperature during a transient as during a steady state. In our theory, we infer this functional form from the granular diffusion flame theory. The GDF theory allows us to include both the chemical reaction and the diffusion characteristics of the flame in our theoretical model. This description of the gas phase flame is then used as a boundary condition on the solid phase. The solid phase is described by the one-dimensional non-steady Fourier heat conduction equation and is integrated numerically. The theoretical predictions were obtained by using the actual experimental pressure-time curves as inputs to the above described theoretical model. A predicted boundary between extinction and non-extinction is determined for each propellant formulation. Generally speaking, these predicted boundaries are in good quantitative agreement with the experimental results. The

theoretical predictions indicate that although the diffusional processes are most important during steady state burning, the chemical reaction processes are the important factors in determining whether or not extinction will occur. It is also shown both experimentally and theoretically that the shape of the entire p-t curve is important in determining extinction, but that the low pressure end is the most sensitive indicator of extinction. Similarly, theoretical results have shown that the shape of the complete steady state burning rate curve is an important indication of the extinction characteristics of a propellant, but again that the low pressure end is most sensitive.

A brief study of double-base propellants concludes this thesis. Our experimental results indicate that double-base propellants are considerably easier to extinguish than are composite propellants. A rough model for the burning of double-base propellants is presented based on the limited experimental evidence which is available on the structure of double-base flames. Although the model is rather crude, it is sufficiently realistic to indicate that a double-base propellant (because of its grossly different flame structure) is easier to extinguish than is a composite propellant. Consequently, these results for double-base propellant serve as a further indication of the importance of the flame structure in determining the extinguishment characteristics of solid propellants.

TABLE OF CONTENTS

			Page
Title Page			i
Acknowledgements			ii
Abstract			iii
Table of Contents			v
List of Tables			viii
List of Figures			ix
Nomenclature			xiii
SECTION I		Introduction	1
SECTION II		A Critique of Previous Studies of the Depressurization Process	3
	A.	Review of Previous Experimental Work	3
	B.	The Quasi-Steady Approximation	4
	C.	Some Incorrect Uses of the Quasi-Steady Gas Phase Approximation	6
	D.	Further Discussions of Previous Theories	7
	E.	Steady State Burning Rate Theories Underlying the Various Depressurization Models	14
SECTION III		Considerations of the Re-Ignition Phenomenon Following Temporary Extinction	17
	A.	Reasons for Studying Temporary Extinction	17
	B.	Theoretical Analysis of Re-Ignition	23
SECTION IV		Combustion Model for Depressurization Analysis	27
	A.	Physical Formulation of the Combustion Model	27
	B.	The Granular Diffusion Flame Model for the Depressurizations Transient--Collapsed Surface Heat Release Model	29
	C.	Application of the Depressurization Model to Steady State Burning	35
	D.	Comparison of Present Depressurization Model to KTSS Model	39
	E.	The Vichnevetsky Numerical Integration Procedure	42
	F.	Plausibility of Transforming from an Infinite Domain to a Finite Domain for the Numerical Solution of the Solid Phase	47

			Page
	G.	The Granular Diffusion Flame Model for the Depressurization Transient--Distended A/PA Flame Model	49
	H.	Qualitative Discussion of the Effect of the Distended A/PA Flame on Extinction	52
SECTION V		Experimental Results for Composite Propellants	54
	A.	General Description of the Experiment	54
	B.	Experimental Depressurization Results for Composite Propellants	55
		a) Effect of Changes in Oxidizer Loading	56
		b) Effect of Changes in Oxidizer Particle Size	57
		c) Effect of Different Fuel Binders	58
		d) Effect of Addition of Aluminum Powder	58
		e) Effect of Combustor Geometry	59
	C.	Steady State Burning Rates of Propellants	60
SECTION VI		Theoretical Predictions for Composite Propellants	63
	A.	Numerical Values for the Parameters in the Theoretical Model	63
	B.	Theoretical Predictions Based on Experimental Pressure-Time Curves	65
		a) Effect of Oxidizer Loading	65
		b) Effect of Oxidizer Particle Size	66
		c) Effect of Fuel Binder Type	66
		d) Effect of Addition of Aluminum Powder	67
	C.	Sensitivity of the Theoretical Predictions to the Depressurization Curve	70
	D.	Theoretical Predictions Based on Exponential Depressurizations	71
	E.	Theoretical Predictions of the Importance of the Shape of the Depressurization Curve	75
SECTION VII		Extinguishment of Double-Base Propellants	77
	A.	Physical Description of the Combustion Process in Double-Base Propellants	77
	B.	The Quasi-Steady Approximation for Double-Base Propellants	79
	C.	Combustion Model for Non-Steady Burning of Double-Base Propellants	80
	D.	Experimental Results for Double-Base Propellants	83
	E.	Theoretical Predictions for Double-Base Propellants	84

			Page
SECTION VIII		Summary and Conclusions	86
References			90
Table I			97
Figures 1-58			98
APPENDIX I		The Analog Computer as an Aid in Solving Non-steady Burning Problems in Solid Propellants	156
	A.	Fundamentals of Analog Computers	156
	B.	Magnitude and Source of Errors in Analog Computers	163
	C.	Solution of Simple Ordinary Differential Equations on the Analog Computer	164
	D.	Solution of the KTSS Model on the Analog Computer	167
	E.	Typical Analog Computer Results for KTSS Analysis	171
	F.	Hybrid Computers	171
	Figures I-1 to I-5		172
APPENDIX II		Adiabatic Flame Temperatures of Various Propellants and Heats of Formation of Various Fuel Binders	178
	Table II		179
	Figures II-1 to II-4		180
APPENDIX III		Experimental Procedures	184
	A.	Procedure Used in Depressurization Experiments	184
	B.	Thermal Conductivity Measurements	185
	C.	Attempts at Measuring the Flame Temperature During the Depressurization	187
	D.	Availability of Experimental Pressure Versus Time Curves for Tested Propellants	189
		Figures III-1 to III-5	190
APPENDIX IV		Distribution List	195
APPENDIX V		DD Form 1473	200

LIST OF TABLES

Table No.	Title	Page
I	Composition and Burning Rate Data of Tested Propellants	97
II	Chemical Properties of Propellant Ingredients	179

LIST OF FIGURES

Figure No.	Title
1.	One-Dimensional Energy Balance at the Burning Surface of a Solid Propellant
2.	Two-Stage Granular Diffusion Flame Model for Ammonium Perchlorate-Type Composite Solid Propellants
3.	Steady State Temperature Profile inside Burning Solid Propellant; Effect of Cold End Boundary Condition on Steady State Solution
4.	Variable Area Combustor for Depressurization Tests
5.	Photograph of Assembled Combustor Used for Depressurization Tests
6.	Required Depressurization Rate for Extinction; 82.5/17.5-PBAA Propellant (Experimental and Theoretical Results)
7.	Required Depressurization Rate for Extinction; 80.0/20.0-PBAA Propellant (Experimental and Theoretical Results)
8.	Required Depressurization Rate for Extinction; 77.5/22.5-PBAA Propellant (Experimental Results)
9.	Required Depressurization Rate for Extinction; 75.0/25.0-PBAA Propellant (Experimental and Theoretical Results)
10.	Required Depressurization Rate for Extinction; Effect of Propellant Oxidizer Loading (Experimental and Theoretical Results)
11.	Required Depressurization Rate for Extinction; 45μ AP Particle Size (Experimental and Theoretical Results)
12.	Required Depressurization Rate for Extinction; 80μ AP Particle Size (Experimental Results)
13.	Required Depressurization Rate for Extinction 180μ AP Particle Size (Experimental and Theoretical Results)
14.	Required Depressurization Rate for Extinction; Effect of Oxidizer Particle Size (Experimental and Theoretical Results)
15.	Required Depressurization Rate for Extinction; PBCT Fuel Binder (Experimental and Theoretical Results)

16. Required Depressurization Rate for Extinction; Polyurethane Fuel Binder (Experimental Results)

17. Required Depressurization Rate for Extinction; Effect of Fuel Type (Experimental and Theoretical Results)

18. Required Depressurization Rate for Extinction; 7.5% Aluminum (Experimental Results)

19. Required Depressurization Rate for Extinction 15.0% Aluminum (Experimental and Theoretical Results)

20. Required Depressurization Rate for Extinction Effect of Aluminum Addition (Experimental Results)

21. Required Depressurization Rate for Extinction for a Propellant Containing Coarse Aluminum (Experimental Results)

22. Required Depressurization Rate for Extinction; Effect of Aluminum Particle Size (Experimental Results)

23. Required Depressurization Rate for Extinction for Large Chamber (Experimental Results)

24. Required Depressurization Rate for Extinction; Effect of Chamber Geometry (Experimental Results)

25. Steady State Burning Rate Data: Effect of Oxidizer Variations

26. Steady State Burning Rate Data: Effect of Particle Size

27. Steady State Burning Rate Data: Effect of Fuel Binder Type

28. Steady State Burning Rate Data for Different Aluminum Loadings

29. GDF Theory Fit of Steady State Burning Rate Data; 82.5/17.5-PBAA

30. GDF Theory Fit of Steady State Burning Rate Data; 80/20-PBAA

31. GDF Theory Fit of Steady State Burning Rate Data; 77.5/22.5-PBAA

32. GDF Theory Fit of Steady State Burning Rate Data; 75/25-PBAA

33. GDF Theory Fit of Steady State Burning Rate Data; AP Particle Size: 45μ

34. GDF Theory Fit of Steady State Burning Rate Data; AP Particle Size: 80μ

35. GDF Theory Fit of Steady State Burning Rate Data; AP Particle Size: 180μ

36. GDF Theory Fit of Steady State Burning Rate Data; PBCT Fuel Binder

37. GDF Theory Fit of Steady State Burning Rate Data; 7.5% Aluminum

38. GDF Theory Fit of Steady State Burning Rate Data; 15% Aluminum

39. Required Depressurization Rate for Extinction; Effect of Change in Depressurization Speed (Theoretical Results)

40. Predicted History of Burning Rate during Rapid Exponential Depressurization

41. Predicted History of Flame Temperature during Rapid Exponential Depressurization

42. Predicted History of Characteristic Times during Rapid Exponential Depressurizations

43. Required Depressurization Rate for Extinction; Theoretical Predictions Based on Exponential Pressure Decay. Effect of Changing Surface Heat Release

44. Required Depressurization Rate for Extinction; Theoretical Results Based on Exponential Pressure Decay, Effect of Changes in Flame Temperature

45. Required Depressurization Rate for Extinction; Theoretical Results Based on Exponential Pressure Decay, Effect of Changes in Surface Activation Energy

46. Required Depressurization Rate for Extinction; Theoretical Results Based on Exponential Pressure Decay, Effect of Changes in Flame Activation Energy

47. Required Depressurization Rate for Extinction; Effect of Changes in Burning Rate Constants (Theoretical Results)

48. Required Depressurization Rate for Extinction; Effect of Changes in Final Pressure (Theoretical Results)

49. Two Part Pressure-Time Curve

50. Effect of Changes in the Shape of the Pressure Decay Curve on the Predicted Extinction Boundary

51. Steady State Burning Rate Curve; Double Base Propellant

52. Required Depressurization Rate for Extinction; Double Base Propellant (Experimental Results)

53. Required Depressurization Rate for Extinction; Theoretical Results Based on Exponential Pressure Decay, Comparison Between Double-Base and Composite Propellants

54. Schematic Showing the Relation Between the Regions of Permanent, Temporary and Non-Extinction

55. Effect of Ambient Pressure and Expansion Time on Extinction

56. Calculated Reduction in Re-ignition Time due to Heating by Hot Environment

57. Comparison of Transient Temperature Profiles (Obtained by Varying the Depressurization Speed) at Extinction, with Various Steady State Temperature Profiles.

58. Typical Experimental Pressure-Time Curve

I-1 Analog Computer Circuit Diagram for Solution of Non-steady Burning Equation (Eq.I-34) for a General Lattice Point in Space

I-2 Analog Computer Circuit Diagram for Lattice Point Representing Burning Surface of Propellant (see Eq. I-38)

I-3 Typical Analog Computer Results

I-4 Comparison Between Analog and Digital Computer Results

I-5 Analog Computer Circuit Diagram for Solution of Non-steady Burning Equation by Serial Method (see Eq. I-43)

II-1 Adiabatic Flame Temperature of PBAA Propellant

II-2 Adiabatic Flame Temperature of PBCT Propellants

II-3 Adiabatic Flame Temperature of Polyurethane Propellants

II-4 Adiabatic Flame Temperature of Aluminized Propellants

III-1 Approximate Diaphragm Thickness vs. Burst Pressure (2-3/4 inch diameter)

III-2 Thermal Conductivity Apparatus

III-3 Form of Output Signal From Brightness-Emissivity Measurement

III-4 Brightness-Emissivity Setup

III-5 Sight Glass Assembly

Nomenclature

Symbol	Definition
A	Proportionality constant in characteristic time for chemical reaction; dimensionless
a	Proportionality constant used in steady state comparison with GDF burning rate formula (related to A), dimensionless
B	Proportionality constant in characteristic time for diffusion; dimensionless
b	Proportionality constant used in steady state comparison with GDF burning rate formula (related to B), dimensionless
C_1, C_2, C_3	Integration constants
C_D	Nozzle discharge coefficient; dimensionless
E	Activation energy cal/mole
H	(No subscript) Non-dimensional surface heat release for collapsed surface heat release model,
H	(With subscript) Non-dimensional heat release
K	Proportionality constant
K'	Proportionality constant, in definition of τ_I
L, L_1, L_2	Linear differential operators used in numerical integration scheme
$L_{DARK\ ZONE}$	Non-dimensional length of dark zone
P	Non-dimensional pressure,
Q	(No subscript) Non-dimensional heat release in the flame
Q	(With subscript) Dimensional heat of reaction, cal/g
R	Non-dimensional burning rate, r/r_o
R_g	Guess value for R used in iterative calculation scheme
$\mathcal{R}$	Universal gas constant, cal/mole ^oK
T	Temperature, ^oK
X	Non-dimensional distance,
Z	Non-dimensional space variable defined as $Z = e^{-X}$

Symbol	Definition
a	Constant in steady state burning rate equation $r = a p^n$. Also, constant in GDF steady state burning rate equation $1/r = a/p + b/p^{1/3}$
a'	Coefficient of Arrhenius term for surface pyrolysis rate, $r = a' e^{-E_s/RT_s}$
b	Constant in GDF steady state burning equation, $1/r = a/p + b/p^{1/3}$
c_g	Specific heat at constant pressure in gas phase, cal/g ^{o}K
c_p	Specific heat in solid phase, cal/g ^{o}K
m	Exponent in pyrolysis law used in Ref. 43
$\dot{m}$	Rate of mass flow per unit area, g/cm^{2}sec
n	Pressure index in steady state burning rate equation,
p	Pressure, dyne/cm^2
r	Propellant burning rate (surface regression rate), cm/sec
t	Time, sec
u	Gas phase velocity, cm/sec
x	Distance perpendicular to burning surface of propellant, cm
α	Thermal diffusivity, $\lambda/\rho c$, cm^2/sec
β	Depressurization speed parameter for exponential depressurizations, dimensionless
δ	Dirac delta function. Also, a constant such that $\delta \ll 1$
ε	Chemical reaction progress variable (describes how far the reaction has proceeded toward completion in per cent)
$\dot{\varepsilon}$	Rate of product generation,
λ	Thermal conductivity, cal/cm sec ^{o}K
λ_1, λ_2	(Numerical subscripts), constants used in numerical integration scheme
μ	Microns (measurement of length), 10^{-4} cm

Symbol	Definition
θ	Non-dimensional temperature, $\theta = (T - T_\infty)/(T_{s,0} - T_\infty)$
ρ	Density, g/cm^3
Φ	Function of pressure only, $\Phi(P)$, used in Ref. 43
$\phi(P,R)$	Function of P and R, shorthand notation for heat flux from gas to solid
τ	(Without subscript) Non-dimensional time,
τ_{solid}, τ_{gas}	Characteristic times for solid and gas, respectively, sec
$\tau_{ch}, \tau_{dif}, \tau_{reac}$	Non-dimensional characteristic times for various processes as denoted by subscript
τ_1, τ_2, τ_3	(With numerical subscript) Functions of space variable X used in numerical integration scheme
τ'	Non-dimensional characteristic time, related to τ_{ch}, τ_{dif}, etc. above. For example $\tau'_{ch} = \tau_{ch}\left(\frac{\lambda_p}{\lambda_g}\frac{c_g}{c_p}\frac{\rho_p}{\rho_g}\right)$
ω_{ch}	Constant equal to area under impulse function representing chemical reaction term
ω_{dif}	Constant equal to height, $\rho_g \dot{\varepsilon}_{dif}$, of step function representing a diffusion controlled flame

Subscripts

ch	pertains to chemical reaction character of O/F flame
dif	pertains to diffusional character of O/F flame
f	conditions inside or at end of flame. When used with P, signifies final pressure
fizz	Fizz zone in double-base propellant
g	gas phase
p	propellant (solid phase)
reac	pertains to overall O/F gas phase flame
s	conditions at the propellant surface
s,g	gas phase side of solid-gas interface

Symbol	Definition
s,ρ	solid phase (propellant) side of solid-gas interface
s,o	reference conditions at surface
ss	steady state condition
o	reference condition
I	end of first stage (A/PA) flame in two-stage flame model
II	end of second stage (O/F) flame in two-stage flame model

Superscripts

$\overline{}$	denotes steady state condition, or mean value
$i, i-1$	superscript related to time in discretized equations representing solid phase for numerical integration.

Abbreviations

AP	Ammonium perchlorate,
A/PA	Ammonia-perchloric acid (reaction between decomposition products of AP)
GDF	Granular diffusion flame (model of steady state burning)
KTSS	Designation given to instability theory presented in Ref. 43
O/F	Oxidizer-fuel (refers to main combustion process between oxidizer decomposition products and fuel binder decomposition products)
PBAA	Polybutadiene acrylic acid (fuel binder)
PBCT	Polybutadiene, carboxyl terminated (fuel binder)
PU	Polyurethane (fuel binder)

SECTION I

INTRODUCTION

This thesis is concerned with the analysis, characterization, and understanding of the non-steady burning process which is induced in solid propellants by the rapid venting of the rocket combustion chamber. It is well-known that the flame in a solid propellant rocket engine can be made to go out by suddenly opening the chamber so that the pressure drops to ambient in a few milliseconds. The extinguishment which is induced by such a pressure drop is characterized by the combustion chamber geometry, the chamber L* at the moment of depressurization, the type of propellant, and various propellant properties. Most important, it is the rate of pressure decline, and the extent of the decline that determines whether the flame will go out. The reasons for studying this depressurization process are of both an engineering and a scientific nature.

The engineering aspects are concerned with the actual application of the depressurization process to practical situations. For example, successful stop-start operation of solid propellant rocket motors requires some method of terminating combustion rapidly on command, and this method must leave the propellant grain in a condition of readiness for a new start. Similarly, some method of combustion termination is necessary to achieve thrust cut-off after a rocket has reached its desired velocity. Several methods can be used to "turn off" a solid propellant rocket motor. For instance, thrust cut-off at the end of a mission can be achieved by allowing the propellant to be completely consumed. Alternatively, foreign liquids or gases can be sprayed into the combustion chamber and onto the burning surface to cause a quench. However, neither of these processes is desirable if the engine is to be re-started. One method which is attractive for both stop-start applications as well as for end-of-mission thrust cut-off, is to use sudden depressurization to accomplish extinguishment.

In addition to the engineering aspects of this research program, equally important scientific aspects also exist. The scientific aspects are concerned with using the depressurization process as a means to another end; namely to obtain further understanding of the combustion processes in a solid propellant. The depressurization transient is somewhat unique from a scientific viewpoint in that it will yield repeatable experimental results with much less ambiguity and data scatter than most other experiments that have been used to study non-steady combustion phenomena. Because of the lack of scatter, the results from an experimental depressurization program are quite useful for testing the validity of a theory of non-steady burning. The only drawback is that a large number of experimental depressurization firings must be made in order to have

a sensitive test of a particular combustion model. Since the proper analysis of the depressurization process requires detailed knowledge of the steady state burning process, the experimental verification of the predictions of the depressurization analysis can serve to substantiate and extend our knowledge of steady state burning of solid propellants as well as non-steady burning.

With these two-fold purposes in mind, this thesis presents both a theoretical model of the depressurization process and the results of extensive experimental testing of the susceptibility of various solid propellant formulations to extinguishment by rapid depressurization. The experimental work is aimed at determining how compositional and environmental conditions can affect the extinguishment characteristics of a solid propellant. The companion theoretical model is based on the granular diffusion flame model of steady state burning, and the predictions which are obtained from this theory are in quite good agreement with the experimental results. Such agreement represents further justification for the steady state flame model that was employed, as well as to justify the form of the non-steady theory.

Finally, it should be noted, that after flame-out occurs, the propellant will sometimes spontaneously re-ignite after a period of several seconds and will continue to burn until the entire supply of propellant has been consumed. Re-ignition is generally caused by long exposure to very small heat sources. Typical sources for re-ignition are radiation and conduction from hot, inert parts inside the motor, as well as from the residual hot gases in the chamber. Residual heat left in the solid can also contribute to re-ignition by giving rise to slow exothermic reactions. Whether re-ignition occurs, depends on a competition between these weak heat sources, and similarly weak heat losses from the solid. Although a discussion and brief analysis of the re-ignition process is included, this thesis is primarily concerned with analyzing the so-called "temporary" extinction behavior of solid propellants.

SECTION II

A CRITIQUE OF PREVIOUS STUDIES OF THE DEPRESSURIZATION PROCESS

This section describes the previous experimental and theoretical work which has been done in the area of depressurization-induced extinguishment. The criticisms of the previous theoretical analyses indicate the reasons for a new approach and set the ground-work for the combustion model which is described in Section III.

A. Review of Previous Experimental Work

A number of researchers have published experimental results on extinction by rapid depressurization during the past few years. Ciepluch[1,2,3] was one of the first researchers to conduct a systematic experimental study of the depressurization transient. He presented his results in terms of the initial chamber pressure decay rate (or the time required to reduce the chamber pressure by 50% of its original value) and the initial chamber pressure. He was able to show that a critical decay rate existed such that any depressurization which was faster than this critical rate (measured in terms of the initial dp/dt) would extinguish, while slower decays would result in continued burning. He found that this critical decay rate increased linearly with the initial chamber pressure. He also found that aluminized propellants are slightly harder to extinguish than non-aluminized and that in general the propellant composition has a substantial effect on extinction. He further showed that propellant re-ignition following extinction becomes increasingly less likely as either the depressurization rate is increased or as the nozzle back pressure is lowered.

The second major experimental work which has been presented in the unclassified literature is the work by Jensen[4,5]. His results are quite extensive (more so than Ciepluch's) in terms of the different fuel compositions tested. Both Jensen's work and Ciepluch's work are referenced in connection with the experimental results which are presented in this thesis.

Besides these two studies, a number of less systematic experimental studies have been reported on the extinguishment process. Ryan[6] has presented experimental results for a few propellant formulations, but unfortunately his results are all for initial pressures of less than ten atmospheres. Horton has reported a number of experimental depressurization tests, but he has used so many variables (different propellant formulations, different propellant orientations, different back pressures, etc.), that it is difficult to deduce more than generalized observations from his results. Similarly Marxman[7,8] and Cohen[9] have reported a small amount of data as have Von Elbe and McHale[10]. Reed, et. al.[11] have similarly presented the results of a few experimental tests,

but their final chamber pressures were near or below the lower deflagration limits of the propellants being tested. Because of this it is impossible to determine whether the extinguishment was due to the depressurization rate or due to the lower deflagration limit. Other workers who have reported some depressurization data include Fletcher, et.al.[12,13,14] and Kling and Brulard[15].

In the practical aspects of the depressurization testing, Fletcher and Paulson[16] have discussed a particular nozzle design which is appropriate for experimental testing of extinction characteristics of solid propellants. A second approach to the area change has been given by Ciepluch[1]. The method discussed in this thesis differs from both of these.

Practical application of experimental findings to actual flight hardware naturally requires some compromises. One such change is that the nozzle opening time becomes quite long. Kalt[17], Dubrow, et. al.[18] and Coates, et. al.[19] have discussed the problem where the rate of the area change is important. This problem has not been considered in this thesis. In fact the more general problem of the coupling between the propellant, the chamber, and the nozzle has not been considered either. The reasons are given later. In this thesis the theoretical approach has been to use a specified pressure-time curve to calculate the transient burning rate. The coupling problem is straightforward (though admittedly it is time consuming) and can be used in conjunction with the theoretical analysis presented herein.

Finally a paper by Slocum[20] has discussed the possibilities of using liquid extinguishants for solid propellants. Experimental testing along with considerations such as expense and toxicity led him to conclude that water was the best potential fluid to use for producing the quench. His experimental results indicated that a large amount of fluid was needed to produce quench and that significant problems had to be overcome before such a system would be reliable.

B. The Quasi-Steady Approximation

The experimental results which were discussed in the previous subsection show that depressurization times which are on the order of a few milliseconds are necessary to extinguish a solid propellant. Since the gas phase characteristic time is much shorter than this (as indicated below), most theoretical analyses of the depressurization process have used a quasi-steady approximation in the gas phase. This has then relegated all dynamic effects in the problem to the solid phase. A brief analysis of the depressurization problem shows that this is an appropriate simplification.

The differential equation in the solid phase is given by

$$\frac{\partial T}{\partial t} = \alpha_p \frac{\partial^2 T}{\partial x^2} + r \frac{\partial T}{\partial x} \tag{1}$$

where the coordinate system is chosen as fixed on the regressing surface of the solid (see Section III). By non-dimensionalizing this equation, we obtain a characteristic time which describes the length of time which is required to alter the temperature profile in the solid. This characteristic time is $\tau_{solid} = \alpha_p / r_o^2$ where r_o is the burning rate of the propellant at some reference pressure. Typical values for the parameters are $\alpha_p = .00029$ in^2/sec (taken from reference 21) and $r_o = .25$ in/sec (see data in Section IV). Hence the characteristic time for the establishment of a temperature profile is

$$\tau_{solid} = .0003/(.25)^2 \text{ sec} \approx 5 \text{ ms}$$

The corresponding equation for the gas phase is

$$\frac{\partial T}{\partial t} = \alpha_g \frac{\partial^2 T}{\partial x^2} + u \frac{\partial T}{\partial x} + Q_f \dot{\varepsilon}/c_g \tag{2}$$

where $d\varepsilon/dt$ is the rate of the chemical reaction. Thus the temperature profile in the gas phase is governed by the corresponding characteristic time

$$\tau_{gas} = \alpha_g / u_o^2 \simeq \frac{\alpha_g}{\alpha_p} \frac{\rho_g^2}{\rho_p^2} \tau_{solid}$$

and assuming the specific heats in the solid phase and gas phase are about equal we obtain

$$\tau_{gas} \approx \frac{\lambda_g}{\lambda_p} \frac{\rho_g}{\rho_p} \tau_{solid} \tag{3}$$

The ratio of the thermal conductivities is approximately, $\lambda_g/\lambda_p \simeq .5$ [21]. A nominal value for the density of the solid phase is $\rho_p = 1.5$ gm/cc [22], and for the gas phase (assuming a perfect gas at a temperature of 3000°K and a pressure of 1000 psia), $\rho_g \simeq .0075$ gm/cc. Thus the ratio of gas to solid phase density is $\rho_g/\rho_p \simeq .005$. Finally we obtain

$$\tau_{gas} \simeq 2.5 \times 10^{-3} \tau_{solid} \quad \text{or} \quad \tau_{gas} \simeq 10^{-5} \text{ sec.} \tag{4}$$

so that the gas phase does indeed relax much faster than the solid phase.

One further characteristic time (which is related to this one) is the time required for the gas phase reaction. References 23 and 24 have reported that the flame thickness is on the order of 0.1 mm. Hence the characteristic time for the gas phase

reaction is approximately given by

$$\tau_{flame} \simeq \Delta x/\bar{u} \simeq \rho_g/\rho_p \; \Delta x/r_o \tag{5}$$

or $\tau_{Flame} \simeq 5\times10^{-5}$ sec. Thus the characteristic time for the gas phase reaction is the same order of magnitude as that for the establishment of the temperature profile in the gas phase.

Finally, we can calculate a characteristic for the gas phase flame from the reaction rate term, $\dot{\varepsilon}$. Later in the thesis, two relations are given for $\dot{\varepsilon}$, one for diffusional processes, and the other for chemical reaction processes. (see equations 30, 33 and 34). The relations are

$$t_{CH} = \frac{1}{Q\dot{\varepsilon}_{CH}} = \frac{\kappa_p \rho_g}{Q \rho_p r_o^2} \simeq .8\times10^{-5} \text{ sec.}$$

and

$$t_{dif} = \frac{1}{Q\dot{\varepsilon}_{dif}} = \frac{\rho_g \Delta x}{\rho_p Q r_o} \simeq 2.5\times10^{-5} \text{ sec}$$

Where Q is the non-dimensional heat release in the flame zone and is taken as about 3. These times are similar to the other two gas phase times which were calculated above.

Recalling again that those depressurizations which lead to extinction must occur in a few milliseconds, we see that the quasi-steady gas phase approximation is justifiable for the typical depressurization problem, because the relaxation time for the gas phase processes is much shorter than the time which characterizes the depressurization process. Similar conclusions have been reached by others[7,8].

C. Some Incorrect Uses of the Quasi-Steady Gas Phase Approximation

Although all the theoretical work which has been done to date has made use of the quasi-steady gas phase approximation in either an expressed or an implied manner, many of these theories have applied the quasi-steady approximation incorrectly. A long series of workers [illegible]ding Von Elbe[25], Paul, et. al.[26], Horton[27], Wal[illegible]8), Ryan[6], Brown, et.al.[29], and Zel'dovich[30], have fallen into the trap of assuming that the heat feedback itself is quasi-steady. That is to say, they assumed that the temperature profile in the quasi-steady gas phase is identical to the temperature profile during a steady state (at the instantaneous pressure). Although such an idea may at first seem plausible, it is wrong. The reason it is wrong is that it neglects the process in the problem that is unsteady. If the heat feedback from the gas phase to the solid were quasi-steady, then the temperature gradient inside the surface of the solid would also be quasi-steady (because the heat transfer must be continuous at the solid-gas interface). However, some part of the overall system must be unsteady in order for extinction by rapid depressurization (i.e. by dynamic effects) to occur.

Thus the temperature profile in the solid must be a non-steady profile. And if the profile in the solid phase is non-steady, we should also expect its gradient at the surface to be non-steady (or at the very least, we should not specify it to be in phase with the pressure). Therefore the heat feedback from the quasi-steady gas phase to the non-steady solid must likewise be non-steady. The heat feedback must depend on both the instantaneous pressure and the rate of change of the pressure. As a consequence we see that even though the gas phase is quasi-steady, its temperature profile will not (in general) be a steady-state profile because of the non-steady boundary conditions (the heat feedback to the solid) on the gas phase.

If we then eliminate the quasi-steady heat feedback assumption (but not the quasi-steady gas phase approximation) we must add some additional information (which this list of authors did not use) in order to uniquely specify the problem. The procedure is entirely straightforward. The gas phase is quasi-steady in terms of both flow processes and chemical processes. Hence the analysis of the quasi-steady gas phase can proceed in a manner which is identical to the analysis which is used for the steady state gas phase except that the amount of heat which is fed back into the propellant is no longer equal to its steady state value. The actual magnitude of this heat feedback must be determined by solving the non-steady Fourier heat conduction equation rather than by using the solution to the steady heat conduction equation in the solid. This is perhaps seen more clearly if we consider a thermodynamic system which includes only the gas phase. This gaseous system is non-adiabatic in either the steady state or during a quasi-steady transient due to the heat feedback to the solid. However because of the quasi-steady approximation, the same equations describe this gas phase system in either the steady state or in the quasi-steady transient, i.e., our purely gas phase system merely shifts through a continuous series of steady states during a depressurization. Meanwhile, the magnitude of the non-adiabaticity (heat loss to the solid) is somewhat different between steady state and transient conditions. Thus during quasi-steady transients, we must solve the steady state gas phase equations with a non-steady boundary condition which represents the non-adiabaticity of the gas phase.

One theory which does treat the heat feedback properly is the Denison and Baum instability model[31]. This analysis has been applied to the depressurization transient by Marxman and Wooldridge[32]. The heat feedback in Denison and Baum's model properly depends on both the instantaneous pressure and on the instantaneous burning rate during a transient. However, they didn't go far enough. They incorrectly used a steady state eigenvalue for the mass flux through the gas phase. The mass flux through the gas phase should also depend on both the pressure and the burning rate. This again is due to the non-steady boundary conditions on the quasi-steady gas phase.

D. Further Discussions of Previous Theories

As indicated in the previous subsection, the quasi-steady approximation has been used incorrectly in several instances.

In this subsection we individually, and in more detail, describe the previous theories which have dealt with the extinguishment process. In so doing, we point out some additional objections to the methods which have been used in these previous studies. Some of these objections are concerned with ill-advised approximations, but others deal with obvious errors in the models.

The theories which have been proposed by Von Elbe[25] and Paul, et. al.[26] are similar and are both based on small perturbation approaches. Von Elbe's analysis is very vague and is based on physical intuition rather than on precise mathematical reasoning. Paul's approach is more straightforward. Both theories are based on perturbing the amount of energy stored in the solid during a steady state. Such a perturbational solution is not unique, nor is the method which is used for obtaining it, consequently one cannot say that the methods Von Elbe and Paul have used are "wrong". However, it is preferrable to perturb the entire non-steady differential equations rather than to perturb the integral solution of the steady state equation as both of these workers did.

In both theories, the resulting equation for the transient burning rate is of the form

$$r_{\text{transient}} = a p^n + K\, dp/dt \tag{6}$$

where

$$r_{\text{steady state}} = a p^n \tag{7}$$

Here the constant, K, depends on the obvious parameters which non-dimensionalize the pressure-time derivative. Between the two theories, this constant differs by a numerical factor. According to Von Elbe and Paul, extinction occurs when the magnitude of dp/dt becomes so large (in a negative sense) that the right hand side of the transient burning rate expression vanishes. Thus the perturbation quantity (K dp/dt) must become equal to the "zeroth" order term (ap^n) for extinction to occur. However, a perturbational approach does not remain valid when the perturbation becomes of the same order of magnitude as the zeroth order term. Consequently it is wrong to use a first order perturbation solution to determine when extinction occurs. A first order perturbation solution can only indicate when the transient burning rate begins to differ significantly from the corresponding steady state burning rate (at the instantaneous pressure).

Paul and his co-workers later modified the constant, K, in their burning rate expression so that it became in effect a function of the rate of change of the pressure, dp/dt[33]. These modifications were based on solutions to the complete non-steady heat conduction equation in the solid and were supposed to have the effect of including higher order terms in the small perturbation expansion. These factors allowed somewhat better correlation of the experimental data in some cases.

Finally, we raise two other objections against these two theories. First of all both Von Elbe and Paul ignored the experimental evidence which has shown that a significant amount of heat release occurs very near to the surface of a burning composite solid propellant (although the effect of this omission is overshadowed by their improper use of the quasi-steady approximation). Second, they used a constant surface temperature for the burning propellant. As discussed below, the constant surface temperature approximation is acceptable from the standpoint of an energy balance, but a constant surface temperature approximation has significant implications on the determination of the burning rate.

When initially published, both these theories were supposed to apply at the initial instant of the depressurization. Since then both authors have postulated that their respective theories should be applied at the moment of extinction. Limited success has been obtained with these formulas using both the initial pressure-time derivative and the derivative at the moment of extinction[9,10,34]. This success is mainly due to the fact that the formulas include some of the most important non-dimensional parameters in the problem. The contribution of these theories is that they offer a justification for the commonly used method of presenting experimental data and they identify one important non-dimensional parameter in the depressurization problem.

Wallis' model[28] includes the same basic assumptions as are in Von Elbe's and Paul's theories, however, he has solved the complete solid phase equation numerically, and in so doing, bypassed some of their difficulties. Like Paul and Von Elbe, Wallis used a constant surface temperature, included no heat source or sink at the surface, and used a quasi-steady heat feedback. He did not make any comparisons between his theoretical predictions and experimental results, but merely indicated his model would predict extinction.

Horton's model of the depressurization process[27] is also similar to those of Paul, et. al. and Von Elbe in that he too uses a quasi-steady heat feedback and a constant surface temperature. Like Wallis, he numerically integrated the complete non-steady heat conduction equation in the solid phase as a function of the instantaneous pressure during the depressurization process. His analysis differs from Wallis' (note that chronologically Horton's work came before Wallis') in only one respect: Horton included an endothermic heat sink at the surface of the solid (latent heat). However, there is no physical evidence to indicate that the solid decomposes endothermically. In fact, experiments have shown that the decomposition is exothermic[22,35]. The predictions based on Horton's model differ from his experimental results by as much as a factor of five in some cases.

Besides using his theory to predict extinction, Horton specialized his model to apply to the "infinite dp/dt" case so that he could infer the magnitude of the "heat sink" at the surface. Ryan[6] also used this "infinite dp/dt" theory. Horton and Ryan reasoned that even for a step change in pressure (infinite dp/dt), a certain minimum pressure drop, ΔP, is required to extinguish a propellant. They determined this minimum ΔP from experimental data by extrapolating the results from a series of extinctions which had been obtained by using successively faster depressurization rates. According to their picture of a burning solid propellant, one portion of the heat feedback from the gas phase goes into overcoming the latent heat of the solid, while the remainder goes into pre-heating the solid. The step function in pressure which would just extinguish combustion was supposed to correspond to a decrease in the heat feedback by an amount just equal to the product of latent heat and the mass flux (before the step change in pressure). The resulting lower heat flux would be just adequate to retain the solid phase temperature profile at its original level with no excess left to go into overcoming the latent heat. Consequently the step in pressure would cause propellant burning rate to go to zero in a step fashion. This poses somewhat of a contradiction from a physical viewpoint because the continued heat flux into the propellant would cause the propellant to re-ignite immediately. The plausibility of such an instantaneous change in the burning rate rests completely upon the constant surface temperature approximation. This is because the temperature at any point in the solid can not change instantaneously when the heat transfer to the surface is changed in a step-wise fashion (as can be shown from the heat conduction equation). Thus, if the burning rate were considered to be a function of the surface temperature (for example an Arrhenius function) as is commonly assumed, the burning rate could not change by a finite amount in zero time. Hence, this "measurement" of the "latent Heat" of a solid propellant has no meaning if we do not use the constant surface temperature approximation.

Considerable experimental evidence has shown that both ammonium perchlorate and typical fuel binders decompose by way of a chemical reaction[22,35], not by a purely physical process. For such a chemical decomposition, the burning (decomposition) rate would certainly depend on the temperature of the material; an Arrhenius function would be more realistic than a constant surface temperature approximation (see discussion in Section IV-A). Nevertheless for the typically high activation energies which have been reported experimentally[22,35], the surface temperature changes by only a small amount for relatively large variations in the burning rate. Thus, the constant surface temperature approximation is a good approximation as far as the energy equation itself is concerned, but its variation is very important for determining the burning rate. If the surface temperature is held constant, the burning rate must be determined from the heat flux rather than from

the temperature of the decomposing solid propellant. This can give the transient burning rate solution a completely different character than when it is based on the surface temperature.

A final comment on the "infinite dp/dt" analysis concerns the quasi-steady approximation. If the pressure change is truly infinite, the gas phase cannot certainly be treated in a quasi-steady manner. However, the term "infinite" is a relative term. It implies the relaxation time of the solid must be much, much longer than the characteristic time which describes the pressure change. On the other hand, the quasi-steady assumption requires the process time to be much longer than the gas phase reaction time. This restricts the characteristic time of this "infinite dp/dt" process to within a very narrow region (if such a region exists). Consequently not only did Horton and Ryan use the wrong quasi-steady approximation in their "infinite dp/dt" theory, the required depressurization processes are probably so fast that the quasi-steady approximation is not applicable in the gas phase anyway. The gas phase should probably be treated in a non-steady manner for the "infinite dp/dt" case.

Zel'dovich[30] also discussed the "infinite dp/dt" model. His reasoning was identical to both Horton's and Ryan's and the criticisms of their work apply to Zel'dovich's work also.

As indicated above, the theory by Marxman and Wooldridge is based on the Denison and Baum[31] instability model which properly recognizes that the heat feedback should depend on both the pressure and the burning rate during a transient. Marxman improved the Denison and Baum theory by recognizing that, from both a physical and a mathematical standpoint, a surface heat release is important in the transient burning process of a solid propellant. However, his first attempt at including the surface heat release led to a violation of the first law of thermodynamics--he assumed the total heat release was constant and independent of pressure, but his model predicted that (despite this assumption) the flame temperature increased with pressure. He later modified his description of the surface heat release so that the laws of thermodynamics were satisfied, but he did so in a completely arbitrary manner. The amount of heat which is released at the surface (in his model) increases with the surface temperature in an Arrhenius fashion. He "borrows" this increase in the surface heat release (with increasing steady-state pressure and surface temperature) from the main flame zone. Consequently the amount of heat released in the main flame <u>decreases</u> in an Arrhenius fashion as the steady state pressure is increased. Further, since he has no physical basis on which to found this surface heat release, its magnitude is completely arbitrary. For instance, he has no manner of deciding whether the surface heat release should increase or decrease with a change in the propellant oxidizer loading.

Fletcher[12,13,14] did not offer a theoretical model to describe the extinction process, but instead used measured values of the chamber pressure during a depressurization to back-calculate the transient burning rate during the depressurization. This calculation was performed by a simple non-steady mass balance on the chamber. By measuring the chamber pressure as a function of time, he was able to determine the net mass outflow (i.e., the difference between outflow and inflow) which was necessary to give the current chamber pressure. From simple nozzle calculations, he determined the total mass outflow and consequently inferred the mass inflow (and transient burning rate) during the depressurization. His results indicate that during a depressurization, the transient burning rate first rapidly increases (to a value equal to about twice the initial steady state burning rate) before decreasing and going to zero. The height of this peak in the burning rate increases with the speed of the depressurization. As indicated above, this calculation is straightforward, but a consideration of the numbers involved shows that it is completely meaningless.

As an example of this calculation, consider a combustor which is burning at a steady state pressure. For definiteness we take this pressure to be 1000 psia, and the corresponding nozzle throat area to be one centimeter squared. For the depressurization process this nozzle area is suddenly opened to (say) 50 cm^2 (this ratio of 50 to 1 is typical of area ratios used in the experimental work presented in this thesis). If we assume the large throat area chokes instantaneously, the mass outflow will increase by a factor of 50 over its previous value while (at least instantaneously) the inflow will remain at approximately the value it had just before the nozzle was opened. Before the nozzle is opened, the mass inflow due to combustion is just equal to the mass outflow due to the nozzle. Thus, at the instant after the nozzle is enlarged by 50 to 1, the ratio of mass outflow to inflow is likewise about 50 to 1. That is to say

$$\left(\dot{m}_{in}/\dot{m}_{out}\right)_{t=0^+} \simeq \frac{1}{50} \qquad \text{or} \quad .02$$

and this 2% is the unknown which we wish to calculate. This represents the fallacy in Fletcher's calculations. The parameter he is trying to calculate influences the parameter he measured by only a small percent.

Again taking a definite case, suppose our p-t curve requires a net mass outflow of 48 units/sec. at a given instant of time. Thus, if the total mass outflow is 50 units/sec., the inflow will be 2 units/sec. However, consider the effect of the nozzle C_D. For the typically small experimental nozzles, a knowledge of C_D within 5% is good. Thus suppose our nozzle which ideally flows 50 mass units/sec. (for $C_D \equiv 1.0$) actually has a $C_D = .96$. Then the total mass outflow becomes 48 units/sec. (instead of 50 units/sec.) so consequently the mass inflow is

zero. Smaller C_D's would give negative mass inflows.

Thus we see that lack of precise knowledge of the nozzle C_D's can give large errors in the back-calculated burning rate. Further errors enter because the pressure measurement is never exact and from the simplifying assumptions which must always be made in any analysis. All these conditions are such that the faster the depressurization (the larger the area change) the larger will be these errors. Consequently Fletcher's calculations (which were made with a C_D of unity) are meaningless. It is further of interest to note that the predictions given in this thesis (which were obtained by a completely different calculation method) indicate that, opposite to Fletcher's results, the transient burning rate is always below the steady state burning rate which corresponds to the instantaneous pressure. There is no possible mechanism to explain how the burning rate could possibly increase over the steady state value it had before the depressurization (although it could conceivably be above the steady state burning rate corresponding to the instantaneous pressure).

Kling and Brulard[15] have used the same method to back-calculate the burning rate during a transient as did Fletcher. They too used a nozzle C_D of unity and like Fletcher's, their calculated burning rate increased at the initial part of the depressurization. They wrongly attributed this increase to erosive burning effects, the actual cause is the same as in Fletcher's calculations.

In Wooldridge and Marxman's latest publications[8,36] they coupled the combustor and the nozzle to the burning solid propellant during a depressurization transient by means of the energy equation and the continuity equation. This approach has not been followed in this thesis. It is felt that the coupling merely adds a source of uncertainty to the comparisons between the experimentally observed extinctions and the theoretically predicted extinctions, i.e., discrepancies could be attributed to either the combustion model or the description of the gas dynamics processes in the chamber and nozzle. In this thesis the experimentally measured p-t curves have been used rather than introduce the conservation equations for the combustion chamber. (For the pressurization problem which Wooldridge and Marxman also worked on, the chamber coupling becomes of utmost importance because of the possibility of large overshoots in the burning rate. The difference between rapid depressurization and rapid pressurization is that during depressurization, the mass inflow due to continued burning is always smaller than the nozzle mass outflow. The opposite is true for pressurizations. In pressurizations the mass inflow must exceed the mass outflow.)

E. Steady State Burning Rate Theories Underlying the Various Depressurization Models

We conclude our discussion of previous depressurization models with a consideration of the steady state theories on which these transient analyses are based. The theoretical representation of the steady state burning rate is important in the depressurization analysis because of the quasi-steady approximation. Those theories which assume the heat feedback is quasi-steady (references 25 through 29) bypass the need for any description of the flame. Thus they can be dismissed in this discussion by noting that all of them use a heat feedback which is proportional to the steady state burning rate which is in turn expressed by the Vielle burning rate relation,

$$q_{Feedback} = Kp^n \sim r_{ss} = ap^n \qquad (8)$$

To fit the complete steady state burning rate curve of virtually any propellant, the burning rate index, n, must be allowed to vary with pressure. In these simple theories, it could be taken as an empirical function of pressure, although to date, all predictions based on these theories have used a constant value of n.

As indicated, Marxman and Wooldridge have been more correct in their usage of the quasi-steady approximation and consequently in their theory (as in ours) the structure of the gas phase flame is very important. Following Denison and Baum[31], they described the gas phase flame as a pre-mixed laminar flame and then used the Von Karman eigenvalue[37] as the speed of this pre-mixed flame. The reaction order was related to the Vielle burning rate index, n, and was determined empirically. In order to fit the steady state burning rate as a function of pressure over the entire pressure range, they allowed the flame activation energy to be an arbitrary function of pressure (8). Thus their steady state burning rate expression is of the form

$$r_{ss} = a' p^n \exp(-E_f(p)/RT_F) \qquad (9)$$

First of all, we note that a composite solid propellant is not at all pre-mixed on a molecular level. Consequently there is no a priori reason for believing that upon decomposition of the solid phase these heterogeneous products mix instantaneously (in comparison with the chemical reaction). In fact the opposite could just as well be true; the diffusional mixing of these heterogeneous products could be so slow in comparison with the chemical reaction that the flame effectively behaves as a purely diffusional flame. The granular diffusion flame theory (which is used in our model) allows both chemical reaction and diffusion to occur simultaneously. Very extensive experience with this (GDF) steady state formulation has shown that at normal rocket pressures, diffusion is a more important process in a composite solid propellant flame than is the chemical

reaction[38]. Hence, it would be more appropriate to use a flame speed formula from a diffusional flame than to use Von Karman's pre-mixed flame eigenvalue. (Note the two separate objections which we raise here. First, a solid propellant flame does not behave like a pre-mixed flame. Consequently a pre-mixed flame theory is not appropriate. Second, even if the flame were pre-mixed, the mass flux eigenvalue as determined from the steady state would not be the correct eigenvalue for the quasi-steady transient.)

One physical indication that diffusion is important in a composite solid propellant flame is based on the experimental observation that propellants with small oxidizer particle sizes burn much faster than propellants with large particle sizes (when both propellants have the same oxidizer to fuel ratio). This fact is clearly shown in the steady state burning rates which are included in this thesis as well as in the burning rates of Steinz[38] and many others. This is readily explained by the GDF theory because as the particle sizes become smaller, diffusion should occur over smaller distances and hence be faster so that the propellant burns faster. A theory which is based on a completely pre-mixed flame can give no plausible explanation for the particle size effect.

Wooldridge and Marxman explain their variable flame activation energy by pointing out that a solid propellant flame is composed of a complicated series of reactions whose average activation energy is given by E_F. As the combustion pressure changes, various reactions assume differing amounts of importance so that the average activation energy changes. Wooldridge and Marxman have further justified the variable activation energy by saying that it doesn't vary by very much. It is indeed correct that the average activation energy could change, but it would be just as appropriate to hold the activation energy fixed and allow the pre-exponential factor, a', to vary with pressure. However, the pre-exponential factor would have to vary by large amounts to give the same effect as the small variation in activation energy.

Steinz[39] has presented a thorough discussion of steady state burning. His results show that the GDF theory accurately fits the steady state burning rate behavior of most (ammonium perchlorate-based) composite solid propellants that have fuel binders that do not melt "readily" on the burning surface, i.e., fuels that burn with a relatively dry surface. Typical examples are PBAA, PBCT and PBAN. The GDF theory does not fit the burning rate behavior of propellants which contain fuel binders that do melt on the surface; the polyurethane binders are a class of fuels which fall into this class. Steinz's results also show that for the "dry" fuel binders, the GDF theory holds for "normal" AP particle sizes, but begins to break down when the AP particle sizes become larger in diameter than the depth of the heat-up zone in the solid. For these large particle sizes, non-one-dimensional

effects are important. Similarly the GDF theory does not fit the burning rate behavior of severely under-oxidized propellants. Fortunately, most composite solid propellants of practical interest have high enough oxidizer loadings, and small enough AP particle sizes that their burning rates do fit the GDF theory.

In summary then, the GDF theory utilizes two free constants for the burning rate expression. These constants are determined empirically. The burning rate correlation which has been proposed by Wooldridge and Marxman, equation 9, utilizes two free constants and an arbitrary function, and should fit any experimental data. Further Marxman and Wooldridge have ignored the effect of diffusional mixing on the flame. As indicated, diffusional mixing is very important in a composite propellant flame.

SECTION III

CONSIDERATIONS OF THE RE-IGNITION PHENOMENON FOLLOWING TEMPORARY EXTINCTION

A. Reasons for Studying "Temporary" Extinctions

When a burning solid propellant is subjected to a rapid pressure decrease, the propellant flame will behave in one of three different ways, depending on the depressurization rate. For relatively slow depressurizations, the propellant will simply resume normal steady state burning at some lower pressure. However, if the rate of pressure decay is increased, a critical rate will eventually be reached above which the flame will extinguish, but for pressure decays which are only slightly faster than this critical rate, the propellant will usually re-ignite after a short delay. That is to say, the propellant will crease burning for a period of from one to ten seconds and will then re-ignite and continue to burn until the entire charge of propellant has been consumed. A further increase in the depressurization rate reveals the existence of a second critical rate above which re-ignition does not occur. For these relatively fast depressurization rates, the propellant flame then remains permanently extinguished. Thus, we can visualize two "extinction" boundaries, such as the ones which are shown schematically on Fig. 54. We shall distinguish the three different end results by referring to them as "non-extinctions", "temporary extinctions", and "permanent extinctions", respectively, as indicated on the figure.

In a stop-start rocket motor, the only extinctions which are of interest are permanent extinctions (for obvious practical reasons). However, in this thesis, we have chosen to investigate the boundary for temporary extinctions, not permanent extinctions. In order to justify this choice, we must consider carefully the causes of re-ignition, and the energy sources which are responsible for re-ignition. It can be shown, both theoretically and experimentally, that the "temporary extinction" characteristics can be connected in a fundamental way to the properties of the particular propellant and the structure of its particular kind of flame, whereas the increase in depressurization rate required to achieve permanent extinction depends sensitively on the residual sources of radiant heat in the chamber at the moment of termination, and therefore on factors which vary from one type of motor geometry to another and from one size to another. It was the purpose of this particular research project to investigate the connection of extinction phenomena with propellant combustion properties, i.e., to conduct a research project aimed at combustion processes, and not at the characteristics of a particular motor. For this reason, the phenomenon of "temporary extinction" was chosen as the focus of attention. The problem of permanent extinction of a motor is considered to be a separate problem, worthy of investigation in its own right. The achievement of extinction of a

motor (i.e., non-re-ignition) can be solved only after the process of temporary extinction (i.e., flame-out) is solved. This is the reason for doing this particular research on the limited, but basic, problem of "temporary extinction".

As its name implies, re-ignition is an ignition phenomenon, and as such, it requires a source of energy. Since the re-ignition takes place in a hot propellant, the amount of energy which is necessary for re-ignition is less than the amount of energy that is required to ignite a cold propellant. Further, since the observed re-ignition times in practical rocket motors or in the usual experimental combustor are very long (on the order of several seconds), the heat flux which produces the re-ignition in such chambers must be quite small in magnitude. We can visualize several potential sources which could supply a small heat flux over a long period of time. Among them are conduction and radiation from the residual hot gases in the combustion chamber and radiation from the hot inert parts of the rocket motor. One further possible energy source is present because of the thermal profile in the solid. The energy stored in the propellant can cause it to undergo a slow exothermic decomposition which can eventually raise the propellant temperature high enough to initiate rapid decomposition and combustion. Any of these possibilities can be the dominant source of re-ignition; it is obvious that all of them must contribute in some part to the re-ignition process. If any one of these small heat sources should be allowed to act over an unlimited period of time, the propellant would always eventually re-ignite. However, it must be realized that non-adiabatic factors are also present; heat losses to the surroundings also occur.

Before we make a more thorough investigation of the sources of the re-ignition energy, let us consider some experimental and theoretical observations which have been made pertaining to the re-ignition phenomenon.

Ciepluch has presented some experimental results which show that the occurrence of re-ignition depends on the operating conditions in the rocket motor, both before and after the depressurization[3]. In tests conducted in an altitude chamber, he showed that re-ignition will not occur if the back-pressure to which the rocket motor exhausts is sufficiently low. This minimum back-pressure (about .25 atm for his experiments) is considerably above the lower deflagration pressure of the propellants he was testing (is about 0.04 atm for those compositions). Ciepluch's Fig. 3, which we have reproduced as our Fig. 55 shows that the boundaries for permanent extinction and for temporary extinction are identical at low back pressures. At higher back pressures where re-ignition occurs, there is a sharp increase in the depressurization rate which is required to cause permanent extinction, whereas the depressurization rate for temporary extinction remains about the same as for low back pressures. Ciepluch suggests that the occurrence of a minimum in the back pressure necessary for re-ignition is due

to the fact that the energy required to ignite a propellant increases rapidly as the ambient pressure is reduced[62]. At lower back pressures, he argues, the available circumstantial heat sources become insufficient to cause re-ignition. Ciepluch's results also show that, in the region in which temporary extinctions occur, the time duration between flame-out and re-ignition increases as the depressurization rate is increased. Thus, depressurization rates which are only slightly faster than the critical depressurization rate for temporary extinction lead to re-ignition after a relatively short time interval, whereas depressurization rates which are nearly as fast as the critical depressurization rate for permanent extinctions lead to re-ignition after a relatively long time interval.

Wooldridge and Marxman tested one propellant at each of three back-pressures and, like Ciepluch, they found that the time which elapsed between a temporary extinction and the ensuing re-ignition increased as the back-pressure was decreased[8]. That is to say, they found that re-ignition became less likely as the back-pressure was lowered. They also reported that re-ignition did not occur at their lowest back-pressure (i.e., infinite time between extinction and re-ignition).

Very recently McDermott and Isom have reported the results of some re-ignition tests in a flight-weight engine[63]. Their results showed that although the back-pressure was below the lower deflagration limit, the propellant could still re-ignite because an "off-gassing" effect could raise the chamber pressure above the lower deflagration limit for the particular propellant. This "off-gassing" effect is due, of course, to decomposition of the (extinguished) propellant, which is caused by heat transfer from hot inert parts inside the rocket motor chamber and residual heat in the propellant, and perhaps by exothermic reaction. Measurements of the rate of loss of mass by a hot (non-ignited) propellant were determined from separate experiments to justify this "off-gassing" effect. It should be remarked that the exothermic decomposition accompanying the off-gassing would also tend to promote re-ignition. McDermott and Isom tested two identical motors. One motor contained a type of internal insulation which induces low levels of radiant energy to the propellant surface from the hot inert components. The other motor contained insulation which gave relatively high radiant heat transfer to the propellant surface. The motor with the low radiation level did not re-ignite, but the motor with the high radiation level did re-ignite. This shows that, for their motor, radiative transfer was an important source of energy for the re-ignition phenomenon, over and above the exothermic reaction source that was undoubtedly present, too. An analytical investigation of the re-ignition process has been presented by Lehmann and Schneiter[64]. Their model predicts the time required for temporary extinction and for re-ignition to occur in the presence of various levels of constant heat flux to the propellant surface. (Their analysis is not concerned with the depressurization rate required to achieve extinction.) The heat flux is modeled as being either radiative (absorbed in depth) or convective (absorbed at the surface) in nature. In their calculations, Lehmann and Schneiter assume that both the

burning rate and the heat feedback from the gas phase to the solid go to zero instantaneously at the moment that the pressure decay is initiated. Specifically, they solve the Fourier heat conduction equation (without a convective term), $\partial T/\partial t = \kappa_p \, \partial^2 T/\partial x^2$, in the solid phase; they use an initial temperature profile that corresponds to the original high pressure steady state temperature profile; and they use a heat flux boundary condition that is constant (in time). The magnitude of the heat flux to the propellant is chosen to be representative of the radiative heat fluxes from the hot, inert parts inside a typical rocket motor which has just extinguished. By solving the problem in this manner, their results are, of necessity, independent of the rate of the pressure decay; their predictions depend only on the initial chamber pressure (burning rate) and the magnitude of the (very small) heat flux. A more realistic approach would be to use the results of our depressurization model (or a similar one) to determine which initial temperature profile to use for their re-ignition model, i.e., start the re-ignition calculation after an extinction model had predicted that temporary extinction would occur. Because the residual temperature profile in the solid depends on the rate of the pressure decay, such re-ignition predictions, which in turn would depend on the initial temperature profile would then become dependent on the pressure decay rate. (Recall that the time interval between temporary extinction and re-ignition depends on the rate of the pressure decay, as has been shown experimentally by Ciepluch[5], and others.)

An example of the effect of sub-surface reactions on re-ignition has been described by Mayer, et al[65]. They found some chemical methods whereby the initial exotherm which is observed when ammonium perchlorate is heated slowly in a DTA experiment could be delayed to higher temperatures, or even eliminated from the temperature range just below ignition. Preliminary tests of propellants which had been treated by one of these methods showed that the tendency to re-ignite was suppressed. This indicates that slow decomposition reaction in a hot (but not ignited) propellant can also affect re-ignition. H. Wise[66,67] and his colleagues have worked for some years to measure the amount of heat generated and the kinetic rate of this exotherm, in the expectation that it alone can explain ignition and burning. However, it is easy to show from their data that insufficient heat is generated to account for ignition in millisecond times (the usual case for start-up) or for burning rates of the order of 1 cm/sec. However, their thermochemical results can account for slow re-ignitions.

Additional insight into the re-ignition phenomenon can be obtained from some of the work on ignition processes. The basic difference between ignition and re-ignition processes is that the initial temperature profiles in the solid are different for the two cases. In the normal ignition case, one usually considers a cold propellant which is uniformly at ambient temperature, but in the re-ignition case, the propellant is hot.

As mentioned above, the actual temperature profile in the solid following a transient extinction is determined by the speed and shape of the pressure decay curve, the transient flame characteristics of the propellant, etc. Our extinction model predicts this residual temperature profile in the solid following an extinction (as will any other complete theory of extinction).

An interesting ignition case which closely parallels the re-ignition process is the marginal ignition transient of a rocket motor (due to low igniter energy flux) or the "hang-fire" case. Most[68] has observed in rocket engine tests that, if the igniter source is cut off when only a small part of the propellant surface has ignited, the rate of flame spread drops to nearly zero for a long period of time (as much as 500 ms), simply because of the sharp decrease in the heat flux to the propellant that occurs when the igniter is terminated. However, after a period of apparent inactivity, the flame rapidly spreads to cover the remainder of the propellant surface, and normal steady state burning is obtained. During this "incubation" period, the non-ignited portion of the propellant is slowly heated by the flow of hot gas from the weak flame which exists on the nearby (ignited) portions of the propellant surface. However, Most has found that in order to match theoretical predictions of flame spread rate with observed experimental values, it is necessary to also include a condensed phase energy source. The magnitudes of the heat release which are necessary to produce agreement with experimental measurements are about the same as those deduced by Steinz[39] from steady state burning. They are also the same as those used by Krier[69] and in this thesis. Thus it appears that condensed phase reactions can have measureable effects on long ignition (or re-ignition) cases. Frazer and Hicks[70] have presented some numerical solutions to an ignition model in which distributed reaction was considered in the solid. For appropriate combinations of igniter flux and duration, their predictions showed that the surface temperature of the propellant would drop for a time (following igniter cut-off), but would then recover and increase again until their ignition criterion was reached. Beyer and Fishman[62] have presented the results of some arc-image igniter experiments which were designed to determine the minimum energy requirement for ignition. In these tests, they routinely obtained ignition <u>after</u> the radiation source had been cut off. These delayed ignitions seem to be qualitatively in accord with the theoretical results of both Most[68] and Frazer and Hicks[70].

Baer and Ryan[71] have presented some data on ignition characteristics of propellants which are exposed to very low radiant heat fluxes. Their experimental results show that fluxes of 5 cal/cm^2 sec produce ignition in about one second. Fluxes of 2 cal/cm^2 sec produce ignition delays of about ten seconds. These measured ignition times establish the order of magnitude of radiant flux which will lead to ignition in a cold propellant after about the same delay which is observed in re-ignitions following temporary extinctions in combustors such as ours.

These results which we have cited above suggest that the re-ignition process is affected by the "boundary conditions" on the experiment. For instance, the magnitude of the radiative heat transfer will depend on the motor geometry, the types of materials that are used inside the motor, the length of time the motor has been operating at steady state conditions, etc. Specifically, the motor geometry will determine the size of the radiating area at the source. The type of material used will determine the surface temperature of the radiating surface; a non-conducting material will retain heat on its surface and will radiate strongly, whereas a metal will allow the heat to diffuse away from the surface and so will radiate less energy because of its lower surface temperature. The length of time at steady state operation previous to depressurization can be very important also, because it will strongly affect the temperature of the internal parts. For instance, in an actual application, the motor may operate for as long as a minute before being stopped, while in a laboratory motor, a steady state operating time of only 0.1 sec. may be used.

Similarly, heat conduction from the hot gases to the propellant, and heat losses from the propellant surface can depend on the motor geometry, etc. The heat release from slow subsurface reactions inside the propellant will depend on the temperature profile in the solid after extinction occurs. This final temperature profile in the solid depends on the shape of the depressurization p-t curve and on the level of the final pressure, as is shown later in the thesis.

Because of these factors, we see that measurements of permanent extinctions which are taken from different laboratory experiments can be compared with each other only if exact data are taken on all these "boundary conditions" to make sure that they are the same in each experiment. Specifically, the motor should be made from the same materials and should have the same geometry. Further, the steady state operating times, previous to the depressurization, should be identical. In order to apply the results from permanent extinction tests to practical motors, one would, in principle, have to carefully correct the permanent extinction results for the re-ignition sources and sinks which were present in the laboratory motor. These corrected data would then have to be corrected a second time to incorporate the effects of the re-ignition sources and sinks in the desired practical rocket motor (which would in all likelihood be quite different from those in the laboratory motor).

Temporary extinctions in cold motors, on the other hand, are independent of the small incidental heat sources which cause re-ignition. (This would not be so if the incidental heat sources were intense.) To apply the results of temporary extinctions to a practical motor, one need only correct the data for the re-ignition sources which are present in the practical motor. (Of course, making such "corrections" as are indicated here and in the previous paragraph can be quite a task and would undoubtedly require experimental testing of the actual motor to characterize those re-ignition sources. Our results can, however, be used to

understand which processes are important in the extinction and re-ignition processes.)

The above discussion represents the justification for dealing with temporary extinctions in this thesis. The experimental measurements of permanent extinction tell you nothing of either extinction or re-ignition (for the particular experimental "boundary conditions" chosen). They only show you the results of both effects, combined together in some undetermined manner.

Several experimental "fringe benefits" are obtained by choosing temporary extinctions in a cool motor, fired for only a short time, as the criterion of interest. Primary among these is that much less data scatter appears in the results. This is because the small heat sources which can lead to re-ignition under more practical circumstances can sensitively affect the re-ignition results. For instance, a few large hot carbon flakes adhering to the chamber walls after depressurization may be enough to lead to re-ignition, whereas one carbon flake may still leave the net heat flux to the propellant negative. A second advantage is that the heat transfer is very difficult to calculate during the period between extinction and re-ignition because of the small heat losses and gains. Consequently, temporary extinction is much easier to predict with reasonable accuracy.

B. Theoretical Analysis of Re-Ignition

Our experimental depressurizations were conducted in a thick-walled, stainless steel motor, and, in addition, we used very short run times (about 100 ms). Both of these factors should tend to diminish the effect of radiative heat transfer on the observed re-ignitions. Ciepluch has estimated that the heat transfer to the solid from the residual hot gas in the chamber is only sufficient to raise the surface temperature of the propellant a few degrees F per second[3]. Since we have gas temperatures which are similar to the ones he used in his calculations, heat conduction from the gas phase to the propellant would probably be small in our problem also. Consequently, one important energy source which is left to cause re-ignition in our experiment is probably the slow exothermic decomposition of the hot (but "extinguished") propellant (similar to the reaction McDermott and Isom[63] considered to be responsible for the "off-gassing" effect, and similar in magnitude to the heat release measured by Wise[66-67]). However, some preliminary calculations of the time interval between flame-out and re-ignition have shown that these reactions alone are not sufficient to produce the re-ignition times which are observed experimentally.

Estimates of the re-ignition time were obtained by solving the diffusion equation with an appropriate heat source as a boundary condition. In non-dimensional form, we have

$$\frac{\partial \theta}{\partial \tau} = \frac{\partial^2 \theta}{\partial X^2} \tag{10}$$

with the boundary conditions

$$\theta(\infty, \tau) = 0$$

$$\frac{\partial \theta}{\partial X}(0,\tau) = H \exp\left[-E_s/RT_{s,o}\left(1/T_{s_{RED}} - 1\right)\right] + \dot{q}_{ENV} \qquad (11)$$

where $\dot{q}_{ENV}$ represents heat received by the propellant surface from the environment.

Our theoretical model for temporary extinctions (which is discussed in Sections IV and VI) includes an exothermic heat release which is placed right at the surface. This heat release represents the combination of the exothermic decomposition of the ammonium perchlorate and the endothermic decomposition of the fuel binder. To be consistent, we have used the same magnitude of this heat release for the energy of decomposition in the very much slower process of re-ignition. Because the decomposition rate is so slow, and because we view it as a solid-phase reaction (with possibly very little change of phase) we have ignored the convective term in the energy equation (see Section IV for complete equation). As a further approximation, the distributed reaction was lumped into an effective heat release occurring right at the surface, whose rate is given by an Arrhenius function of the surface temperature. (Various approximate ways of including the effect of distributed solid phase heat release have been given by Culick[72]). The initial condition for this re-ignition problem is the temperature profile in the solid phase at the moment of extinction. This profile is determined from the temporary extinction model, and yields

$$\theta(X, 0) = f(X) \qquad (12)$$

where $f(X)$ is a numerically tabulated function.

The partial differential equation, 10, can be converted to an integral form by using the exact solutions given by Carslaw and Jaeger[73] (pages 58 and 62) as

$$\theta(X,\tau) = \frac{1}{\sqrt{2\pi\tau}} \int_0^\infty f(y)\left\{e^{-(x+y)^2/4\tau} + e^{-(x-y)^2/4\tau}\right\} dy$$

$$+ \frac{1}{\sqrt{\pi}} \int_0^\tau g(\tau - y)\, e^{-X^2/4y}\, dy/\sqrt{y} \qquad (13)$$

where $g(\tau)$ is the temperature gradient at the surface of the solid, i.e., $g(\tau) = (d\theta/dX)_{s,p}$. This integral equation can then be solved numerically. However, since only the surface temperature appears inside the integral, we need only solve for the surface temperature as a function of time. Thus we have

$$\theta(0,\tau) = \frac{1}{\sqrt{\pi\tau}} \int_0^\infty f(y) e^{-y^2/4\tau} dy + \frac{1}{\sqrt{\pi}} \int_0^\tau g(\tau-y)/\sqrt{y}\, dy \qquad (14)$$

The solution to this integral equation then gives us the behavior of the surface temperature as a function of time following extinction. Since this model is adiabatic (no heat losses are considered) it will <u>always</u> predict re-ignition.

Some numerical solutions to equation 14 have been obtained, and are presented in Fig. 56. These results show the manner in which the re-ignition time increases as the non-dimensional speed, β, of the depressurization is increased. For example, near the temporary extinctions limit (i.e., for values of β which are just barely fast enough to cause temporary extinction to occur), the re-ignition time increases very rapidly with small increases in the depressurization rate, β. Thus, according to these results, the depressurization rate that extinguishes a propellant and yet allows it to re-ignite just 0.1 seconds later is only very slightly less than the rate which keeps it extinguished for times on the order of seconds. For large re-ignition times the opposite is true. The reason for this is that the depressurization rate only serves as an initial condition on the re-ignition calculation. For long re-ignition times, the initial condition has occurred so far away in time that it has only a minor influence on the re-ignition time. The figure also shows that the re-ignition time is strongly affected by the environmental heat sources that are present. Once temporary extinction has occurred, the time required for re-ignition to take place is most critically dependent on the external sources of heat that are present, but it is also mildly dependent on the depressurization rate that caused the temporary extinction. This partially justifies the approach by Lehmann and Schneiter[64], in which they predicted re-ignition times without even considering the depressurization rate. However, it is preferable to also include the effects of the depressurization. Nevertheless, in order for permanent extinction to occur, the rate of depressurization must first be sufficiently fast to cause temporary extinction to occur. Once temporary extinction has occurred, the incidental heat sources must be weak enough that they do not cause re-ignition.

Some typical, residual temperature profiles in the solid phase at the onset of temporary extinction are shown in Fig. 57 for several different exponential depressurizations. As can be seen the faster depressurization rates leave more shallow temperature profiles in the solid than do the slower depressurization rates. (These solid phase temperature profiles were

used as initial conditions to make the re-ignition predictions described above.) Several steady-state profiles are also shown (dashed lines) for visual comparison.

Experimentally, re-ignition times of more than ten seconds are generally never observed. Thus we conclude that predicted re-ignition times of more than about ten seconds are equivalent to permanent extinctions because, over time periods this long, the heat losses (which we have ignored) would prevent re-ignition from occurring. Note that, if we choose 5 seconds as the criterion for permanent extinction, we can define a boundary for permanent extinction, having in mind a certain very small heat loss rate. If, however, we declared that the heat loss rate is still smaller, we could just as well pick 10 seconds re-ignition time as our criterion for permanent extinction. But these two theoretical boundaries happen to be relatively far from each other (see Fig. 56). This illustrates the point that, if the hypothetically small heat losses from the propellant are still further reduced so that longer re-ignition times are observed, the permanent extinction boundary is quite strongly affected. As we have indicated above in our discussion of permanent extinction, the result is very sensitive to the practical motor conditions.

Throughout this thesis, we have presented the boundary for temporary extinctions for which the re-ignition time is on the order of a few seconds. That is to say, a depressurization rate which is very near, but just above, any of our reported extinction boundaries will leave the propellant temporarily extinguished for several seconds. This is the meaning of our temporary extinction boundaries.

We should also note that we could use our temporary extinction model to calculate re-ignition by simply continuing our computer calculations for long times after the propellant has temporarily extinguished. However, since re-ignition times are some 100 times longer than the temporary extinction times, this would mean computer operating times (IBM 360/67) on the order of hours. The cost of this would be prohibitive, so the alternative method described above has been used.

SECTION IV

COMBUSTION MODEL FOR DEPRESSURIZATION ANALYSIS

In this section the theoretical model for the transient combustion process is developed. The depressurization analysis requires a fairly elaborate description of the gas phase processes because of the wide range of pressure conditions which are encountered during the depressurization transient. The granular diffusion flame theory provides such a description as discussed below. The development which is presented here follows Reference 40 closely. An earlier version of the theory was given in Reference 41.

A. Physical Formulation of the Combustion Model

In formulating the combustion model for the depressurization analysis, we visualize a semi-infinite, homogeneous propellant which is burning on its surface in a one-dimensional manner (see Fig. 1). The one-dimensional approximation implies that the thickness of the temperature profile in the solid phase, and the thickness of the gas phase flame are both large in comparison with the effective roughness dimension of the regressing propellant surface. Steinz[80] has estimated the surface roughness of a burning solid propellant as being less than 10μ. The flame thickness is on the order of 0.1 mm (100μ) as noted in Section II. The solid phase heat-up zone thickness is given by $\Delta X = \alpha_p / r$, and taking $\alpha_p = .002\ cm^2/sec$ and $r = .5\ cm/sec$ (which are typical values, see Section VI), we find $\Delta X \simeq 40\mu$ at about 1000 psia. Consequently a one-dimensional approximation is not a bad approximation. For low pressures and burning rates it becomes increasingly better. (Steinz[80] has concluded that a one-dimensional approximation can be used as high as 1500 psia.)

The approximation of a homogeneous solid phase, requires that the solid phase heat-up zone be large in comparison with the effective heterogeneity of the propellant. The best measure of the heterogeneity is the mean AP particle size. Most of the propellants which were used in the experimental work for this thesis were composed of 70% - 180μ AP and 30% - 45μ AP (by weight). This indicates there were 4 or 5 times as many of the smaller AP particles than of the large. Thus we take 45μ as an effective measure of the heterogeneity in a solid propellant. Consequently, at high pressures, the heterogeneity is of the same order of magnitude as the thermal profile depth. However, the homogeneous approximation is still applicable, because the burning surface is so much larger than the average particle size that local differences are averaged out over the burning surface giving the effect of a homogeneous propellant.

The one-dimensional combustion wave which is used for the theoretical model of the depressurization process, pictures

a sub-surface heat-up zone in the solid, an exothermic surface heat release, and a gaseous oxidizer/fuel (O/F) flame (see Fig. 2). The solid phase is described mathematically by the non-steady Fourier heat conduction equation. Because of its non-linearity, this equation is solved numerically. The solid phase is coupled to the gas phase by the heat flux at the solid-gas interface. Part of this heat flux comes from the O/F flame while the rest comes from the surface heat release.

Following Steinz and Summerfield[22], this "surface" heat release is subdivided into an endothermic decomposition of the solid occurring right at the surface, followed by an exothermic gas phase reaction occurring very close to the surface (very thin with respect to the O/F flame thickness) (See Fig. 2.). The endothermic process decomposes the fuel into gaseous vapors and decomposes the ammonium perchlorate into ammonia and perchloric acid. The exothermic process represents the very rapid reaction of these last two components, ammonia and perchloric acid, in an ammonia/perchloric acid (A/PA) flame, in which the gaseous fuel acts only as a diluent. At high pressures this A/PA flame is effectively collapsed and, being very thin, all its heat release is conducted back into the solid (hence the term "surface" heat release). However, at low pressures, the A/PA flame becomes distended (finite kinetics) and only a portion of its heat release is conducted back into the solid; the remainder is carried downstream into the subsequent oxidizer/fuel flame by the gaseous products. Steinz[39] has shown that the kinetics of this A/PA reaction are not slow enough to cause it to distend significantly, except at pressures of about one atmosphere or lower. Thus the effect of the distended surface reaction is important in those extinguishment cases in which the theoretical results are to be compared with experiments which were conducted by exhausting to sub-atmospheric pressures. Since all of our experimental data were obtained by exhausting to atmospheric pressures, and since extinction normally occurred some 10 to 20 psi above ambient, we have used the collapsed surface heat release approximation in all cases. For completeness, the equations for the distended surface reaction are given in subsection IV-E.

This A/PA flame is sufficiently exothermic to make the overall process at the surface appear exothermic. The extent of the exothermicity of this "surface" heat release increases with the AP content of the propellant. At normal AP loadings, about two thirds of the heat received by the solid phase comes from this surface heat release. The second-stage oxidizer/fuel flame contributes the remainder of the heat to the solid phase.

Finally, the granular diffusion flame theory[42] is used along with the proper application of the quasi-steady gas phase analysis to describe the gaseous oxidizer/fuel flame and to deduce the heat feedback from the gas phase. In order to

apply the GDF theory to the particular type of transient which typifies the depressurization process, a slightly different interpretation of the GDF model is necessary. This modification is discussed below. The reason for choosing this physical model of the solid propellant flame is that the GDF model includes both the diffusional mixing and the chemical reaction characteristics of the flame. Both of these processes are important in the depressurization process.

B. The Granular Diffusion Flame Model for the Depressurization Transient-Collapsed Surface Heat Release Model

The coordinate system which has been chosen for the analysis of the depressurization process is taken to be fixed on the burning propellant surface so that the solid is translating at a velocity, $r(t)$, equal to the instantaneous burning rate of the propellant (see Fig. 1). The energy equation for the solid phase can then be written as

$$\lambda_p \frac{\partial^2 T}{\partial x^2} + \rho_p c_p r(t) \frac{\partial T}{\partial x} = \rho_p c_p \frac{\partial T}{\partial t} \tag{15}$$

The surface pyrolysis rate is given by the usual Arrhenius law,

$$r = a' e^{-E_s/RT_s} \tag{16}$$

Experimental measurements of the surface temperature of a burning solid propellant have been attempted by several investigators. A compilation of these experimental results is given in Fig. 24 of Reference 80. Although the data scatter between the various experiments is considerable, there is a decided increase in the surface temperature as a function of pressure. From these results, we conclude that as the burning rate increases, the surface temperature increases, but that large changes in the burning rate (pressure) are required to cause a small change in the surface temperature. This evidence seems to support the use of an Arrhenius relation between the burning rate and the pressure. In addition, the complex hydrocarbon chain of which the fuel binder is composed, decomposes into small gaseous fragments at the surface. The return of these fragments to the complex solid phase is virtually impossible, so that a one-way decomposition, such as our Arrhenius function, seems quite plausible for the binder (i.e., there is no mass flux from the gas back into the solid). A similar argument holds for the ammonium perchlorate for a different reason. It is generally accepted that AP decomposes by dissociative sublimation to gaseous ammonia and perchloric acid, and that two gases react violently upon decomposition (because they are mixed on a molecular level) to form oxygen rich products. They probably react so rapidly that there is little chance for the ammonia or perchloric acid to return to the solid phase, so that the ammonium perchlorate decomposition is also a one-way (far from equilibrium) process.

The surface heat release is treated by the collapsed approximation that was described in the previous subsection (i.e., the entire heat release is deposited right at the surface), so that the surface heat release appears in the heat balance for the solid-gas interface. (Section IV-G presents the equations for a distended surface heat release, and it is shown there, that by taking the limit as the surface heat release zone goes to zero length, one obtains the equations described in this subsection). The heat balance at the solid gas interface is

$$-\lambda_p\left(\frac{\partial T}{\partial x}\right)_{s,p} = r\rho_p Q_s - \lambda_g\left(\frac{\partial T}{\partial x}\right)_{s,g} \tag{17}$$

In the gas phase, the continuity equation is given by

$$\frac{\partial \rho}{\partial t} + \frac{\partial(\rho u)}{\partial x} = 0 \tag{18}$$

and the energy equation takes the form

$$\lambda_g \frac{\partial^2 T}{\partial x^2} + \rho_g c_g u \frac{\partial T}{\partial x} + Q_f \dot{\varepsilon} \rho_g = \rho_g c_g \frac{\partial T}{\partial t} \tag{19}$$

With regard to conservation of momentum in the gas phase, it is assumed that viscous terms are small, and that the velocity is much less than the speed of sound, so that the momentum equation may be replaced by the statement that the pressure is constant across the thickness of the flame zone. We also use the perfect gas law in the gas phase,

$$p = \rho_g R T_g \tag{20}$$

We now invoke the quasi-steady gas phase approximation. As mentioned previously, this approximation implies that the time derivatives of the gas phase fluid dynamic equations are small and can be neglected. Thus the continuity equation (Eq. 18) becomes the simple one-dimensional, steady state relation

$$\rho_g u = \rho_p r \tag{21}$$

and the gas phase energy equation becomes

$$\lambda_g \frac{d^2 T}{dx^2} + \rho_p r c_g \frac{dT}{dx} + Q_f \dot{\varepsilon} \rho_g = 0 \tag{22}$$

By defining the following non-dimensional variables

$$H = \frac{Q_s}{c_p(T_{s,p} - T_\infty)} \qquad Q = \frac{Q_f}{c_p(T_{s,0} - T_\infty)} \qquad \Theta = \frac{T - T_\infty}{T_{s,0} - T_\infty}$$

$$R = r/r_0 \qquad \tau = t/(\alpha_p/r_0^2) \qquad X = x/(\alpha_p/r_0) \tag{23}$$

we can re-write Equations 15, 17, and 22, in a more convenient non-dimensional form. The equation for the solid phase, Eq. 15, becomes

$$\frac{\partial^2\theta}{\partial X^2} + R(\tau)\frac{\partial\theta}{\partial X} = \frac{\partial\theta}{\partial\tau} \tag{24}$$

The heat balance at the solid-gas interface, Eq. 17, becomes

$$\left(\frac{\partial\theta}{\partial X}\right)_{s,p} = \frac{\lambda_g}{\lambda_p}\left(\frac{\partial\theta}{\partial X}\right)_{s,g} - HR \tag{25}$$

and the gas phase energy equation, 22, becomes

$$\frac{d^2\theta}{dX^2} + \frac{c_g}{c_p}\frac{\lambda_p}{\lambda_g}R(\tau)\frac{d\theta}{dX} + \frac{Q\dot{\varepsilon}\alpha_p^2\rho_g c_p}{\lambda_g r_o^2} = 0 \tag{26}$$

This gas phase equation must now be integrated in order to determine the heat feedback from the gas to the solid. We can symbolically perform such an integration by considering Eq. (26) to be a first order ordinary differential equation having $(d\theta/dX)$ as a dependent variable. This integration gives

$$\left(\frac{d\theta}{dX}\right)_f e^{-\frac{c_g}{c_p}\frac{\lambda_p}{\lambda_g}RX_f} - \left(\frac{d\theta}{dX}\right)_{s,g} = -\int_0^{-X_f}\frac{Q\dot{\varepsilon}\rho_g\alpha_p^2 c_p}{\lambda_g r_o^2}e^{\frac{c_g}{c_p}\frac{\lambda_p}{\lambda_g}RX}dX \tag{27}$$

Although $(d\theta/dX)_f$ is not identically zero in the transient case, the approximation is made that

$$\left(\frac{d\theta}{dX}\right)_f e^{-\frac{c_g}{c_p}\frac{\lambda_p}{\lambda_g}RX_f} \ll \left(\frac{d\theta}{dX}\right)_{s,g} \tag{28}$$

Physically, this approximation implies that the amount of heat which is conducted from the flame to the burned gases (i.e., in the downstream direction) is much less than the amount of heat which is conducted upstream into the cooler propellant. The reason for this is that the downstream gases are at nearly the same temperature as the local flame temperature (because they have just emerged from the flame themselves), whereas the surface is considerably cooler than the flame (by virtue of the exothermic reaction that is taking place inside the flame), and so, the amount of heat conducted from the hot flame to the cool solid is much larger than the amount of heat conducted from the hot burned gases to the hot flame. The negative exponential also enters in such a way as to strengthen the inequality; the exponential term is always less than unity. Thus the equation for the heat feedback, Eq. 27, becomes

$$\left(\frac{d\theta}{dX}\right)_{s,g} \simeq \int_0^{-X_f}\frac{Q\dot{\varepsilon}\rho_g\alpha_p^2 c_p}{\lambda_g r_o^2}e^{\frac{c_g}{c_p}\frac{\lambda_p}{\lambda_g}RX}dX \tag{29}$$

In order to proceed further, we need an expression for the (spatial) reaction rate of the oxidizer/fuel flame. Following the GDF theory, we visualize two limiting cases. In the first case, the burning is considered to be completely

controlled by diffusional mixing (such as would be the case at high pressure and high temperature). For this limiting case we represent $\rho_g \dot{\varepsilon}_{dif}$ as a step function

$$\rho_g \dot{\varepsilon}_{dif} = \omega_{dif} \qquad 0 \le X \le X_f$$
$$\rho_g \dot{\varepsilon}_{dif} = 0 \qquad X > X_f \,, \quad X < 0 \tag{30}$$

In the second limiting case, the burning is considered to be controlled by the chemical reaction (low pressures and low temperatures). Here we represent $\rho_g \dot{\varepsilon}_{CH}$ as an impulse function occurring at $X = X_f$, and having the area ω_{CH}, *i.e.*, $\rho_g \dot{\varepsilon}_{CH} = \omega_{CH}\,\delta(X - X_f)$. This corresponds to allowing all the reaction to take place at the highest temperature.

The magnitudes of the two constants, ω_{CH} and ω_{dif}, must be determined such that the proper amount of heat is released in the flame. A heat balance carried out over the entire gas phase (43) gives

$$\theta_f = \theta_s + Q\frac{c_p}{c_g} + \frac{c_p}{c_g}\frac{\lambda_g}{\lambda_p}\left(d\theta/dX\right)_{s,g} / R \tag{31}$$

and, by integrating Eq. 26, the gas phase energy equation, from zero to minus infinity, we obtain

$$-\left(\frac{d\theta}{dX}\right)_{s,g} + \frac{c_g}{c_p}\frac{\lambda_p}{\lambda_g} R\left[\theta_f - \theta_s\right] + \frac{Q\,\alpha_p^2 c_p}{\lambda_g r_0^2}\int_0^{-\infty} \rho_g \dot{\varepsilon}\, dX = 0 \tag{26a}$$

Re-arranging both Eqs. 30 and 26a we find

$$Q\frac{c_p}{c_g} = \left[\theta_f - \theta_s\right] - \frac{1}{R}\left(\frac{c_p}{c_g}\frac{\lambda_g}{\lambda_p}\right)\left(\frac{d\theta}{dX}\right)_{s,g} \tag{30a}$$

$$-\frac{Q}{R}\frac{\alpha_p}{\rho_g r_0^2}\frac{c_p}{c_g}\int_0^{-\infty} \rho_g \dot{\varepsilon}\, dX = \left[\theta_f - \theta_s\right] - \frac{1}{R}\frac{c_p}{c_g}\frac{\lambda_g}{\lambda_p}\left(\frac{d\theta}{dX}\right)_{s,g} \tag{26b}$$

By comparison of Eqs. 30a, and 26b, we find

$$\int_0^{-\infty} \rho_g \dot{\varepsilon}\, dX = -R\left(\rho_p r_0^2/\alpha_p\right) \tag{32}$$

Thus for the chemical reaction controlled flame

$$\int_0^{-\infty} \rho_g \dot{\varepsilon}_{CH}\, dX = \omega_{CH}\int_0^{-\infty} \delta(X - X_f)\, dX = -\omega_{CH}$$

or

$$\omega_{CH} = \left(\rho_p r_0^2/\alpha_p\right) R \tag{33}$$

And for the diffusionally controlled flame,

$$\int_0^\infty \rho_g \dot{\varepsilon}_{dif}\, dX = \omega_{dif} \int_0^{X_f} dX = \omega_{dif} X_f$$

or

$$\omega_{dif} = (\rho_p r_o^2/\alpha_p)(R/X_f) \tag{34}$$

Functional forms for the characteristic times of these two limiting cases are given in Ref. 42. In terms of our non-dimensional variables, these are

$$\tau_{CH}' = \frac{\lambda_p}{\lambda_g}\frac{c_g}{c_p}\frac{\rho_p}{\rho_g}\tau_{CH}$$

$$= \frac{A^2 T_{f_{REO}}^2}{P^2} \exp\left[\frac{E_f}{RT_{f,o}}\left(1/T_{f_{REO}} - 1\right)\right] \tag{35}$$

and

$$\tau_{dif}' = \frac{\lambda_p}{\lambda_g}\frac{c_g}{c_p}\frac{\rho_p}{\rho_g}\tau_{dif} = \frac{B^2 T_{f_{REO}}^{5/3}}{T_{s_{REO}}^{7/4}\, P^{2/3}} \tag{36}$$

where A and B are constants to be determined from the pressure dependence of the steady state burning rate of the particular propellant. In keeping with our quasi-steady gas phase assumption, we postulate that these same functional forms hold during the (quasi-steady) transient as well as during the steady state. During the transient we simply use the instantaneous values of the pressure, flame temperature, and surface temperature. Thus concisely, our quasi-steady assumption implies (a) the steady state fluid dynamic equations hold (the time derivatives in the gas phase are negligible), and (b) the combustion process has the same temperature and pressure dependence during the transient as during the steady state (the combustion process is quasi-steady). However, the gas phase does have a non-steady character which arises from the non-steady surface boundary conditions, and which results in a non-steady condition at the downstream edge of the flame.

Having obtained expressions for the pressure and temperature dependence of the two limiting flame types, we now choose a simple combination of their characteristic times to define the characteristic time of the overall solid propellant flame. Let

$$\sqrt{\tau_{REAC}'} = \sqrt{\tau_{dif}'} + \sqrt{\tau_{CH}'} \tag{37}$$

This choice is identical to that used in the original GDF formulation (40) but it is expressed in a different form. This combination was originally picked because it recovers the proper pressure dependence at the low and high pressure regimes of steady state burning, and also because of its simplicity. It has since been shown to be the best such (simple) combination and represents the pressure dependence of the burning rate quite accurately for a wide range of composite solid propellant formulations (38).

For our transient analysis, we must add one further extension to the GDF theory. In order to integrate the gas phase energy equation, we need some combination of ω_{CH} and ω_{dif}. By analogy with the GDF assumption, we choose to weight these two functions by the square root of their characteristic times. Thus the spatial dependence of the overall reaction is described by

$$\rho_g \dot{\varepsilon} = \sqrt{\frac{\tau_{CH}'}{\tau_{REAC}'}}\ \omega_{CH}\ \delta(X - X_f) + \sqrt{\frac{\tau_{dif}'}{\tau_{REAC}'}}\ \omega_{dif} \tag{38}$$

The justification for this choice is that it has the desired limiting behavior as we go to either the purely diffusional controlled limit, or the purely chemical reaction controlled limit and provides a smooth transition between these extremes. Further, this form is normalized so that the proper amount of heat is always evolved. Finally, it is an algebraically manageable expression.

Returning to our Eq. 29 we can now perform the indicated integration by using Eq. 38. We find

$$\left(\frac{d\theta}{dX}\right)_{s,g} = -\frac{\lambda_p}{\lambda_g}\frac{QR}{\sqrt{\tau_{REAC}'}}\left[\sqrt{\tau_{CH}'}\, e^{-\frac{c_p}{c_g}\frac{\lambda_g}{\lambda_p}RX_f} + \sqrt{\tau_{dif}'}\left(1 - e^{-\frac{c_p}{c_g}\frac{\lambda_g}{\lambda_p}RX_f}\right)\Big/\left(\frac{c_p}{c_g}\frac{\lambda_g}{\lambda_p}RX_f\right)\right] \tag{39}$$

and if we consider $\bar{u}$ as an average gas velocity, we can assume that $\bar{u} \simeq x_f / t_{REAC}$ or in non-dimensional form,

$$R = \frac{\rho_g}{\rho_p} X_f / \tau_{REAC} = \frac{\lambda_p}{\lambda_g}\frac{c_g}{c_p} X_f / \tau_{REAC}' \tag{40}$$

From this we obtain the final form for the heat feedback from the gas phase,

$$\frac{\lambda_g}{\lambda_p}\left(\frac{d\theta}{dX}\right)_{s,g} = -\frac{QR}{\sqrt{\tau_{REAC}'}}\left[\sqrt{\tau_{CH}'}\, e^{-R^2\tau_{REAC}'} + \left(1 - e^{-R^2\tau_{REAC}'}\right)\frac{\sqrt{\tau_{dif}'}}{R^2\tau_{REAC}'}\right] \tag{41}$$

A relation for the flame temperature is given in Eq. 31,

$$\theta_f = \theta_s + Q + \left(\lambda_g/\lambda_p\right)\left(d\theta/dX\right)_{s,g} / R \tag{42}$$

At this point let us consider the physical characteristics of this gas phase model. First of all, we are dealing with a solid which is inhomogeneous. Thus the gaseous decomposition products will likewise be unmixed and will include separate "pockets" of oxidizer and of fuel vapors. Before chemical reactions can occur, these constituents must mix by diffusion. At low pressures, this diffusional mixing will occur rapidly whereas the chemical reaction will be relatively slow. At high pressures the converse will be true; the chemical reaction will be rapid while the diffusional mixing will be relatively slow. The existence of these two pressure limits must be accepted, although they need not both be important. For example, the "high" pressure limit may occur so low in pressure that the chemical reaction is always so fast that it is never important in normal solid propellant burning. Similarly, the low pressure limit may occur so high in pressure that, at normal pressures, diffusion is so fast that the flame always behaves as if it were pre-mixed. Our problem is to determine at which pressures these two processes are important, and to do so, we use the GDF theory. Extensive previous experience with the GDF theory (38) has shown that at normal, high pressure, steady state burning, the flame is primarily controlled by diffusion; the chemical reaction is considerably faster than the diffusional mixing. However, at pressures around one atmosphere the chemical reaction begins to become the more important process.

In addition to its pressure dependence, the chemical reaction will have a strong dependence on the flame temperature through an Arrhenius term. A decrease in the flame temperature will measurably slow the chemical reaction. Diffusion will be only weakly dependent on the temperature. During the depressurization transient the flame temperature drops considerably below its steady state level so that the chemical reaction becomes markedly slower, and eventually as the point of extinction is approached, the chemical reaction becomes the dominating process in determining whether or not extinction will actually occur. The analytical form we have chosen for the description of the gas phase flame allows for the change-over from a diffusionally controlled flame (at high pressure, steady state conditions) to a chemical reaction controlled flame (at low pressure, transient conditions). (Note that in order to evaluate the chemical reaction part of the flame accurately we must know the low pressure steady state burning rate behavior of the propellant, because at high pressures the chemical reaction characteristics are so rapid that they scarcely influence the pressure dependence of the burning rate.)

C. Application of the Depressurization Model to Steady State Burning

The depressurization model developed above includes two constants, A and B. These constants are to be determined from the steady state burning rate of the particular propellant of interest. In order to determine these constants, we now specialize the equations of our combustion model to apply specifically to the steady state case.

During a steady state condition, the solid phase is described by the ordinary differential equation (set the time derivative equal to zero in Eq. 24)

$$\frac{d^2\bar{\theta}}{dX^2} + \bar{R}\,\frac{d\bar{\theta}}{dX} = 0 \tag{43}$$

The cold end boundary condition requires that

$$\bar{\theta}(\infty) = 0 \tag{44}$$

Interface conditions require that

$$\left(\frac{\partial\bar{\theta}}{\partial X}\right)_{s,p} = \frac{\lambda_g}{\lambda_p}\left(\frac{\partial\bar{\theta}}{\partial X}\right)_{s,g} - H\bar{R} \tag{45}$$

and

$$\bar{\theta}_{s,p} = \bar{\theta}_{s,g} \tag{46}$$

The general solution of Eq. 43 is

$$\bar{\theta}(X) = C_1 + C_2\, e^{-\bar{R}X} \tag{47}$$

By applying the cold end boundary condition (Eq. 44) and the temperature matching condition at the solid-gas interface (Eq. 46), we obtain

$$\bar{\theta}(X) = \bar{\theta}_s\, e^{-\bar{R}X} \tag{48}$$

By differentiation, we find the gradient at the surface of the solid,

$$\left(\frac{\partial\bar{\theta}}{\partial X}\right)_{s,p} = -\bar{R}\,\bar{\theta}_s \tag{49}$$

The heat balance at the surface then requires that

$$\frac{\lambda_g}{\lambda_p}\left(\frac{\partial\bar{\theta}}{\partial X}\right)_{s,g} = -\bar{R}(\bar{\theta}_s - H) \tag{50}$$

In the previous sub-section, we integrated the gas phase energy equation (under the quasi-steady approximation) and obtained (Eq. 41)

$$\frac{\lambda_g}{\lambda_p}\left(\frac{\partial\theta}{\partial X}\right)_{s,g} = -\frac{QR}{\sqrt{\tau'_{REAC}}}\left[\sqrt{\tau'_{CH}}\, e^{-R^2\tau'_{REAC}} + \left(1 - e^{-R^2\tau'_{REAC}}\right)\frac{\sqrt{\tau'_{dif}}}{R^2\tau'_{REAC}}\right] \tag{51}$$

For the present steady state case we merely replace the general non-steady gradient $(\partial\theta/\partial X)_{s,g}$ by the specialized steady state gradient which is given in Eq. 50 above. Thus we obtain the relation

$$\bar{\theta}_s - H = \frac{Q}{\sqrt{\bar{\tau}'_{REAC}}}\left[\sqrt{\bar{\tau}'_{CH}}\, e^{-\bar{R}^2\bar{\tau}'_{REAC}} + \left(1 - e^{-\bar{R}^2\bar{\tau}'_{REAC}}\right)\frac{\sqrt{\bar{\tau}'_{dif}}}{\bar{R}^2\bar{\tau}'_{REAC}}\right] \tag{52}$$

These equations are used in conjunction with the experimentally measured pressure dependence of the steady state burning rate to determine the burning rate constants, A and B, in the manner described in the following paragraphs.

For completeness, we group (and re-number) the equations which are used to solve for the burning rate constants, A and B. The specific equations are the pyrolysis relation (Eq. 16); the relations for the two characteristic times (Eqs. 35 and 36) and the combination of these two times to form the characteristic time of the overall flame (Eq. 37); and the steady state heat feedback equation (Eq. 52).

$$\bar{R} = \exp\left[E_s / \mathcal{R} T_{s,o} \left(1/T_{s_{RED}} - 1 \right) \right] \tag{53}$$

$$\sqrt{\bar{\tau}'_{CH}} = \frac{A \bar{T}_{f_{RED}}}{\bar{P}} \exp\left[E_f / \mathcal{R} T_{f,o} \left(1/\bar{T}_{f_{RED}} - 1 \right) \right] \tag{54}$$

$$\sqrt{\bar{\tau}'_{dif}} = B \bar{T}_{f_{RED}}^{5/4} / \bar{T}_{s_{RED}}^{7/8} \bar{P}^{1/3} \tag{55}$$

$$\sqrt{\bar{\tau}'_{REAC}} = \sqrt{\bar{\tau}'_{CH}} + \sqrt{\bar{\tau}'_{dif}} \tag{56}$$

$$\bar{\theta}_s - H = \frac{Q}{\sqrt{\bar{\tau}'_{REAC}}} \left[\sqrt{\bar{\tau}'_{CH}}\, e^{-\bar{R}^2 \bar{\tau}'_{REAC}} + \left(1 - e^{-\bar{R}^2 \bar{\tau}'_{REAC}} \right) \frac{\sqrt{\bar{\tau}'_{dif}}}{\bar{R}^2 \bar{\tau}'_{REAC}} \right] \tag{57}$$

Note the Eq. 53 is the non-dimensionalized form of the pyrolysis relation, Eq. 16.

The reference surface temperature, $T_{s,o}$, and the reference flame temperature, $T_{f,o}$, are assumed known, as are the flame activation energy, E_f, the surface activation energy, E_s, and the surface heat release, H (see Section VI-A). The steady state flame temperature is determined as a function of pressure from adiabatic flame temperature calculations for the particular propellant composition. The steady state burning rate is known as a function of pressure from experimental measurements. Thus the only unknowns in this set of equations are the burning rate constants, A and B.

The determination of the burning rate constants, A and B, proceeds as follows. First, a particular pressure at which the burning rate has been measured, is chosen. The corresponding surface temperature is calculated from the pyrolysis relation, Eq. 53. The flame temperature is determined from

adiabatic flame temperature calculations. An arbitrary value is then chosen for the constant, A, and $\bar{\tau}'_{CH}$ is then calculated from Eq. 54. The constant, B, is then calculated from Eqs. 55 and 57 (by iteration). (Note that if the burning rate were measured at only one point, our system would have an arbitrariness in it, such that for any "A" chosen, a corresponding "B" could be found. However, the pressure dependence of the burning rate is used to remove the arbitrariness.) Then, using the same arbitrary value for the constant, A, corresponding constants, B, are found for the experimental burning rate at each of the measured pressures. The mean square deviation from the average value of B is then determined. Successive values of the constant, A, are chosen until some value of A is found which minimizes the sum of the mean square deviations of each of the calculated constants, B (at each pressure at which the burning rate had been measured), from the average B (for the particular value of A). The "A" and the average "B" at this minimum are taken as the "best" fit of the steady state burning rate theory to the measured burning rate data. In actual practice, a decisive minimum was always found (except as noted in Section VI-B).

It is interesting to now compare this modified version of the GDF theory with the standard GDF model for steady state burning. These models become similar when the product $\bar{R}^2 \bar{\tau}'_{REAC}$ is greater than (say) two. In such a case we can neglect the exponential terms, because

$$e^{-\bar{R}^2 \bar{\tau}'_{REAC}} \ll 1 \tag{58}$$

With this approximation, the feedback Eq. 52 becomes

$$\frac{\bar{\theta}_s - H}{Q} = \frac{\sqrt{\bar{\tau}'_{dif}}}{\bar{R}^2 \bar{\tau}'^{3/2}_{REAC}} \qquad \text{or} \qquad \frac{1}{\bar{R}} = \sqrt{\frac{\bar{\theta}_s - H}{Q}} \left(\frac{\bar{\tau}'_{REAC}}{\bar{\tau}'_{dif}}\right)^{1/4} \sqrt{\bar{\tau}'_{REAC}} \tag{59}$$

If we further consider the flame temperature and the surface temperature as constants (which is a good approximation during steady state), we can write the expressions for the characteristic times as (see Eqs. 54 and 55),

$$\bar{\tau}'_{CH} \simeq a^2/\bar{p}^2 \qquad \text{and} \qquad \bar{\tau}'_{dif} \simeq B^2/p^{2/3} \tag{60}$$

so that the steady state burning rate is approximately given by

$$\frac{1}{\bar{R}} \simeq \sqrt{\frac{\bar{\theta}_s - H}{Q}} \left(\frac{\bar{\tau}'_{REAC}}{\bar{\tau}'_{dif}}\right)^{1/4} \left[a/p + B/p^{1/3}\right] \tag{61}$$

Neglecting the pressure dependence of the fourth power of the indicated ratio of the characteristic times, this expression is of the same form as the standard GDF burning rate expression, namely

$$\frac{1}{r} = \frac{a}{p} + \frac{b}{p^{1/3}} \tag{62}$$

In a steady state situation, the approximation, $e^{-\bar{R}^2 \bar{\tau}'_{REAC}} \ll 1$, holds from high pressure down to nearly atmospheric pressure, because although $\bar{R}^2$ decreases with pressure, the characteristic time increases with pressure. However note that during the depressurization transient this exponential cannot be ignored. In extinguishment cases, R goes to zero while τ'_{REAC} remains finite. Hence during extinguishment $e^{-R^2 \tau'_{REAC}} \rightarrow 1.0$.

D. Comparison of Present Depressurization Model to the KTSS Model

A theory of non-steady burning has previously been published by the Princeton group (43). This previous model, which will be referred to here as the KTSS model, is intended for the analysis of combustion instability problems. In this sub-section we present a comparison between the theoretical model which is presented in this thesis and the KTSS model. The difference between these two models is in the handling of the quasi-steady gas phase. Because the instability problem is concerned with small excursions about some mean burning level, the instability model need be only a local theory (in the sense that it applies to only small changes in pressure and temperature). The depressurization problem on the other hand, requires a more global analysis because the analysis must apply all the way from normal operating pressures down to atmospheric (or sub-atmospheric) pressures. The depressurization analysis must also deal with large flame temperature variations.

In the KTSS analysis of the gas phase, they derive a relation for the heat feedback which is of the form

$$\lambda_g \left(\frac{\partial T}{\partial x}\right)_{s,g} = -\frac{\phi(p)}{r}\left[1 - \exp\left(-\rho_p^2 c_p r^2 / \dot{\varepsilon} \lambda_g \rho_g\right)\right] \tag{63}$$

where the term, $\phi(p)$, is a function of pressure only, which is determined from the steady state burning characteristics of the propellant. They argue that the exponential term is negligible at high pressures, and hence can be ignored. From steady state relations, they evaluate $\phi(p)$ as

$$\phi(p) = -\left(\frac{\partial \bar{\theta}}{\partial \bar{X}}\right)_{s,g} \bar{R} \tag{64}$$

But as noted before (see Eq. 50), the steady state heat feedback from the gas phase to the solid is given by

$$\left(\frac{\partial \theta}{\partial \bar{X}}\right)_{s,g} = -\left(\bar{\theta}_s - H\right) \bar{R} \tag{50}$$

So

$$\phi(P) = (\bar{\theta}_s - H)\,\bar{R}^2 \tag{65}$$

and the KTSS feedback law is (for the transient case)

$$\left(\frac{\partial \theta}{\partial X}\right)_{s,g\ KTSS} = -\frac{\bar{R}^2(\bar{\theta}_s - H)}{R} \tag{66}$$

In the KTSS model, a steady state burning rate equation of the form $\bar{R} = P^n$ was used, and the pyrolysis law was of the form, $R = \theta_s^{\,m}$, where m is a constant. Thus the KTSS feedback equation is

$$\left(\frac{\partial \theta}{\partial X}\right)_{s,g\ KTSS} = -\frac{P^{2n}(P^{n/m} - H)}{R} \tag{67}$$

where $P^{n/m}$ is the steady state surface temperature corresponding to the instantaneous pressure P.

Returning to our depressurization model, let us, for reference, re-write Eq. 41 which specifies the heat feedback from the gas phase during a transient.

$$\frac{\lambda_g}{\lambda_p}\left(\frac{\partial \theta}{\partial X}\right)_{s,g} = -\frac{QR}{\sqrt{\tau'_{REAC}}}\left[\sqrt{\tau'_{CH}}\,e^{-R^2\tau'_{REAC}} + \left(1 - e^{-R^2\tau'_{REAC}}\right)\frac{\sqrt{\tau'_{dif}}}{R^2\tau'_{REAC}}\right] \tag{41}$$

The corresponding equation for steady state burning is (rearranging Eq. 52)

$$\frac{\bar{\theta}_s - H}{Q} = \frac{1}{\sqrt{\bar{\tau}'_{REAC}}}\left[\sqrt{\bar{\tau}'_{CH}}\,e^{-\bar{R}^2\bar{\tau}'_{REAC}} + \left(1 - e^{-\bar{R}^2\bar{\tau}'_{REAC}}\right)\frac{\sqrt{\bar{\tau}'_{dif}}}{\bar{R}^2\bar{\tau}'_{REAC}}\right] \tag{52a}$$

In order to obtain the KTSS feedback law, we now make the approximation that the flame is purely diffusionally controlled and hence that

$$\sqrt{\tau'_{dif}} \gg \sqrt{\tau'_{CH}}$$

so that as a consequence

$$\sqrt{\tau'_{REAC}} \simeq \sqrt{\tau'_{dif}}$$

Thus the transient and steady state feedback Eq. 41 and 52a become

$$\frac{\lambda_g}{\lambda_p}\left(\frac{\partial \theta}{\partial X}\right)_{s,g} = -\frac{Q}{R\tau'_{dif}}\left(1 - e^{-R^2\tau'_{dif}}\right) \tag{68}$$

$$\frac{\bar{\theta}_s - H}{Q} = \frac{1}{\bar{R}^2\bar{\tau}'_{dif}}\left(1 - e^{-\bar{R}^2\bar{\tau}'_{dif}}\right) \tag{69}$$

Now, as in the KTSS development, we neglect the exponential terms in Eqs. 68 and 69, and we have for the transient case

$$\frac{\lambda_p}{\lambda_g}\left(\frac{\partial\theta}{\partial X}\right)_{s,g} = -Q/R\tau'_{dif} \tag{70}$$

whereas for the steady state equation we have

$$\frac{Q}{\bar{\tau}'_{dif}} = \bar{R}^2(\bar{\theta}_s - H) \tag{71}$$

By comparison with the KTSS theory, we see that their $\phi(p)$ term (Eq. 65) in non-dimensionalized form is equivalent to $Q/\bar{\tau}'_{dif}$ in our development. Thus if we assume $\tau'_{dif} \simeq \bar{\tau}'_{dif}$, i.e., if we ignore the temperature dependence of the diffusional time we have

$$\tau'_{dif} = \frac{B^2\, T_{F_{RED}}^{5/3}}{T_{S_{RED}}^{7/4}\, p^{2/3}} \simeq B/p^{2/3} \tag{72}$$

Hence for the transient feedback we have

$$\frac{\lambda_g}{\lambda_p}\left(\frac{\partial\theta}{\partial X}\right)_{s,g} = -\frac{\bar{R}^2(\bar{\theta}_s - H)}{R} \tag{73}$$

which is identical to the KTSS feedback law, Eq. 67, when written in the linearized form (in which the exponential term is dropped)

$$\frac{\lambda_g}{\lambda_p}\left(\frac{\partial\theta}{\partial X}\right)_{s,g\,KTSS} = -p^{2n}(p^{n/m} - H)/R \tag{67a}$$

In summary, we see that if we neglect the chemical-reaction-rate part of our model, and if we drop the temperature dependence of the diffusional time, we will obtain the KTSS feedback law as a special case of our depressurization model. At high pressures, the approximation $\tau'^{1/2}_{dif} \gg \tau'^{1/2}_{dk}$ does indeed hold, so that a small perturbation solution of the depressurization model at high pressures would be similar to the KTSS small perturbation solution. However at low pressures (which are generally not of interest in instability) the two models would predict quite different results because the chemical reaction term could no longer be ignored.

Despite the fact that the chemical reaction term can be legitimately ignored in the instability problem, it cannot be ignored in the depressurization analysis. As we have indicated before, the chemical reaction term is the most important term in determining whether or not extinction will occur. Also the GDF steady state theory is a better representation of the pressure dependence of the burning rate over the wide pressure ranges of interest than is the $\bar{R} \simeq p^n$ formulation which is used in the KTSS model.

Finally it should be pointed out that the linearized form of the KTSS feedback law, Eq. 67a, can never predict extinction because the entire feedback expression is multiplied by a factor of 1/R. Thus as R approaches zero, the heat feedback becomes infinite so that extinction can not occur. A similar problem is encountered if we try to use the straight line integration of the gas phase energy equation as was done in the original formulation of the GDF theory (42). It is for this reason that we have had to modify the integration of the gas phase in our development of the GDF model for the depressurization analysis.

E. The Vichnevetsky Numerical Integration Procedure

The numerical integration procedure which was used for the solution of the solid phase equation (Eq. 24) is based on a method suggested by Vichnevetsky[44]. The method consists of initially discretizing the time coordinate so as to obtain a system of ordinary differential equations in the spatial coordinate X. The resulting equations are non-linear due to the presence of the burning rate term, R. The normal method for solving these ordinary differential equations is to choose a guess value for the burning rate, R, and obtain the solution of the ordinary differential equation and then use the solution to guess a better value for the burning rate. Thus eventually the solution is found by iteration. However each time a numerical value is chosen for the burning rate, the resulting equation becomes linear (i.e., the non-linear term is replaced by a constant). Vichnevetsky's method uses this fact to separate the second order equation into three first order ordinary differential equations by means of linear differential operators. These first order equations are then integrated numerically in such a direction (i.e., either positive or negative) as to make the integration stable. The resulting system is computationally stable as has been shown by Vichnevetsky. Stability has also been shown empirically by comparing results obtained with the Vichnevetsky integration with the results of standard numerical integration schemes which are easily shown to be stable. An outline of the method follows.

Rewriting Eq. 24 for the solid phase

$$\frac{\partial^2\theta}{\partial X^2} + R\frac{\partial\theta}{\partial X} = \frac{\partial\theta}{\partial\tau} \tag{24}$$

and the corresponding boundary conditions,

$$\theta(\infty) = 0 \tag{44}$$

$$\left(\frac{\partial\theta}{\partial X}\right)_{S,P} = \phi(R,P) \tag{74}$$

where $\phi(R,P)$ is the function given in Eq. (41). Representing the time derivative by a finite difference approximation, we obtain the ordinary differential equations

$$\frac{d^2\theta^i}{dX^2} + R^i \frac{d\theta^i}{dX} - \frac{\theta^i}{\Delta\tau} = -\frac{\theta^{i-1}}{\Delta\tau} \tag{75}$$

We then replace the unknown R by a "guess" value, Rg, and obtain a linear, constant coefficient equation. Hence we can identify the linear operators L, L_1 and L_2 as

$$L = d^2/dX^2 + R_g\, d/dX - 1/\Delta\tau \tag{76a}$$

$$L_1 = d/dX - \lambda_1 \tag{76b}$$

$$L_2 = d/dX - \lambda_2 \tag{76c}$$

where L_1 and L_2 are defined such that

$$L = L_1 L_2 = L_2 L_1$$

(the operators are commutative). The values for $\lambda_{1,2}$ are

$$\lambda_{1,2} = \frac{R_g}{2} \pm \sqrt{\left(\frac{R_g}{2}\right)^2 + 1/\Delta\tau} \tag{77}$$

Let λ_1 be the positive definite root, and λ_2 the negative definite root. We now define three new functions $\tau_1(X)$, $\tau_2(X)$ and $\tau_3(X)$ such that they satisfy the equations

$$L_1(\tau_1) = (d\tau_1/dX) - \lambda_1 \tau_1 = \tau_3 \tag{78a}$$

$$L_2(\tau_2) = (d\tau_2/dX) - \lambda_2 \tau_2 = 0 \tag{78b}$$

$$L_2(\tau_3) = (d\tau_3/dX) - \lambda_2 \tau_3 = -\theta^{i-1}/\Delta\tau \tag{78c}$$

and since

$$L(\tau_1) = L_2[L_1(\tau_1)] = L_2[\tau_3] = -\theta^{i-1}/\Delta\tau \tag{79}$$

and

$$L[\tau_2] = L_1[L_2(\tau_2)] = L_1[0] = 0 \tag{80}$$

we see that any linear combination of τ_1 and τ_2 will satisfy the differential equation. Hence we set

$$\theta^i(X) = \tau_1(X) + C_3\, \tau_2(X) \tag{81}$$

We must now pick the boundary conditions for τ_1, τ_2, and τ_3 such that θ^i, as defined, will satisfy the required boundary conditions. First we note that in order to obtain stable integrations, we must integrate the L_1 operator in the negative-X direction and the L_2 operator in the positive-X direction. In this manner the solution we obtain will always be of the form $e^{-\lambda X}$ (where $\lambda > 0$) so that any error will decay exponentially as the integration proceeds. (Note that if our solution were of the form $e^{+\lambda X}$, and we integrated in the positive-X direction, any errors would grow without bound, however, by integrating from infinity to zero any errors decay.) Thus, we will want to specify boundary conditions for τ_2 and τ_3 at X=0 (and integrate positively), but we must specify the boundary condition for τ_1 at X=∞ (and integrate negatively). This also allows us to satisfy the split boundary conditions without iteration.

By substitution it can be shown that the following choices for the boundary conditions for the functions τ_1, τ_2 and τ_3

$$\tau_1(\infty)=0 \qquad \tau_2(0)=1 \qquad \tau_3(0)=\lambda_2\,\theta^{i-1}(0) \tag{82}$$

will satisfy the boundary conditions which have been specified for θ^i (Eqs. 44 and 74) provided we choose the constant c_3 as indicated below. Substitution of the boundary conditions into Eq. 81 gives

$$\theta^i(\infty) = \tau_1(\infty) + c_3\,\tau_2(\infty) = 0 \tag{83}$$

and

$$\left(\frac{d\theta^i}{dX}\right)_{s,p} = \phi(P,R) = \left(\frac{d\tau_1}{dX}\right)_{X=0} + c_3\left(\frac{d\tau_2}{dX}\right)_{X=0} \tag{84}$$

Now, the equation for $\tau_2(X)$ can be solved analytically to give

$$\tau_2(X) = e^{\lambda_2 X} \qquad 85)$$

and since $\lambda_2 < 0$ we see that $\tau_2(\infty)=0$, so that the first condition, Eq. 83, on θ^i is satisfied, because $\tau_1(\infty)$ is also zero, see Eq. 82. From equations 78a and 78b we see that

$$\left.\frac{d\tau_1}{dX}\right|_{X=0} = \lambda_1\tau_1 + \tau_3\Big|_{X=0} \tag{86a}$$

$$\left.\frac{d\tau_2}{dX}\right|_{X=0} = \lambda_2\,\tau_2\Big|_{X=0} \tag{86b}$$

Inserting these in Eq. (84) and solving for C_3, we find

$$C_3 = \frac{\phi(R,P) - \lambda_1 \tau_1(0) - \tau_3(0)}{\lambda_2 \tau_2(0)} \tag{87}$$

and using the boundary conditions, Eq. 82, we have

$$C_3 = \frac{\phi(R,P) - \lambda_1 \tau_1(0) - \lambda_2 \theta'^{-1}(0)}{\lambda_2}$$

Thus we can solve for the functions τ_3 and τ_2 by integrating in the positive-X direction. Then, knowing τ_3, we can solve for τ_1 by integrating in the negative-X direction. From these we can determine the constant C_3 and then tabulate the non-dimensional temperature, θ', as a function of X.

In the actual integration, the fourth-order Runge-Kutta method of integration was used. This method is advantageous in that it requires no starting routine. Rather than apply the cold-end boundary conditions at infinity (which is impossible in a numerical solution), the boundary conditions were applied at some "large" value of X. The actual position at which the boundary conditions were applied was determined by calculating the depth (into the propellant) at which the temperature would drop to 10^{-5} times its value at the surface if the current burning rate were a steady state burning rate. As the burning rate drops during the depressurization, the temperature profile penetrates deeper and deeper into the solid. Correspondingly the number of intervals used in the X coordinate during the depressurization was increased as the burning rate decreased (the interval size was held constant). When the non-dimensional burning rate dropped lower than about R=.05, the number of X intervals was no longer increased. (Specifically, the cold end boundary condition was applied at a non-dimensional depth X = 10/R, when R is the instantaneous non-dimensional burning rate. The actual physical depth at which the boundary condition was applied, is given by $x = X\kappa_p/r_0$. Using the same value for the thermal diffusivity which is used throughout the rest of the thesis, namely κ_p =.00029 in^2/sec., and using a nominal value of .25 in/sec for the reference burning rate, r_0, we find for the two extremes, R = 1.0 and R = .05, that the cold-end boundary condition is applied at depths of 0.01 inches and 0.20 inches respectively. In our experiments, propellants which were .5 inches thick were used. Consequently, these depths for the cold-end boundary condition seem acceptable, i.e., they are still inside the propellant.) The number of mesh points used in the X coordinate varied between about 150 and 1600 for any given depressurization. Variations in step size and number of steps showed this approximation was adequate.

A variable time step was used in the computer solution. For each computer run, the computation was started with an initial time step, $\Delta\tau$ = 0.01, in non-dimensional units. As the computation progressed (and the magnitudes of the time derivatives decreased) the time step was gradually increased

to a maximum step size of $\Delta\tau = 1.0$. Various checks of this time step interval indicated that it was adequate. The checks consisted of using constant time steps, and of halving the time step interval. If the time step were increased by very much over the magnitudes indicated above, the computed results began to show a weak dependence on the size of the time step which was used. The numerical results based on the Vichnevetsky integration were also compared with numerical results which were obtained by using the more conventional finite differencing method for Eq. 24, namely the explicit method

$$\frac{\theta_j^{i+1}-\theta_j^i}{\Delta\tau} = \frac{R^i[\theta_{j+1}^i-\theta_{j-1}^i]}{2\Delta X} + \frac{\theta_{j+1}^i - 2\theta_j^i + \theta_{j-1}^i}{\Delta X^2} \qquad (90)$$

where superscripts represent the time coordinate, and subscripts represent the spatial coordinate. The integration by means of Eq. 90 requires a stability condition, $\Delta\tau/\Delta X^2 < .5$, and this condition was observed in the calculations based on Eq. 90. The results of the Vichnevetsky integration agreed very well with the integrations based on Eq. 90.

A final check on the numerical solutions was to ascertain that the computer program would calculate steady state conditions (without drift or offset) at each of several pressure levels. These steady state checks were of especial usefulness because the complete steady state solutions could be obtained analytically, so that a direct determination of the computing error could be made. Thus, this check was used to ensure that no programming errors, algebraic or sign errors, or computational errors were present in the final computer program. The steady state checks were made in two ways. First, an initial temperature profile corresponding to a given pressure level was input to the computer as an initial condition. The corresponding pressure was then input as a forcing function independent of time (i.e., the pressure was specified as a constant for all time). The check consisted of observing that the calculated results did not drift from their initial values as time progressed. This steady state check was run for a sufficient time to ensure that very slow drift rates were not present (specifically, the steady state was computed for time intervals which were similar to the time intervals necessary for the prediction of extinction). The second steady state check was to ensure that, after starting from one steady state profile, the computer solution would eventually move to the proper second steady state profile, if the pressure were held constant at the level corresponding to the second steady state profile. Thus, of the two steady state checks, one ensured that, given an initial steady state, the transient computer solution would maintain that steady state without drift (if the pressure were held constant). The second ensured that the computer solution would "home" towards a desired steady state level if it were started at some other level.

Conceptually speaking, the overall calculation process for the transient burning rate as a function of time, proceeds

as follows. At any given time step in the solution, the temperature profile in the solid for the previous time is known as a tabulated function of the spatial coordinate, X. For the first time step, the temperature profile at the previous time is just the initial condition; for all other times, it is the most recently calculated temperature profile. To obtain the temperature profile for the next instant of time, an initial guess value for the burning rate is first chosen. The heat feedback from the gas phase to the solid is then calculated for the particular guess value of the burning rate. Then the equation for the solid phase, Eq. 75, which is now linear (since R(t) has been replaced by a constant) is solved as indicated above to give the temperature profile in the solid. The surface temperature corresponding to this profile gives a second value of the burning rate through the Arrhenius pyrolysis relation, Eq. 53. This burning rate is then compared with the previously guessed value of the burning rate, and a new guess is made for the burning rate. This establishes an iterative loop which proceeds until the guess value of the burning rate is within a certain, specified tolerance of the calculated (from the pyrolysis relation) burning rate. Eq. 24 and its associated boundary conditions, Eqs. 41 and 44 were programmed in the Fortran IV computer language (according to the method described above, see Eqs. 75, 78, 81, 82, and 88) and was solved on the following IBM computers; the IBM 7094, the IBM 360/30, the IBM 360/67, and the IBM 360/91. An average computation time for one depressurization was about 30 seconds on the 360/67 computer when a Fortran "H" compiler was used.

F. Plausibility of Transforming From an Infinite Domain to a Finite Domain for the Numerical Solution of the Solid Phase

In several previous studies (4, 8, 43) which dealt with non-steady burning of solid propellants, an exponential coordinate transformation of the form $Z = e^{-x}$ has been used to transform the semi-infinite solid into a finite domain $(0, 1)$. If we apply such a transformation, Eq. 24 takes the form

$$Z^2 \frac{\partial^2 \theta}{\partial Z^2} + (1-R) Z \frac{\partial \theta}{\partial Z} = \frac{\partial \theta}{\partial \tau} \qquad 0 \le Z \le 1 \qquad (91)$$

The numerical solution of the problem in this coordinate system is made simpler because of the finite domain. However we also note that this form of the equation has a singularity at Z = 0 (the cold end). This singularity can create problems which will more than offset the convenience obtained by eliminating the semi-infinite domain. One example of the type of problem this singularity can introduce is seen by considering the steady state solution. An analytical expression can be obtained for the steady state solution, hence we can make an exact error analysis of a numerically determined steady state solution by a simple comparison. Of course, even if our numerical scheme predicts the correct steady state solution, we cannot

infer that it will produce correct transient solutions, but certainly the converse is true; if our numerical scheme predicts incorrect results for a steady state, it will also give incorrect transient predictions for excursions between two steady states.

Thus we consider the solutions of the equation

$$Z^2 \frac{d^2\bar{\theta}}{dZ^2} + (1-\bar{R}) Z \frac{d\bar{\theta}}{dZ} = 0 \qquad 0 \leq Z \leq 1 \tag{92}$$

with the boundary conditions

$$\bar{\theta}(\delta) = 0 \tag{93}$$

$$\left(\frac{\partial\bar{\theta}}{\partial Z}\right)_{Z=1} = \phi(P,\bar{R}) \tag{94}$$

where we have chosen to apply the cold boundary condition, Eq. 93, at $Z = \delta$ (where $\delta \ll 1$) rather than at $Z = 0$ in order to show the importance of this boundary condition. The solution of Eq. 92 which satisfies boundary conditions 93 and 94 is

$$\bar{\theta}(Z)_{EXACT} = \frac{\phi(P,\bar{R})}{\bar{R}} \left(Z^{\bar{R}} - \delta^{\bar{R}}\right) \tag{95}$$

The "exact" solution (for the cold boundary condition applied at $Z = 0$) is given by setting $\delta = 0$ is this expression, i.e.,

$$\bar{\theta}(Z)_{\substack{EXACT \\ \delta=0}} = \frac{\phi(P,\bar{R})}{\bar{R}} Z^{\bar{R}}$$

Note that because of the $Z^{\bar{R}}$ term, this steady state solution is non-analytic at $Z = 0$ except in the special case when $\bar{R}$ is an integer. However, the application of finite difference methods to the solution of this problem assumes the solution can be expanded in a Taylor's series at every point. (Alternatively, finite difference approximations can be thought of as locally representing the solution by a polynomial in Z, but there are no polynomials in Z which are non-analytic at the origin.) Thus the region near $Z = 0$ cannot be approximated accurately by finite differences.

One simple alternative for the case in which $\bar{R} > 1$ is to apply the boundary condition, 93, at $Z = \delta \neq 0$. In this manner the integration doesn't have to go all the way to the singularity. From the analytical expression for the steady state solution we see that this approximation will give an error of the order $\delta^{\bar{R}} < \delta$ (i.e., for $\bar{R} > 1$, $\delta^{\bar{R}} < \delta$) which becomes an increasingly better approximation as the magnitude of $\bar{R}$ increases. Numerical solutions of the steady state problem have indicated

that this procedure does indeed give accurate results during a steady state. In fact for the case of $\bar{R} > 1$, the boundary condition can be applied at Z = 0 (i.e., we can use a Taylor's series expansion about the non-analytic point) without creating large (steady state) errors.

The case in which $\bar{R} < 1$ (which is of interest in the depressurization problem where R must approach zero) is quite different. In this case the first derivative ($\partial\bar{\theta}/\partial\tau$) of the steady state solution is infinite at Z = 0. Applying the boundary condition at $Z = \delta$ is completely unacceptable even for very small values of δ. An example of the magnitude of the error involved in applying the boundary condition at $\delta = .005$ is shown in Fig. 3 for the case when $\bar{R} = 0.3$. Visual inspection of the corresponding "exact" steady state profile immediately shows why such errors are encountered. Numerical tests in which the boundary condition was applied at Z = 0, but in which the non-analytic solution was represented by finite difference formulas, indicated errors of this same order of magnitude in the steady state solutions. (This merely implies that it is impossible to find a polynomial in Z which has an infinite slope at Z = 0.)

Numerical solutions were obtained for transient problems in both the finite domain "Z" and the semi-infinite domain "X". Considerable differences were noted in the predicted extinction boundaries (on the order of a factor of 2). For this reason and in view of the discussion presented above, we conclude that the exponential coordinate transformation cannot be used for the depressurization problem. It is however appropriate (and useful) for pressurization problems in which the transient non-dimensional burning rate remains greater than unity.

A recent paper which discusses various ways of transforming infinite and semi-infinite problems into finite domains has been published by Sills (45). Sills suggests the above discussed exponential transformation as being appropriate for this purpose. He mentions the necessity of ensuring that the quantity $\partial\theta/\partial\tau$ (in terms of our variables) remain bounded as $Z \to 0$. However he states that he has found no physical situation in which this derivative does become unbounded and hence that it is not a serious drawback. Our problem represents a case where the gradient is unbounded so that we should expect to find problems.

G. The Granular Diffusion Flame Model for the Depressurization Transient -- Distended A/PA Flame Model

In this subsection we modify the equations which describe the depressurization transient to include the effects of a distended A/PA reaction. Following Steinz and Summerfield[22], we visualize the A/PA reaction as a pre-mixed flame (because the reactants, ammonia and perchloric acid, are premixed on a molecular scale following their generation by the decomposition

of the AP crystals), and as having a first order pressure dependence.

We visualize a model which includes two separate gas phase flame structures as shown in Fig. 2. The energy equations for these two flames are given as

$$\frac{\partial^2\theta}{\partial X^2} + \frac{\lambda_p}{\lambda_g}\frac{c_g}{c_p} R\frac{\partial\theta}{\partial X} + \frac{\lambda_p \dot{\varepsilon}\, \alpha_p Q}{r_o^2 c_g \rho_p \alpha_g} = 0 \qquad X_I \le X \le X_{II} \tag{97}$$

and

$$\frac{\partial^2\theta}{\partial X^2} + \frac{\lambda_p}{\lambda_g}\frac{c_g}{c_p} R\frac{\partial\theta}{\partial X} + \frac{\lambda_p \dot{\varepsilon}\, \alpha_p H_I}{r_o^2 c_g \rho_p \alpha_g} = 0 \qquad 0 \le X \le X_I \tag{98}$$

for the O/F flame and the A/PA flame respectively.

The integration of the O/F flame proceeds exactly as before except for the change in the lower integration limit. In a manner analogous to that used in Subsection B to obtain Eq. 27, we find

$$\left(\frac{d\theta}{dX}\right)_{I^+} e^{-\frac{\lambda_p}{\lambda_g}\frac{c_g}{c_p} R X_I} = \int_{-X_I}^{-X_{II}} \frac{\lambda_p \dot{\varepsilon}\, \alpha_p}{r_o^2 c_g \rho_g \alpha_g} Q\, e^{\frac{\lambda_g}{\lambda_p}\frac{c_p}{c_g} R X}\, dX \tag{99}$$

and applying the same approximations for $\dot{\varepsilon}$ as before (see Eq.30)

$$\frac{\lambda_p}{\lambda_g}\left(\frac{d\theta}{dX}\right)_{I^+} = -\frac{QR}{\sqrt{\tau'_{REAC}}}\left[\sqrt{\tau'_{CH}}\, e^{-\frac{\lambda_g}{\lambda_p}\frac{c_p}{c_g} R(X_{II}-X_I)} + \frac{\left(1-e^{-\frac{\lambda_g}{\lambda_p}\frac{c_g}{c_p} R(X_{II}-X_I)}\right)}{\frac{\lambda_p}{\lambda_g}\frac{c_g}{c_p} R(X_{II}-X_I)/\sqrt{\tau'_{dif}}}\right] \tag{100}$$

where $X_{II} - X_I$ is the flame thickness which we previously called X_f. Again making the approximation that $\bar{u} \simeq (X_{II} - X_I)/t_{reac}$, we finally obtain

$$\frac{\lambda_g}{\lambda_p}\left(\frac{d\theta}{dX}\right)_{I^+} = -\frac{QR}{\sqrt{\tau'_{REAC}}}\left[\sqrt{\tau'_{CH}}\, e^{-R^2\tau'_{REAC}} + \left(1-e^{-R^2\tau'_{REAC}}\right)\frac{\sqrt{\tau'_{dif}}}{R^2\tau'_{REAC}}\right] \tag{101}$$

which represents the heat feedback from the O/F flame to the outer edge of the A/PA flame (and is analogous to Eq. 41).

We now symbolically integrate the A/PA flame as in Eqs. 27 and 99

$$\left(\frac{d\theta}{dX}\right)_{I^-} e^{-\frac{\lambda_p}{\lambda_g}\frac{c_g}{c_p} R X_I} - \left(\frac{d\theta}{dX}\right)_{s,g} = -\int_0^{-X_I} \frac{\lambda_p \dot{\varepsilon}\, \alpha_p}{r_o^2 c_g \rho_p \alpha_g} H_I\, e^{\frac{\lambda_p}{\lambda_g}\frac{c_g}{c_p} R X}\, dX \tag{102}$$

Since the A/PA reaction is a premixed flame, we approximate $\dot{\varepsilon}_I$ as a delta function (to be consistent with our handling of the O/F flame).

Thus we let

$$\rho_g \dot{\varepsilon}_I = \omega_{CH}\, \delta(X_f) \tag{103}$$

and the resultant integration gives

$$\frac{\lambda_g}{\lambda_p}\left(\frac{\partial\theta}{\partial X}\right)_{s,g} = \frac{\lambda_g}{\lambda_p}\left(\frac{d\theta}{dX}\right)_I e^{-RX_F} + H_I R e^{-RX_I} \tag{104}$$

and as before we approximate

$$R \simeq \frac{\lambda_p}{\lambda_g}\frac{c_g}{c_p}\frac{\rho_g}{\rho_p} X_I/\tau_I = X_I/\tau_I' \tag{105}$$

Or, finally

$$\frac{\lambda_g}{\lambda_p}\left(\frac{d\theta}{dX}\right)_{s,g} = \left[\frac{\lambda_g}{\lambda_p}\left(\frac{d\theta}{dX}\right)_{I^-} + H_I R\right] e^{-R^2\tau_I'} \tag{106}$$

Where the characteristic time for the first order A/PA reaction is given by[22]

$$\tau_I = \frac{K}{P} \exp\left[E_I/RT_{I,0}\left(1/T_{I\,REO} - 1\right)\right] \tag{107}$$

To complete the solution, we have two interface conditions. The first is the trivial relation between the A/PA flame and the O/F flame

$$\left(\frac{d\theta}{dX}\right)_{I^-} = \left(\frac{d\theta}{dX}\right)_{I^+} \tag{108}$$

At the solid-gas interface we have

$$\left(\frac{\partial\theta}{\partial X}\right)_{s,p} = \frac{\lambda_g}{\lambda_p}\left(d\theta/dX\right)_{s,g} - H_s R \tag{109}$$

where H_s is the endothermic heat sink associated with the decomposition of the AP and fuel binder.

For comparison with the results for the collapsed surface reaction case we now write

$$\left(\frac{d\theta}{dX}\right)_{s,p} = \left\{\phi + H_I R\right\} e^{-R^2\tau_I'} - H_s R \tag{110}$$

where

$$\phi \equiv -\frac{QR}{\sqrt{\tau_{REAC}'}}\left[\sqrt{\tau_{CH}'}\, e^{-R^2\tau_{REAC}'} + \left(1 - e^{-R^2\tau_{REAC}'}\right)\frac{\sqrt{\tau_{diff}'}}{R^2\tau_{REAC}'}\right] \tag{111}$$

Using similar notation, the results for the collapsed A/PA approximation are expressed as (see Eq. 41)

$$\left(d\theta/dX\right)_{s,p} = \phi + HR \tag{112}$$

From the definitions of H_I and H_s we see that $H = H_I - H_s$ so that in the limit as τ_I' goes to zero, the distended A/PA model approaches the collapsed model (as it should).

This expression implies that as the surface reaction begins to distend it not only decreases the "effective" surface heat release where

$$H_{eff} \equiv H_I \, e^{-R^2 \tau_I'} - H_s \tag{113}$$

but it also acts as a barrier between the O/F flame and the solid surface so that less heat is fed back from the O/F flame as well.

H. Qualitative Discussion of the Effect of the Distended A/PA Flame on Extinction

Before discussing the effect of the distended surface reaction we must carefully specify the situation which we are considering. Two distinct cases can be noted. In Case I, we will analyze a given set of steady-state P-R burning rate data in either of two ways; with a distended or a collapsed surface heat release. In Case II, we will compare a fictitious propellant whose surface heat release is completely collapsed with a propellant which has a distended ammonia/perchloric acid (A/PA) flame such that the steady state burning rate characteristics of the two propellants differ because of (and only because of) the differences in the surface heat releases.

In Case I, where we consider two different methods for analyzing the same propellant, the amount of heat which is conducted into the solid during a steady state must necessarily be the same in both analyses. As usual, this heat comes from two sources, the oxidizer/fuel (O/F) flame and the surface heat release. In the collapsed A/PA flame analysis, all the surface heat release goes into the solid, whereas in the distended A/PA flame analysis, only part is conducted back into the solid. Thus, in the distended reaction case, the O/F flame has to feed <u>more</u> heat back into the solid and it must conduct it through the "insulating" layer of the distended A/PA flame. As a consequence the GDF theory predicts the O/F flame will be thinner in the distended A/PA flame analysis than in the collapsed analysis. This shows up in terms of different values for the burning rate constants, A and B, for the two analyses. The term which includes the effects of the distended surface reaction is the exponential, $e^{-R^2 \tau_I'}$ (see Eq. 110). During a transient, the instantaneous burning rate drops below the corresponding steady state burning rate while the characteristic time increases over its steady state value. The overall effect is that this exponential is closer to unity during a transient than during steady state (i.e., the A/PA flame is more distended in a steady state than in a transient). Thus for the distended A/PA flame analysis, the transient effectively compresses the distended A/PA zone from its steady state

thickness and brings a thin (relatively) O/F flame closer to the surface. For the collapsed model no such compression is possible. Meanwhile changes in the O/F flame from steady state to transient are about comparable for the two analyses so that because of the "compression" of the A/PA region during a transient, the distended A/PA flame model predicts that a given propellant is more difficult to extinguish than does the collapsed surface heat release model.

In Case II, where two different propellants (which are distinguished by different steady state burning rate characteristics) are considered, the opposite conclusion is reached. Since we visualize the same O/F flame for these two fictitious propellants, the burning rate constants, A and B, are the same for the distended as for the collapsed reaction. (But the amount of heat conducted into the solid is different for the two propellants.) In this comparison, the distended surface reaction acts only as an "insulator" between the O/F flame and the solid so that the propellant with the distended A/PA flame is easier to extinguish.

SECTION V

EXPERIMENTAL RESULTS FOR COMPOSITE PROPELLANTS

An extensive experimental program has been undertaken to determine the extinction characteristics of several propellant formulations. The results of these experimental tests are presented in this section. Comparison of the theoretical extinction predictions with these experimental results is deferred until Section VI.

A. General Description of the Experiment

Experimental tests of the extinction characteristics of various solid propellant formulations were conducted by using the combustor which is shown schematically in figure 4. The combustor consists of a cylindrical section which is open on both ends. A blank plate is bolted to one face of the cylindrical section to form the bottom of the combustor and to support the propellant sample. The other end of the combustor is enclosed by a copper plate which contains the primary (large) nozzle. A double diaphragm mechanism similar to ones used in shock tubes is then placed on top of the copper nozzle and is used to obtain the desired pressure decrease. As indicated by the schematic, the combustor has been carefully designed so as to minimize erosive burning effects and to cause the propellant to burn in a one-dimensional manner and hence to be as similar as possible to the one-dimensional theoretical model. Visual inspection of many extinguished propellant samples has verified that the burning surface is remarkably level and smooth. A photograph of the assembled combustor is shown in figure 5.

The propellant samples were cast into circular steel cups which were either of two heights; 3/8 inch or 5/8 inch. The sides of the cups served as inhibitors for the edges of the propellant and insured that combustion occurred only on the end surface of the propellant sample. The cups filled the entire cross-section of the combustor which is nominally two inches in diameter.

In conducting the experiment, the propellant sample is placed in the bottom of the combustor as indicated in figure 4. Two burst diaphragms are positioned as shown, and the cavity between them is pressurized. The propellant is then ignited by means of a bag of propellant shavings and a hot wire. The exhaust gases initially pass through both the primary (large) nozzle and the secondary (small) nozzle which is situated in the side wall of the double diaphragm apparatus (see figure 4). Because of its much smaller size, the secondary nozzle controls both the flow and the chamber pressure so long as the diaphragms remain in place. The primary (large) nozzle does not affect the flow until after the diaphragms are removed. The diaphragms are chosen so that they are strong enough to withstand the differential in pressure between the combustion chamber and the pre-pressurized cavity, but not strong enough

to withstand the differential between the chamber pressure and atmospheric pressure. Consequently when the propellant has reached the desired steady state operating pressure (which is determined by the size of the small nozzle) the pressurized space between the two diaphragms is vented so that the chamber pressure causes both diaphragms to shear cleanly at the wall. The exhaust gases are then restricted only by the primary nozzle and the chamber pressure drops rapidly. Both the initial pressure level and the depressurization rate can be varied by choosing nozzles of different diameters. The available sizes for the large nozzles ranged between .138 inches and 2.0 inches in diameter. The smaller nozzles ranged between .063 inches and .116 inches in diameter.

Sheet aluminum of four different thicknesses ranging between .020" and .040" was used for the burst diaphragms. In order to protect the diaphragms from the hot exhaust gases, the exposed surface of the lower diaphragm was coated with a thin layer of silicone rubber. This provided adequate thermal insulation for the duration of a test run and prevented the diaphragms from bursting prematurely due to heating effects.

The instantaneous chamber pressure was measured by a pressure transducer which was mounted flush in the wall (except for a 1/16 inch protective coating of silicone rubber). A PT76 Model Dynisco transducer was used. This transducer has a response time of better than 0.1 millisecond, and is more than adequate for the depressurizations of interest. In addition to the pressure measurement, the flame radiation (in the visible region) was monitored by a photomultiplier tube. Extinction was determined to have occurred when (or if) the photomultiplier output went to zero. The transducer output and the photomultiplier signal were recorded on an oscillograph at a chart speed of 120 inches per second. The more rapid depressurization were also recorded simultaneously on a sensitive tape recorder which has a frequency response which is flat to 20 Kc. These tape recordings were later played back at a reduced speed and re-recorded on the oscillograph. This allowed better time resolution of the fast depressurizations.

B. Experimental Depressurization Results For Composite Propellants

The experimental results which have been obtained with this apparatus are presented in figures 6 through 24. For economy of space and for ease of comparison, the corresponding theoretical results are also shown in these figures, but these theoretical predictions will be discussed separately in a later section. All the results in these figures are given in terms of the initial chamber pressure prior to depressurization, and the initial rate of depressurization, $(dp/dt)_o$. The initial value of the depressurization rate is <u>not</u> a unique variable for determining when extinction occurs <u>unless</u> the initial rate, by inference, specifies the entire p-t curve. For example, if the curve were exponential, then specifying the initial depressurization rate (and the initial pressure) would completely

specify the entire depressurization curve. Similarly for a combustor of given geometry, the initial depressurization rate will also specify the entire depressurization curve. Such is the case for the data in figures 6 through 24. However, for combustors of different geometries, the same initial $(dp/dt)_o$ will in general correspond to different depressurization curves as discussed in Section V-B-e, entitled "Effect of Combustor Geometry".

All the experimental extinction data which are presented in this thesis were obtained by venting to atmospheric pressure. Because of this, nearly all the "extinctions" were followed by re-ignition. As indicated previously, extinction was said to have occurred when the flame radiation went to zero. However in almost all cases, the re-ignition and burnout which followed these "transient" extinctions could also be verified audibly. This audible verification proved to be a useful check for determining extinguishments and was used in conjunction with the cessation of flame radiation.

The time interval between extinction and re-ignition was generally on the order of one to five seconds. Permanent extinction did occasionally occur and although no trends were apparent as to when the extinction remained permanent, it was generally possible to achieve permanent extinction by going to very high depressurization rates. It should be noted that the extinction data which were reported by Jensen (4,5) were also obtained by venting to atmospheric pressure, but he chose to present the boundary for permanent extinction. Still, most of the data in this thesis are in qualitative agreement with his in terms of the effects of different propellant formulations.

Experimental results are presented for the following series of variations in propellant formulation: (a) variations in propellant oxidizer (AP) loading, (b) variations in oxidizer (AP) particle size, (c) different fuel binder types and (d) addition of varying amounts of aluminum powder. For each propellant formulation, the experimental data is presented in terms of go/no-go extinction testing. Experimental runs which did not extinguish but which merely resumed burning at some lower steady state pressure are indicated by darkened circles (see figure 6). Experimental runs which extinguished and either remained permanently extinguished or re-ignited are denoted by open circles. An "extinction boundary" is drawn between these experimental extinction and non-extinction points for each propellant formulation. Following these detailed results, a composite curve showing the extinction boundaries for each propellant in the current series of propellant formulation variations is given.

a. Effect of Changes in Oxidizer Loading

The effect of oxidizer loading on the extinction characteristics of a solid propellant was determined experimentally

for four different oxidizer loadings, 75%, 77.5%, 80.0% and 82.5%. A 70%/30% bimodal mixture of 180μ and 45μ particle size ammonium perchlorate was used. The fuel binder was PBAA. The detailed experimental results for each oxidizer concentration are shown in figures 6 through 9. These results, as well as all the other experimental results, showed that the extinction region could be separated from the non-extinction region by a straight line boundary (in terms of initial pressure-initial dp/dt coordinates). The boundaries which were determined from figures 6 through 9 are shown together on figure 10 for comparison. This comparison shows that as the oxidizer loading is increased, the propellant becomes more difficult to extinguish. Increasing the oxidizer loading from 75% to 82.5% makes the propellant more than twice as difficult to extinguish (in terms of the initial dp/dt). These results are supported qualitatively by experimental results obtained by both Jensen (4) and Ciepluch (2), who also showed that increasing the oxidizer loading makes a propellant more difficult to extinguish.

b. Effect of Changes in Oxidizer Particle Size

The second series of propellant variations deals with the effect of changes in the oxidizer particle size. Three different propellants, each having the same 75%/25% oxidizer - to - fuel ratio, were tested. Unimodal ammonium perchlorate particles which had average particle diameters of 45μ, 80μ and 180μ respectively were used in the three propellants. The detailed experimental results are shown in figures 11 through 13. A composite curve showing the three experimentally determined extinction boundaries is given in figure 14. From these results, we see that propellants having smaller AP particle sizes are more difficult to extinguish (although for depressurizations which start at relatively low pressures - below about 300 psia - the opposite effect may be noticed due to the fact that the boundaries cross). As in the case of the oxidizer variation, the extinction boundary for the two extremes in particle size variation differs by more than a factor of two at high pressures. Although the effect of particle size is quite distinct in these figures, Jensen (4) has shown a somewhat different effect. His results for propellants with different oxidizer particle sizes again cross at about 300 psia, but above 300 psia, the larger particle size propellant is the more difficult to extinguish. However, several variables were different between his experiment and ours: First, as mentioned above, his results include the effects of re-ignition. Second, his results are for comparisons between larger particle sizes than ours--200μ and 400μ -- and he was using bimodal particle size distributions (small size being held constant in both size and quantity). Finally he used a different fuel binder. Ciepuch also indicated that propellants having smaller particle sizes were easier to extinguish, however, he was testing an aluminized propellant. Thus the effect of changes in particle size does not seem to always be the same. No specific reason can be given for these differences.

c. Effect of Different Fuel Binders

Three different fuel binders were used to determine the effect of fuel binder type on extinction. For each of the three binders, the oxidizer loading was 80% by weight. The results for the PBAA propellant are shown in figure 7 which was discussed previously. The detailed experimental results for the PBCT binder are given in figure 15; those for the PU binder are given in figure 16. Figure 17 gives the composite results for all three binder systems. In general there is little difference between the extinction boundaries for the three different fuels. They are all within a 20% spread at all pressure levels. At high initial chamber pressures (around 1000 psia), the PBAA propellant is the most difficult to extinguish while the PBCT is least difficult to extinguish. At low chamber pressures (around 200 psia), the extinction boundaries cross so that the PBAA and the PBCT propellants have similar extinction characteristics whereas the PU propellant is slightly easier to extinguish. Ciepluch (2) made a similar comparison of PBAA and PU binders at one initial chamber pressure, 500 psia. His results, like ours, showed that the two binders were similar in their extinction characteristics (but again his results were for aluminized propellants). Jensen (4) did not test a PBAA propellant, but he obtained results which showed that a PBCT propellant was nearly twice as hard to extinguish as PU. The probable explanation for Jensen's results is again that he considered permanent extinctions. For example, while obtaining the experimental results reported herein, it was noted that reignition was not nearly so prominent in PU propellants as it is in PBAA propellants. Thus it appears that we would also have shown a large difference between PU and PBCT propellant had we determined the boundary for permanent extinction. However this difference in "extinction" characteristics merely reflects the fact that polyurethane propellants are more difficult to ignite (and hence difficult to re-ignite).

d. Effect of Addition of Aluminum Powder

Varying amounts of aluminum powder were added to one propellant formulation to determine the effects of aluminum on the propellant's extinction characteristics. Three different aluminum concentrations were used; 0%, 7.5% and 15%. The propellant oxidizer-to-fuel binder ratio was held constant at 77.5/22.5 for all three aluminum loadings. This particular ratio was picked because it has sufficient binder to provide a castable propellant even at the 15% aluminum level (the highest solids loading). The aluminum powder particles were about 16μ in diameter. Results for the 7.5% and the 15% aluminum loadings are presented in figures 18 and 19 respectively. The 0% aluminum case is presented in figure 8, and was discussed previously. The composite curve for aluminum addition, which is shown on figure 20 indicates that, in general, the addition of aluminum (at constant oxidizer-to-fuel binder ratio) makes the propellant more difficult to extinguish. However the effect is quite small; an increase from 0% to 15% in aluminum concentration only raises the extinction boundary by some 15%. Here again the story is somewhat different at lower pressures. For initial chamber pressures

below about 400 psia the addition of aluminum tends to make the propellant easier to extinguish.

One propellant formulation which contained 15% of a coarser aluminum powder (120 μ versus 16 μ) was also tested. The detailed experimental results are shown in figure 21. Figure 22 compares the differences between the extinction boundaries of a propellant having 15% coarse (120 μ) aluminum, 15% fine (16 μ) aluminum and 0% aluminum. As can be seen, the effect of the change in the aluminum particle size proved to be larger than the effect of changing the aluminum content from 0% to 15%. The propellant with the coarse aluminum was easier to extinguish than the propellant with the fine aluminum, but it was also easier to extinguish than the unaluminized propellant. (In actual practice, aluminum particle sizes which are larger than 40 μ are seldom used in solid propellants.) It is hypothesized that the coarse particles were so large that they could not melt before they were ejected into the gas phase. Hence their effect on the surface heat release term (which is discussed in the next section) is less than for small aluminum particles and this effect probably explains the difference between the two different aluminum particle sizes.

e. Effect of Combustor Geometry

Finally, experimental results have been obtained which indicate the effects of chamber geometry on extinguishment. The effects of chamber geometry were determined by inserting a spacer in the experimental combustor. This new combustor had the same surface burning area and the same cross-sectional area as the original, but it had a larger volume due to its increased length. The ratio of the lengths (and the volumes) of the two combustors was about three to one. The detailed experimental results for the larger combustor are shown in figure 23. The propellant which was used for this testing was composed of 75% AP and 25% PBAA. The AP was unimodal with an average particle size of 180 μ. The results of testing this propellant in the regular chamber were discussed previously and are shown in figure 13. A comparison of the results which were obtained with the two different chambers is shown in figure 24. Since the same propellant was used in both chambers, the extinction boundaries obtained with the two chambers should coincide (i.e. the extinction boundary should depend only on the propellant formulation). However they differ by a factor of two. Clearly, then, the initial rate of depressurization is not an adequate method for correlating extinctions which are obtained with combustors having different geometries. In other words, as the combustor geometry is changed, the critical L^* (based on the final throat area) which is required to just extinguish the propellant, also changes. It might appear that the critical L^* for a given propellant formulation would be the same no matter what the combustor geometry. For example, in the case of a simple "blowdown" process with constant temperature and with no mass inflow, chambers of different shapes and sizes would all have identical p-t curves so long as they all had the same

value of L^*. Thus one might expect that as the chamber length is increased, the critical throat area (which would just extinguish combustion) would increase proportionately, i.e., that extinguishment of a given propellant would depend only on the intial pressure and the chamber L^*. However, our experiments have shown this to be untrue; when the combustor length was increased by a factor of 3, the critical throat area (for extinction) increased by only a factor of about 1.2, not by a factor of 3. The reason for this is that the shape of the depressurization curves of the two combustors is not alike; two separate phenomena combine to change the shape of the p-t curve. First is the effect of the final pressure. If both chambers had the same L^*, the smaller combustor would have a higher final chamber pressure than the larger (if the propellant continued to burn) by virtue of its smaller nozzle. Hence, because of the higher final pressure, the smaller chamber would be more difficult to extinguish. Second is the mass inflow effect due to continued combustion during the depressurization. This effect is negligible during the initial part of the p-t curve, but at the low pressure end, the inflow and the outflow must become equal (if the propellant continues to burn). For the same L^*, the smaller chamber has a proportionately smaller mass outflow but about the same inflow. Therefore on a percentage basis, the smaller chamber has a larger mass inflow effect and so, for the same initial depressurization rate, the lower end of the p-t curve from the small chamber has a gentler slope. This can be seen by comparing a chamber with no mass inflow (i.e. a pure "blow-down" process) with a chamber which has finite mass inflow during the depressurization. Clearly the chamber with finite mass inflow would require a longer time to empty and its p-t curve would have a gentler slope -- especially at the low pressure end of the depressurization. In terms of extinguishment, this inflow process would require a larger initial dp/dt to extinguish the smaller chamber. Thus both of these effects show that the smaller chamber is more difficult to extinguish in terms of the initial dp/dt.

C. Steady State Burning Rates of Propellants

The pressure dependence of the steady state burning rates of each of the propellant formulations which were used in the depressurization experiments were measured in a strand burner. The apparatus and procedure is discussed in detail in reference 39. The measurement consists of burning a 5 x ¼ x ¼ inch strand of propellant in an inert N_2 atmosphere. The nitrogen serves both as a means of pressurizing the strand burner and as a purge to remove the exhaust products. Six wires are threaded through the propellant strand at ½ inch intervals along its length. As the strand burns, these wires are broken in sequence. An electrical impulse is used to determine when each wire breaks. This impulse is recorded on an oscillograph. The burning rate is then determined by averaging the time required to break each of the wires. Each strand of propellant was leached in water, dried, and then coated with a thin layer of butyrate dope in order to

inhibit combustion on the sides of the strand.

For each propellant formulation, the steady state burning rate was measured at each of twelve different pressure levels. These pressures were chosen to be about equally spaced, in a logarithmic sense, between ambient pressure and 1000 psia. The results of these steady state measurements are presented in figures 25 through 28 on log-log coordinates. These figures show the dependence of the burning rate on the pressure (log P versus log R). $P^{2/3}$ versus P/R plots of the same data are also shown on figures 29 through 38. The coordinates of this latter set of curves are taken from the regular granular diffusion flame theory in which the burning rate of a solid propellant is given by (40)

$$1/r = a/p + b/p^{1/3} \quad \text{or} \quad p/r = a + bp^{2/3}$$

where a and b are constants to be determined from the steady state burning rate data. In nondimensional form this relation becomes

$$\frac{P}{R} = \left(a r_0/p_0\right) + \left(b r_0/p_0^{1/3}\right) P^{2/3}$$

so that according to this equation the steady state burning rate of a solid propellant would be given by a straight line in P/R - $P^{2/3}$ coordinates. The two terms "a" and "b" are not actually constants but really depend on the flame temperature and the surface temperature, both of which vary so slowly with pressure that they are normally assumed constant for steady state work. However, we must include variations in flame temperature and surface temperature because they become very important during a transient. In addition, because of our interest in the transient, we are forced to use a different approximation in the integration of the gas phase flame. For these two reasons, our theoretical predictions of the steady state burning rate will not be exactly linear when presented in the $P^{2/3}$-P/R coordinates. However the results will be nearly linear, and to emphasize the similarity between this approach and the regular GDF theory approach, we have chosen to present all our data in terms of $P^{2/3}$-P/R.

The steady state burning rate data was fit to the burning rate equation by determining the "best" values of the constants A and B. The fitting was done by a least-squares method on the computer as described previously in Section IV-C.

A tabulation of the A's and B's for each propellant formulation is given in Table I. This table also includes the burning rate at 1000 psia, and the pressure index, n, in the burning rate relation, $r=ap^n$, at 1000 psia. The $P^{2/3}$-P/R burning rate curves given in figures 29-38 show both the data points and the computer curve fits. The burning rates of several of the propellant formulations are not exactly described by the GDF theory. (A thorough discussion of the region of validity of the GDF theory

is given in reference 39.) Precise values of the burning rate constants, A and B, are difficult to determine for such propellants which don't fit the GDF theory precisely. This is especially true for the constant, A, the constant in the chemical reaction term. There is no problem in obtaining precise values for the constants, A and B, for those propellants whose burning rates follow the GDF theory quite closely.

One propellant formulation, the polyurethane, differed grossly from the GDF theory. It exhibited a negative pressure exponent of burning in the region above 500 psia. Because of this, no meaningful values could be obtained for the constants, A and B, for the PU propellant. Hence, in the following section on theoretical results, no predictions are given for the PU propellant.

SECTION VI

THEORETICAL PREDICTIONS FOR COMPOSITE PROPELLANTS

Various computer solutions to the combustion model have been obtained and are presented in this section. Two different types of depressurization p-t curves have been used to obtain these solutions. One is an exponential decay which was chosen for convenience in theoretical work and for easy comparison with the results of other theories. The second is the actual experimental pressure-time curves. Using the exponential pressure decays, and correlating the results in terms of the initial time derivative of the pressure, the model predicts the correct qualitative behavior for responses to changes in oxidizer loading, AP particle size, propellant flame temperature, etc. However, since the experimental p-t curves are not exactly exponential, the theoretical results based on exponential pressure decays cannot be expected to give precise quantitative predictions. It is for this reason that the experimental pressure-time traces have been used.

A. Numerical Values for the Parameters in the Theoretical Model

In order to make qualitative theoretical predictions, it is necessary to specify definite numerical values for the various physical parameters. The sources for these constants and the methods used for determining them are given in this subsection.

The ambient temperature was taken to be 300°K for all our theoretical work.

An approximate value of 16 Kcal/mole was used for the surface activation energy. This value is based on measurements reported by Schultz and Decker[46] and Coates[47]. See also the extensive reviews of references 22 and 35 .

Surface temperatures which are around 850-950°K have been reported for steady state burning of solid propellants at low pressures (below 10-20 atmospheres[39,48,49]. For our calculations, we arbitrarily chose the steady state surface temperature of 80%/20%, AP/PBAA propellant to be 1000°K at 1000 psia. Then, using the measured steady state burning rate of this propellant (at 1000 psia), we calculated the magnitude of the pre-exponential factor, a', from the dimensional form of the pyrolysis relation, $r = a' \exp(-E/RT_s)$. This value for the pre-exponential factor, a', was then used along with the 16 Kcal/mol activation energy (see above) to define the absolute value of the surface temperature, T_s, for <u>all</u> propellant formulations as a function of their burning rates.

To facilitate the actual detection of extinction by the computer, an "extinction" temperature (analogous to an ignition temperature) of 600°K was specified. It was assumed that all decomposition ceased at this temperature. Tests of the combustion model have shown that the actual magnitude which is chosen for the extinction temperature has a negligible effect on the predicted extinction boundary so long as the cutoff is less than about 650 or 700°K. This insensitivity justifies the use of an "extinction" temperature (see also the discussion in Section III).

The numerical values for the surface heat release were determined by mass weighting an assigned exothermic heat release of 250 cal/gm for AP along with an endothermic heat of decomposition of 225 cal/gm for the fuel binder. These are considered to be nominal values and are taken from the review which Steinz has presented[39]. Because of a lack of data, the latent heat of the fuel binder was considered to be the same for all binder systems which were tested. In the case of aluminized propellants, the heat of fusion of aluminum, 68 cal/gm endothermic[50], was also included in the calculation of the surface heat release term so long as the surface temperature was above the temperature at which aluminum melts.

Because of a similar lack of data, the thermal diffusivity of the solid phase was taken to be the same for all propellant formulations except the aluminized propellant. The ratio between the thermal diffusivity of aluminized propellants and unaluminized propellants was obtained from measurements in our laboratory as discussed in Appendix III. These results showed that a 15% aluminum content increases the thermal diffusivity by about 35% (with respect to a non-aluminized propellant). A value of .00030 in^2/sec for the thermal diffusivity of an unaluminized propellant was used. This typical value was taken from Barrere[21].

For each propellant, the non-dimensional heat release, Q, in the oxidizer/fuel flame was determined from the calculated adiabatic flame temperatures (see Appendix II) and the surface heat release. The variation in the adiabatic flame temperature with pressure was included in the theoretical calculations by specifying the heat release Q to be a function of the instantaneous pressure. In general, the heat release should also depend on the flame temperature during a transient, but this effect was neglected (see discussion in the next paragraph).

Within our quasi-steady approximation, the change in the heat release, Q, with changes in the flame temperature (from its steady state value) is readily calculable. We can visualize the quasi-steady transient as a non-adiabatic condition in which the non-adiabaticity is given by the difference between the transient and the steady state heat feedback from the gas phase. Thus as the flame temperature changes from its steady state value, corresponding changes in the chemical equilibrium

constants (K_p's) for the various reactions will also occur as in a non-adiabatic flame. As a consequence, the heat release depends on the flame temperature. Although these changes might be as important as the effect of pressure on the heat release, they were, because of their complexity, ignored as mentioned above.

B. Theoretical Predictions Based on Experimental Pressure-Time Curves

The comparisons between the theoretical predictions of the model which was developed in Section III and the experimental results which were presented in Section IV are given in figures 6 through 20. These predictions are all based on the experimental pressure-time curves. To make the comparison between theory and experiment as concise as possible, the figures which show individual data points have been drawn with open circles representing those cases which extinguished experimentally and darkened circles representing cases which did not extinguish experimentally. For a particular depressurization curve for which the theoretical prediction agreed with the experimental result, no other notation is made. Depressurization curves for which the theoretical predictions disagree with the experimental results are denoted by flags. Thus, an unflagged point represents agreement between theory and experiment, while a flagged point indicates disagreement. A few of the depressurization curves whose $(dp/dt)_o$-P coordinates are far removed from the theoretical extinction boundary were not actually run on the computer; it was only inferred that they would behave as indicated on the figures. It must be emphasized that the only depressurization curves whose outcomes were not predicted theoretically were those points which were sufficiently far from the boundary that their final result was not in doubt. As indicated on the curves, the theoretical extinction boundaries were generally quite distinct so that such omissions are justifiable.

A typical experimental pressure-time curve is shown on figure 58, on semi-logarithmic coordinates. Note that an exponential p-t curve would be a straight line in this coordinate system, so that, consequently, this figure shows how far the experimental curve differs from an exponential curve. A single experimental curve has been plotted in three ways (namely, absolute pressure, gage pressure, and as initial pressure minus final pressure), but none of the three curves are exponential in form (i.e., none are straight lines).

a. Effect of Oxidizer Loading

The detailed theoretical predictions of the effect of oxidizer loading variations on the extinction characteristics of a propellant are shown on figures 6 through 9. The composite of the experimentally and theoretically determined extinction boundaries for all the propellant oxidizer variations is given

in figure 10. All these figures show excellent agreement between the theoretical predictions and the experimental results.

Changes in the propellant AP loading were accounted for in the theoretical model by three major parameters. First, changes in the structure of the gas phase flame were taken into account by changes in the burning rate constants, A and B, of the GDF theory. Second, the magnitude of the surface heat release, H, was changed in accordance with the AP content of the propellant in the manner which was previously prescribed. Third, the gas phase heat release, Q, was varied with the oxidizer loading according to the calculated adiabatic flame temperatures.

b. Effect of Oxidizer Particle Size

The comparisons between theory and experiment for the AP particle size variations is given in figures 11 and 13. As in the case of the oxidizer variations, changes in the flame structure due to AP particle size changes are taken into account theoretically by the GDF description of the flame. However, since only the oxidizer particle size was changed, and not the oxidizer loading, the value of the surface heat release remained constant. Similarly the adiabatic flame temperature remained unchanged because the chemical composition of the propellants was the same. Again the predicted extinction boundaries are quite close to the experimental boundaries.

c. Effect of Fuel Binder Type

The comparisons between theory and experiment for the different fuel binder types are given in figures 7,15, and 17. The predictions for the PBCT propellant (figure 15) are again relatively good (the maximum error is 20%), but these results are not as close as some of the other predictions. The primary reason for the error in the predicted extinction boundary for the PBCT propellant is that the steady state burning rate of this propellant is not described exactly by the GDF theory. The region of validity of the GDF theory has been thoroughly explored by Steinz, Stang and Summerfield[38]. Their results show that the solid propellants which are used for most practical applications fall into the region where the GDF theory is valid. However, in an experimental study of the effects of propellant parameters, propellants which are easy to process and to cast must be used. Hence it is not always possible to use propellants which follow the GDF burning rate law.

Even if a given propellant deviates slightly from the GDF theory (such as the PBCT propellant), it is still possible to determine values for the burning rate constants, A and B. However, in such cases the steady state burning rate data form a line which is not quite linear in $P^{2/3}$-P/R coordinates and it becomes difficult to determine precise values for A and B. The

value of A, the constant in the chemical reaction term, is especially difficult to define precisely in such a situation. For example, visual inspection of the steady state burning rate data for the PBCT propellant (Fig. 36) shows that the fitted curve could be moved slightly and still (visually) fit the data as well as the computer fit. Small changes in the lower end of this curve can cause fairly significant changes in the burning rate constant A. This situation could be improved somewhat by measuring burning rates at subatmospheric pressures (but there the distended surface reaction starts to become important). A check of the other steady state burning rate curves shows that some of them also did not fit the GDF theory exactly. This is particularly true of the particle size variations. Nevertheless the extinction results turned out somewhat better in these cases than for the PBCT. The highly oxidized PBAA propellants are closely described by the GDF theory so that the determination of the burning rate constants, A and B, was quite precise for these propellants.

The propellant which contained the third type of fuel binder, polyurethane, deviated drastically from the GDF theory. The burning rate of this PU propellant exhibited a negative pressure exponent of burning in the region above 500 psia. Because of this, no meaningful values could be obtained for the burning rate constants. Consequently no theoretical predictions have been made for the PU propellant. The negative pressure exponent of burning is caused by the phenomenon of intermittent burning as discussed by Steinz [39]. To the author's knowledge, no steady state theory exists which can properly describe this phenomenon. However, if such a steady state theory becomes available, it could in principle be inserted into the present depressurization model in place of the GDF theory, and predictions could be obtained for the PU propellant.

d. Effect of Addition of Aluminum Powder

In our description of the non-steady burning process in an aluminized propellant, three separate factors were used to account for the presence of aluminum in the propellant. First, the addition of aluminum increases the thermal diffusivity of the solid (as described earlier). Second, the aluminum changes the magnitude of the surface heat release, and third, the addition of aluminum changes the structure of the gas phase flame so as to require a modification in the treatment of the gas phase heat release.

In considering the effect of aluminum on the surface heat release, we first of all note that there is no reason to suspect that the aluminum alters the actual chemical decomposition process of either the oxidizer or the fuel binder in any direct manner. The aluminum can, however, produce indirect effects. For example, if the aluminum melts while it is still inside solid phase of the propellant, its heat of fusion can serve as an important heat sink

inside the solid phase, and can lower the effective surface heat release. On the other hand, if the aluminum does not melt while it is inside the solid phase, it will not affect the magnitude of the surface heat release. Accordingly, we distinguish two separate cases as determined by the instantaneous temperature of the surface of the solid propellant.

We first consider the case where the surface temperature of the propellant is above the melting point of aluminum. Then, appealing to an equilibrium argument, we require that the aluminum must melt before the oxidizer and fuel binder decompose. We approximate this melting by a heat sink which is concentrated right at the surface of the propellant. Its magnitude is given by the heat of fusion of aluminum (as suggested above). Thus, when the surface temperature of the propellant is above the melting point of aluminum, the aluminum serves to decrease the surface heat release.

The second case occurs when the surface temperature of the propellant drops below the melting point of aluminum. In this case, the decomposition of the oxidizer and the fuel binder can proceed before the aluminum melts. In fact, the aluminum can not possibly melt until it reaches a region in the combustion zone where the local temperature is above its melting point. Thus, when the surface temperature of the propellant is below the melting temperature of the aluminum, the oxidizer and fuel binder decompose around an inert (solid phase) metal. Consequently the aluminum has no effect on the surface heat release (save for the amount of AP and fuel binder it displaces). In this case, we assume the aluminum receives its heat of fusion directly from the gas phase (in some distributed manner).

Thus in our theoretical model, the surface heat release of an aluminized propellant is discontinuous in the manner indicated above. This is obviously an oversimplification. Such an abrupt change certainly does not occur. However since the melting point of aluminum is 932°K[50], and since the propellant surface temperature ranges between about 1000°K down to about 600°K (our extinction temperature), both of these extremes in the behavior of aluminum will probably be encountered. Our calculations predict that, during steady state burning conditions, the surface temperature of the propellant will remain above the melting point of aluminum almost all the way down to atmospheric pressure. This indicates that the aluminum on the surface will be molten during most steady state burning conditions, as has been frequently observed experimentally.

Our modified treatment of the gas phase flame of an aluminized propellant is based on the physical observation that the aluminum burns relatively far from the propellant surface (essentially downstream of the O/F flame). In addition, our steady

state burning rate curves show that the burning rate of a propellant is almost completely unaffected by the addition of aluminum, provided the propellant oxidizer to fuel binder ratio is left unchanged when the aluminum is added. Thus, both of these observations indicate that the aluminum burns so far from the surface that the combustion of the aluminum does not constitute an important driving mechanism for the combustion process. Consequently we view the combustion of the aluminum as a sort of "afterburning" process which doesn't affect the propagation of the combustion zone. In view of this, we set the "effective" heat release in the gas phase flame of an aluminized propellant equal to the heat release in the gas phase flame of a non-aluminized propellant (which has the same oxidizer and fuel binder concentrations). We ignore the added heat release due to the combustion of the aluminum and merely treat the aluminum as an inert in the O/F flame. This gives an "effective" flame temperature which is slightly lower than the flame temperature for the corresponding unaluminized propellant (by an amount equal to the heat of fusion of the aluminum plus the energy needed to raise the temperature of aluminum to that of the gaseous combustion products).

It is well known that the addition of aluminum to a propellant will generally eliminate high pressure instability. Summerfield and Krier[81] have attributed this stabilizing effect to a change in the surface heat release term (similar to the one discussed above) and to a "thermal inertia" effect caused by the globules of molten aluminum on the surface. They have shown that this thermal inertia effect is very important in an instability analysis, however, for the depressurization case, the thermal inertia effect becomes quite small. The reason for this is that the characteristic time associated with the depressurization process is longer than the characteristic time associated with the frequencies at which instabilities occur. For this reason, the thermal inertia effect has not been included in this analysis. If it were included, its effect would be to raise the extinction boundary (make the propellant harder to extinguish) by less than about 5%.

The comparison between theory and experiment for a propellant which contains 15% aluminum is shown on figure 19. As can be seen, the theoretical predictions once again show good agreement with the experimental results. It should, however, be noted that it would perhaps be more realistic to disregard any heating of the molten aluminum droplets by the hot, reacting gases in the flame zone. Such a calculation would raise the effective flame temperature by about 100°K. This increased flame temperature would then raise the extinction boundary by an estimated 15-20%. This would then give predicted results which were within about 25-30% of the experimental results, the predictions indicating that an aluminized propellant is more difficult to extinguish than is actually the case.

C. Sensitivity of the Theoretical Predictions to the Depressurization Curve

The preceding subsection has shown that the theoretical predictions are, generally speaking, in excellent agreement with the experimental results. As a further check of the model, we have taken several runs which were near the theoretical (and experimental) extinction boundary and changed the time scale of their p-t curves to determine the sensitivity of the theoretical results to the p-t curve. Such a sensitivity check was also made by Horton[27] who, like us, used experimental p-t curves for his theoretical predictions.

Horton's experimental results were less extensive than ours in terms of the number of experimental data points taken with each propellant formulation. Consequently he was unable to determine extinction boundaries as a function of pressure as we have done. Thus Horton had to evaluate the accuracy of his theoretical predictions on the basis of a purely statistical tabulation. That is to say, each experimental run gave him a "no" (the propellant did not extinguish) or "yes" (the propellant did extinguish) result. Similarly, his theoretical model gave either a "yes" or "no" prediction corresponding to each experimental pressure-time curve. The percent of correct predictions (i.e., theoretical and experimental results of either "yes"-"yes" or "no"-"no", respectively) was used to determine the "accuracy" of his model. Such a statistical comparison is a relatively insensitive check. For example, if all the experimental results are near the extinction boundary, a very accurate model could give poor statistical results. Similarly, by taking all the experimental points far enough away from the extinction boundary, any theory (even those based on dimensional analysis) should give good predictions in a statistical sense. (Note that the prediction that a propellant would <u>never</u> extinguish would be 50% accurate statistically if exactly half of the experimental runs extinguished.)

In an attempt to obtain further information as to the accuracy of his theoretical predictions, Horton tried changing the time scale of the p-t curves of some of the points which his theory had predicted incorrectly. He found that the time scale had to be changed by a factor of ten in some cases to obtain the correct results. This, then, gives more of an indication of the accuracy of his theoretical model than do his statistical tabulations.

By comparing experimental and theoretical extinction boundaries, we have obtained a realistic measure of the accuracy of our theoretical predictions, however a change of the time scale of the p-t curve can still give added information as to the sensitivity of our model. A total of three experimental runs were chosen for use in this sensitivity check. One of these runs had extinguished experimentally but the theoretical predictions

had indicated that it would continue to burn. The other two points had continued to burn both experimentally and theoretically. The time scales of the entire experimental p-t curves for these three points were then "speeded up" by a multiplicative factor of .80 (i.e. 20% faster) to determine if they were really as close to the extinction boundary as indicated. The 20% increase in the entire p-t curves naturally corresponded to a 20% increase in their initial depressurization rates and was sufficient to move all three points into the extinction region of the map as shown in figure 39. Using these "new" p-t curves, the theory correctly predicted that all three points which had previously continued to burn (according to the theory) would now extinguish. Inspection of other runs occurring near the extinction boundary indicated that their final outcome could similarly be changed (i.e., extinction to non-extinction, or vice-versa) by a small change in the time scales of their respective p-t curves. Thus our model proves to be quite sensitive to the speed of the p-t curve in the region near the theoretical extinction boundary.

D. Theoretical Predictions Based on Exponential Depressurizations

The results which are presented in this subsection are all based on exponential p-t curves given by the equation, $P = P_f + [(P_o - P_f)\exp(-\beta\tau)]$, where β is a non-dimensional measure of the rate of the depressurization and is analogous to $(dp/dt)_o$. Figures 40-42 show the variations of the burning rate, the flame temperature and the characteristic times, as a function of time during two exponential depressurizations. These two p-t curves differ only by the values of β which were used. The p-t curve with the larger β (i.e. the faster depressurization) led to extinction, whereas the p-t curve with the smaller β (the slower depressurization) resulted in continued combustion. The results are plotted against the product $\beta\tau$ rather than against the non-dimensional time, τ, alone. This coordinate was chosen so as to make the two curves coincide at the start. (Note, that when plotted against $\beta\tau$, the exponential p-t curves for all values of β fall on the same line.) Hence this choice allows us to compare those changes which are due only to the dynamics of the problem.

The predicted transient burning rates for the two exponential depressurizations are shown in figure 40. The corresponding steady state burning rate is also included for reference. Note that the predicted transient burning rates for both of these two depressurizations are always less than the corresponding steady state burning rate.

The predicted transient flame temperatures for these depressurizations are shown on figure 41. The steady state flame temperature, which was taken to be constant for these two runs, is also included on the curve. The results show that the predicted flame temperature drops considerably below the

the steady state value during both depressurizations. In the case which continued to burn, the flame temperature recovered and returned to its steady state level. In the extinction case, the flame temperature continued to decrease until the extinction criterion was reached.

The importance of this decrease in flame temperature is reflected in figure 42 which shows the characteristic times for chemical reaction and for diffusional mixing during an exponential depressurization which leads to extinction. Again the steady state values are given for comparison. This curve dramatically shows that the diffusional mixing term is the dominant (slowest) term at high pressure, steady state operation, but that during the transient the powerful Arrhenius term causes the chemical reaction term to become the more important characteristic in the gas phase flame. Note that because the characteristic diffusion term is nearly directly proportional to the flame temperature, diffusion actually occurs faster during the transient than during the steady state. This unexpected result occurs because we include the gas phase density in our characteristic time terms.

The sensitivity of the predicted extinction boundaries to changes in the various parameters in the theoretical model, are shown in figures 43-46. Each of these figures shows the effects of two different types of changes in one particular parameter. These two changes will be referred to as Case I, and Case II (analogous to the cases discussed in Section IV-G). In Case I, the change in the particular parameter is accompanied by changes in the burning rate constants, A and B (see equations 35 and 36), in such a manner that the change in the particular parameter does not cause a change in the steady state burning rate behavior. This corresponds to choosing two different numerical values of the particular parameter when analyzing a given propellant. In Case II, the burning rate constants were not changed when the parameter was changed, so that the end result was a shift in the steady state burning rate behavior of the "propellant" due to the change in the parameter. This case compares two separate (fictitious) propellants which differ only by this one parameter.

The effects of changes in the surface heat release, H, are shown on figure 43. The solid line represents the base case. The line which is composed of both long and short dashes corresponds to Case II (above). This curve represents the case where the change in the surface heat release causes a change in the steady state burning rate behavior of the propellant, i.e., it shows the predicted effect of changes in the surface heat release on the extinction boundary. The line which is composed of all dashes, represents the result of using two different numerical values for H in the theoretical predictions. For example, if one is uncertain of the magnitude of H by this amount, the predicted results will be uncertain by the (large) amount shown by the comparison between this

curve and the base curve. Thus, it is imperative that the surface heat release be known accurately. (A .05 uncertainty in H, corresponds to about a 10% uncertainty in the heat release given off upon decomposition of AP, or about a 30% uncertainty in the latent heat of the fuel.) However, despite the sensitive dependence of the predictions on the surface heat release, the model is capable of predicting the effect of changes in oxidizer loading quite accurately (see Section VI-B-a), even though the surface heat release varies rapidly with the percentage of oxidizer in the propellant. This indicates that the method that was used to estimate the surface heat release must be reasonably accurate (or else the model would not properly predict the effect of changes in the oxidizer content of the propellant).

Figure 44 shows the effects of a 300°K decrease in the flame temperature. Again, the solid line represents the base case, the line composed of long dashes represents Case I (above), and the line composed of both long and small dashes represents Case II. The results show that the shift in the extinction boundary due to a change in the flame temperature, that also causes a change in the steady state burning behavior (Case II), is quite large. However, the error introduced into the extinction predictions by the use of an incorrect flame temperature is quite small (in view of the fact that flame temperatures can probably be estimated to within 100°K).

Figure 45 shows that the error introduced in the computer predictions by the use of an incorrect surface activation energy is quite small, but that if the surface activation energy is somehow magically increased without affecting the other characteristics of the propellant, extinction occurs much more easily.

For our exponential depressurizations, changes in the steady state flame temperature with pressure have been ignored. For most practical propellants, this is a good approximation (see flame temperature calculations in Appendix II). Since the flame temperature is constant, the steady state burning rate is completely independent of the flame activation energy. Consequently Cases I and II are identical in this case. Figure 46 shows that if the activation energy of the flame of an actual propellant is increased, the propellant becomes much easier to extinguish. (This is because of the importance of the Arrhenius term during depressurization.) Similarly, the use of an incorrect flame activation energy in the theoretical model would strongly affect the theoretical predictions. This is especially important since the flame activation energy is so poorly known.

By way of summarizing figures 43-46, we note that uncertainties introduced into the theoretical predictions by uncertainty in the flame temperature or the surface activation

energy are quite small. However, uncertainties in the flame activation energy and surface heat release cause large uncertainties in the theoretical predictions. By testing several propellants with different surface heat releases, we have been able to increase our confidence in the values of the surface heat release which have been used. Unfortunately, no such check is available for the flame activation energy.

Figure 47 shows that a 25% change in either of the burning rate constants, A or B (see equations 35 and 36), causes a change of about the same magnitude in the extinction boundary. However, a 25% change in B, the constant in the diffusional term, corresponds to a much larger change in the steady state burning rate than does a similar change in A. An increase in B essentially corresponds to lowering the entire burning rate curve by a relatively large, constant percentage, while an increase in A corresponds to lowering the entire curve by a small, constant <u>increment</u>. At high pressures, this latter effect is not even noticeable, but at low pressures it becomes significant. Thus the value of the constant, A, in the chemical reaction term is relatively sensitive to small changes in the low pressure end of the burning rate curve. Because of its importance in determining "A", we see that the low pressure end of the steady state burning rate curve is just as important to the prediction of extinction as is the high pressure end. The converse argument also applies. The chemical kinetics affect only the low pressure end of the burning rate curve. If there is a change in the chemical kinetics, the high pressure end of the burning rate curve remains unchanged, but the extinction characteristics of the propellant can change significantly.

From a physical viewpoint, an increase in either of the constants, A or B corresponds to an increase in the respective characteristic time. Consequently when either A or B is increased, the propellant becomes easier to extinguish (because the gas phase flame moves farther away from the surface). Increasing either of the constants, A or B, corresponds to <u>decreasing</u> the steady state burning rate. Thus all other things being equal (i.e. surface heat release, flame temperature, etc.), a propellant which has a high burning rate (at all pressures) will be difficult to extinguish. This explains the limited success (and the short-comings) of the "non-dimensionalization" theories; in general, all other things are not equal so that the effect on extinction of an increase in the steady state burning rate cannot be determined without also including a complete analysis of the changes in the other propellant parameters.

Figure 48 compares the extinction boundary as a function of the initial pressure for two different final chamber pressures, 40 psia and 20 psia. The predicted extinction boundaries differ by about a factor of two for these two different final pressures. These results show that a lower final pressure favors extinction.

E. Theoretical Predictions of the Importance of the Shape Depressurization Curve

The experimental results of Section V have shown that changing the combustor geometry, and hence the shape of the p-t curves, has a significant effect on extinguishment (when expressed in terms of $(dp/dt)_o$ and p_o). To obtain further insight into this problem, an analytical study of the importance of the shape of the p-t curve on extinction was undertaken. In this study, two exponentials with different decay rates were connected together to determine which part of the p-t curve is the most sensitive indicator of the occurrence of extinction. The two exponentials were joined so that the pressure was continuous at their junction, but so that the slope of the pressure was discontinuous. The point of the junction of the two exponentials was chosen as the time at which the pressure had dropped one "e-fold" below its initial value (see figure 49). The relative rate of decay of the two exponentials was then varied and the extinction boundary was determined as a function of this ratio between the two decay constants.

Results have been obtained for two cases in which the pressure was varied between 1000 and 40 psia, and 250 and 20 psia, respectively. The results are shown in figure 50 where the abscissa represents the final decay constant, β_2, and the ordinate represents the initial decay constant, β_1. The line along which $\beta_2 = \beta_1$ is shown by a dashed curve. This special case represents the smooth, one step exponential curve which was used in the previous subsection. These results show that as the ratio between the decay rates of the two parts of the p-t curve is changed, the value of the initial derivative of the pressure which is required to just extinguish combustion varies over very wide limits. This agrees with the experimental results which showed that for combustors of different geometries (between which the shape of especially the low pressure end of the p-t curve differed), the initial pressure derivative was not a good indicator of the extinction characteristics of a propellant. For example, note that when the initial decay constant is changed by a factor of 10 (from 0.1 to 1.0), the final exponential decay constant which is required to just extinguish combustion, changes by only some 15 to 20%. This implies that the rate of depressurization at the low pressure end of the p-t curve is a much more sensitive indication of whether or not extinction will occur than is the intial rate of depressurization.

It must be understood that the point of intersection of the two exponentials is very important in determining the relative sensitivity of the two parts of the p-t curve. For instance, had we positioned the junction point after a one-and-one-half or two "e-fold" drop in the pressure, the initial exponential would have taken on more importance. Thus these predictions justify the suggestions which have been made by Von Elbe[10], Cohen[9], and others, that as an engineering

approximation, the pressure decay rate at the low pressure end is a better measure of extinction than is the intial decay rate. A corresponding physical argument is that since the actual extinction process does take place at low pressures, phenomena at low pressures are likely to be most influential ir causing extinction. Again, we caution that still the entire pressure decay curve can be important in the extinction process.

SECTION VII

EXTINGUISHMENT OF DOUBLE-BASE PROPELLANTS

In this section, we consider the extinguishment characteristics of double-base propellants. Double-base propellants are distinguished from ammonium perchlorate composite propellants in that the fuel and oxidizer are homogeneously mixed on a molecular scale, and because the constituents are (generally speaking) primarily a mixture of nitrocellulose and nitroglycerin. Some brief experimental results are presented and a theoretical model of the depressurization transient in a double-base propellant is described. Because of the present limited understanding of the steady state combustion process in a double-base propellant, it has been impossible to present as accurate and thorough an analysis here as was done for the composite propellants. However, there are several reasons for including a section on double-base propellants. First of all, any theory for double-base propellants indicates how the depressurization model for composite propellants can be modified to include other steady state theories. Second, the work on double-base propellants serves to emphasize the fact that there are significant differences between the physical characteristics of the flames of a composite propellant and a double-base propellant. Because of these differences, the previous GDF description of the depressurization process is limited to composite propellants and should not be used to describe double-base propellants. Finally, it emphasizes the fact that a proper physical description of the flame is necessary in order to obtain accurate transient predictions.

A. Physical Description of the Combustion Process in Double-Base Propellants

One obvious difference between composite and double-base propellants is that different ingredients are used in the two propellants (generally speaking, double-base propellants are composed of nitrocellulose and nitroglycerin). However, in addition to this compositional difference, the fuel and oxidizer in a double-base propellant (unlike those in a composite propellant) are pre-mixed on a molecular level. A given molecule in a double-base propellant can contain both the oxidizer and the fuel for the ensuing chemical reaction. As a result of these two differences, the flame of a double-base propellant is considerably different from the flame of a composite propellant. However, despite the fact that the ingredients in a double-base propellant are pre-mixed, the flame of a double-base propellant is more complex than that of a composite solid propellant.

A physical description of the combustion process in a double-base propellant can be obtained from various experimental observations. The combustion wave in a double-base propellant consists of the following parts. First is the heat-up zone in the solid which is accompanied by sub-surface chemical reactions.

These reactions decompose the solid and eject reactive particles into the gas phase. These particles combine exothermically very near to the surface in the so-called "fizz zone" and cause a steep rise in the temperature profile. This rapid gaseous reaction is followed by the so-called "dark zone" which is characterized by a plateau in the temperature profile. At high pressures, a luminous flame appears at the end of the dark zone and the temperature profile rises rapidly to the adiabatic flame temperature.

It is generally accepted that the sub-surface reaction is exothermic[51,52,53]. Crawford, et. al.[51] have indicated that the energy contributed by the solid phase reactions represents a significant portion of the energy which is required to decompose the surface. Klein, et. al.[52] have further contended that this heat production must occur very near to the surface of the burning propellant because of the low thermal conductivity of the solid and because of the Arrhenius dependence of the reaction on the local temperature. Samples of gas taken near the surface of a burning double-base propellant by Tajima, et. al.[34] have shown that free radicals are present, but there has been no evidence of high molecular weight products. Tajima, et. al. have interpreted this to mean that extensive degradation must take place in the condensed phase. Crude estimates of the depth of the sub-surface reactions have been set at 10μ by Klein, et.al. and 50-300μ by Heller and Gordon[55].

As suggested above, the surface decomposition is followed immediately by a reaction between the decomposition products. This reaction yields such intermediate products as NO, CO, and H_2[55] and raises the gas temperature to about 1500°K very near the surface[51,52]. The thickness of this reaction zone has been estimated as one millimeter by Heller and Gordon[55] and as tenths of a millimeter by Sarner[56].

At low pressures no further reaction takes place and the final combustion temperature remains at about 1500°K (far below the calculated abiabatic temperature of about 3000°K). Thus at low pressures, the entire combustion process is nonluminous except for a weak radiation from the surface of the propellant[57,58]. However, as the pressure is increased to about 250 psia, a bright, sharply defined, luminous flame suddenly appears[51,55,57,58]. When it first appears, the luminous flame is about 15 mm from the surface and being so far away, it has no noticeable effect on the burning rate. As the pressure is increased still further, the dark zone shrinks and the luminous flame moves closer to the surface. Crawford, et. al.[51] have found that the length of the dark zone is proportional to p^{-3}, while, for a slightly different propellant formulation, Heath and Hirst[58] have found that the length varies as $p^{-1.9}$.

At high pressures, the luminous flame eventually moves so near the burning surface that it becomes a controlling factor in the burning rate. Reid[57] has estimated that heat feedback from the luminous flame starts to become important around 500-600 psia. The effect of the flame can sometimes be noted by a change in the slope of the steady state burning rate curve.

The dark zone is apparently a region in which a critical concentration of active particles is built up, after which a nearly instantaneous branched chain reaction takes place (luminous flame). Consequently while the dark zone becomes very thin above 1000 psia, there is no reason to believe that it ever vanishes entirely. Finally, ignition temperature measurements by Tajima, et. al.[54] and Crawford, et. al.[51] have indicated that a double-base propellant ignites at about 500°K. Surface temperature measurements by Crawford, et. al.[51], Klein, et. al.[52], and Cotton and Austin[59], have been reported between 500°K and 1000°K.

B. The Quasi-Steady Approximation for Double-Base Propellants

Before describing the model for non-steady burning of double-base propellants, it is necessary to again review the applicability of the quasi-steady approximation for the gas phase. This review is especially necessary in view of the relatively thick reaction zone in double-base propellants. Using an overall flame thickness of 15 millimeters (taken from the previous sub-section), and using a steady state burning rate of .5 in/sec, we obtain a gas residence time of about five milliseconds in the reaction zone. For such long residence times, the validity of the quasi-steady approximation begins to become questionable. However, this flame thickness includes the luminous flame. At low pressures (where the flame reaches this 15 millimeter thickness), the luminous flame is insignificant as a driving mechanism for the combustion process. The fizz zone thickness is a more appropriate measure of the characteristic time of the gas phase reaction. Consequently, using a thickness of one millimeter (again taken from the previous subsection) for the fizz zone, we obtain a residence time of 0.5 ms. This time is fast enough to justify the quasi-steady approximation (depressurization times for double-base propellants are on the order of ten milliseconds).

At high pressures, the luminous flame does become important in the combustion process of a double-base propellant. However, in order for the flame to feed a significant amount of heat back to the solid, it is necessary that the flame move very close to the surface. We make the approximation that when the luminous flame is so near the surface that it adds significant heat to the surface, it is thin enough to be assumed quasi-steady. Conversely, at low pressures, where the flame moves away from the surface, it is no longer important in the burning process so that the quasi-steady approximation can be based on the thickness of the fizz zone alone.

In our theoretical model, we will always include the luminous flame in our description of the combustion process. In addition, we will always assume that the entire flame zone is quasi-steady, but this is not in disagreement with the statements in the above paragraph for the following reasons. At pressures below 500-600 psia, the heat feedback from the luminous flame is negligible (less than 0.1%) in our model, consequently, at low pressures the luminous flame has no effect on the transient burning rate so that the actual method which is used to describe them becomes irrelevant. We are in effect applying the quasi-steady approximation to only the fizz zone.

C. Combustion Model For Non-Steady Burning of Double-Base Propellants

As previously indicated, the physical description of the combustion process in double-base propellants is not as well documented as is the burning rate process for composite solid propellants. Because of this, our double-base theory should be considered as preliminary and should be revised and updated as more detailed knowledge of the flame structure becomes available. The theory we shall use is basically similar to the one presented by Rice and Ginell[60], but it philosophically follows the model for composite solid propellants which was described in Section III.

We visualize the combustion process as being composed of three exothermic regions; one inside the solid phase, one near to the solid surface but in the gas phase (fizz zone), and one in the luminous flame. For simplicity we approximate the sub-surface reaction as being collapsed and occurring entirely at the surface. We treat the fizz reaction as a pre-mixed flame. As before, we approximate the spatial reaction rate in this gaseous reaction zone by a delta function. Note that the approximations for the sub-surface reaction and the fizz reaction are mutually consistent (all reaction occurs at the highest temperature). The actual "thickness" of the fizz zone (i.e. the distance of the delta function from the surface) is to be determined from steady state data in a manner analogous to that used for composite propellants.

Because of the heat release in the solid, this combustion model predicts a steady state burning rate which is independent of pressure in the low pressure region. The level of this pressure independent region in the burning rate is proportional to the amount of heat which is released in the solid. Steady state burning rate data of double-base propellants frequently exhibit such a plateau, and the magnitude of the sub-surface heat release can be estimated from the level of this plateau. However, in these preliminary studies, the split in the heat release between the sub-surface reaction and the fizz zone reaction has been arbitrarily picked as 25%/75%. (The total heat release of the two reactions is known from experimental measurements of the temperature in the dark zone.)

Finally, we model the dark zone as having a length which is an empirically determined function of pressure (only). From Crawford's observations[51], we take this function to be proportional to p^{-3}. We visualize the dark zone as being a region in which a critical concentration of a reactive species is developed. As soon as this critical concentration is reached, a chain reaction occurs right at the end of the dark zone and gives rise to the luminous flame. The biggest drawbacks to this assumption are that the model requires measurements of the length of the dark zone as a function of pressure during steady state burning and, more fundamentally, that it ignores the mechanisms which contribute to the length of the dark zone. The justification for such a crude model is that the luminous flame is only of minor importance at intermediate pressures and that it will probably disappear altogether before the pressure has dropped low enough to cause extinction. At pressures above 1000 psia, the model is expected to become less and less valid.

The mathematical description of the model is as follows. First, since all the sub-surface reaction is placed right at the surface, the equation for the solid phase is the same as the one we used for composite propellants (see Section IV-B). In non-dimensional form, the equation for the solid phase is

$$\frac{\partial^2\theta}{\partial X^2} + R\frac{\partial\theta}{\partial X} = \frac{\partial\theta}{\partial\tau} \tag{24}$$

The quasi-steady approximation in the gas phase also leads to the same equation as the one that was used for composite propellants. Both the fizz zone and the dark zone (plus luminous flame) are described by similar equations,

$$\frac{d^2\theta}{dX^2} + \frac{c_g}{c_p}\frac{\lambda_p}{\lambda_g}R\frac{d\theta}{dX} + \frac{Q\,\dot{\varepsilon}_g\,\alpha_p^2\,\rho_g\,c_p}{\lambda_g\,r_0^2} = 0 \qquad \text{dark zone and luminous flame} \tag{114}$$

$$\frac{d^2\theta}{dX^2} + \frac{c_g}{c_p}\frac{\lambda_p}{\lambda_g}R\frac{d\theta}{dX} + \frac{H_{fizz}\,\dot{\varepsilon}_{fizz}\,\alpha_p^2\,\rho_g\,c_p}{\lambda_g\,r_0^2} = 0 \qquad \text{fizz zone} \tag{115}$$

In order to integrate the gas phase equations, we take both $\dot{\varepsilon}_g$ and $\dot{\varepsilon}_{fizz}$ to be delta functions. Thus we obtain

$$\left(\frac{d\theta}{dX}\right)_{I^+} = -QR\frac{\lambda_p}{\lambda_g}\,e^{-\frac{c_p}{c_g}\frac{\lambda_g}{\lambda_p}R(X_z - X_I)} \qquad \text{dark zone and luminous flame} \tag{116}$$

and

$$\left(\frac{d\theta}{dX}\right)_{s,g} = \left[\left(\frac{d\theta}{dX}\right)_{I^+} + \frac{\lambda_p}{\lambda_g}H_{fizz}R\right]e^{-R\frac{c_p}{c_g}\frac{\lambda_g}{\lambda_p}X_I} \qquad \text{fizz zone} \tag{117}$$

In order to determine the "thickness" of the fizz zone reaction,

X_I, we again relate it to a characteristic time

$$X_I = R\,\tau_{fizz}\,\rho_p/\rho_g = \frac{\lambda_g}{\lambda_p}\frac{c_p}{c_g}\,R\,\tau'_{fizz} \tag{118}$$

We express this characteristic time as

$$\tau'_{fizz} = \frac{A^2\,T_{fizz\,RED}}{P^m}\exp\left[E_{fizz}/RT_{fizz_0}\left(\frac{1}{T_{fizz_{RED}}}-1\right)\right] \tag{119}$$

where m is the order of the reaction, and A is an undetermined constant. (Rice and Ginell[60] similarly used a reaction of order m). However, for the length of the dark zone, we use a slightly different approximation. We assume the luminous flame occurs immediately at the end of the dark zone, and we determine the dark zone length, $X_{II}-X_I$, from Crawford, et. al's data[51],

$$X_{II} - X_I = L_{DARK\ ZONE} = K/P^3 \tag{120}$$

The constant k is also determined from the same source to be, k = 3.

The final form of the equations describing the heat feedback from the gas phase to the solid phase of a double-base propellant is

$$\frac{\lambda_g}{\lambda_p}\left(\frac{d\theta}{dX}\right)_{s,g} = \left[QR\,e^{-3R/P^3} + H_{fizz}\,R\right]e^{-R^2\tau'_{fizz}} \tag{121}$$

and

$$\left(\frac{\partial\theta}{\partial X}\right)_{s,p} = \frac{\lambda_g}{\lambda_p}\left(\frac{d\theta}{dX}\right)_{s,g} - H_s R \tag{122}$$

The steady state burning rate curve is obtained by inserting the steady state temperature gradient inside the solid, $(d\theta/dX)_{s,p} = \bar{\theta}_s\,\bar{R}$, into the above equations to give

$$\bar{R} = \sqrt{\log\left(\frac{Q\,e^{-3R/P^3} + H_{fizz}}{\bar{\theta}_s - H_s}\right)}\;\frac{P^{m/2}}{A\,T_{fizz_{RED}}\exp\left[E_{fizz}/2RT_{fizz_0}\left(\frac{1}{T_{fizz_{RED}}}-1\right)\right]} \tag{123}$$

A plot of this equation is shown on figure 51. Nominal values have been assumed for all the parameters as shown on the curve. As this figure shows, this equation predicts a constant burning rate at low pressures. At intermediate pressures the burning rate behaves as $P^{m/2}$. At high pressures, the heat feedback from the luminous flame begins to become important and the burning rate increases rapidly.

D. Experimental Results for Double-Base Propellants

As indicated in the introductory remarks at the beginning of this section, a small number of experimental depressurizations have been made using double-base propellants. Only one double-base formulation was tested. The particular formulation which was chosen was an ICRPG double-base reference propellant. This propellant was purchased from the Naval Ordnance Station, Indian Head, Maryland and carries the designation N-5. The propellant is basically composed of 50% nitrocellulose and 35% nitroglycerin. Complete properties and specifications are given in reference 61.

The experimental methods and apparatus which were used for testing the double-base propellant are identical to those described in Section IV and Appendix I for composite propellants. As discussed in Section IV, a photomultiplier was used to monitor the visible radiation from the propellant flame during a depressurization. The propellant was said to extinguish if (and when) the flame radiation went to zero. However, as indicated above, the luminous flame in double-base propellants disappears at pressures below about 250 psia-the dark zone becomes effectively infinite in length at this pressure. In our experiments, the photomultiplier faithfully recorded this disappearance of the flame. Whether the propellant extinguished permanently, extinguished momentarily and later re-ignited, or continued to burn, the photomultiplier output went to zero and stayed there. As a result, the photomultiplier was of no use in determining which of these three end conditions actually occurred. Furthermore, re-ignition and burnout following a temporary extinction in a composite propellant always produced a noise which was loud enough to be heard audibly, and so served as a second method for identifying runs which extinguished temporarily. However, the re-ignition and burnout of the double-base propellants could not be detected audibly. Consequently the only way to positively identify which runs extinguished, was to actually observe propellant remaining in the combustion chamber following a depressurization. That is to say, the only extinctions which could be detected were permanent extinctions; it was impossible to discern between transient extinctions and runs which continued to burn.

The experimental results for the double-base propellants are shown in figure 52. In order to allow easy visual comparison with the results for composite propellants, the double-base results have been plotted on the same scale as were the results for the composite propellants. Those points for which the final outcome is uncertain (i.e. temporary extinctions and non-extinctions) are indicated by semi-darkened symbols. Despite the many inconclusive runs, a sufficient number of runs extinguished permanently to prove that this double-base propellant is much easier to extinguish than were any of the composite solid propellants which were tested.

Since the only points on this plot whose outcome is definite are the runs which extinguished permanently, the only experimental "extinction boundary" we can draw is a boundary between permanent extinction and non-extinction plus extinction followed by re-ignition (i.e. a boundary like those drawn by Jensen[4]). The data scatter which is shown on this figure is representative of the apparently random way in which re-ignition occurred throughout the entire experimental program (for both double-base and composite propellants). As we discussed in Section III, this scatter is due to variations in the re-ignition process, not the depressurization process.

E. Theoretical Predictions for Double-Base Propellants

As seen in the previous sub-section, the experiments with double-base propellants have only been adequate to ascertain the qualitative conclusion that double-base propellants are easier to extinguish than are composite propellants. Our aim is to use our theoretical model for double-base propellants to show this same qualitative result, namely that double-base propellants are easier to extinguish than are composite propellants.

With this in mind, we have chosen nominal values for the parameters in our equations as shown on figure 51. The steady state burning rate which corresponds to these values of the parameters is also shown on figure 51. This burning rate curve is similar in shape to the burning rates which were measured by Crawford, et. al.[51].

The theoretical extinction boundary for this double-base propellant is shown in figure 53. Exponential pressure-time curves have been used to obtain this extinction boundary. For comparison, a similar theoretical extinction boundary for a composite propellant (which is essentially 80%/20% PBAA) is also shown on this figure. This graphically shows that the extinction predictions for double-base propellants do have the qualitative agreement with our limited experimental results which we had hoped for. The data definitely show that double-base propellants extinguish more easily than composite solid propellants.

This then represents another justification for one of the ideas which we have tried to put forward in this thesis: an accurate physical description of the flame is necessary if one is to obtain accurate transient (in this case depressurization transient) predictions for a solid propellant. The difference between the extinction characteristics of double-base and composite solid propellants can only be explained in terms of the differences in their flame structures. For example, the theories of Von Elbe and Paul, which were discussed previously, predict that as the steady state burning rate of a propellant increases, the propellant becomes more difficult to extinguish. The degree

of difficulty increases as the square of the steady state burning rate. Thus their theory predicts

$$\left(\frac{dP}{dt}\right)_{CRITICAL} \sim \frac{\rho \bar{r}^2}{n \alpha_p}$$

The burning rate of double-base propellants is generally considerably higher than that of composite propellants. Consequently these "non-dimensionalization" theories would predict that a double-base propellant is more difficult to extinguish than is a composite. This prediction is qualitatively in the wrong direction. The reason for this incorrect prediction is that they did not include the flame structure in their theoretical models.

SECTION VIII

SUMMARY AND CONCLUSIONS

In the preceding sections of this thesis, we have developed separate theories to explain the depressurization transient in both composite propellants and in double-base propellants. We have also presented experimental results which show the extinguishment characteristics of both types of propellants and which serve to provide a test for the theoretical models. Most of the work which is reported in this thesis pertains to composite propellants; a lesser amount pertains to double-base propellants.

In the experimental program for composite propellants, the extinction characteristics of several families of propellants were determined through extensive testing. Sufficient experimental data were obtained to determine the boundary between the region of extinction and the region of non-extinction for each individual propellant formulation. A corresponding theoretical boundary was then determined from the theoretical model. The accuracy of the theoretical predictions was checked by comparing the theoretically predicted boundaries with the experimentally determined boundaries. In order to obtain meaningful, quantitative agreement between theory and experiment, the actual experimental pressure-time curves were used as the forcing functions for obtaining the theoretical predictions. The comparisons showed that the predictions for the effect of changes in the propellant oxidizer loading and for the effect of changes in the oxidizer particle size are in excellent agreement with the experimental results. The predictions for different fuel binder types are also satisfactory, but are not as exact as the predictions for the first two series. The propellants for which the theoretical predictions begin to deviate from the experimental results are, in general, those propellant formulations for which the steady state theory (on which the depressurization model is based) begins to break down.

The experimental testing which was done with double-base propellants was only sufficient to indicate that double-base propellants are considerably easier to extinguish than are composite propellants. The corresponding theoretical predictions for the double-base propellants agreed with this qualitative experimental observation.

In our theories for both composite and double-base propellants, a quasi-steady approximation has been used to analyze the gas phase. It is this approximation which makes the problem tractable. In developing these theoretical models, we have been especially careful in the application of this quasi-steady approximation. Other authors have used similar "quasi-steady" approximations, but they have frequently been less careful, and have gotten into difficulties on this point.

When the quasi-steady approximation is used properly, an accurate physical description of the flame structure becomes imperative. In most of the theories which mis-use the quasi-steady approximation, the flame structure doesn't even appear in the analyses. Consequently it is impossible for such models to predict the qualitative differences between the extinction characteristics of composite and double-base propellants which we have observed experimentally, and which we have shown to be due to differences in the flame structure.

Both of our theoretical models include as accurate a description of the flame structure as present knowledge allows. In fact, it is only in the description of the flame structure that our model for composite propellants differs from our model for double-base propellants, and as noted above, our models do predict the qualitative differences between the extinction characteristics of double-base and composite propellants. In addition, our theoretical model gives accurate, quantitative predictions for composite propellants.

Our depressurization model for composite propellants is based on the granular diffusion flame theory of steady state burning. The GDF theory was originally chosen for use in the depressurization analysis because extensive studies of steady state burning have shown that the GDF theory more closely predicts the pressure dependence of the burning rates of a wide variety of propellant formulations than does any other existing steady state theory. Furthermore, the GDF theory allows us to incorporate the two physical phenomena which are most important in the description of the gas phase flame; the model allows for both the diffusional mixing of the originally heterogeneous mixture of fuel and oxidizer, and for the chemical reaction which follows the mixing.

A number of modifications to the GDF theory were necessary in order to apply it to the depressurization analysis, but the critical test of the theory is in its ability to represent the temperature dependence of the gas phase reaction rate. The steady state formulation of the GDF theory originally included a dependence on the flame temperature, however since the steady state flame temperature is nearly constant (independent of pressure), the actual dependence on the flame temperature had never been tested - it was only a latent hypothesis. The depressurization results, on the other hand, are strongly dependent on the temperature in the gas phase and the agreement between theory and experiment indicates that the manner in which the dependence on the flame temperature is incorporated into the GDF theory is basically correct. Thus the results of our transient analyses support the basic GDF postulate, namely that the flame of a composite solid propellant is composed of both diffusional and chemical reaction effects. Further, our results indicate that the GDF theory yields an appropriate estimate of the relative importance of these two effects.

Previous results on the steady state burning of composite propellants have shown that, at normal rocket pressures, diffusion is the most important process in the flame of a composite solid propellant. Our results have confirmed this, but they have also shown that at the onset of extinction the opposite is true; the extinguishment process depends strongly on the chemical processes. A proper theoretical model should therefore include both of these effects.

Our results have also shown that it is inadequate to relate the occurrence of extinction to a single value of dp/dt (the rate of change of pressure) at some point in the p - t curve. We have shown that extinction is most sensitive to the low pressure end of the p - t curve, but that the entire curve must be considered if we are to obtain a proper solution to the depressurization problem. These remarks apply equally well to the steady state burning rate curve. Since the chemical reaction rate is important in the extinction process, it follows that the low pressure end of the steady state burning rate is also important in determining the extinction characteristics of a propellant. This is because the effect of chemical kinetics appears only in the low pressure portion of the burning rate curve and not at the high pressure end where they are swamped by the slower diffusion processes.

Both our experimental and our theoretical results support the experimental findings of others . showing that more highly oxidized propellants are more difficult to extinguish. Similarly, propellants with smaller AP particle sizes are more difficult to extinguish. The addition of aluminum (at constant oxidizer-to-fuel binder ratio) makes a propellant slightly more difficult to extinguish.

Our depressurization model for double-base propellants visualizes a flame which is completely controlled by chemical reactions. Diffusion is unimportant in a double-base flame because the reactants are pre-mixed on a molecular scale inside the solid. At low and intermediate pressures, the combustion process in a double-base propellant is almost entirely driven by a region of concentrated heat release which occurs near and inside the surface of the solid. The reaction which occurs near the surface is referred to as the fizz zone. The luminous flame is generally so far from the surface at these pressures (or during typical depressurizations) that it is of little consequence. We have approximated the stand-off distance of the luminous flame from an empirically determined formula which gives the length of the dark zone as a function of pressure (only). Because of the minor importance of the luminous flame on the extinguishment process, we feel this rather gross approximation is adequate. We have represented the fizz zone heat release by a delta function -- our approximation for a premixed reaction.

Finally, some of the more important points which have been brought out in this thesis are condensed and listed here

in a very concise fashion. We have found:

(a) The flame structure is very important in determining the extinction characteristics of a solid propellant.

(b) The granular diffusion flame theory can be applied to the depressurization transient. (For propellants having fuel binders which do not melt readily, and which are not strongly under-oxidized, and for propellants which do not have very large AP particles sizes).

(c) The depressurization results add further justification to the granular diffusion flame model of the steady state burning of composite solid propellants.

(d) Although the steady state burning process in a composite solid propellant is largely controlled by diffusional processes, the extinction process depends in large part on the chemical processes.

(e) The entire p - t curve is significant in determining extinction, not just the rate of change of pressure at one specific point on the p - t curve.

(f) Similar to the above, the entire steady state burning rate curve is important in determining the extinction characteristics of a propellant.

(g) Increasing the oxidizer loading, or decreasing the ammonium perchlorate particle size in a composite propellant tends to make the propellant more difficult to extinguish.

(h) Double-base propellants are easier to extinguish than are composite propellants. The difference is directly attributable to differences in their flame structures.

(i) The occurrence of extinction depends primarily on the depressurization rate whereas re-ignition is most strongly influenced by the environment inside the motor. Temporary extinction is a characteristic of a particular propellant. Permanent extinction is a characteristic of not only the propellant, but also the internal configuration of the combustion chamber.

REFERENCES

1. Ciepluch, Carl C., "Effect of Rapid Pressure Decay on Solid Propellant Combustion", ARS Journal, Vol. 31, No. 11, November 1961, pp. 1584-1586.

2. Ciepluch, Carl C., "Effect of Composition on Combustion of Solid Propellants During a Rapid Pressure Decrease", NASA TN D--1559, (1962).

3. Ciepluch, Carl C., "Spontaneous Reignition of Previously Extinguished Solid Propellants", NASA TN D-2167, March 1964.

4. Jensen, G. E., "A Start-Stop Study of Solid Propellants", NASA CR-66488, Nov. 1967.

5. Jensen, G. E., "An Experimental Study of Solid Propellant Extinguishment By Rapid Depressurization", NASA CR-66747, Final Report, Contract No. NAS 1-7815, United Technology Corporation, March, 1969.

6. Ryan, N. W. et. al., "Ignition and Combustion of Solid Propellants", University of Utan, Department of Chemical Engineering, Technical Report No. 9711-01, pp. 36-41 (1966). Also Mantyla, R. G., Baer, A. D., and Ryan, N. W., "Extinction by Rapid Depressurization: A Means to Other Ends", ICRPG 3rd Combustion Conference, CPIA Publication No. 138, Vol. 1, p. 227, (1966)

7. Wooldridge, C. E., Marxman, G. A., and Capener, E. L., "Propellant Combustion Phenomena During Rapid Depressurization", Final Report, NASA CR-66500, October, 1967.

8. Wooldridge, C. E., Marxman, G. A., and Krier, R. J., "A Theoretical and Experimental Study of Propellant Combustion Phenomena Druing Rapid Depressurization", NASA CR-66733, Final Report, Contract No. NAS 1-7349, Stanford Research Institute, February, 1969.

9. Cohen, N. S., "A Theory of Solid Propellant Extinguishment by Pressure Perturbation", ICRPG 2nd Combustion Conference, 1965, CPIA Publication No. 105, May, 1966.

10. Von Elbe, G. and McHale, E. T., "Extinguishment of Solid Propellants By Rapid Depressurization", AIAA J. 6, 1417 (1968).

11. Reed, R., Nelson, C., McDonald, A., Ramnarace, J., "Extinction Characteristics of Carboxyl Terminated Polybutadiene Propellant", ICRPG 3rd Combustion Conference, CPIA Publication No. 138, Vol. I, October, 1966.

12. Fletcher, E. A. and Bunde, G. W., "Gas Evolution From A Solid Rocket Propellant During Depressurization To Produce A Quench", AIAA J. 4, 181 (1966).

13. Fletcher, E. A. and Hiroki, T., "Gas Evolution From Solid Propellants During Pressure Decays", AIAA J. 4, 2222 (1966).

14. Fletcher, E. A., Bunde, G., Paulson, R., "Study of Reignitable Solid Propellant Grains Leading To Extinguishable And Restartable Solid Propellant Rocket Motors", NASA CR-53960, Fifth Quarterly Progress Report, Contract No. NAS 3-2554, April, 1964.

15. Kling, R. and Brulard, J., "Les Vitesses de Combustion des Propergols Solides Composites en Regime Transitoire", La Recherche Aerospatiale, No. 115, November-December, 1966.

16. Fletcher, E. A. and Paulson, R. A., "Chamber Pressure Balanced Piston-Nozzle for Fast Depressurization", J. Spacecraft and Rockets 3, 152, (1966).

17. Kalt, S., "Thrust Termination in Solid Propellant Rocket Motors - Evaluation of Ballistic Test Data", ARS J. 31, 84 (1961).

18. Dubrow, B., Guth, E. D., and Wong, M. W., "Ballistics of Solid Propellants During Thrust Modulation", J. of Spacecraft and Rockets 2, (1965).

19. Coates, R. L., Polzien, R. E., and Price, C. F., J. Spacecraft and Rockets 3, 419 (1966).

20. Slocum, R. W., "Result of Solid Motor Extinguishing Experiments", AIAA J. 1, 1419 (1963).

21. Barrere, M., Jaumotte, A., de Veubeke, B. F., and Vandenkerckhove, J., Rocket Propulsion, Elsevier Publishing Company, 1960.

22. Steinz, J. A. and Summerfield, M., "Mechanism of Burning of Solid Propellants With Special Reference To Low Pressure Combustion Phenomena", in Advances in Chemistry Series, American Chemical Society, 1969.

23. Sutherland, G. S. "The Mechanism of Combustion of an Ammonium Perchlorate-Polyester Resin Composite Propellant", Ph.D. Thesis, Aeronautical Engineering Department, Princeton University, (May, 1956).

24. Povinelli, L. A., "A Study of Composite Solid Propellant Flame Structure Using a Spectral Radiation Shadowgraph Technique", AIAA J. 3, 1593 (1965).

25. Von Elbe, G., "Theory of Solid Propellant Ignition and Response to Pressure Transients", Bulletin of Interagency Solid Propulsion Meeting, Vol. III, 95, (July, 1963). Also "Solid Propellant Ignition and Response of Combustion to Pressure Transients", AIAA Preprint 66-668, (June 1966).

26. Paul, B. E., et al., "A Ballistic Explanation of the Ignition Pressure Peak", AIAA Preprint 64-121, 1964.

27. Horton, M. D., Bruno, P. S., and Graesser, E. C., "Depressurization Induced Extinction of Burning Solid Propellant", AIAA J. 6, 292 (1968).

28. Wallis, F. R., "Initial Pressure Peaks in Rocket Motors and Interruption by Venting", Journal of Spacecraft and Rockets, Vol. 5, April, 1968, pp. 481-483.

29. Brown, R. S., Muzzy, R. J., and Steinle, M. E., "Surface Reaction Effects on the Acoustic Response of Composite Solid Propellants", AIAA J. 6, 479 (1968).

30. Zel'dovich, Y. B., "The Burning Rate of a Solid Propellant Under Variable Pressure", PMTF (USSR), No. 3, 1964.

31. Denison, M. P. and Baum, E., "A Simplified Model of Unstable Burning in Solid Propellants", ARS Journal, Vol. 31, 1961, 1112-1122.

32. Marxman, G. A. and Wooldridge, C. E., "Effect of Surface Reactions on the Solid Propellant Response Function", AIAA J. 6, 471 (1968).

33. Landers, L. C. and Lou, R. L., "Development of an Extinguishable Solid Propellant (u)", Report No. AFRPL-TR-65-147, Contract AF 04(611)-9889, Aerojet-General Corporation, Sacramento, Calif., 19 July 1965 (Confidential). Cited in Ref. 34.

34. Lou, R. L. and Landers, L. C., "Solid Rocket Motor Extinguishment by Rapid Depressurization", CPIA Publication No. 111, Vol. III, Oct., 1966 (Confidential). (The entirety of Volume III is classified; this individual article is unclassified.)

35. Hall, A. R. and Pearson, G. S., "Ammonium Perchlorate as an Oxidizer", Oxidation and Combustion Reviews 3, 129 (March, 1968).

36. Wooldridge, C. E. and Marxman, G. A., "Nonlinear Solid Propellant Burning Rate Behavior During Abrupt Pressure Excursions", AIAA Preprint 69-172. Presented at AIAA 75h Aerospace Sciences Meeting, New York City, N. Y., Jan. 20-22, 1969.

37. von Karman, T., "The Present Status of The Theory of Laminar Flame Propagation", Sixth Symposium (International) on Combustion, The Combustion Institute, Reinhold Publishing Corporation, 1956.

38. Steinz, J. A., Stang, P. L. and Summerfield, M., "The Burning Mechanism of Ammonium Perchlorate-Based Composite Solid Propellants", AIAA Preprint No. 68=638. Presented at AIAA 4th Propulsion Joint Specialist Conference, Cleveland, Ohio, June, 1968.

39. Steinz, J. A., "The Burning Mechanism of Ammonium Perchlorate-Based Composite Solid Propellants", Ph.D. Thesis, Aerospace and Mechanical Sciences Department, Princeton University, February, 1969.

40. Merkle, C. L., Turk, S. L., and Summerfield, M., "Extinguishment of Solid Propellants by Depressurization: Effects of Propellant Parameters", AIAA Preprint 69-176, AIAA 7th Aerospace Sciences Meeting, New York, January 20-22, 1969.

41. Merkle, C. L. and Summerfield, M., "Extinguishment of Solid Propellants by Rapid Depressurization: A Theory Based on a New Feedback Law", Presented at the 3rd ICRPG/AIAA Solid Propulsion Conference, Atlantic City, N. J., June 1968.

42. Summerfield, M., Sutherland, G. S., Webb, M. J., Taback, H. J., and Hall, K. P., in M. Summerfield (Editor), Solid Propellant Rocket Research, Progress in Astronautics and Rocketry, Vol. I, Academic Press, New York, 1960.

43. Krier, H., T'ien, J. S., Sirignano, W. A., and Summerfield, M., "Nonsteady Burning Phenomena of Solid Propellants: Theory and Experiments", AIAA J. 6, 278 (1968).

44. Vichnevetsky, R., "A New Stable Computing Method for the Serial Hybrid Computer Integration of Partial Differential Equations", Proceedings of the 1968 Spring Joint Computer Conferences, AFIPS, Vol. 32, Thompson Book Company, 1968.

45. Sills, J. A., "Transformations For Infinite Regions and Their Application to Flow Problems", AIAA J. 7, 117 (1969).

46. Schultz, R. D. and Dekker, A. O., "Transition-State Theory of the Linear Rate of Decomposition of Ammonium Perchlorate", Sixth Symposium (International) on Combustion, p. 260, Reinhold Publishing Co., New York, 1957.

47. Coates, R. L., "Linear Pyrolysis Rate Measurements of Propellant Constituents", AIAA J. 3, 1257 (1965).

48. Sabadell, A. J., Wenograd, J., and Summerfield, M., "Measurement of Temperature Profiles through Solid-Propellant Flames Using Fine Thermocouples", AIAA J. 3, 1580 (1965).

49. Powling, J., "Experiments Relating to the Combustion of Ammonium Perchlorate-Based Propellants", Eleventh Symposium (International) on Combustion, p. 447, The Combustion Institute, Pittsburgh, 1967.

50. Weast, R. C. (Editor), Handbook of Chemistry and Physics 48th Edition, p. 0-33, The Chemical Rubber Company, Cleveland, 1967.

51. Crawford, B. L., Huggett, C. and McBrady, J. J., "The Mechanism of the Burning of Double-Base Propellants", J. of Physical and Colloid Chemistry 54, 854 (June, 1950).

52. Klein, R., Mentsen, M., von Elbe, G., and Lewis, B., "Determination of the Thermal Structure of a Combustion Wave by Fine Thermocouples", J. of Physical and Colloid Chemistry 54, 877 (June, 1950).

53. Shorr, M. and Zaehringer, A. J., Solid Rocket Technology, John Wiley and Sons, New York, 1967.

54. Tajima, Y. A., Dauerman, L. and Salser, G. E., "A New Experimental Technique and New Results on the Mechanism of Combustion and Catalysis of Double-Base Propellants", ICRPG 2nd Combustion Conference, CPIA Publication 105, p. 379 (May, 1966).

55. Heller, C. A. and Gordon, A. S., "Structure of the Gas Phase Combustion Region of a Solid Double Base Propellant", J. Physical Chemistry 59, 773, (August, 1955).

56. Sarner, S. F., Propellant Chemistry, Reinhold Publishing Corporation, New York, 1966.

57. Reid, D. L., "The Dependence of Several Solid Propellant Burning Anomalies on Flame Structure", MSE. Thesis, Department of Aeronautical Engineering, Princeton University (July, 1957).

58. Heath, G. A. and Hirst, R., "Some Characteristics of the High Pressure Combustion of Double-Base Propellants", Eighth Symposium (International) on Combustion, p. 711, Williams and Wilkins Company, Baltimore, 1962.

59. Cotton, D. J. and Austin, T. D., Navweps Report 8573 (1964). Cited in reference 56.

60. Rice, O. K. and Ginell, R. "The Theory of the Burning of Double-Base Rocket Powders", J. of Physical and Colloid Chemistry, 54, 885, (June, 1950).

61. Anon., "Available ICRPG Standard Propellant Samples", Indian Head Special Publication 68-8, Naval Ordnance Station, Indian Head, Maryland (June, 1968).

62. Beyer, R. and Fishman, N., "Solid Propellant Ignition Studies with High Flux Radiant Energy as a Thermal Source", Solid Propellant Rocket Research, Academic Press, 1960.

63. McDermott, C. E. and Isom, K. B. "Spontaneous Reignition Analysis for Solid Restartable Motors", AIAA Preprint 69-444, AIAA 5th Propulsion Joint Specialist Conference, USAF Academy, Colorado (June, 1969).

64. Lehmann, G. M. and Schneiter, G. R. "Analytical Investigation of the Reignition of a Solid Propellant", Air Force Systems Command Contract No. F04695-67-C-0158, Report No. TOR-0158(53801-04)-4 Aerospace Corporation, April 1968.

65. Mayer, S. W., Weinberg, E. K. and Schieler, L. "Procedures for Suppressing Premature Exothermic Decomposition in Ammonium Perchlorate", AIAA Preprint 69-503, AIAA 5th Propulsion Joint Specialist Conference, USAF Academy, Colorado (June 1969).

66. Inami, S. H., Rosser, W. A. and Wise, H. "Heat-Release Kinetics of Ammonium Perchlorate in the Presence of Catalysts and Fuel", Combustion and Flame, Vol. 12, No. 1, 1968, pp. 41-44.

67. Rosser, W. A., Fishman, N. and Wise, H. "Ignition of Simulated Propellants Based on Ammonium Perchlorate", AIAA Journal, Vol. 4, No. 9, September 1966, pp. 1615-1621.

68. Most, W. J., "Ignition Transient Prediction and Control of Solid Propellant Rocket Motors", Ph.D. Thesis, Aerospace and Mechanical Sciences Department, Princeton University (June 1969).

69. Krier, H. "Solid Propellant Burning in Nonsteady Pressure Fields", Ph.D. Thesis, Princeton University (September, 1968). See also Ref. 43.

70. Frazer, J. H. and Hicks, B. L. "Thermal Theory of Ignition of Solid Propellants", J. of Physical and Colloid Chemistry 54, 872 (June, 1950).

71. Baer, A. D. and Ryan, N. W. "Ignition of Composite Propellants by Low Radiant Fluxes", AIAA Journal. Vol. 3, No. 5, May 1965, pp. 884-889.

72. Culick, F. E. C. "Calculation of the Admittance Function for a Burning Surface", Astronautica Acta, Vol. 13, No. 3 (1967) pp. 221-237.

73. Carslaw, H. S. and Jaeger, J. C. Conduction of Heat in Solids, Clarendon Press, 1959.

74. Millman, J., Vacuum-Tube and Semiconductor Electronics, McGraw-Hill, 1958.

75. Karplus, W. J. and Soroka, W. W., Analog Methods: Computation and Simulation, McGraw Hill, 1959.

76. Hartley, M. G. An Introduction to Electronic Analogue Computers, Methuen and Co., Ltd., London, 1962.

77. McKay, D. M. and Fisher, M. E. "Analogue Computing at Ultra High Speed, Chapman and Hall, Ltd., London, 1962.

78. Electronic Associates, Inc., Handbook of Analog Computation, 1964.

79. James, M. L., Smith, G. M., and Wolford, J. C., Analog and Digital Computer Methods, International Textbook Co., Scranton, Pennsylvania, 1964, pp. 1-126.

80. Steinz, J. A. , Stang, P.L., and Summerfield, M. "The Burning Mechanism of Ammonium Perchlorate-Based Solid Propellants", Princeton University Aerospace and Mechanical Sciences Report No. 830, (February 1959) p. 25.

81. Summerfield, M. and Krier, H. "Role of Aluminum in Suppressing Instability in Solid Propellant Rocket Motors", Problems of Hydrodynamics and Continuum Mechanics, Society for Industrial And Applied Mathematics, 1969, p. 703.

82. Zeleznik, F. J. and Gordon, S. "A General 704 or 7090 Computer Program for Computation of Chemical Equilibrium Compositions, Rocket Performance, and Chapman-Jouguet Detonations", NASA TN D-1454, (Oct. 1962).

83. Janaf Interim Themochemical Tables, Vol. I U. S. Air Force Contract No. AF33(616)-6149 Dow Chemical Company, Midland, Michigan (December 1960).

84. Syrkin, Y.K. and Dyatkina, M.E. Structure of Molecules and The Chemical Bond, Intersciences Publishers, New York, 1950, pp. 237-261

85. Shorr, M. and Zaehringer, A. J. Solid Rocket Technology, Wiley and Sons, 1967, Chapter 2.

86. Flory, P. J. Principles of Polymer Chemistry, Cornell University Press, Ithaca, 1953.

TABLE I

COMPOSITION AND BURNING RATE DATA OF TESTED PROPELLANTS

Propellant Batch No.	Propellant Composition			Burning Rate Constants		Burning Rate at 1000 psia (in./sec.)	Burning Rate Index "n" at 1000 psia	Calculated Flame Temperature at 1000 psia
	% AP	% Fuel % Binder	% Al	A	B			
944	82.5	17.5 PBAA	0.0	.22	2.78	.30	.24	2625°K
941	80.0	20.0	0.0	.20	2.35	.29	.28	2430
945	77.5	22.5	0.0	.13	2.21	.25	.26	2175
949	75.0	25.0	0.0	.08	1.92	.22	.27	1840
951	75.0 (45μ)	25.0	0.0	.08	1.71	.35	.45	1840
958	75.0 (80μ)	25.0	0.0	.16	1.68	.29	.43	1840
955	75.0 (180μ)	25.0	0.0	.20	1.64	.26	.33	1840
966	80.0	20.0 PBCT	0.0	.21	2.32	.29	.41	2355
970	80.0	20.0 PU	0.0	A and B could not be determined		.18	-.43	2710
960	71.7	20.8 PBAA	7.5	.13	2.37	.26	.25	2630
961	65.9	19.1	15.0	.07	1.82	.24	.25	2990

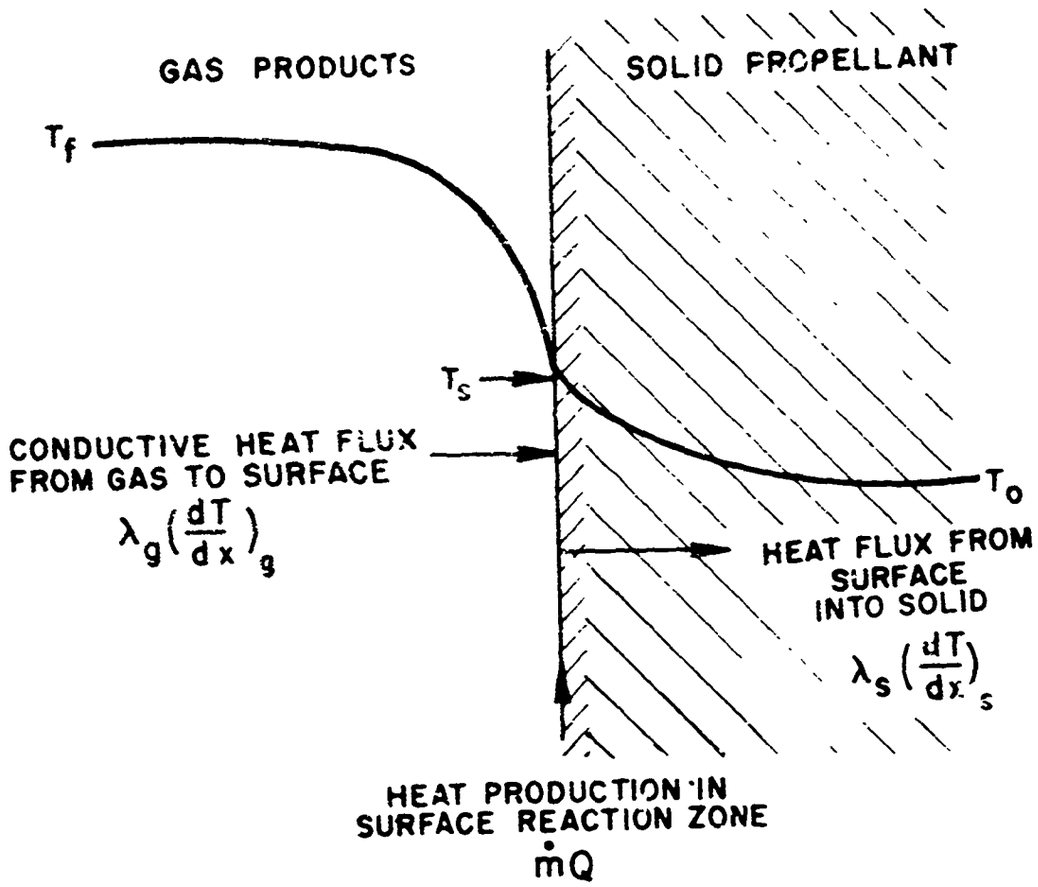

$$\lambda_g \left(\frac{dT}{dx}\right)_g = \lambda_s \left(\frac{dT}{dx}\right)_s - \dot{m}Q$$

ONE DIMENSIONAL ENERGY BALANCE AT SURFACE OF BURNING SOLID PROPELLANT

JP 19 R 4253

FIGURE 1

TWO-STAGE GRANULAR DIFFUSION FLAME MODEL FOR AMMONIUM PERCHLORATE-TYPE COMPOSITE SOLID PROPELLANTS

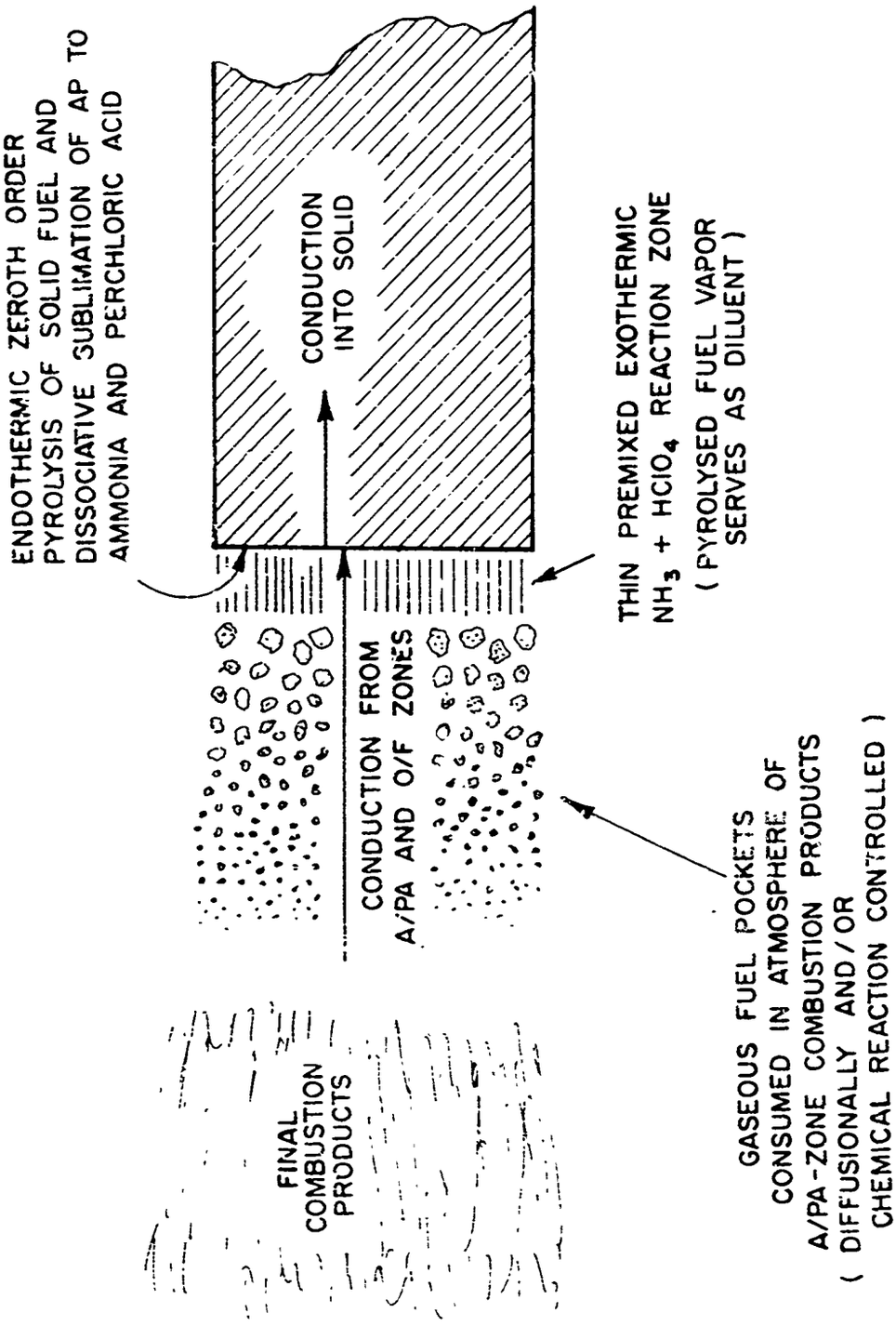

JP 19 2 4254 63

FIGURE 2

STEADY STATE TEMPERATURE PROFILE
INSIDE BURNING SOLID PROPELLANT; EFFECT
OF COLD BOUNDARY CONDITION ON
STEADY STATE SOLUTION

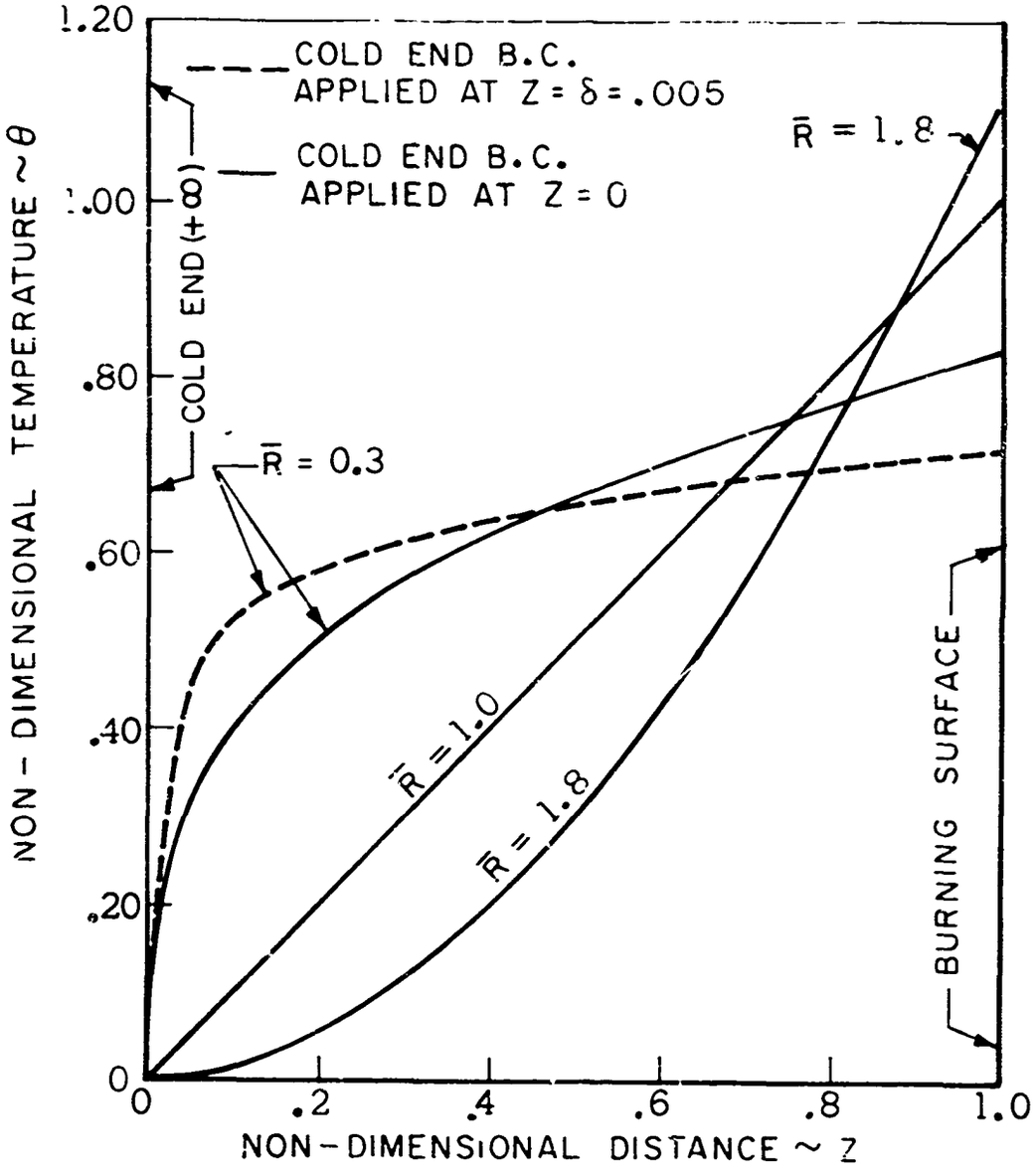

FIGURE 3

JF 19 K 4755 .J

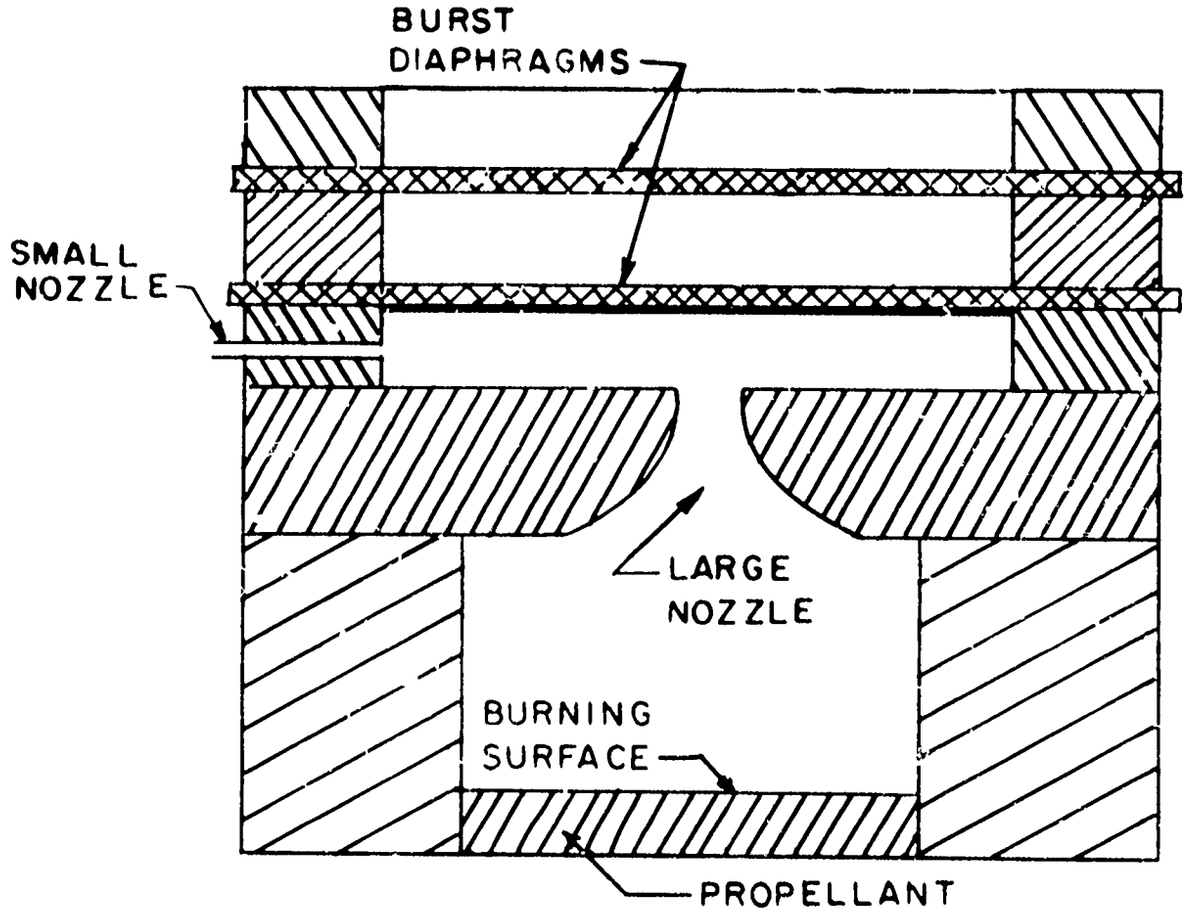

VARIABLE AREA COMBUSTOR
FOR DEPRESSURIZATION TESTS

FIGURE 4

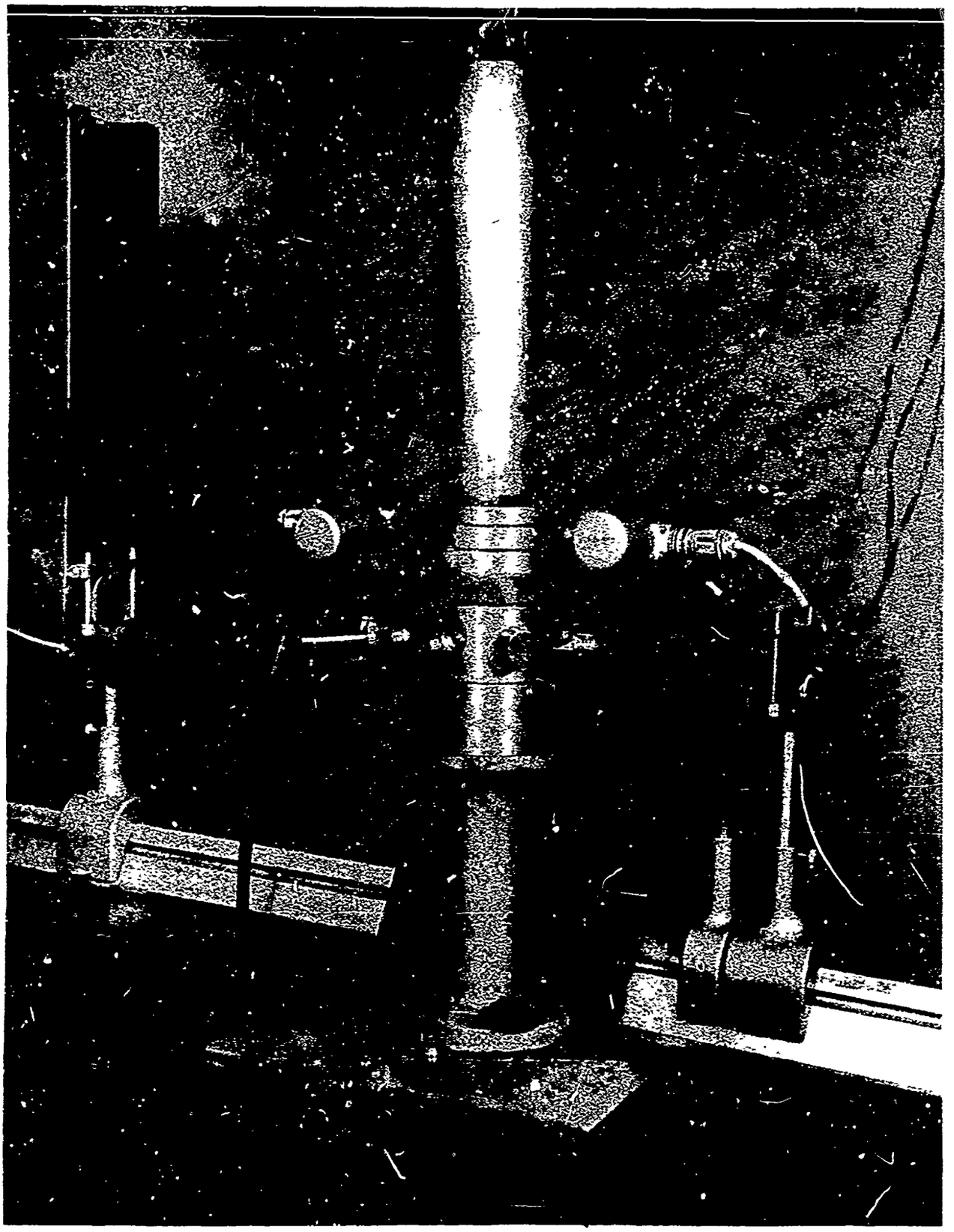

PHOTOGRAPH OF ASSEMBLED COMBUSTOR USED FOR DEPRESSURIZATION TESTS

FIGURE 5

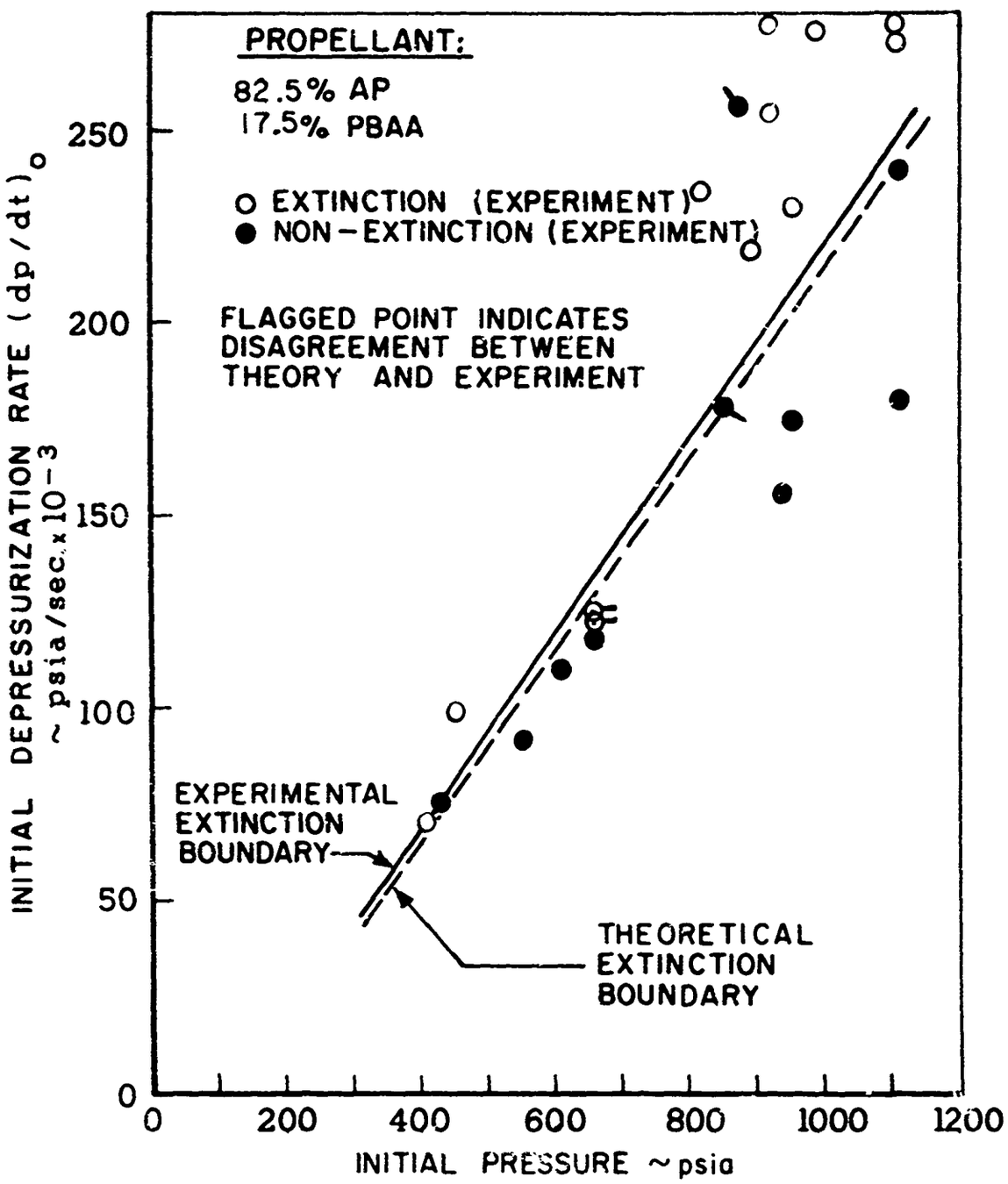

FIGURE 6 REQUIRED DEPRESSURIZATION RATE FOR EXTINCTION EXPERIMENTAL AND THEORETICAL RESULTS 82.5/17.5 - PBAA PROPELLANT

JP 19 R 4257 69

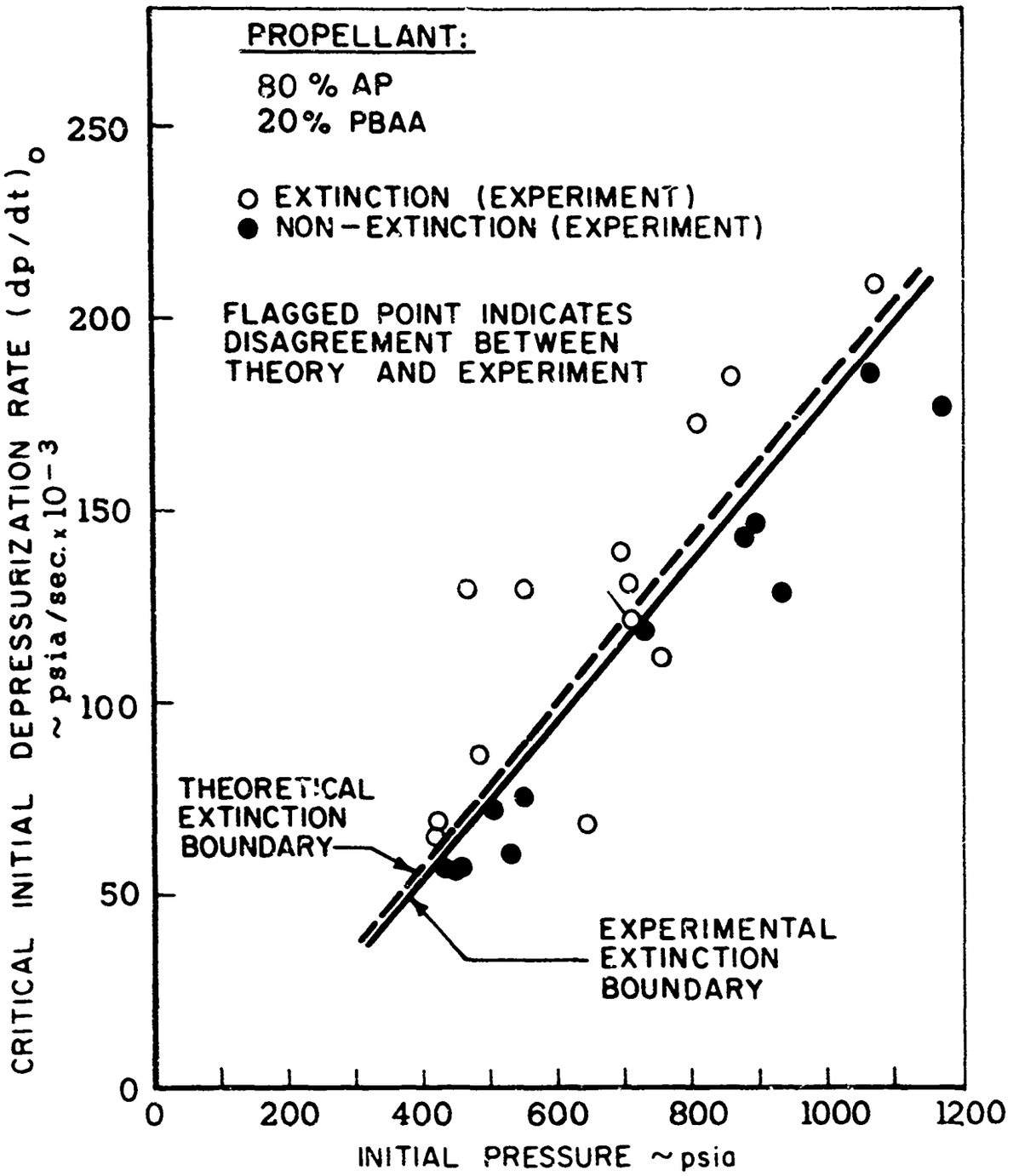

REQUIRED DEPRESSURIZATION RATE FOR EXTINCTION
EXPERIMENTAL AND THEORETICAL RESULTS
80.0/20.0 - PBAA PROPELLANT

FIGURE 7

JP 19 R 409 1-69

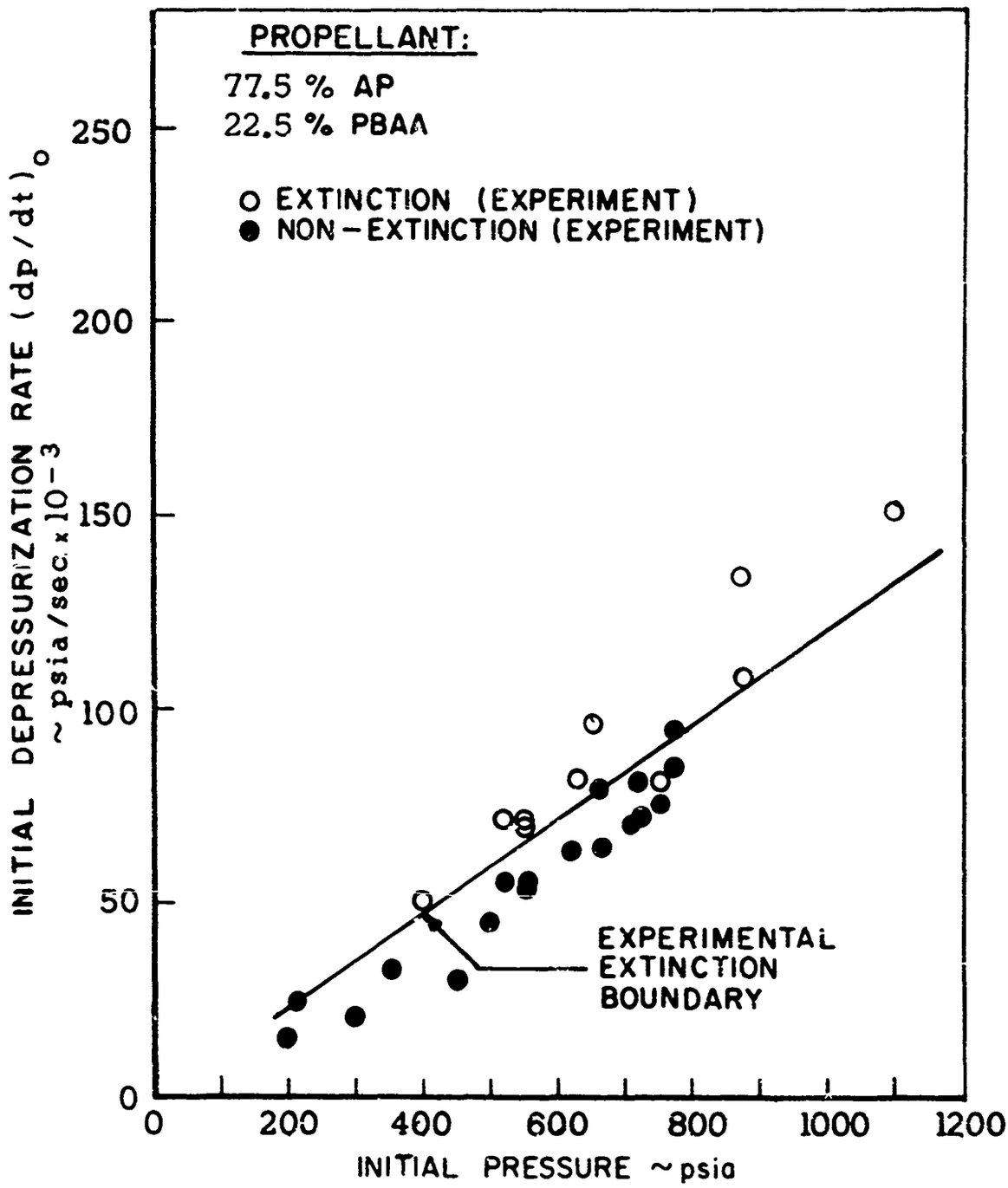

FIGURE 8 REQUIRED DEPRESSURIZATION RATE FOR EXTINCTION
EXPERIMENTAL RESULTS
77.5/22.5 - PBAA PROPELLANT

JP19 R 4258 69

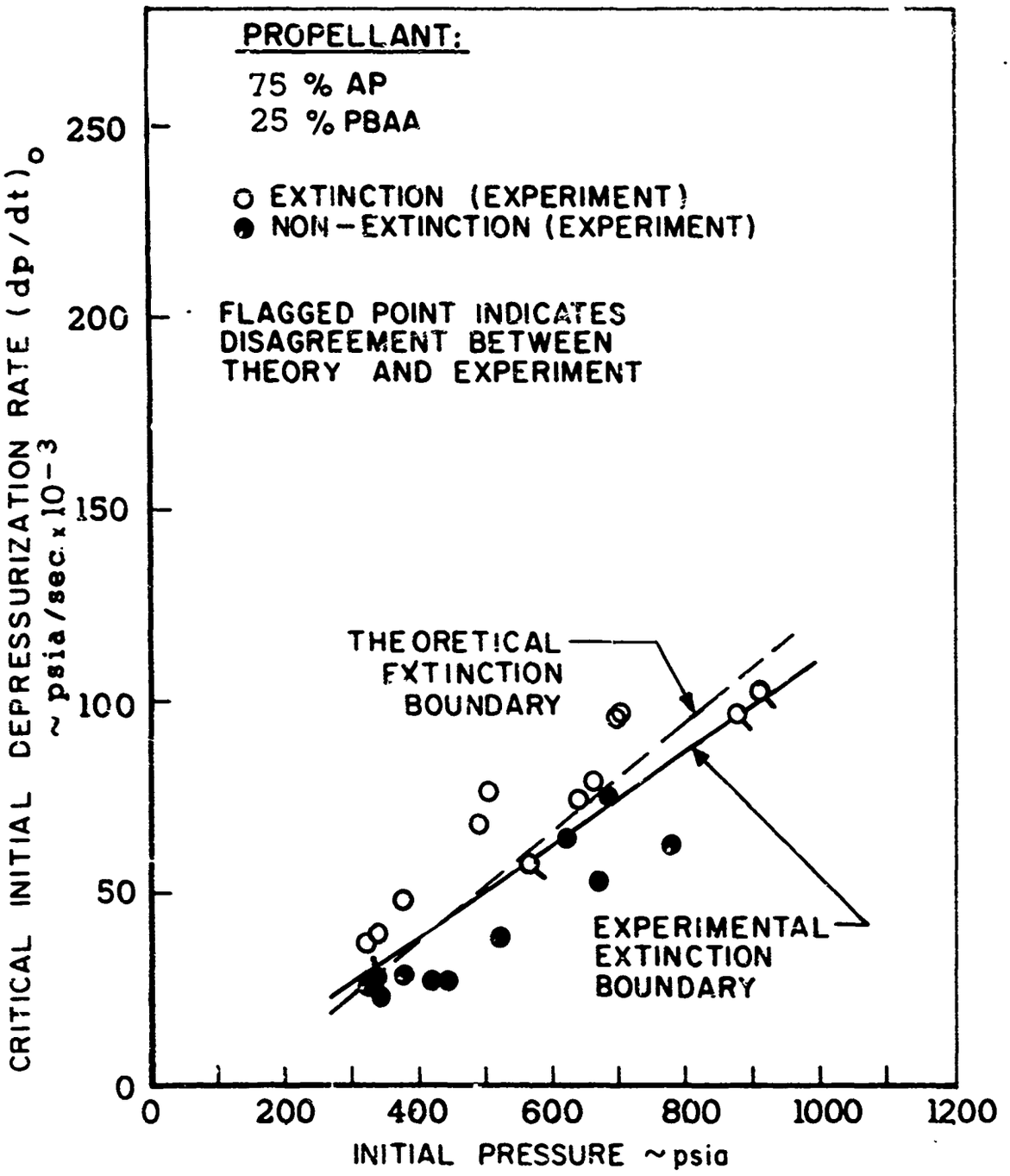

REQUIRED DEPRESSURIZATION RATE FOR EXTINCTION
EXPERIMENTAL AND THEORETICAL RESULTS
75/25 - PBAA PROPELLANT

FIGURE 9

JP 19 R 4259 69

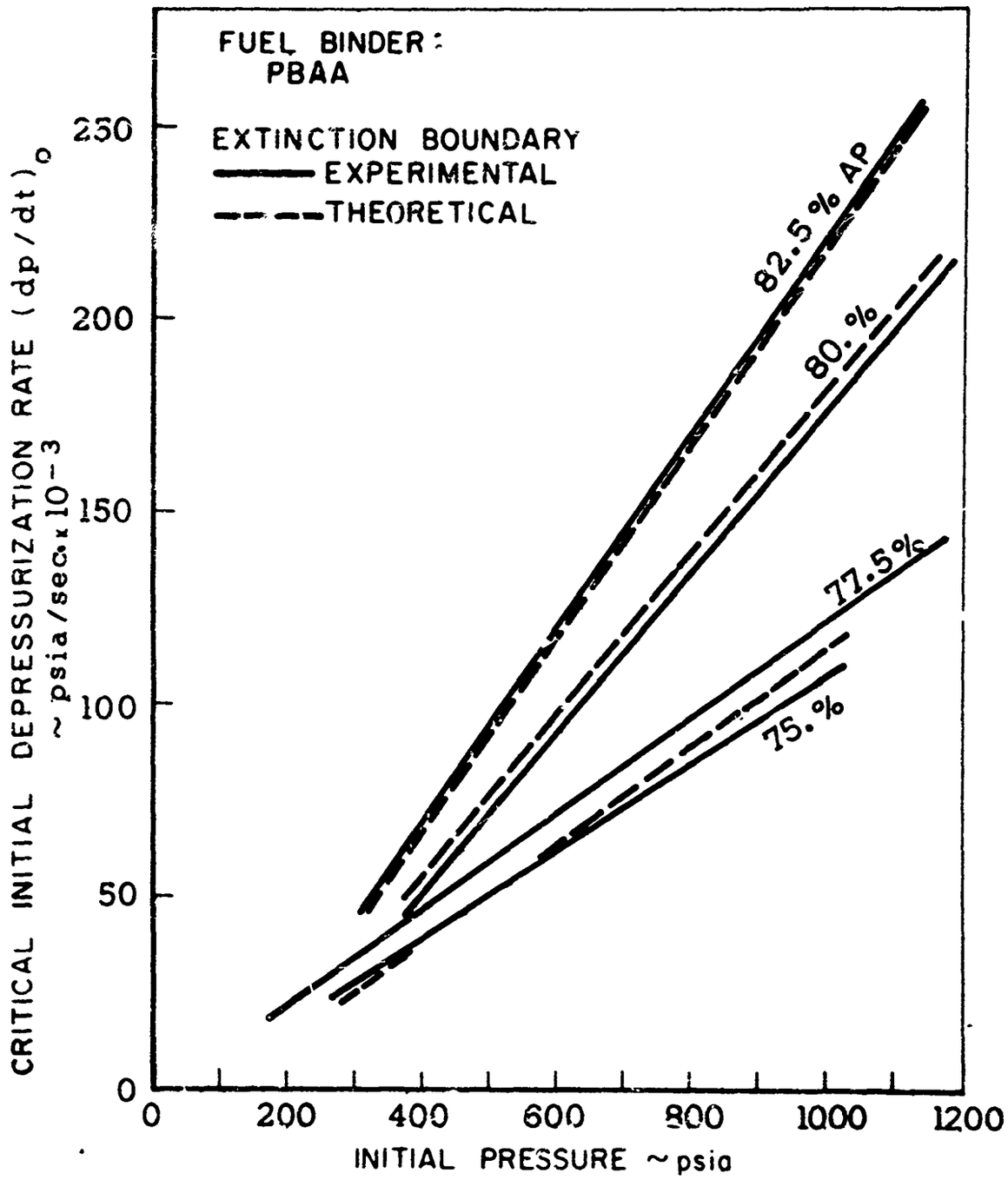

FIGURE 10 REQUIRED DEPRESSURIZATION RATE FOR EXTINCTION
EXPERIMENTAL AND THEORETICAL RESULTS
EFFECT OF PROPELLANT OXIDIZER LOADING

JPL R 4093 - 69

FIGURE 10

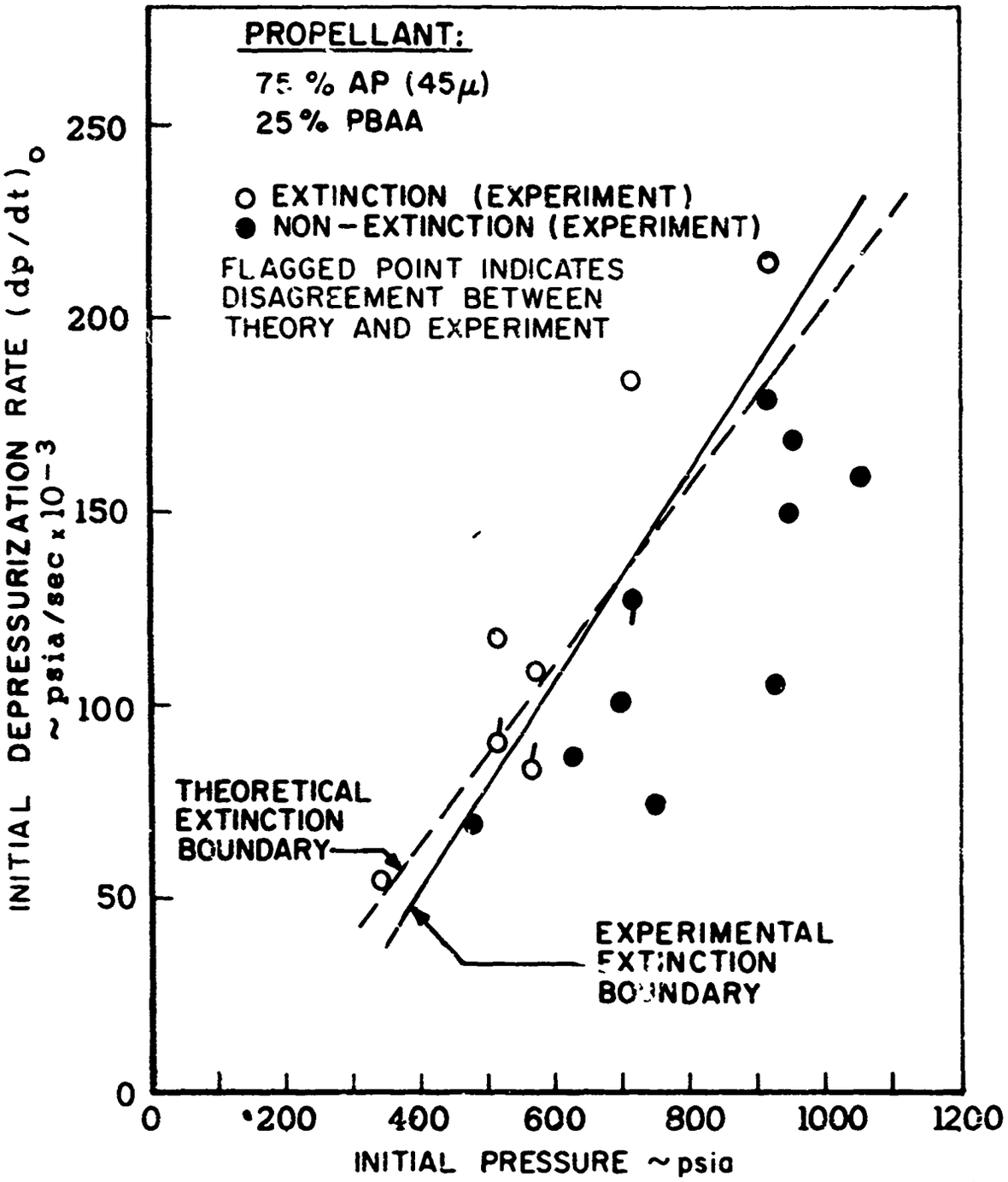

REQUIRED DEPRESSURIZATION RATE FOR EXTINCTION
EXPERIMENTAL AND THEORETICAL RESULTS
45μ AP PARTICLE SIZE

FIGURE 11

JP 19 R 4260 69

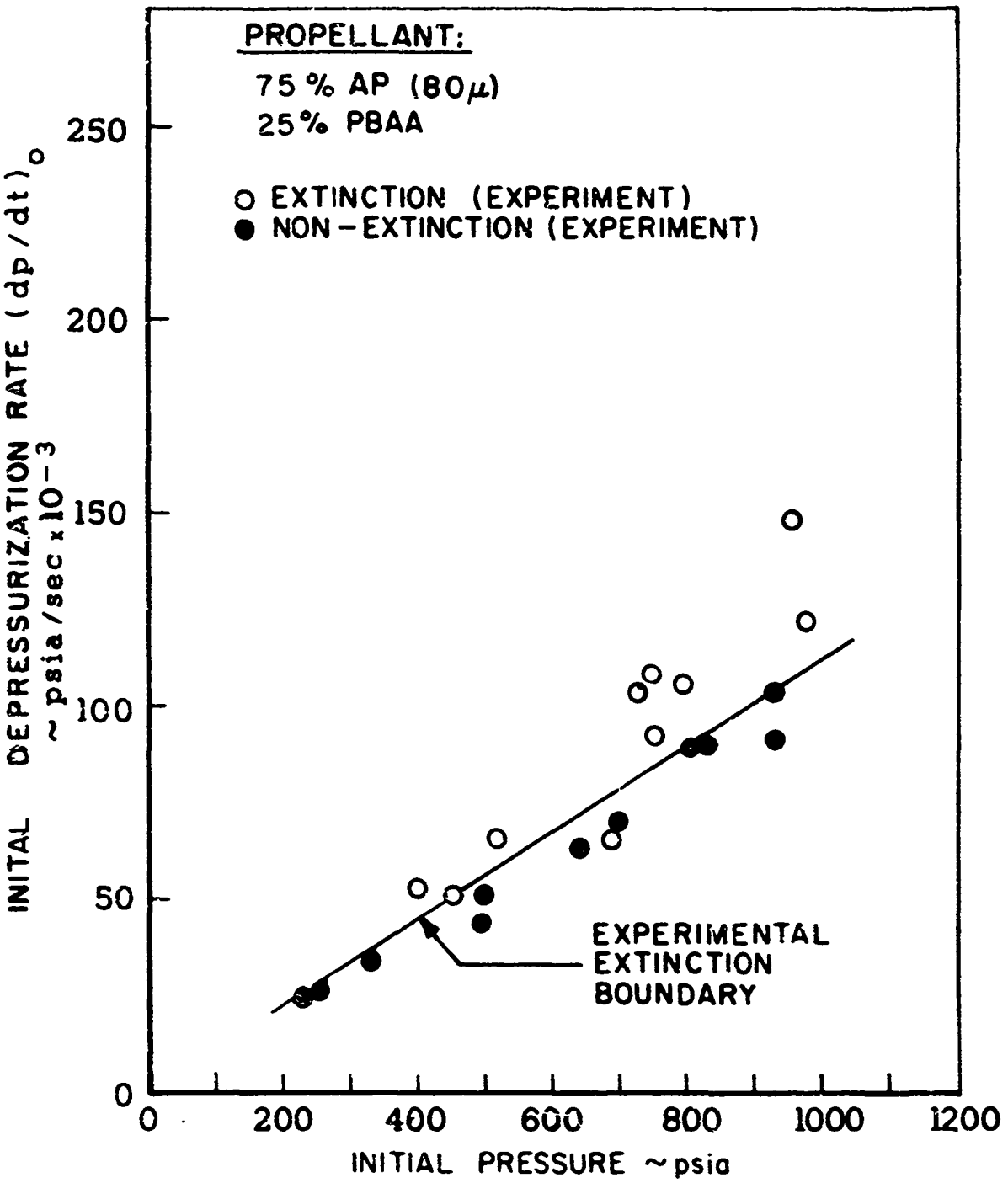

FIGURE 12 REQUIRED DEPRESSURIZATION RATE FOR EXTINCTION
EXPERIMENTAL RESULTS
80μ AP PARTICLE SIZE

JP 19 R 4261 69

FIGURE 12

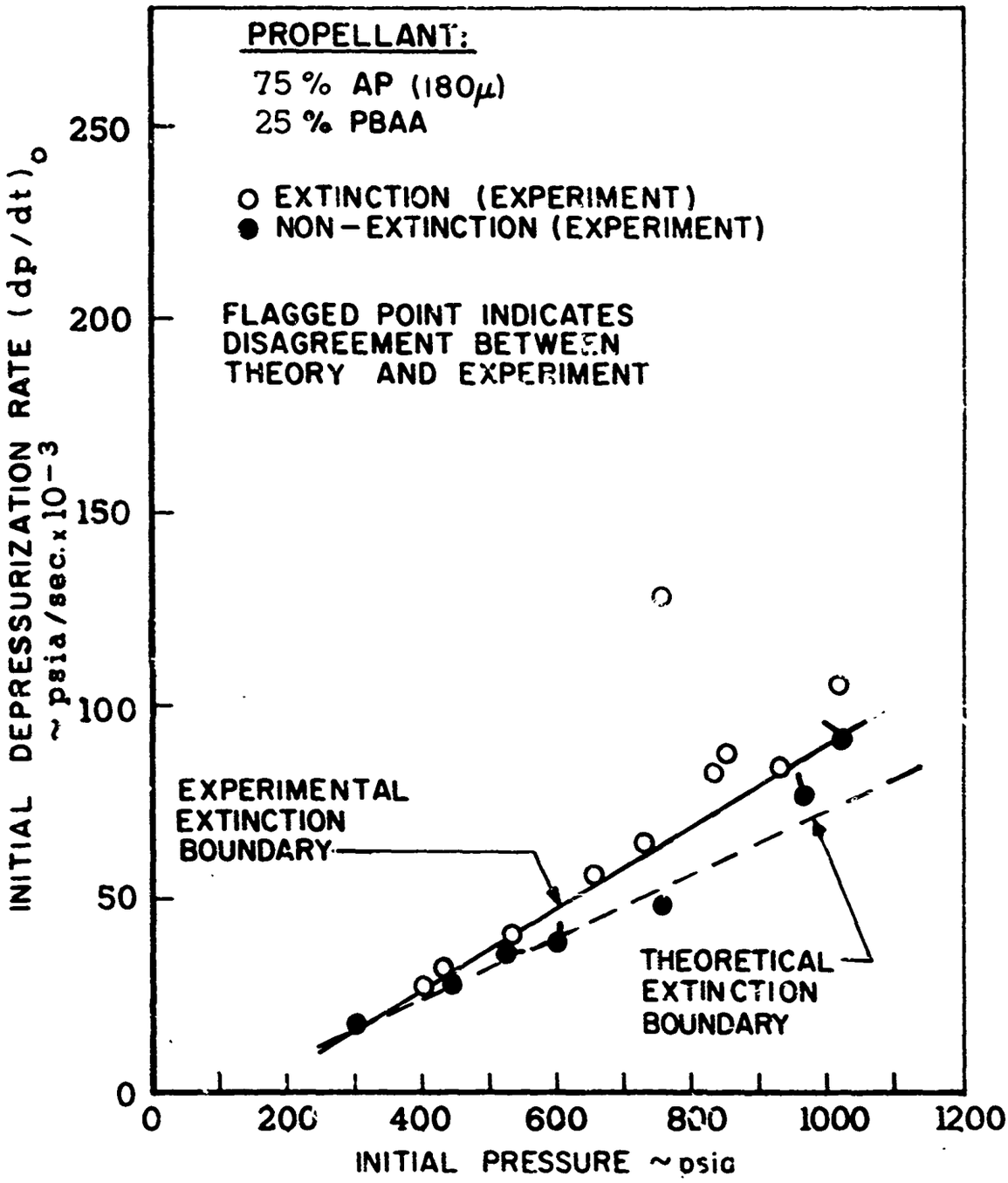

REQUIRED DEPRESSURIZATION RATE FOR EXTINCTION
EXPERIMENTAL AND THEORETICAL RESULTS
180μ AP PARTICLE SIZE

JP 19 R 4262 69

FIGURE 13

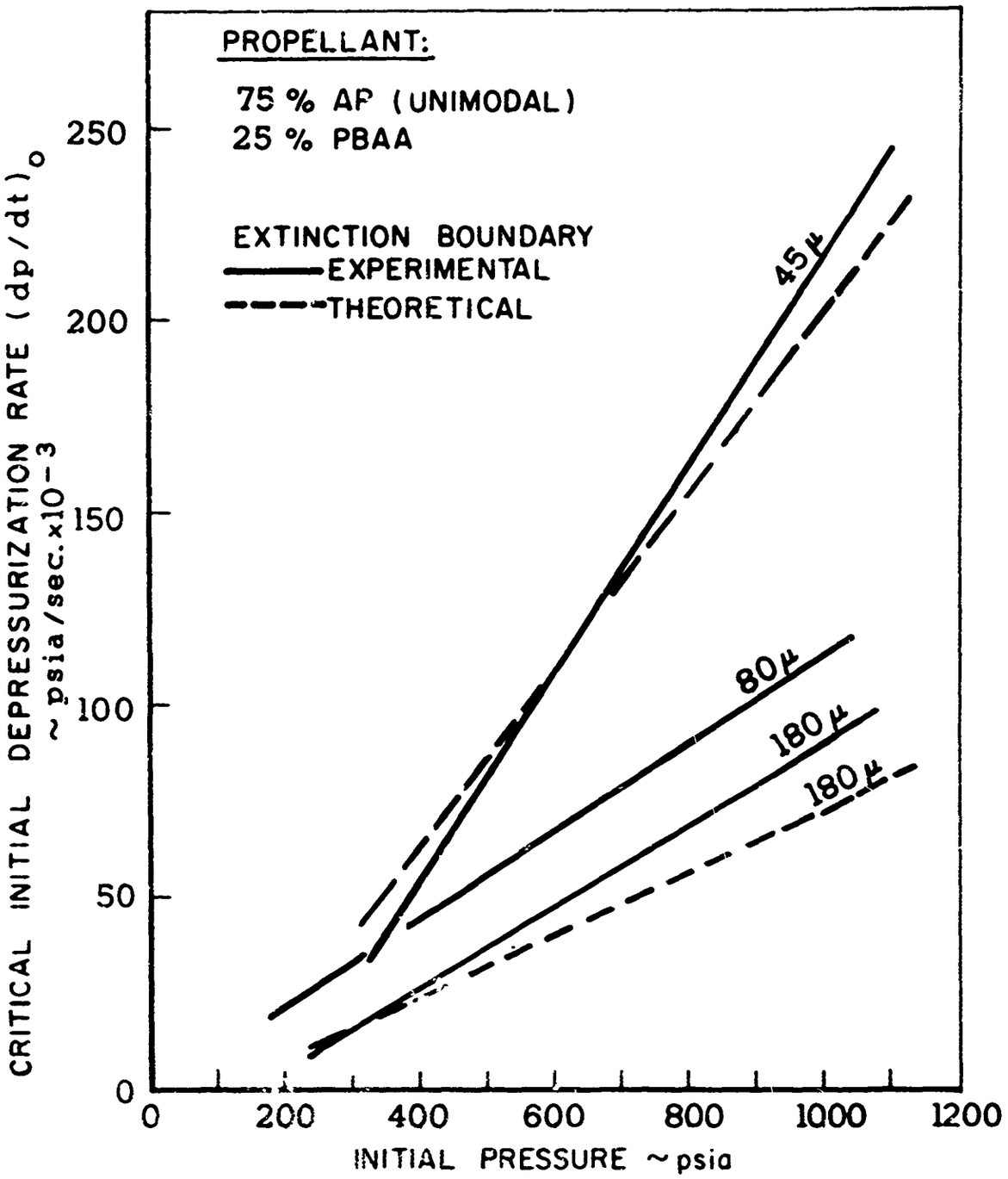

FIGURE 14 REQUIRED DEPRESSURIZATION RATE FOR EXTINCTION
EXPERIMENTAL AND THEORETICAL RESULTS
EFFECT OF OXIDIZER PARTICLE SIZE

JP 19 R 4092 - 69

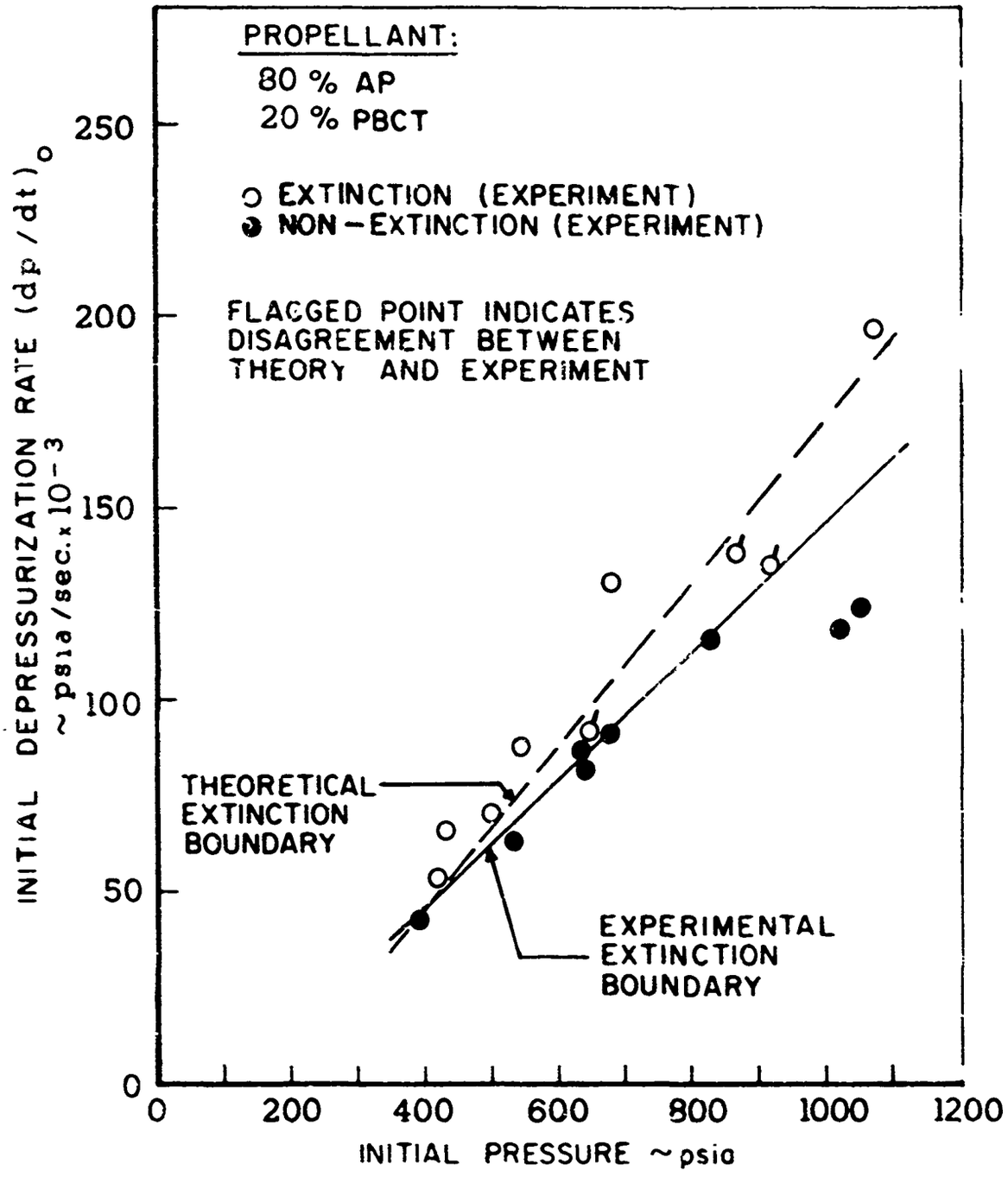

REQUIRED DEPRESSURIZATION RATE FOR EXTINCTION
EXPERIMENTAL AND THEORETICAL RESULTS
PBCT FUEL BINDER

FIGURE 15

JP 19 R 4263 69

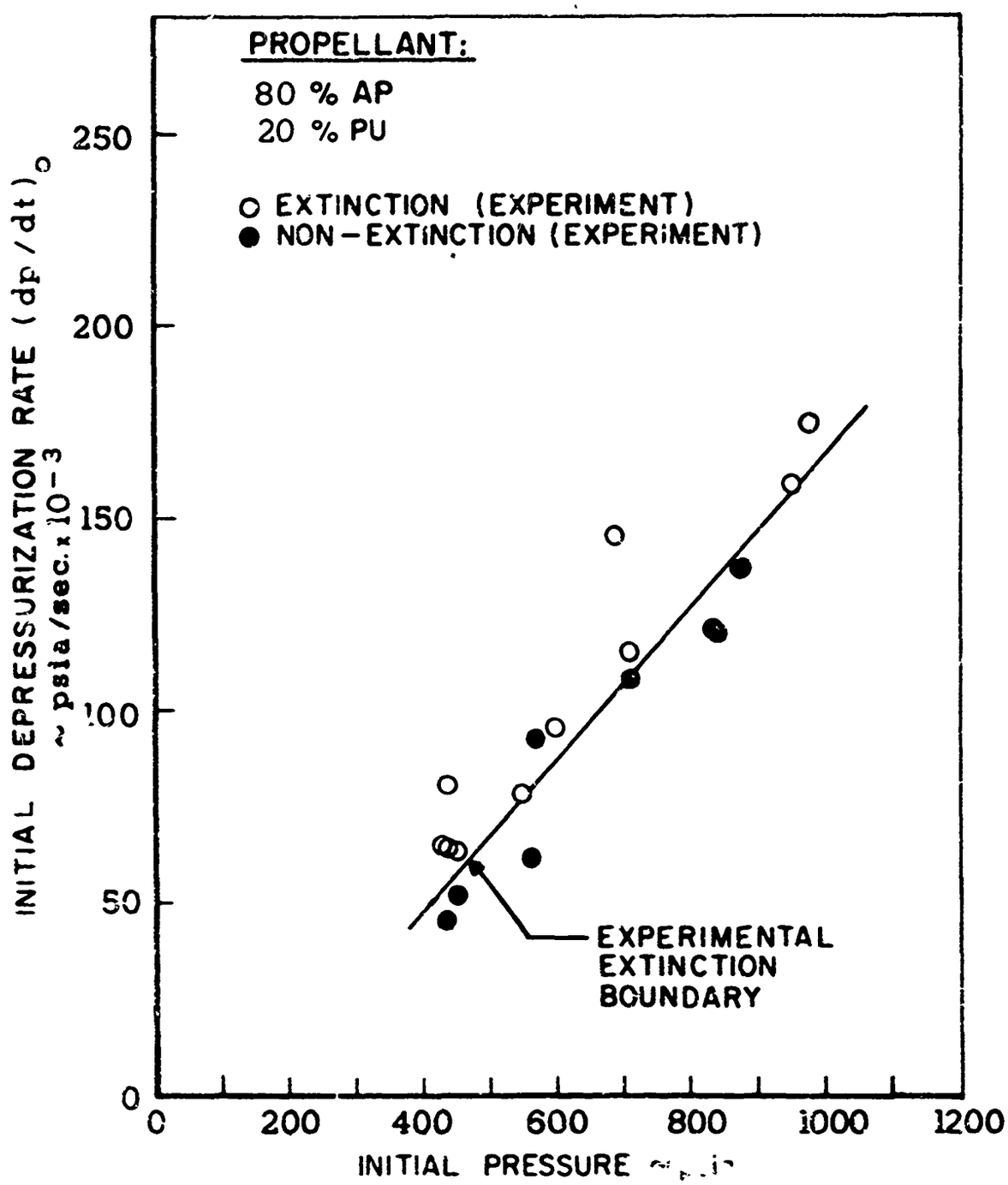

FIGURE 16 REQUIRED DEPRESSURIZATION RATE FOR EXTINCTION
EXPERIMENTAL RESULTS
POLYURETHANE FUEL BINDER

JP19R4264 69

FIGURE 16

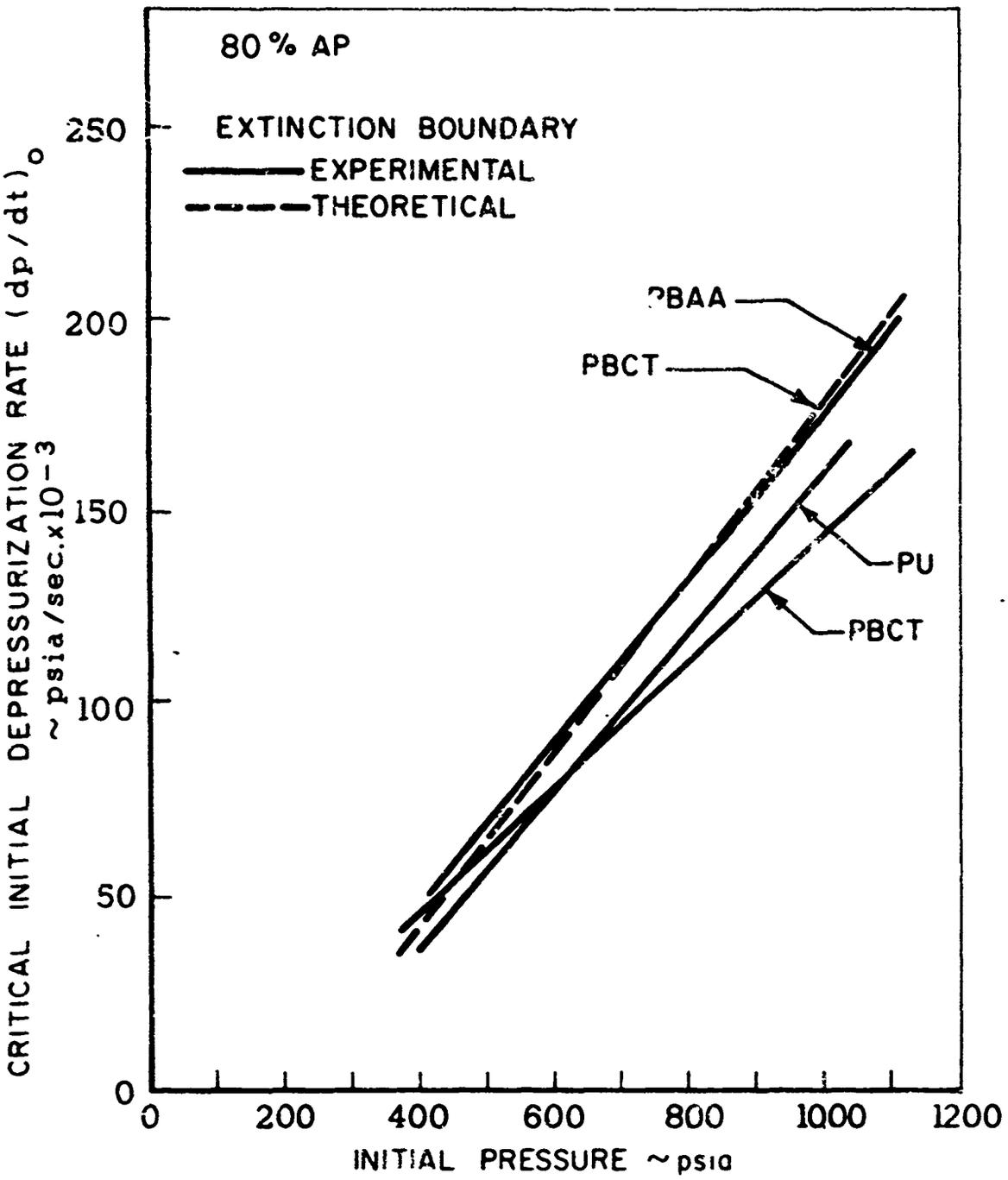

REQUIRED DEPRESSURIZATION RATE FOR EXTINCTION
EXPERIMENTAL AND THEORETICAL RESULTS
EFFECT OF FUEL TYPE

JP 19 R 4094-69

FIGURE 17

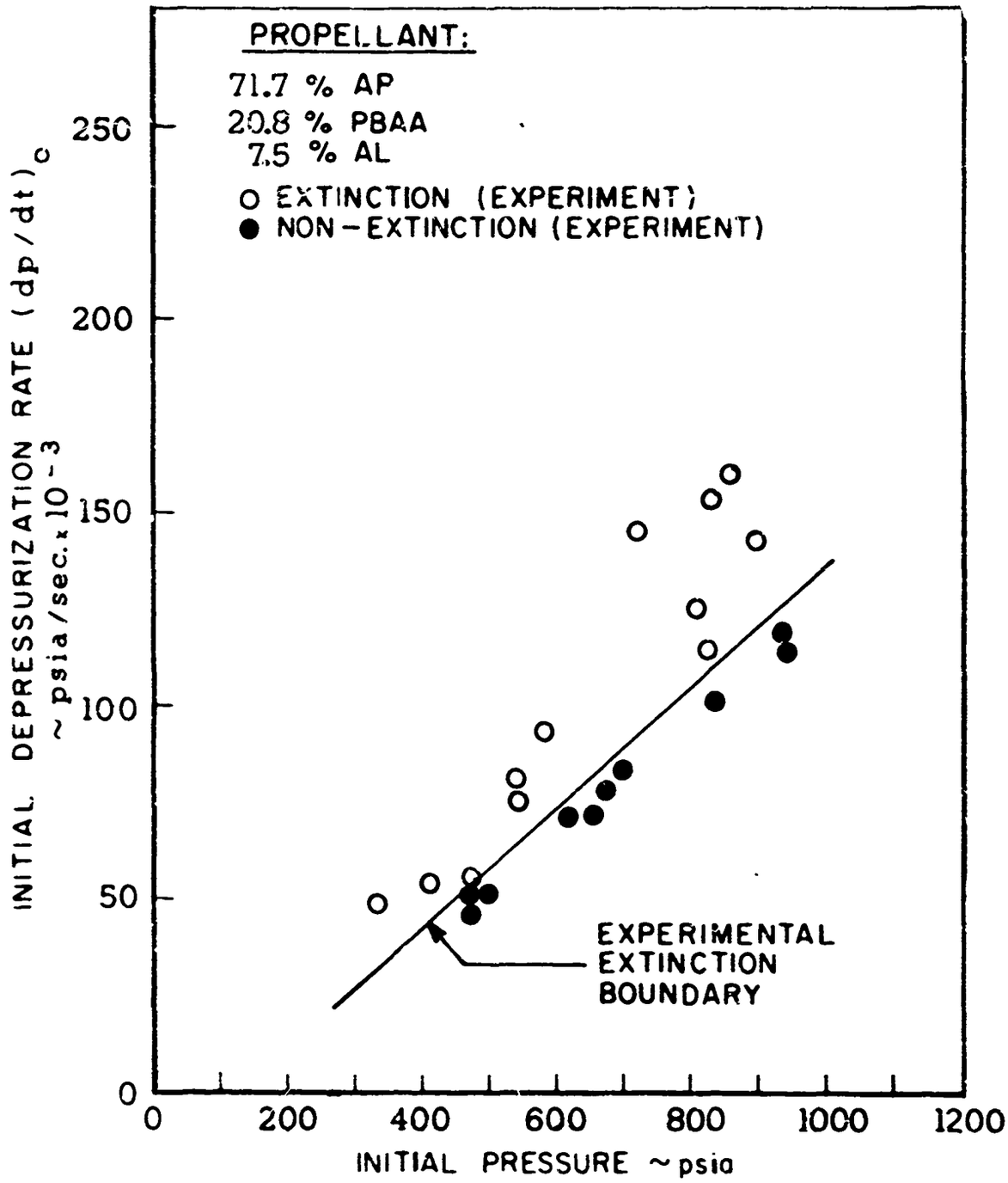

FIGURE 18 REQUIRED DEPRESSURIZATION RATE FOR EXTINCTION
EXPERIMENTAL RESULTS
7.5% ALUMINUM

JPIS R 4265 69

FIGURE 18

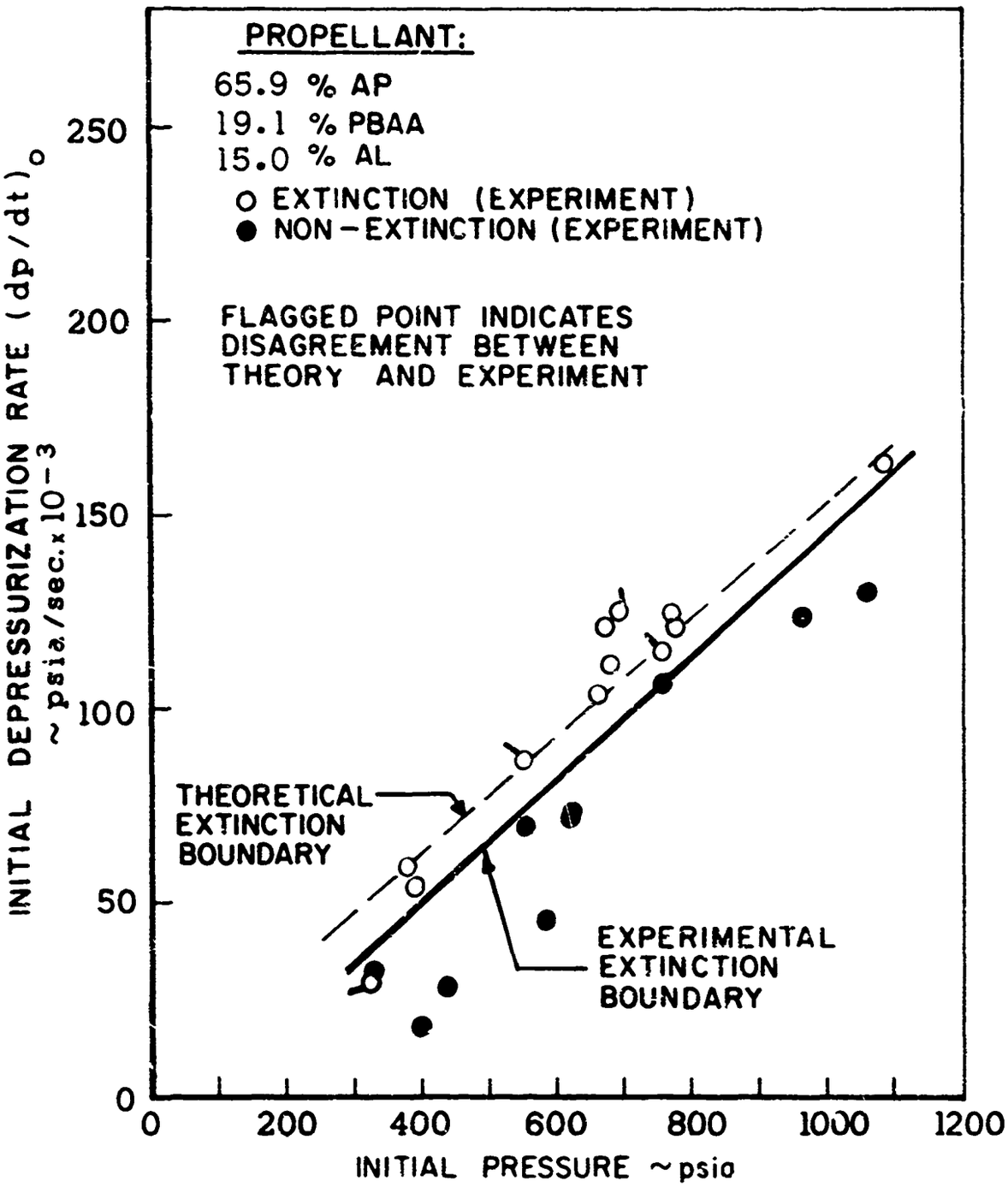

REQUIRED DEPRESSURIZATION RATE FOR EXTINCTION
EXPERIMENTAL AND THEORETICAL RESULTS
15% ALUMINUM

FIGURE 19

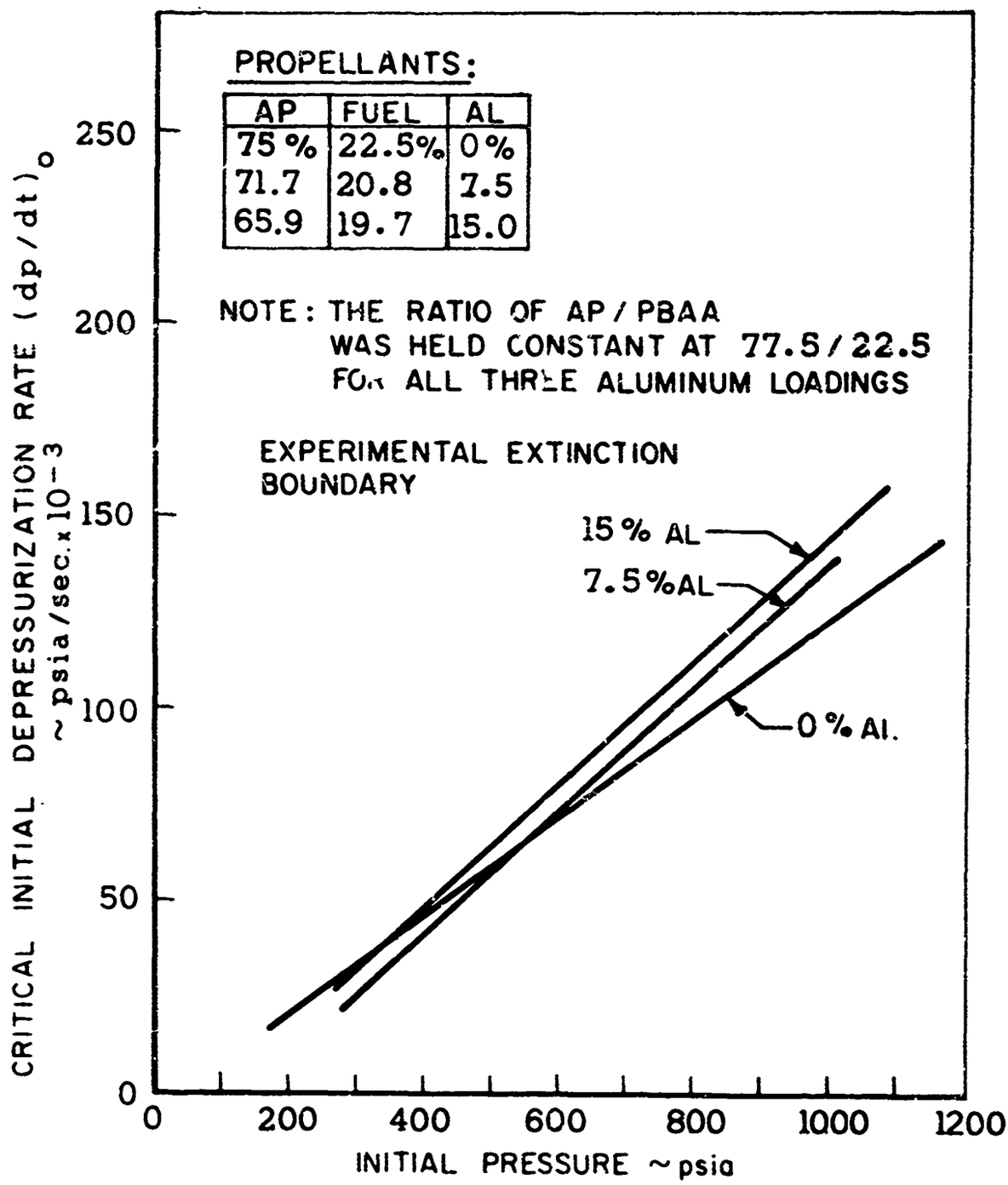

FIGURE 20 REQUIRED DEPRESSURIZATION RATE FOR EXTINCTION
EXPERIMENTAL RESULTS
EFFECT OF ALUMINUM ADDITION

JP 19 X 4090 - 6.5

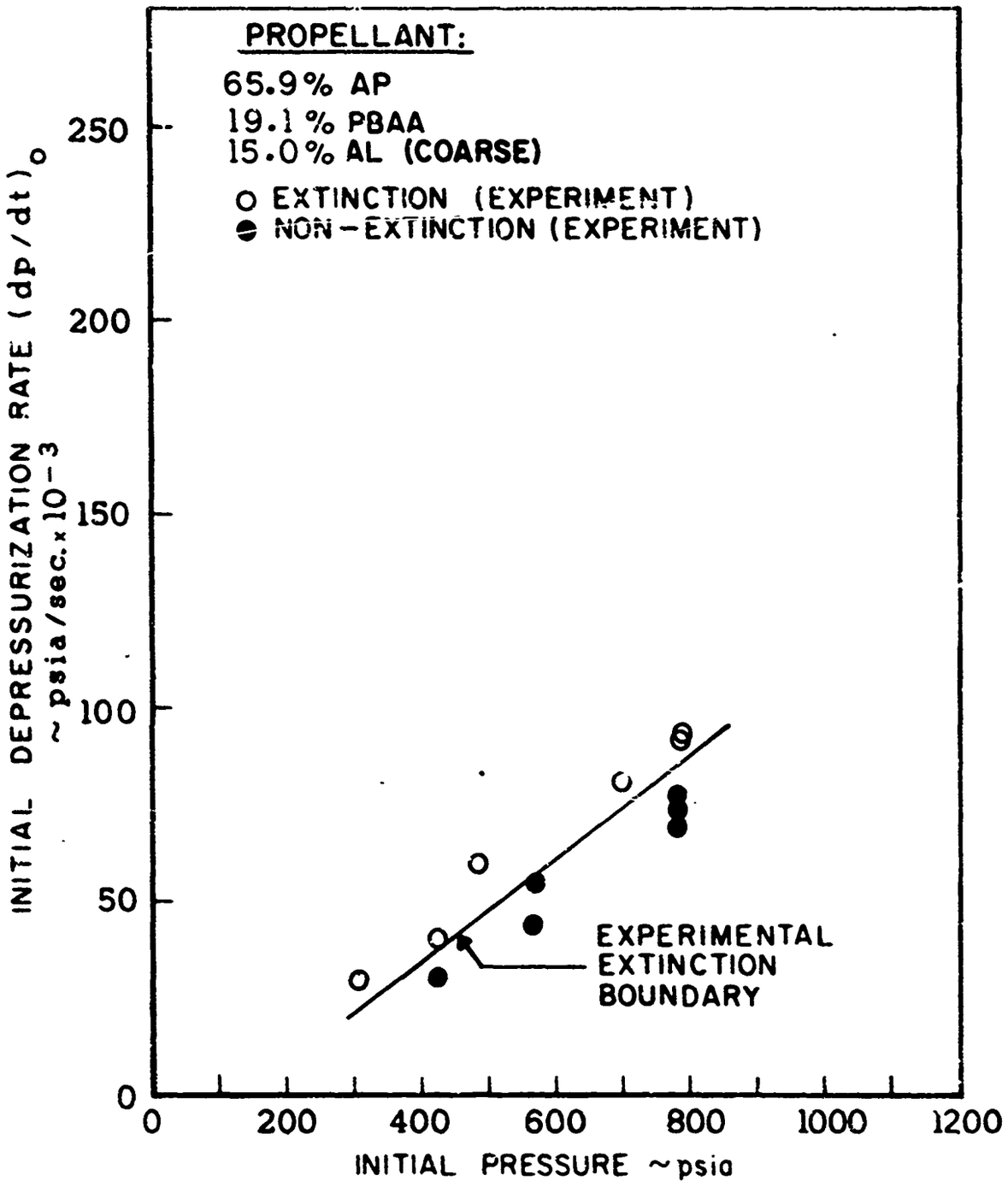

REQUIRED DEPRESSURIZATION RATE FOR EXTINCTION
EXPERIMENTAL RESULTS
FOR A PROPELLANT CONTAINING COARSE ALUMINUM

FIGURE 21

JP 19 R 4267 69

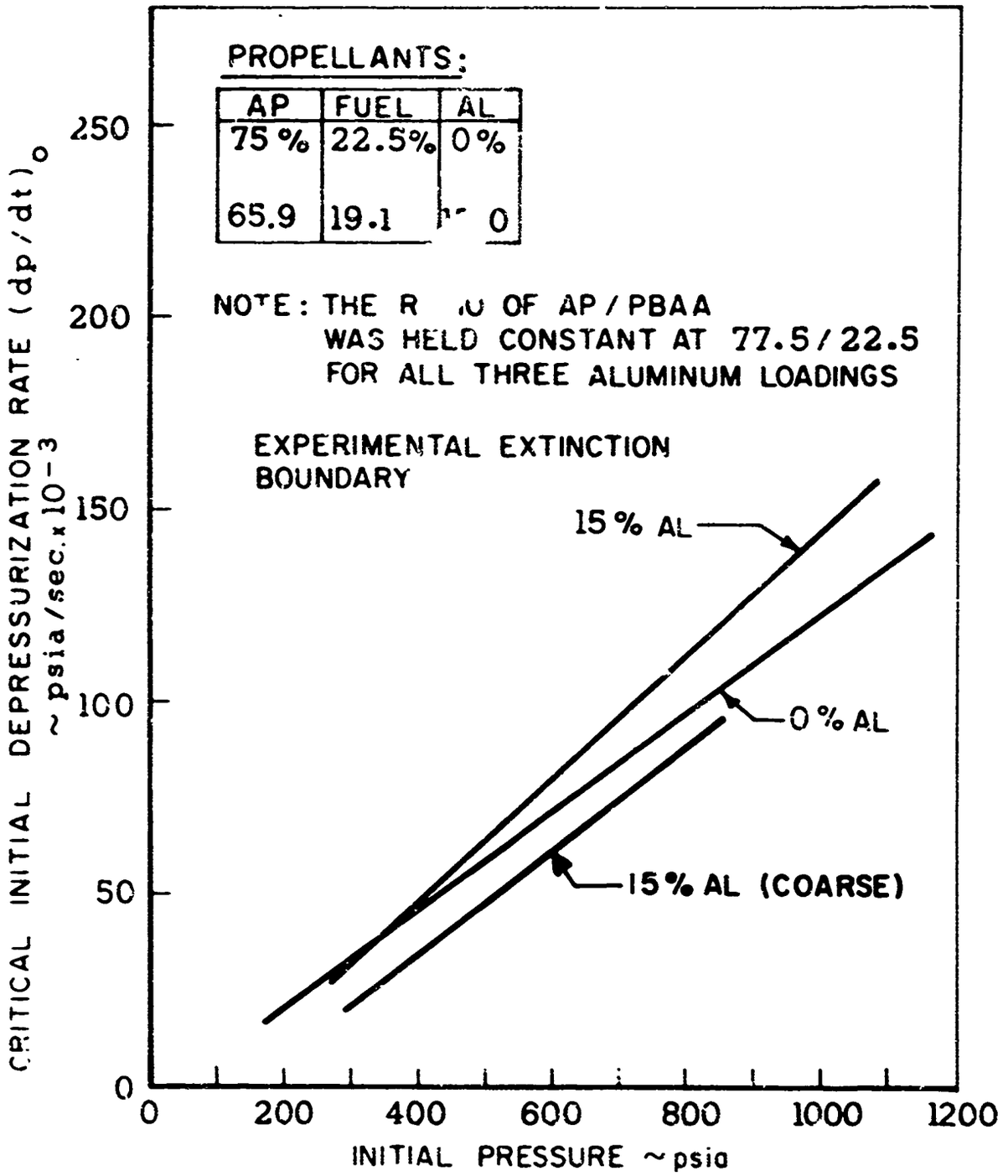

FIGURE 22 REQUIRED DEPRESSURIZATION RATE FOR EXTINCTION
EXPERIMENTAL RESULTS
EFFECT OF ALUMINUM PARTICLE SIZE

JP 19 R 4268 69

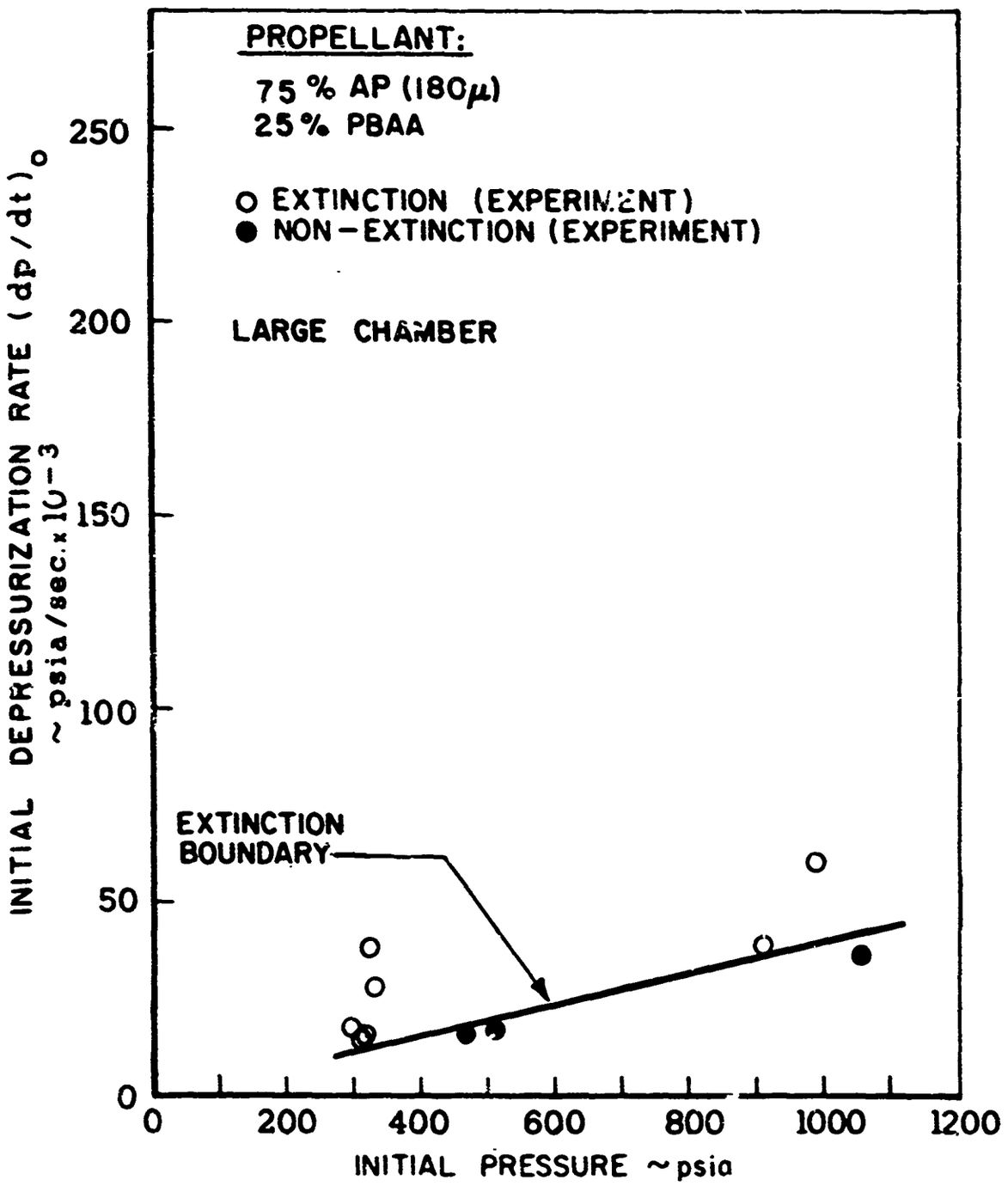

REQUIRED DEPRESSURIZATION RATE FOR EXTINCTION
EXPERIMENTAL RESULTS
FOR LARGE CHAMBER

FIGURE 23

JPL R 4269 69

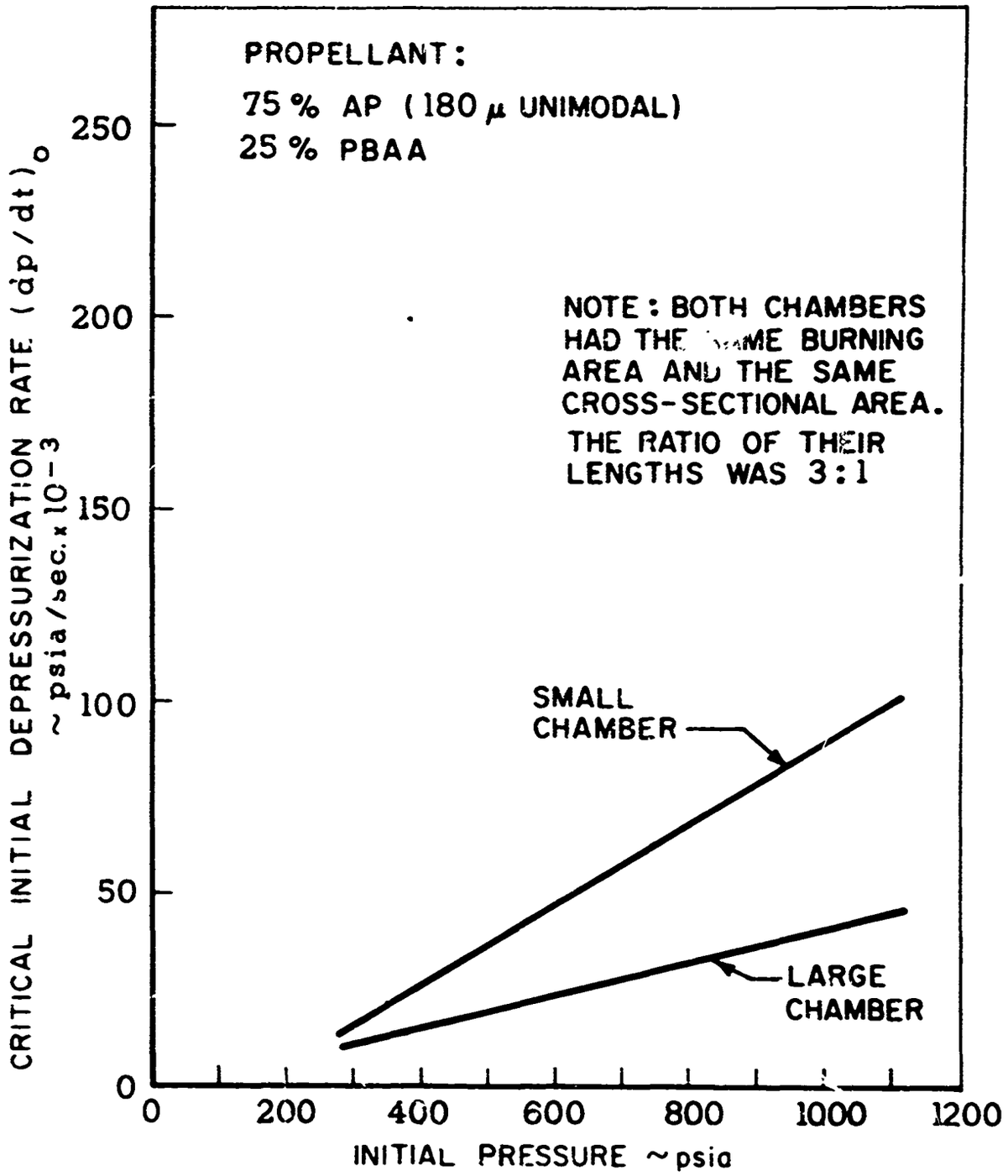

FIGURE 24 REQUIRED DEPRESSURIZATION RATE FOR EXTINCTION
EXPERIMENTAL RESULTS
EFFECT OF CHAMBER GEOMETRY

JP 19 R 4089-69

FIGURE 25

STEADY STATE BURNING RATE DATA:
EFFECT OF OXIDIZER LOADING

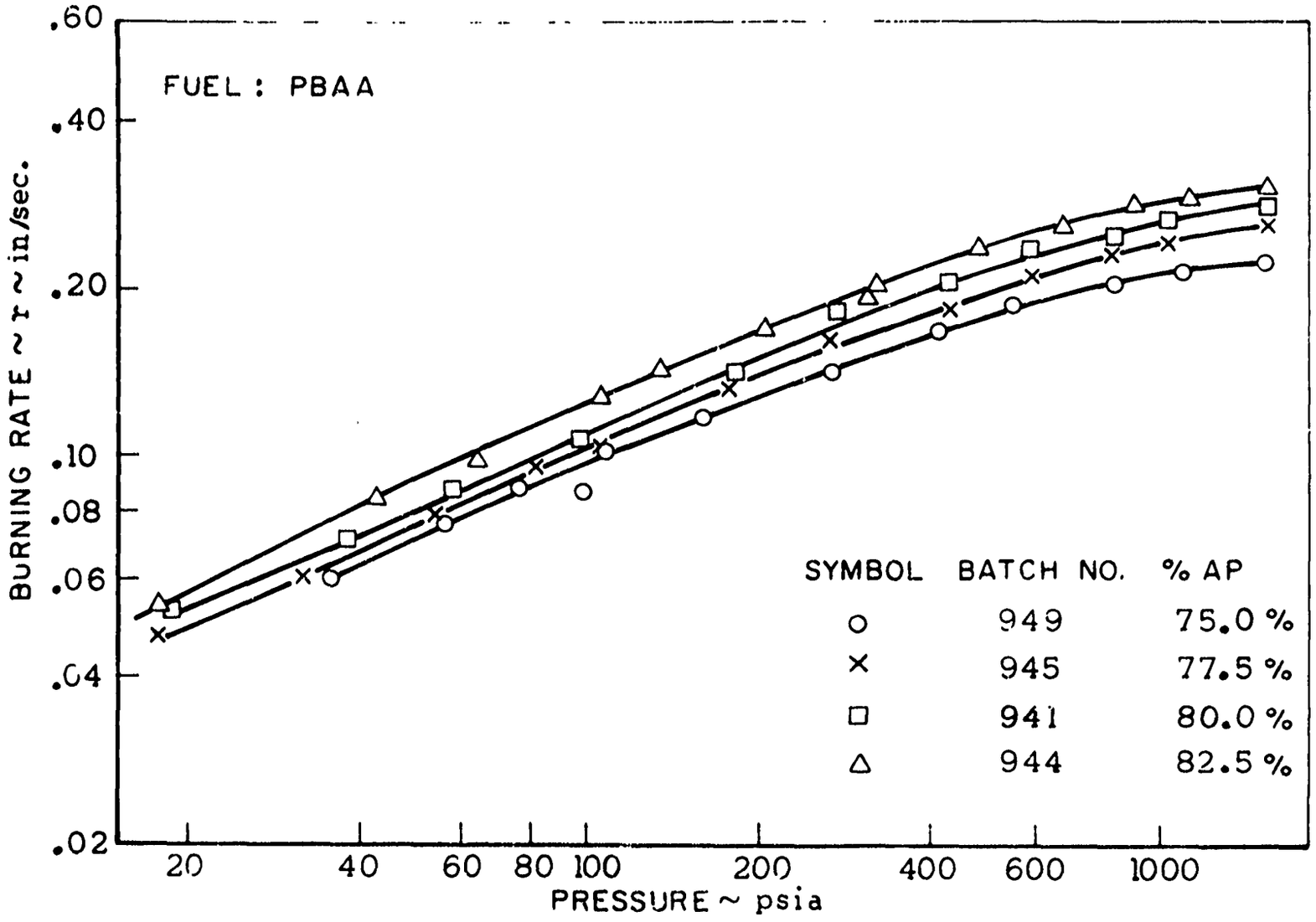

STEADY STATE BURNING RATE DATA:
EFFECT OF PARTICLE SIZE

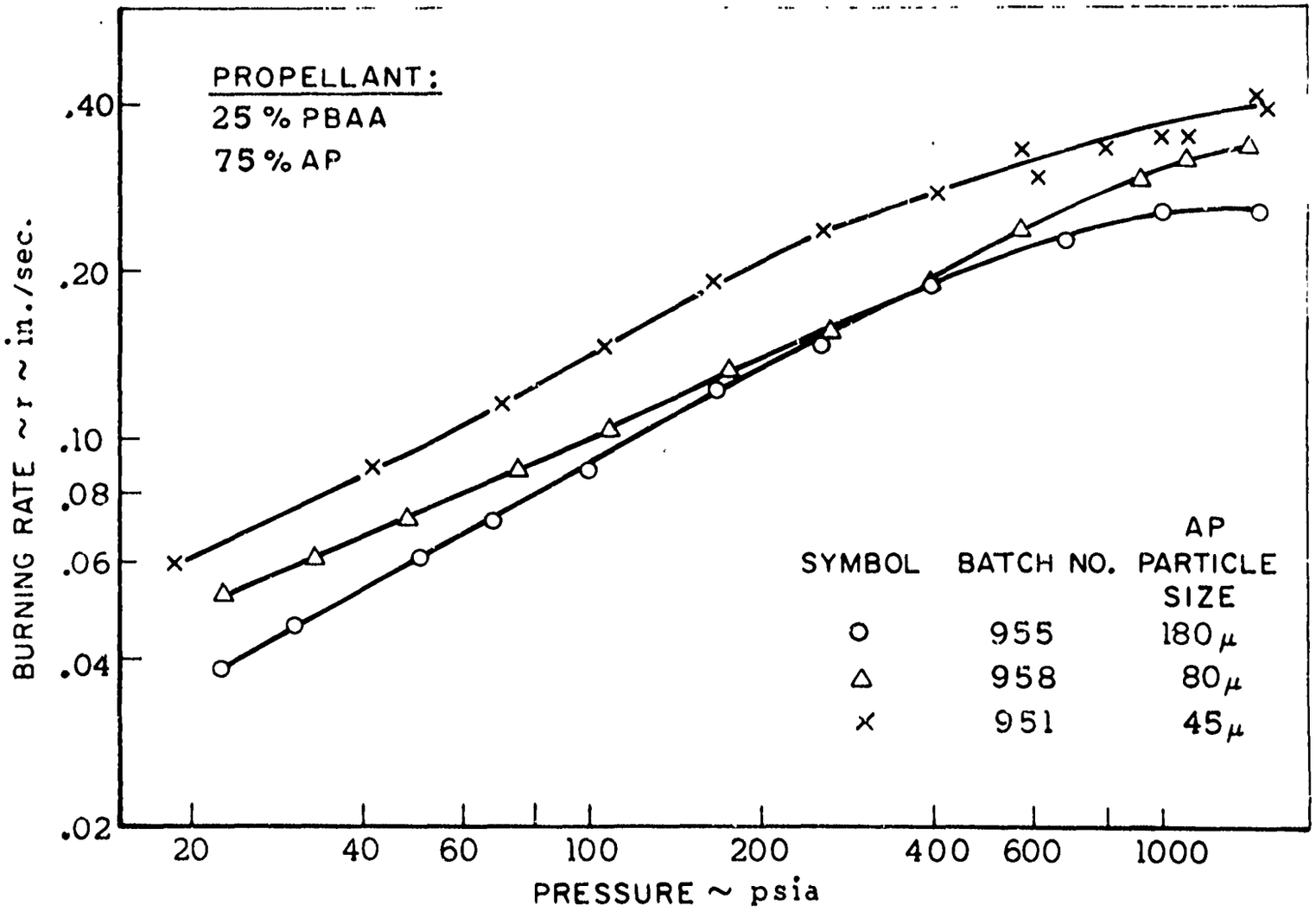

FIGURE 26

STEADY STATE BURNING RATE DATA:
EFFECT OF FUEL BINDER TYPE

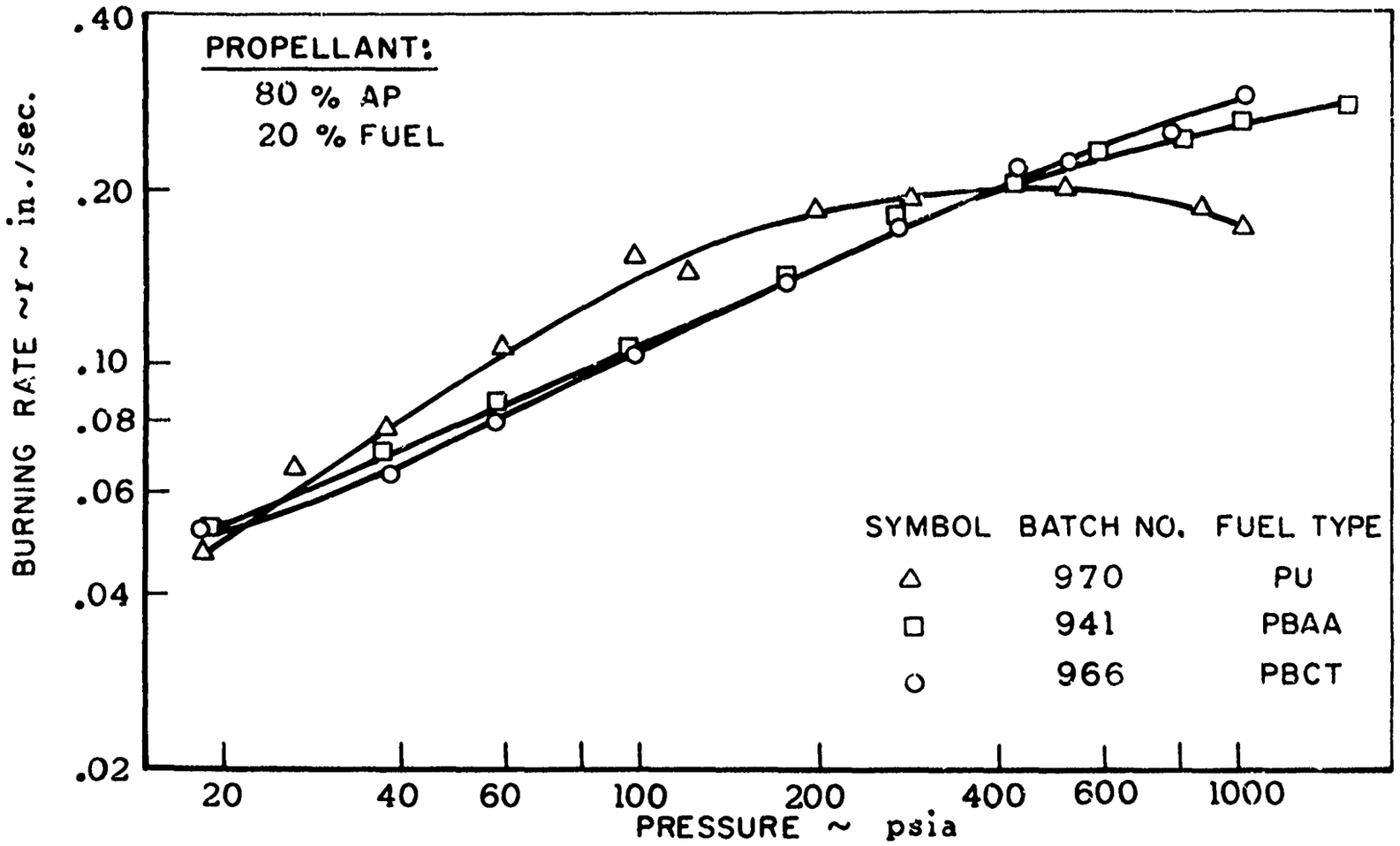

FIGURE 27

JP19 R 4272 69

JP19 K 4213 59

STEADY STATE BURNING RATE DATA FOR DIFFERENT ALUMINIUM LOADINGS

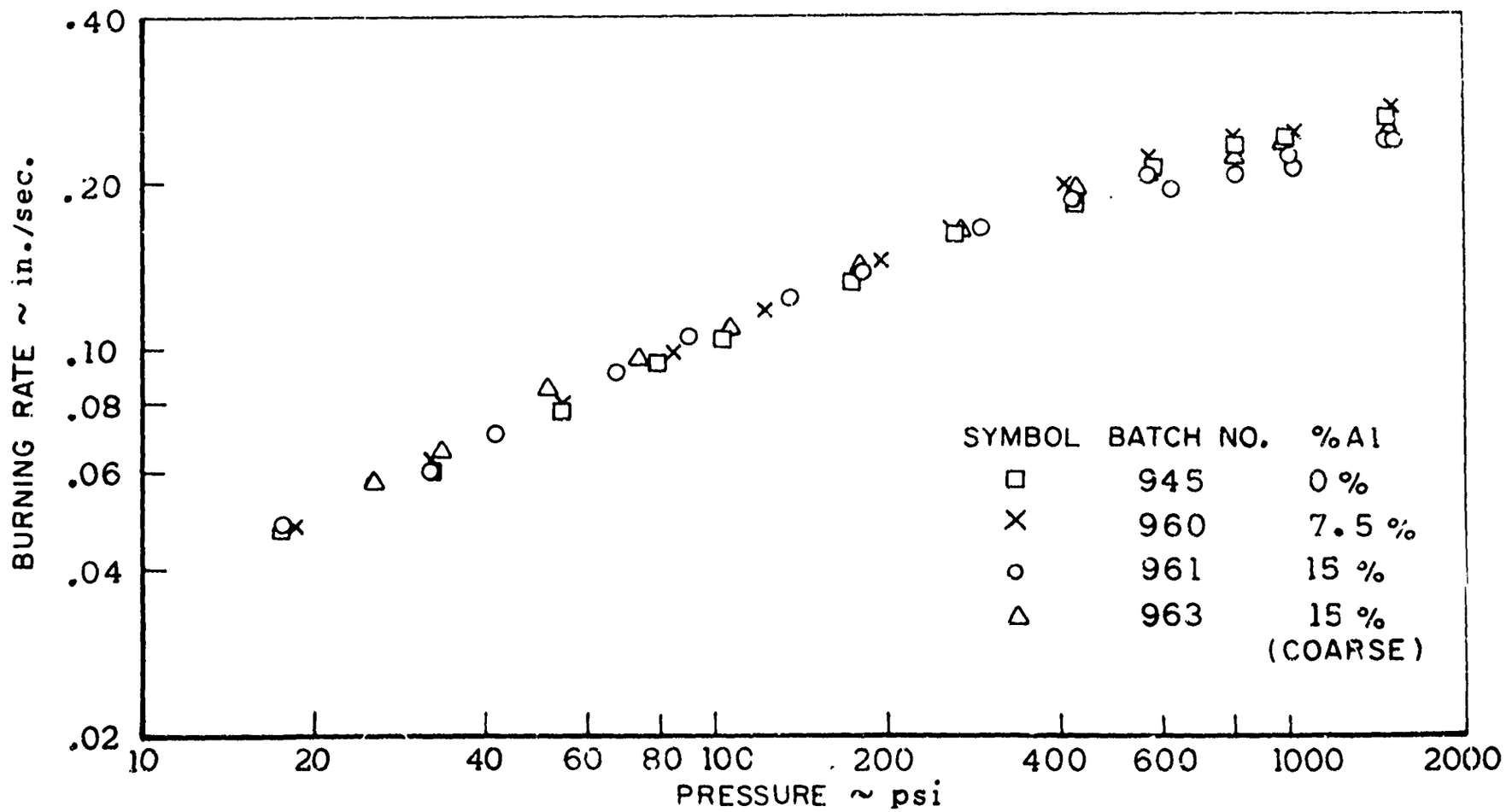

FIGURE 28

GDF THEORY FIT OF
STEADY STATE BURNING RATE DATA
82.5/17.5 PBAA

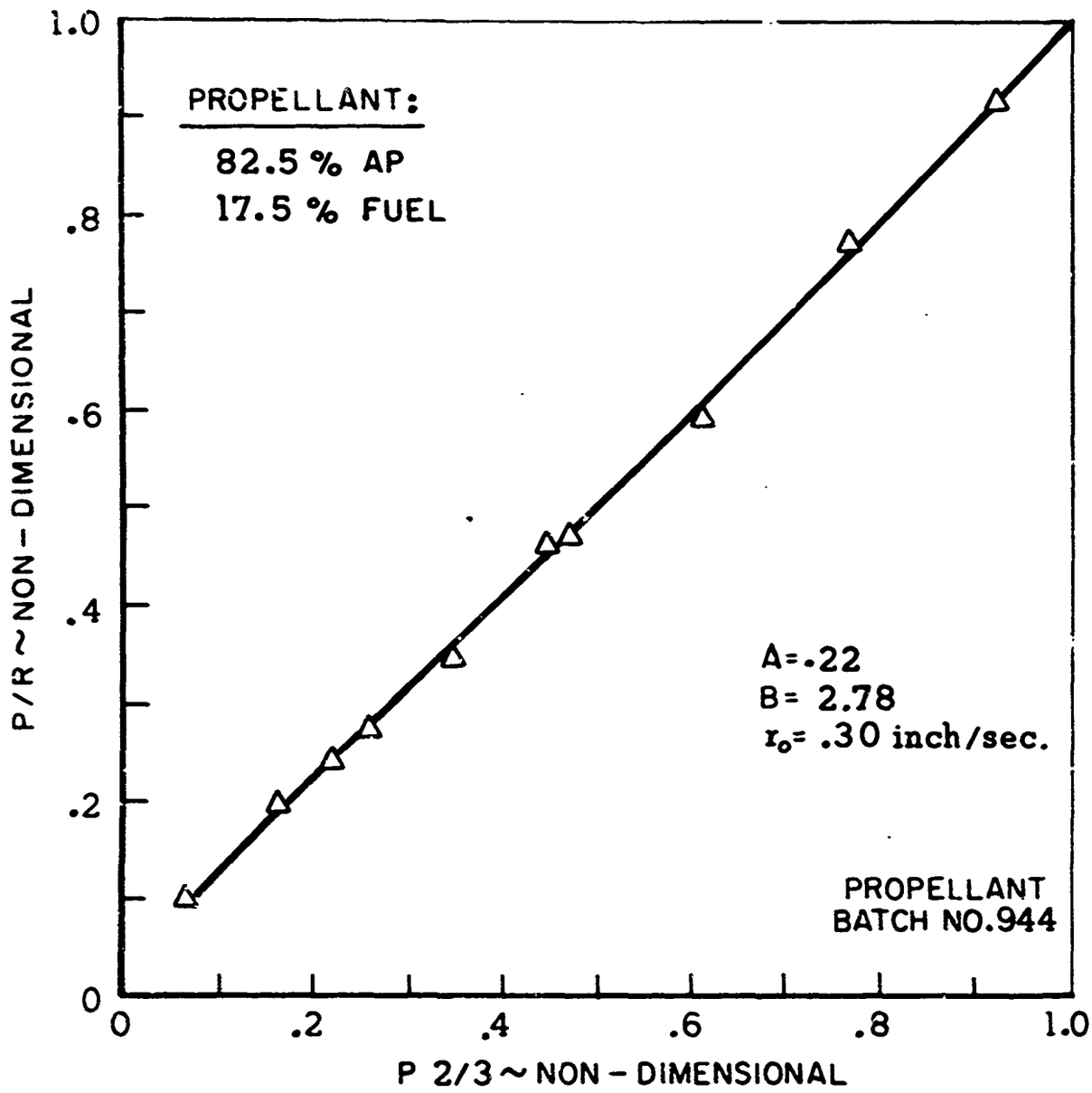

JP 19 R 4274 69

FIGURE 29

GDF THEORY FIT OF
STEADY STATE BURNING RATE DATA
80/20 PBAA

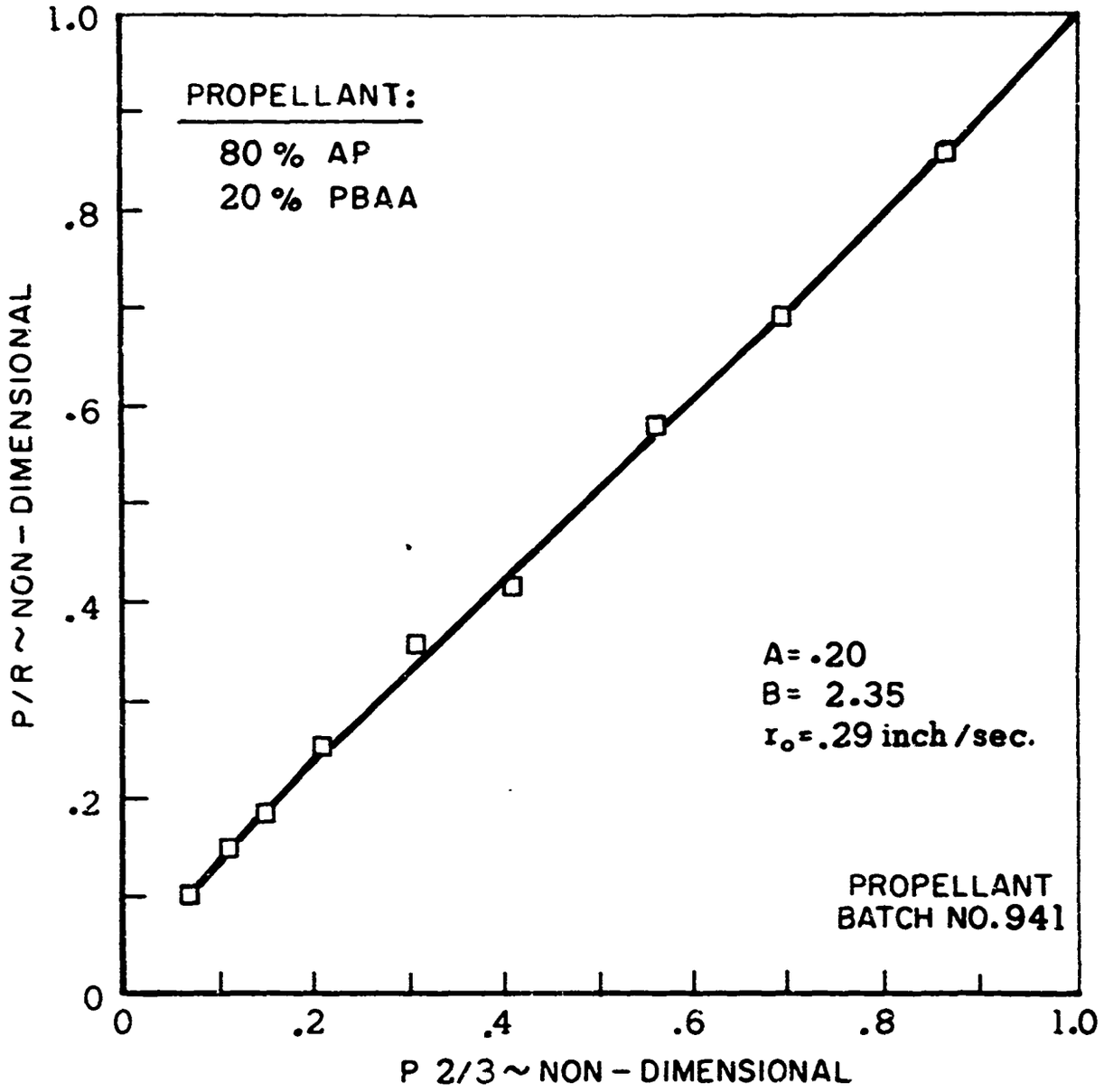

JP 19 R 4275 69

FIGURE 30

GDF THEORY FIT OF
STEADY STATE BURNING RATE DATA
77.5/22.5 – PBAA

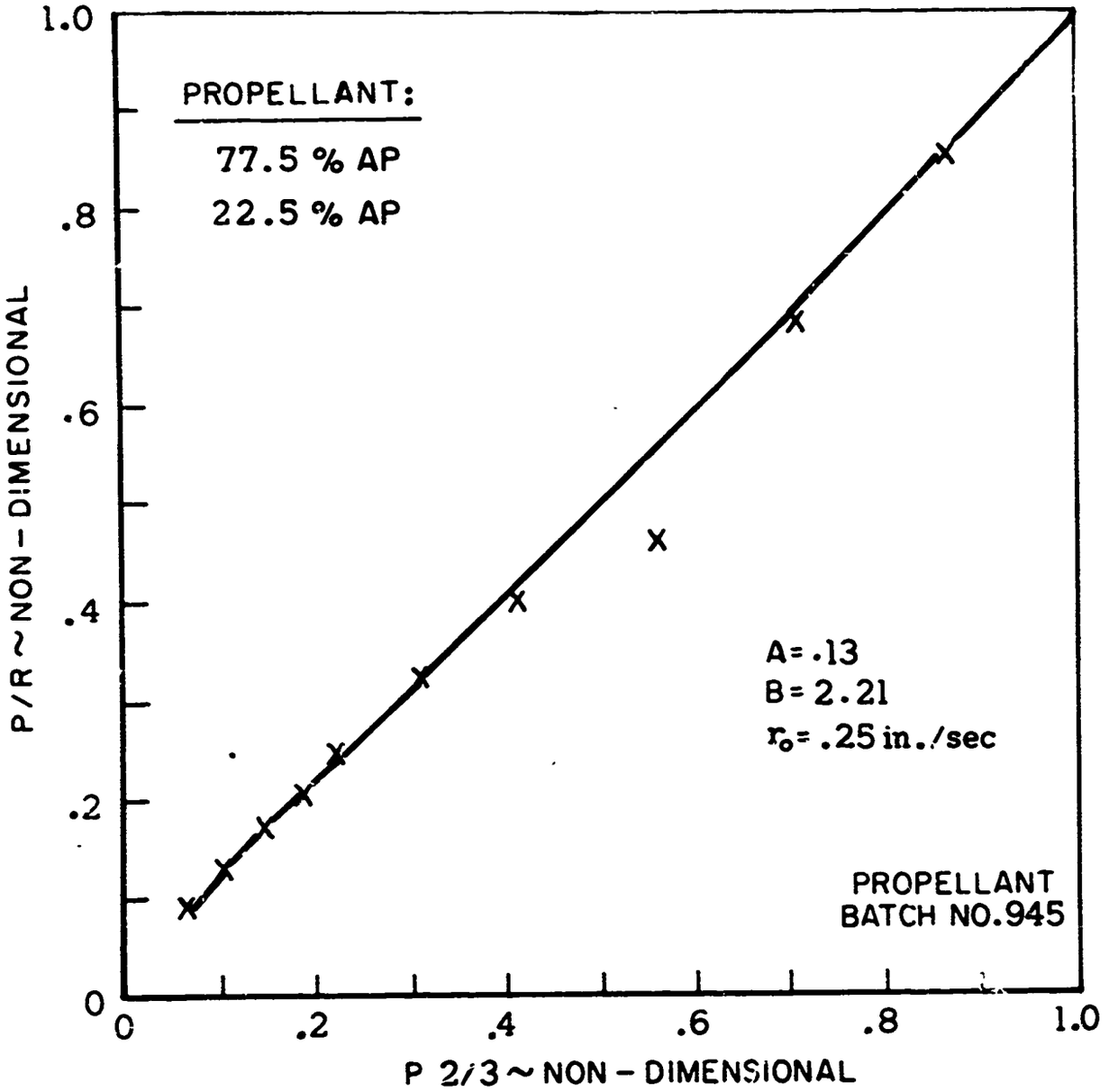

JP 19 R 4276 69

FIGURE 31

GDF THEORY FIT OF
STEADY STATE BURNING RATE DATA
75/25 – PBAA

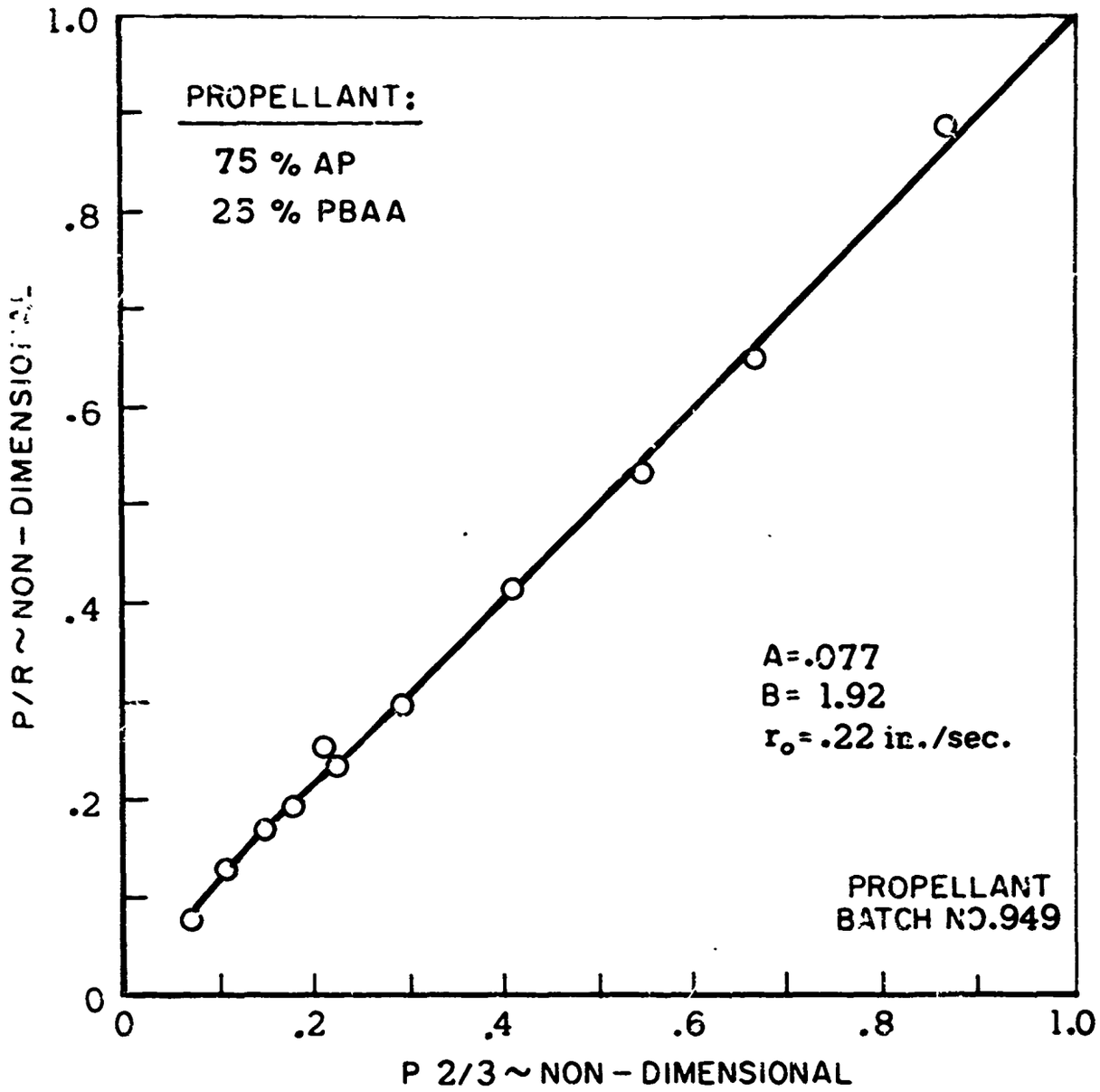

JP19 R 4277 69

FIGURE 32

GDF THEORY FIT OF
STEADY STATE BURNING RATE DATA
AP PARTICLE SIZE: 45 μ

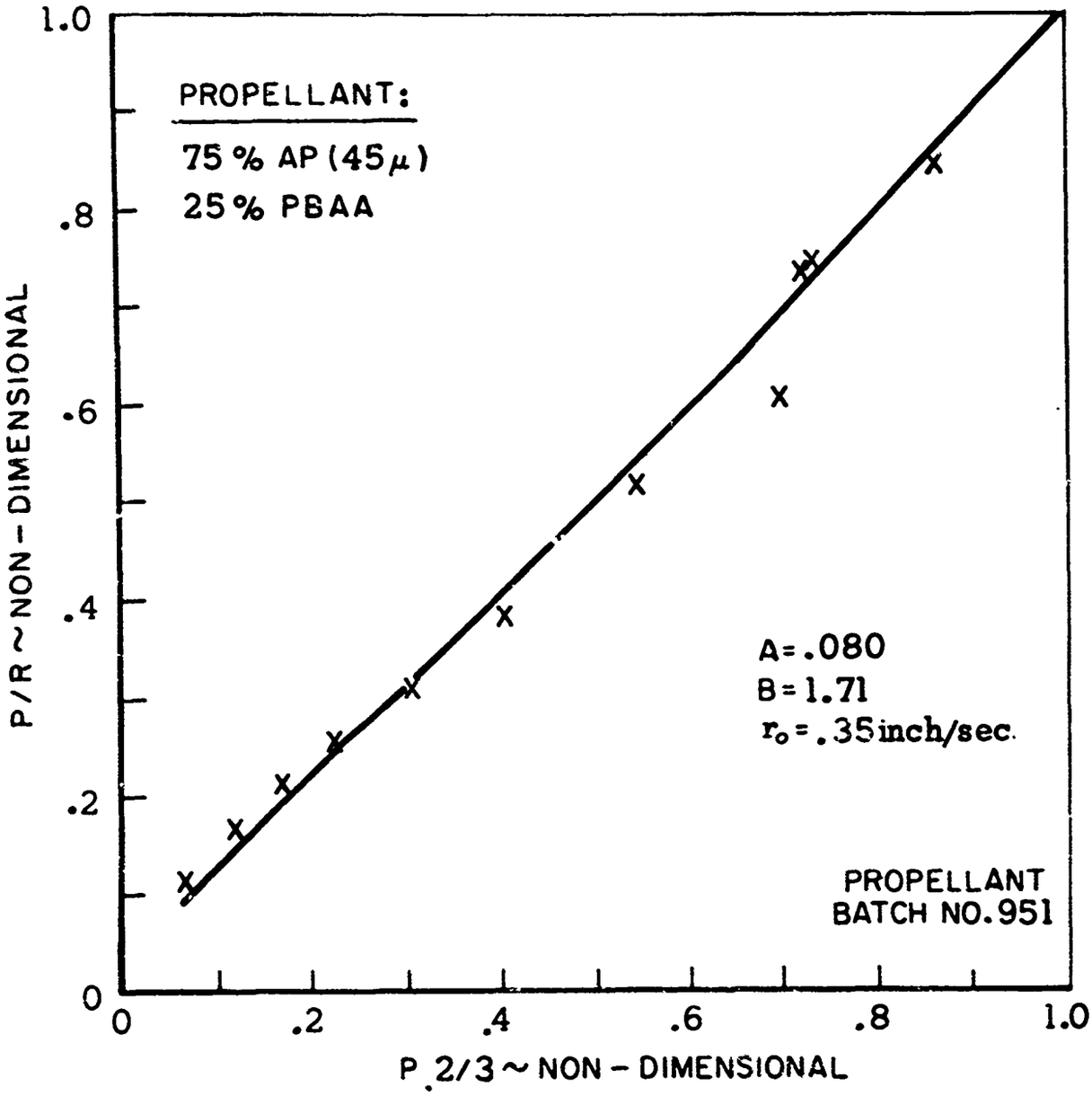

JP 19 R 4278 69

FIGURE 33

GDF THEORY FIT OF
STEADY STATE BURNING RATE DATA
AP PARTICLE SIZE: 80 μ

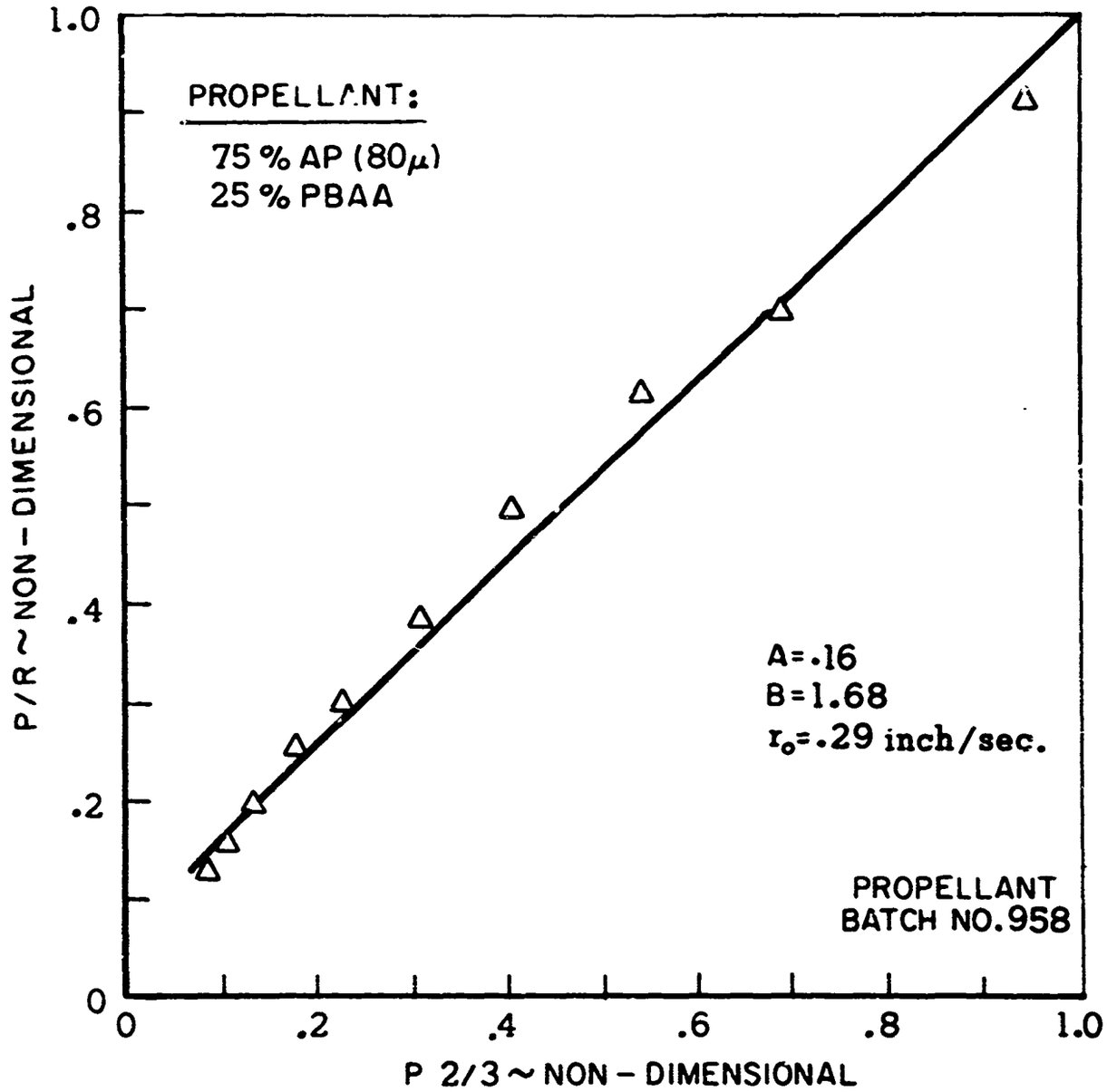

JP19 2 4279 69

FIGURE 34

GDF THEORY FIT OF
STEADY STATE BURNING RATE DATA
AP PARTICLE SIZE: 180 μ

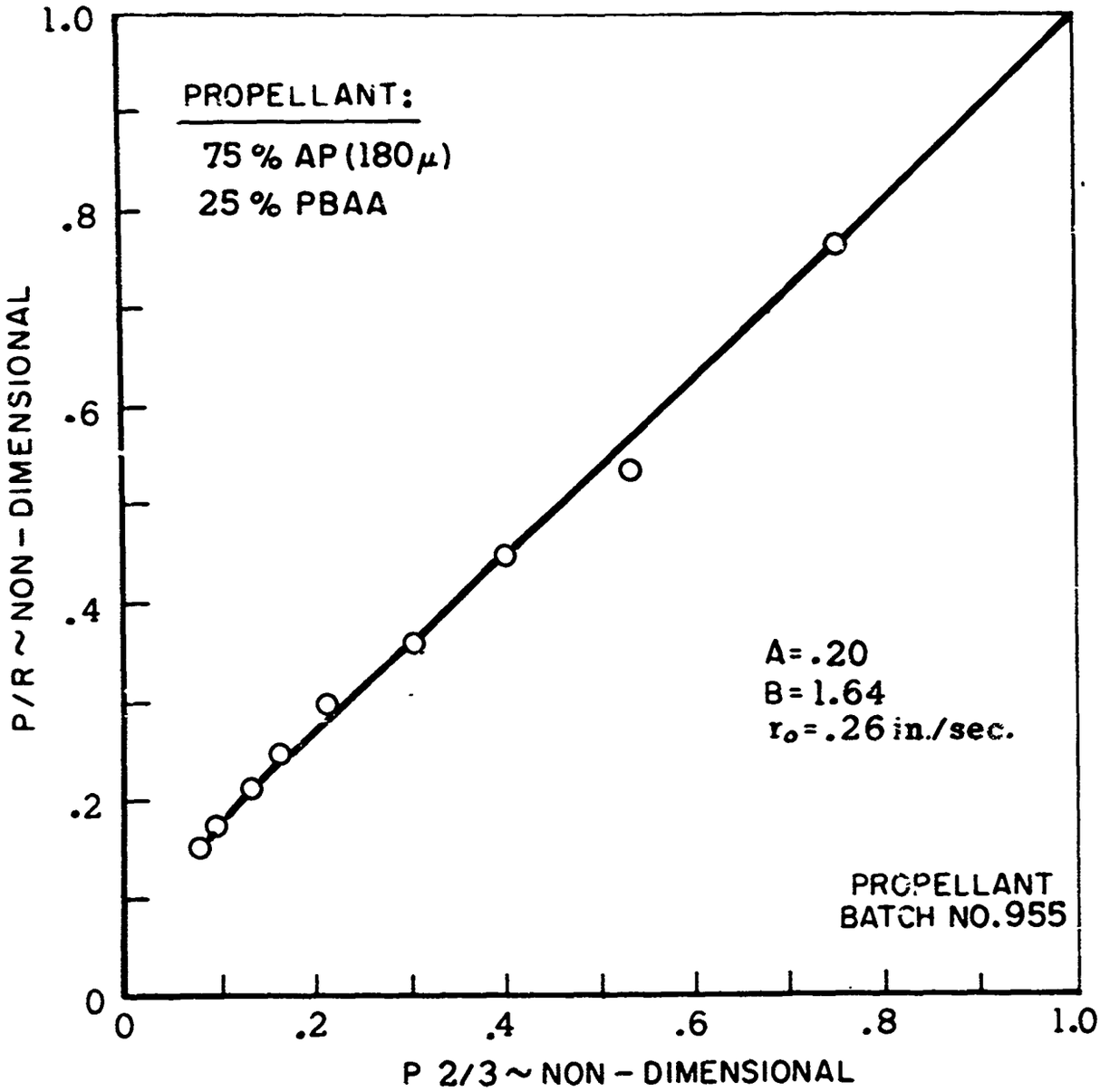

JP 19 R 4280 69

FIGURE 35

GDF THEORY FIT OF
STEADY STATE BURNING RATE DATA
PBCT FUEL BINDER

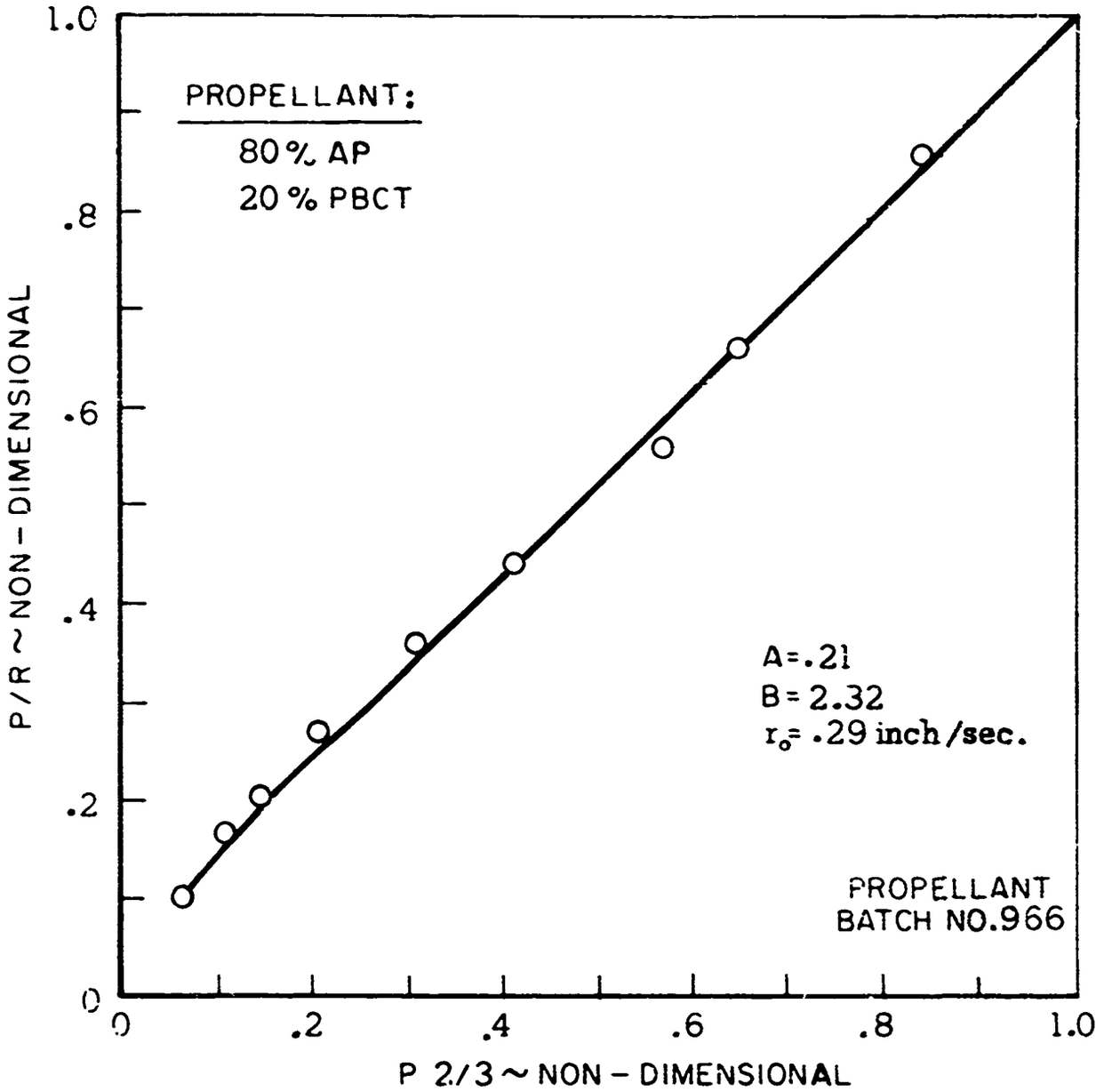

JPL R 4281 69

FIGURE 36

GDF THEORY FIT OF
STEADY STATE BURNING RATE DATA
7.5 % ALUMINIUM

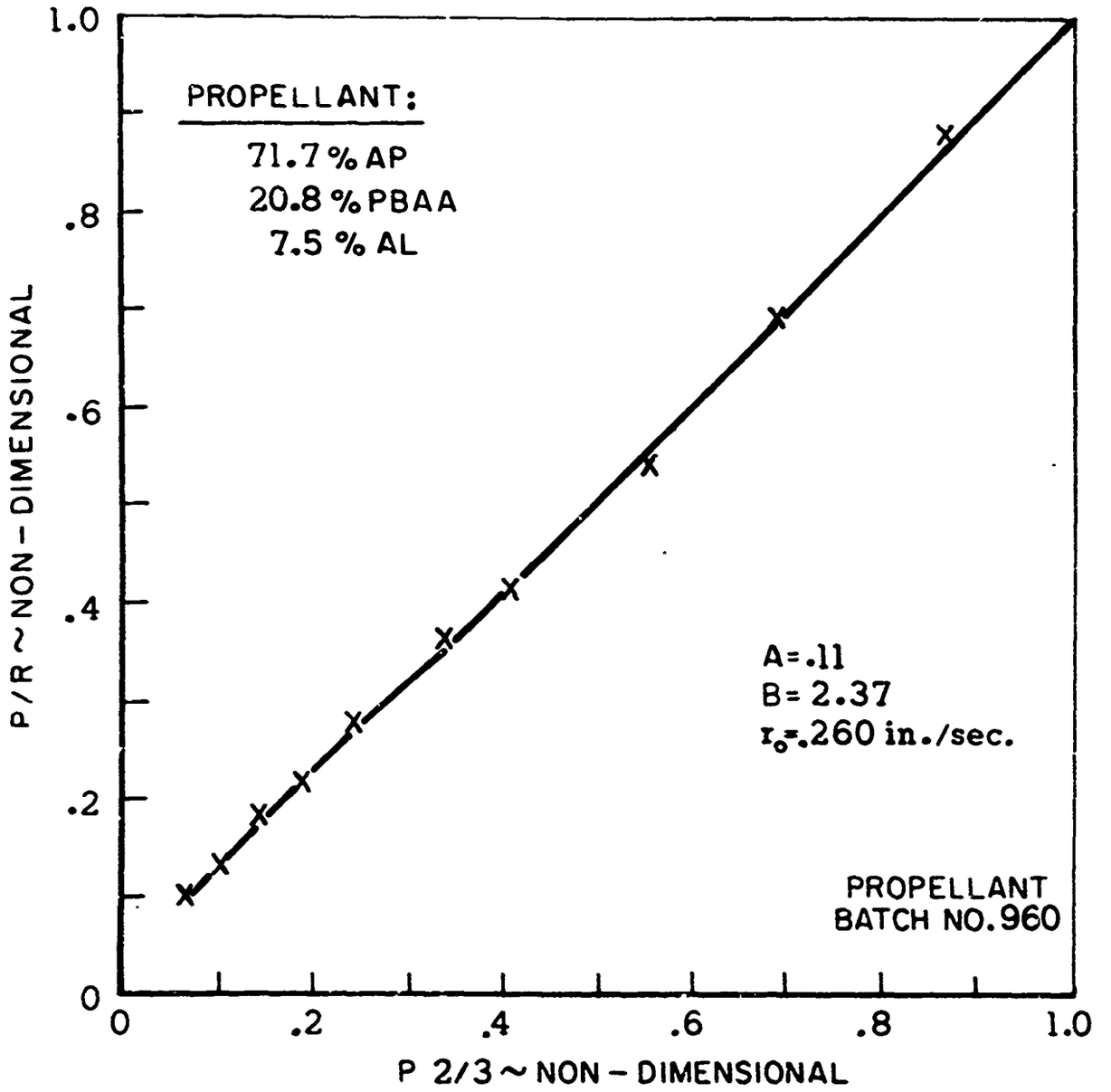

JP 19R4316 69

FIGURE 37

GDF THEORY FIT OF
STEADY STATE BURNING RATE DATA
15 % ALUMINIUM

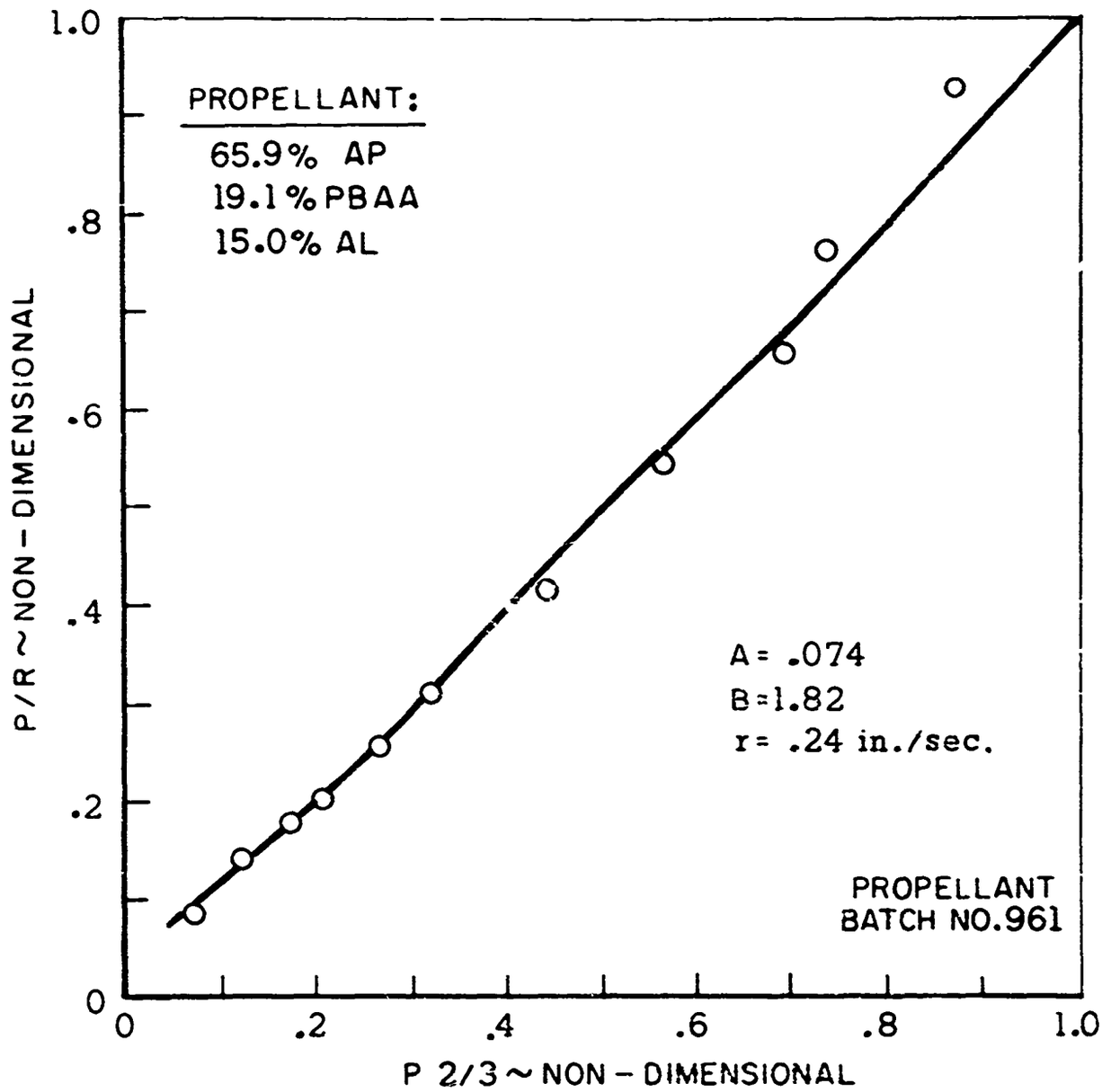

JPL R 4283 69

FIGURE 38

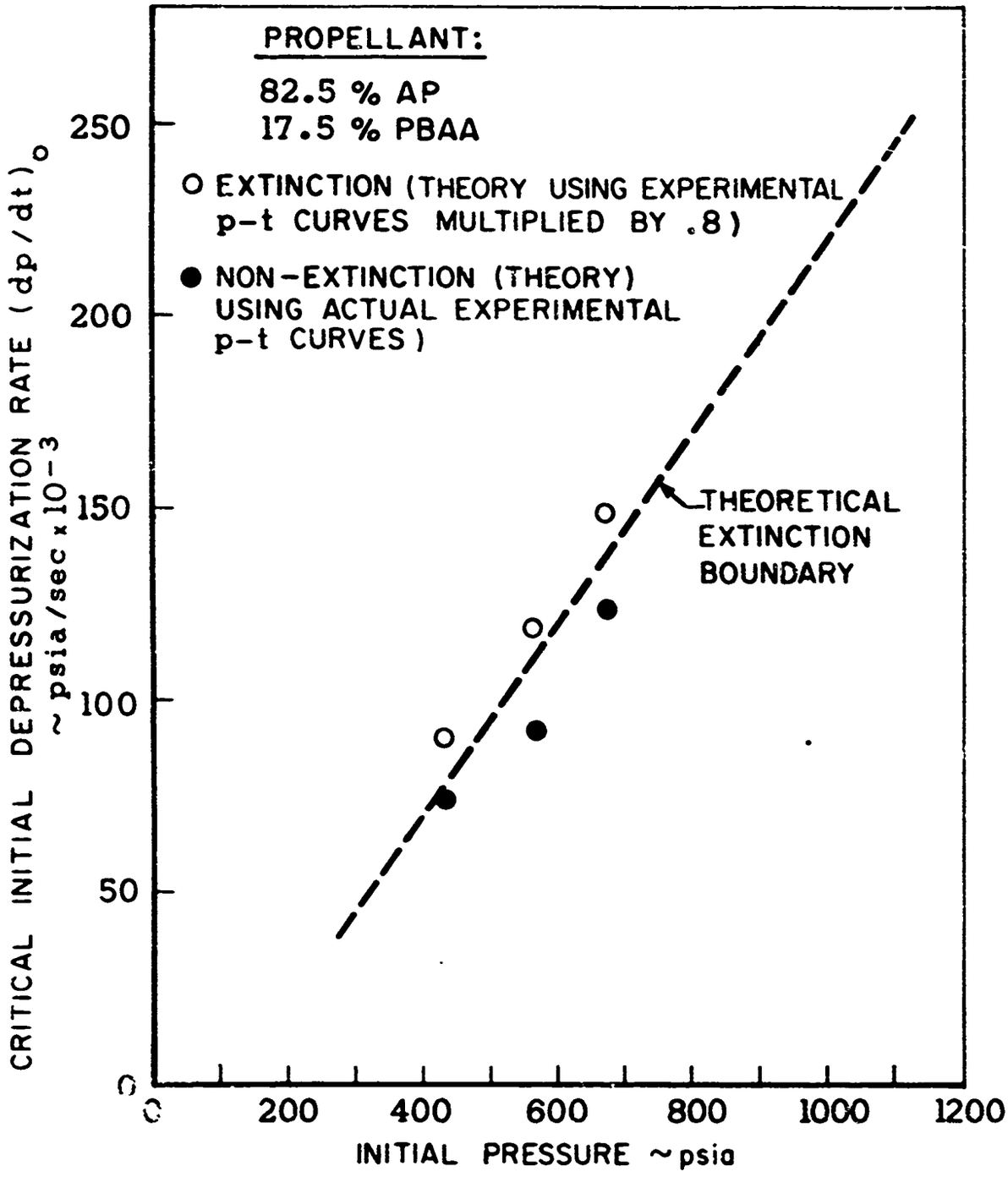

REQUIRED DEPRESSURIZATION RATE FOR EXTINCTION
THEORETICAL RESULTS
EFFECT OF CHANGE IN DEPRESSURATION SPEED
[FOR EXPLANATION, SEE SECT. VI, PART C]

FIGURE 39

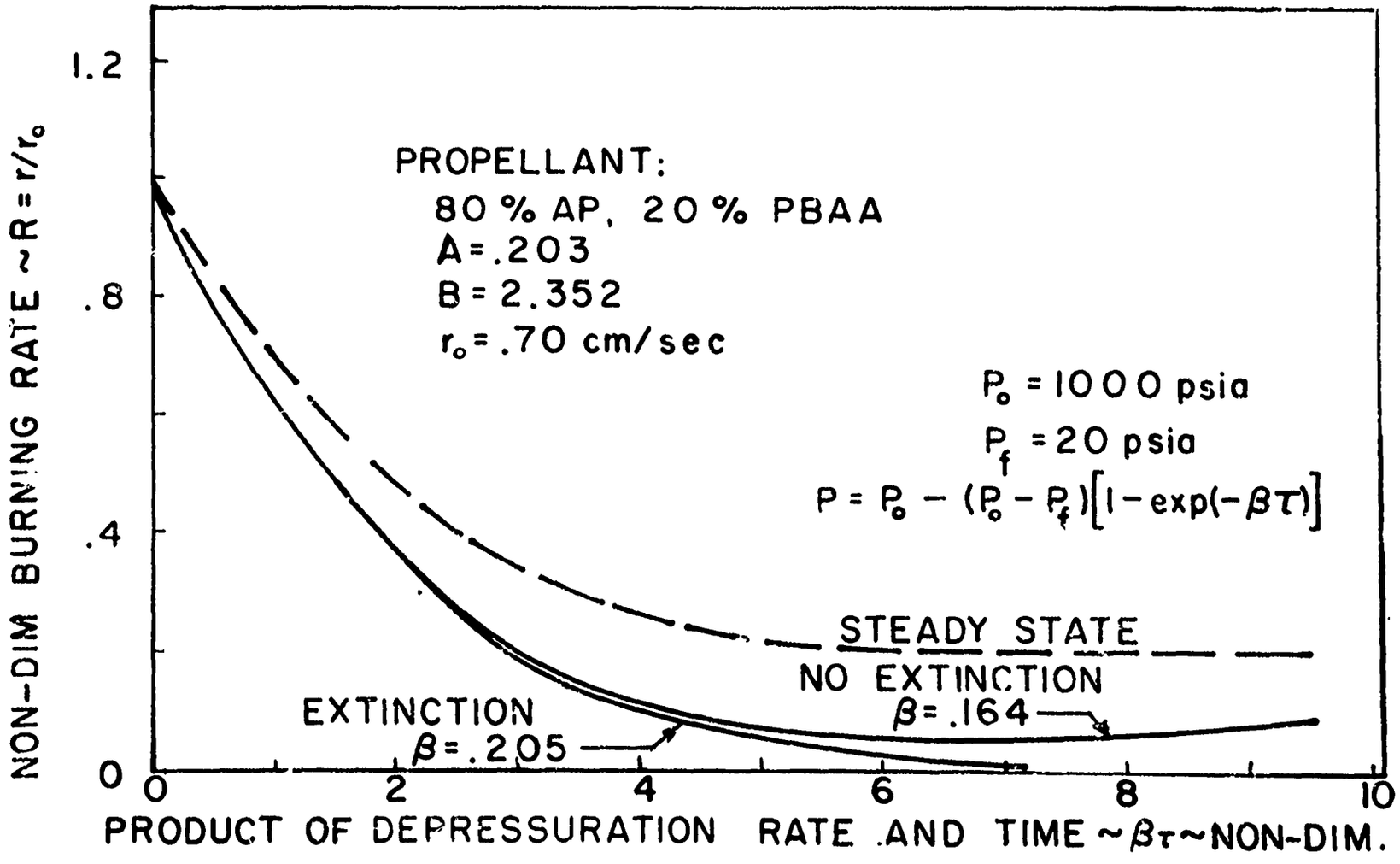

FIGURE 40 PREDICTED HISTORY OF BURNING RATE ~R DURING RAPID EXPONENTIAL DEPRESSURIZATION

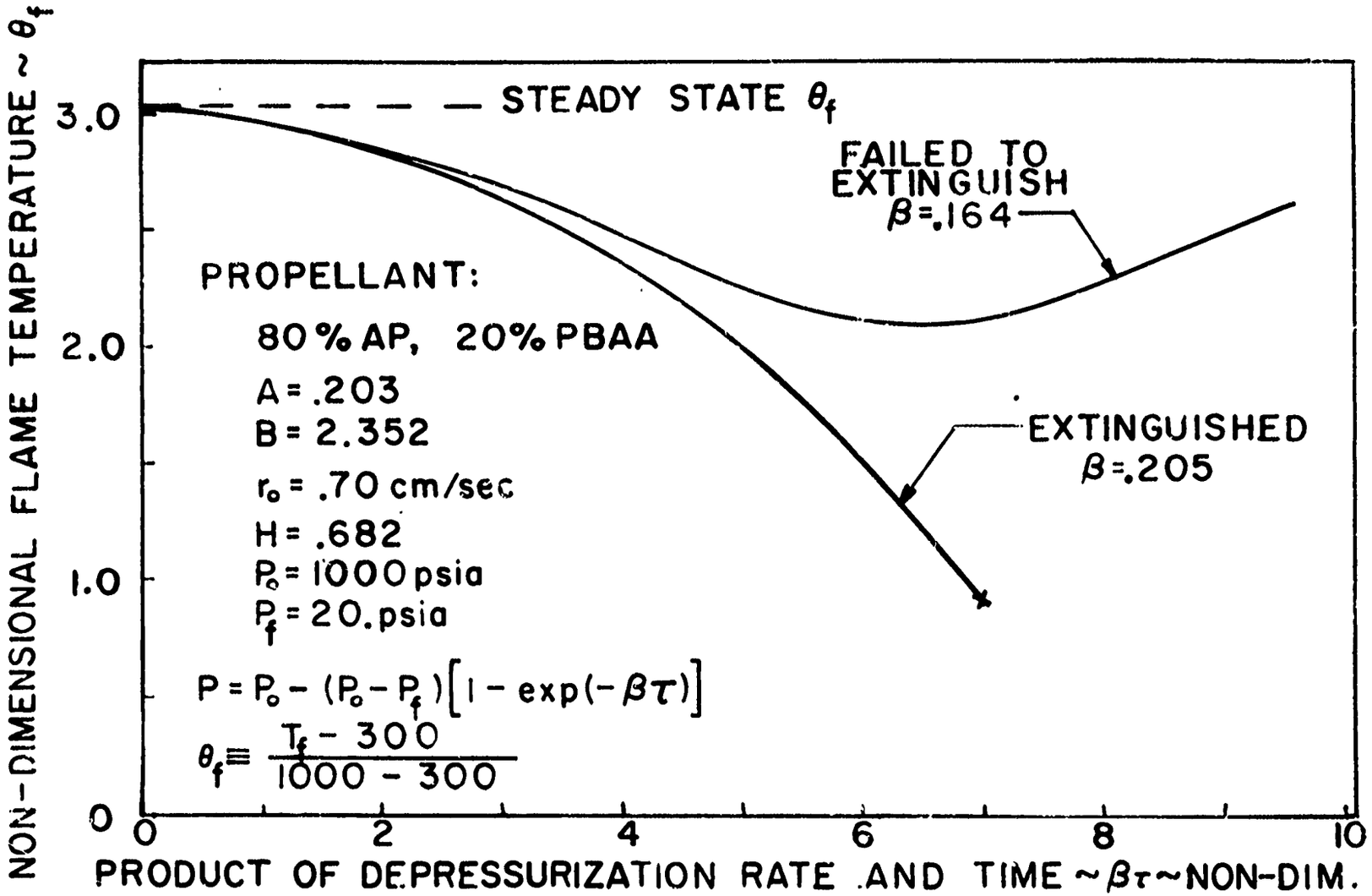

FIGURE 41 PREDICTED HISTORY OF FLAME TEMPERATURE DURING RAPID EXPONENTIAL DEPRESSURIZATION

JPIG R 4285 69

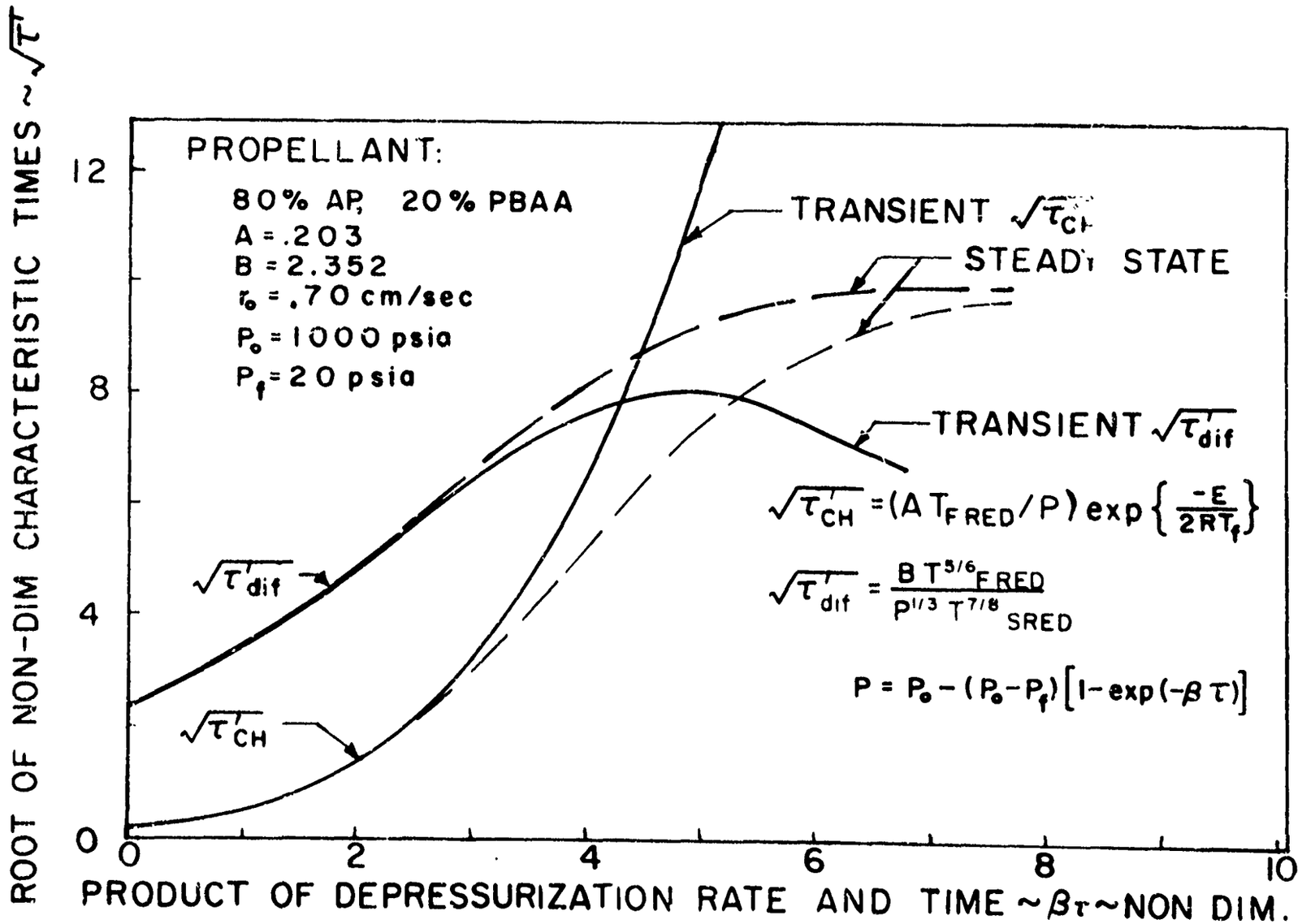

FIGURE 42 PREDICTED HISTORY OF CHARACTERISTIC TIMES DURING RAPID EXPONENTIAL DEPRESSURIZATION

NOT REPRODUCIBLE

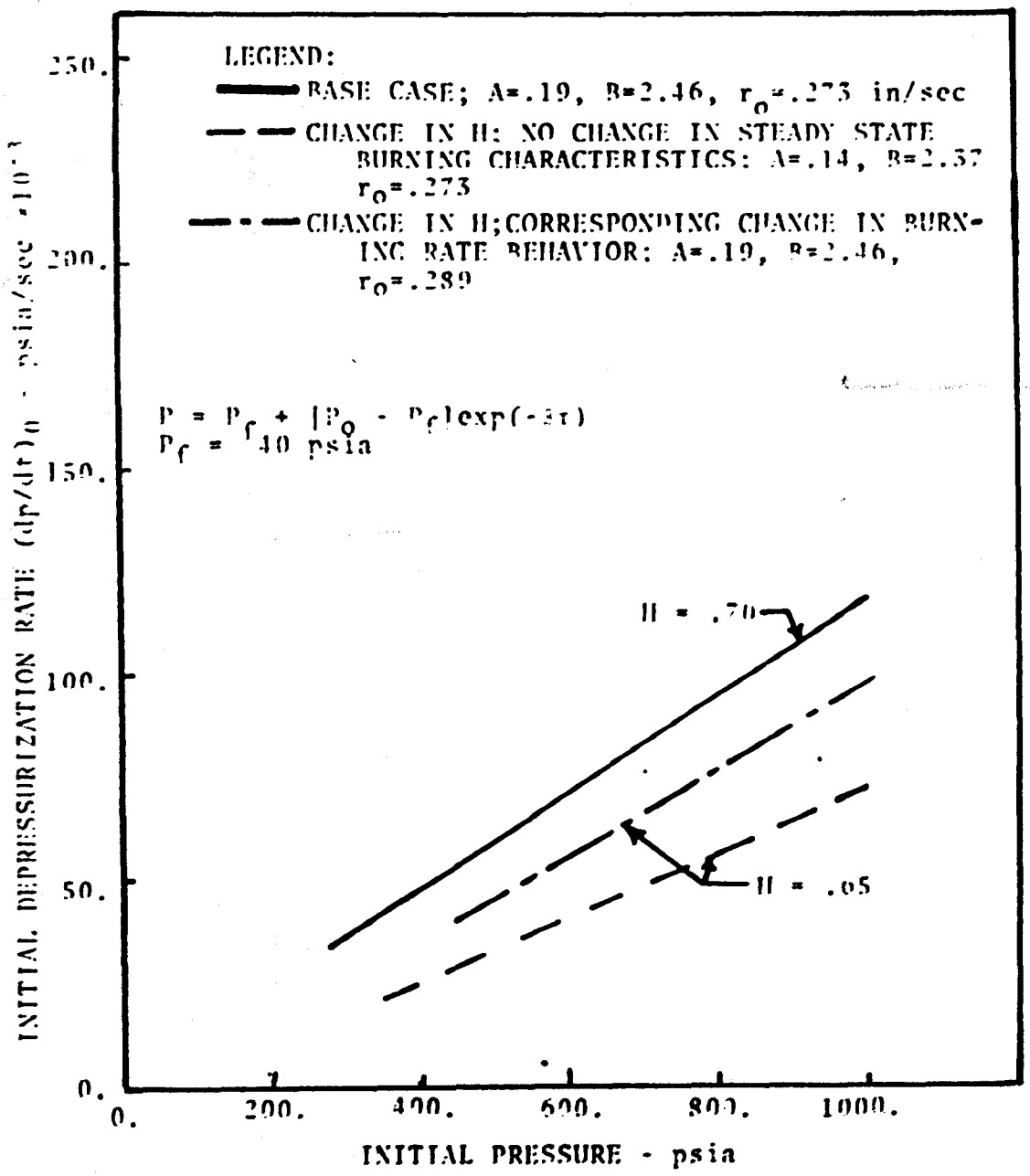

FIGURE 43. REQUIRED DEPRESSURIZATION RATE FOR EXTINCTION THEORETICAL PREDICTIONS BASED ON EXPONENTIAL PRESSURE DECAY EFFECT OF CHANGING SURFACE HEAT RELEASE

JP 19 R 4287 69

FIGURE 43

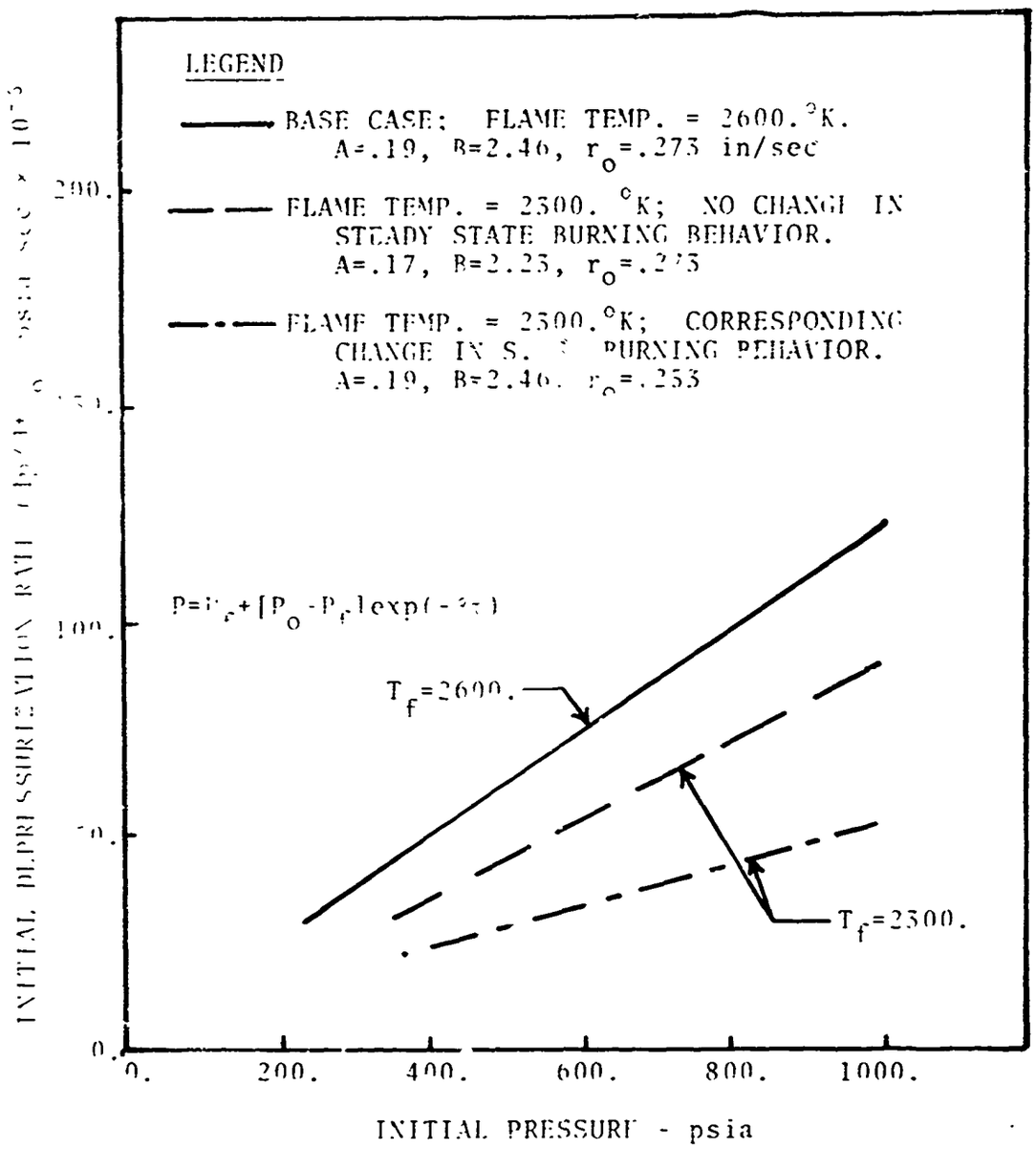

FIGURE 44. DEPRESSURIZATION RATE REQUIRED FOR EXTINCTION THEORETICAL RESULTS BASED ON EXPONENTIAL PRESSURE DECAY EFFECT OF CHANGES IN FLAME TEMPERATURE

FIGURE 44

JPL R 4289 69

NOT REPRODUCIBLE

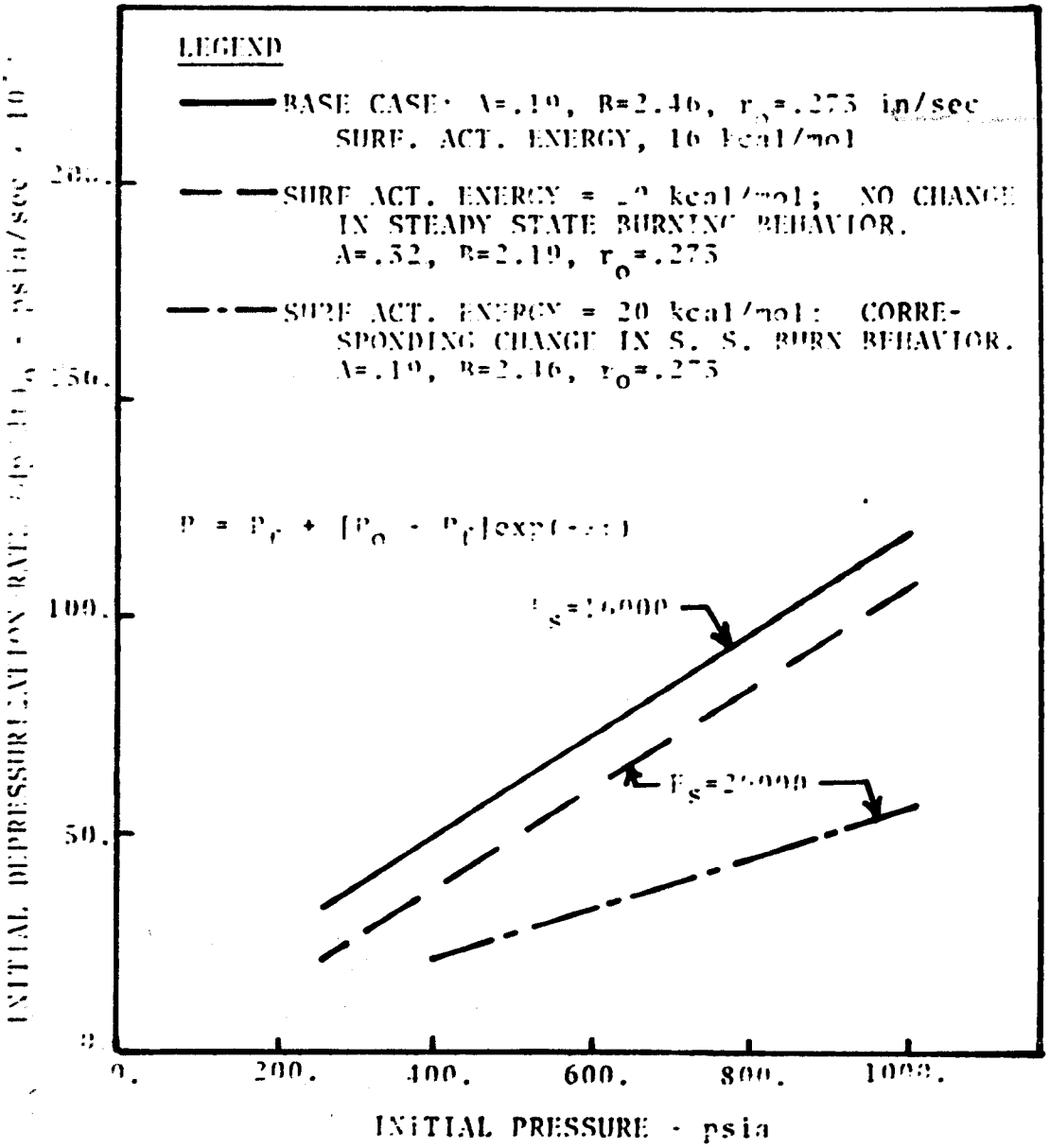

FIGURE 45. REQUIRED DEPRESSURIZATION RATE FOR EXTINCTION THEORETICAL PREDICTIONS BASED ON EXPONENTIAL PRESSURE DECAY EFFECT OF CHANGES IN SURFACE ACTIVATION ENERGY

FIGURE 45

JP 19 R 1290 69

NOT REPRODUCIBLE

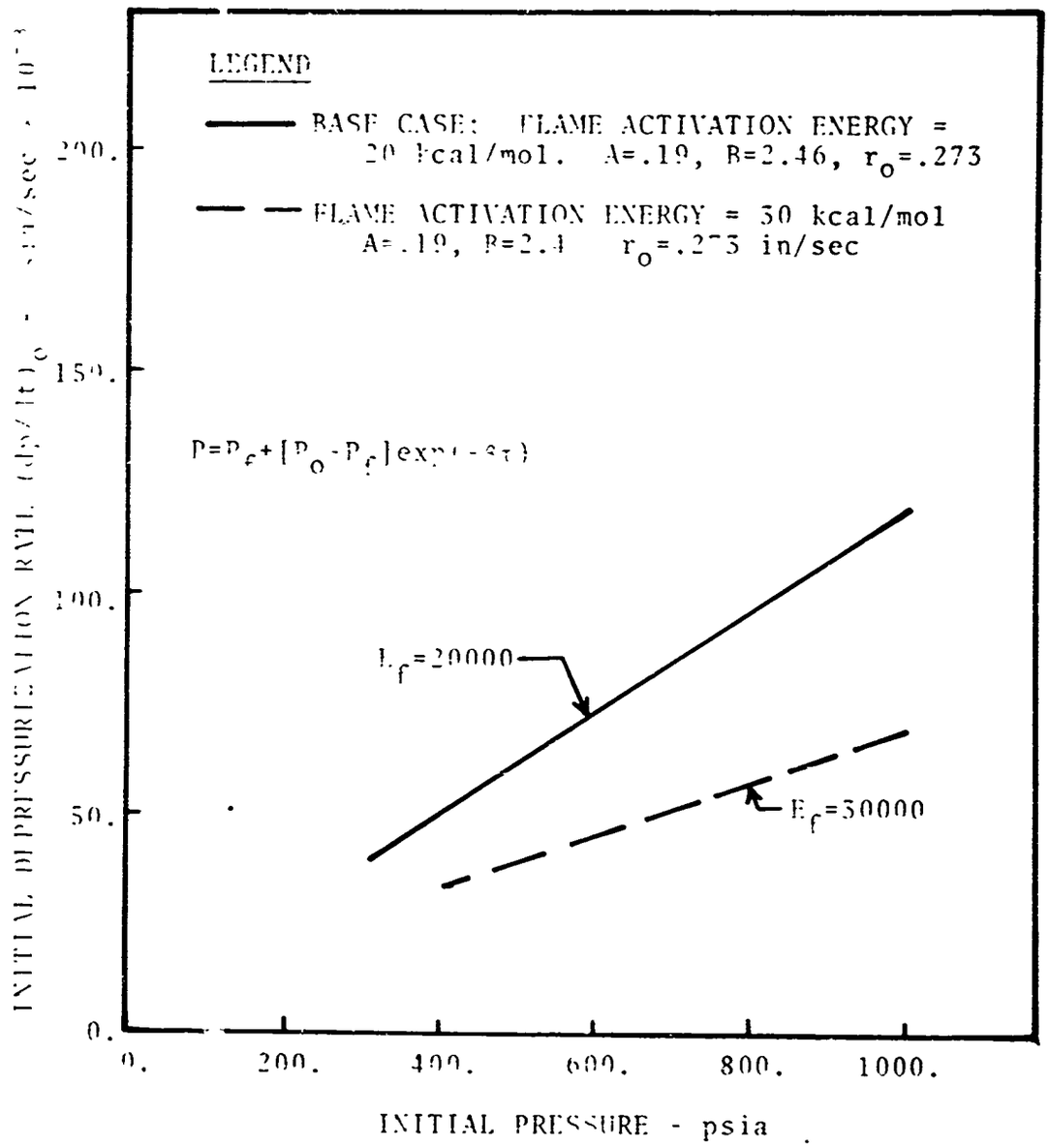

FIGURE 46. DEPRESSURIZATION REQUIRED FOR EXTINCTION THEORETICAL PREDICTIONS BASED ON EXPONENTIAL PRESSURE DECAY EFFECT OF CHANGES IN FLAME ACTIVATION ENERGY

JP19 R 4289 69

FIGURE 46

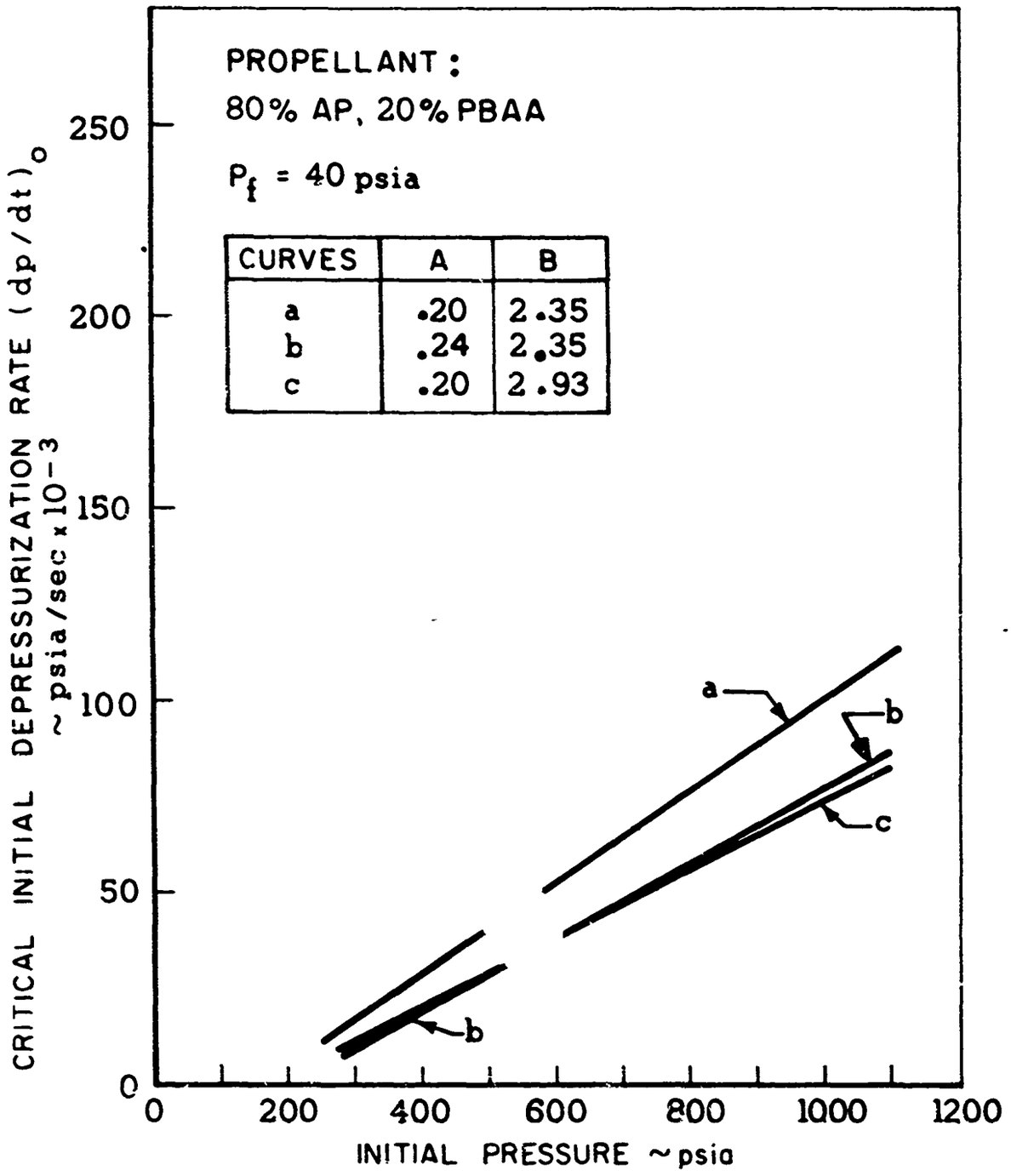

REQUIRED DEPRESSURIZATION RATE FOR EXTINCTION
THEORETICAL RESULTS
EFFECT OF CHANGES IN BURNING RATE CONSTANTS

FIGURE 47

JP 19R4087-69

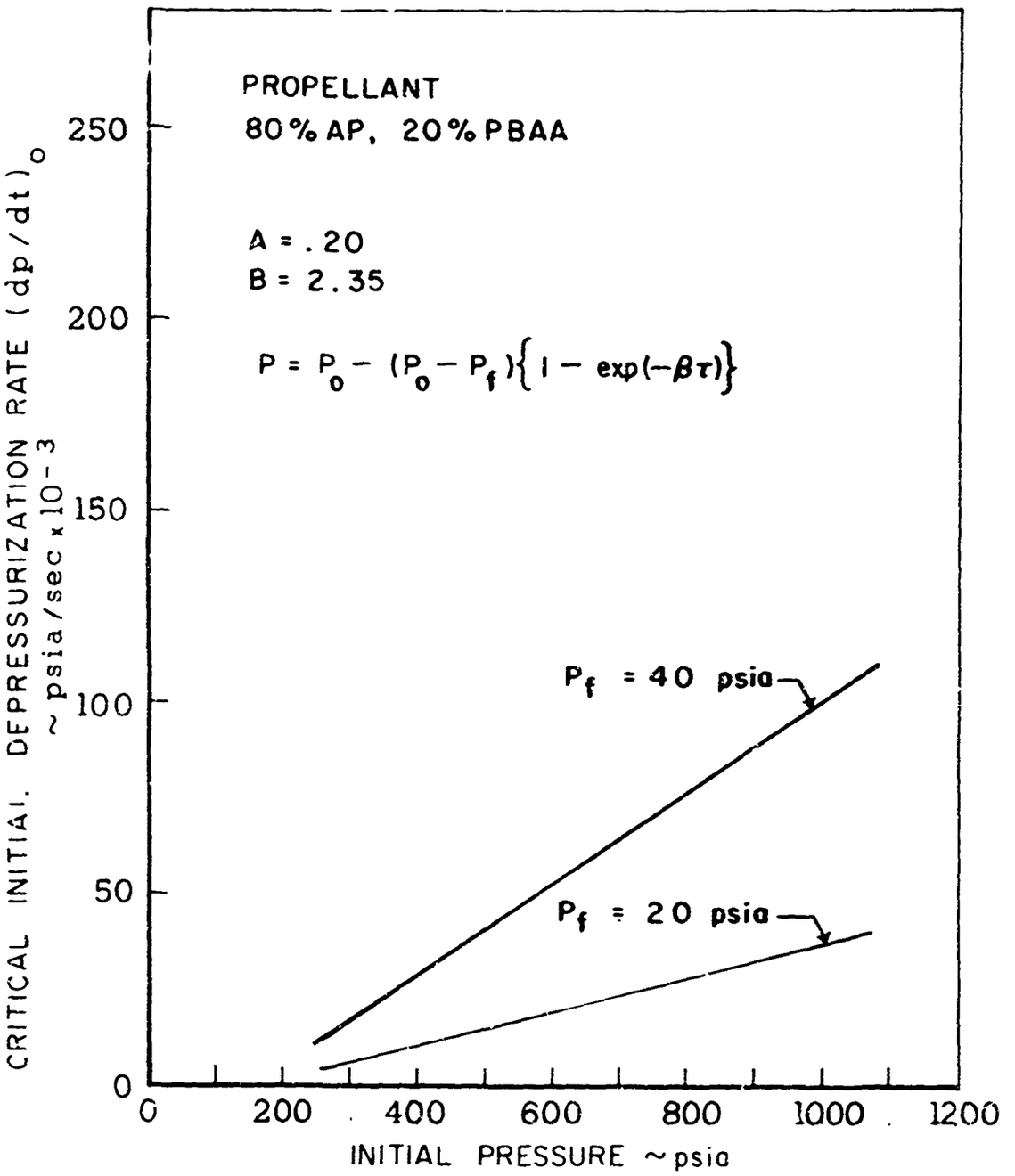

FIGURE 48 REQUIRED DEPRESSURIZATION RATE FOR EXTINCTION
THEORETICAL RESULTS BASED ON EXPONENTIAL PRESSURE DECAY
EFFECT OF CHANGES IN FINAL PRESSURE

FIGURE 48

TWO PART PRESSURE-TIME CURVES

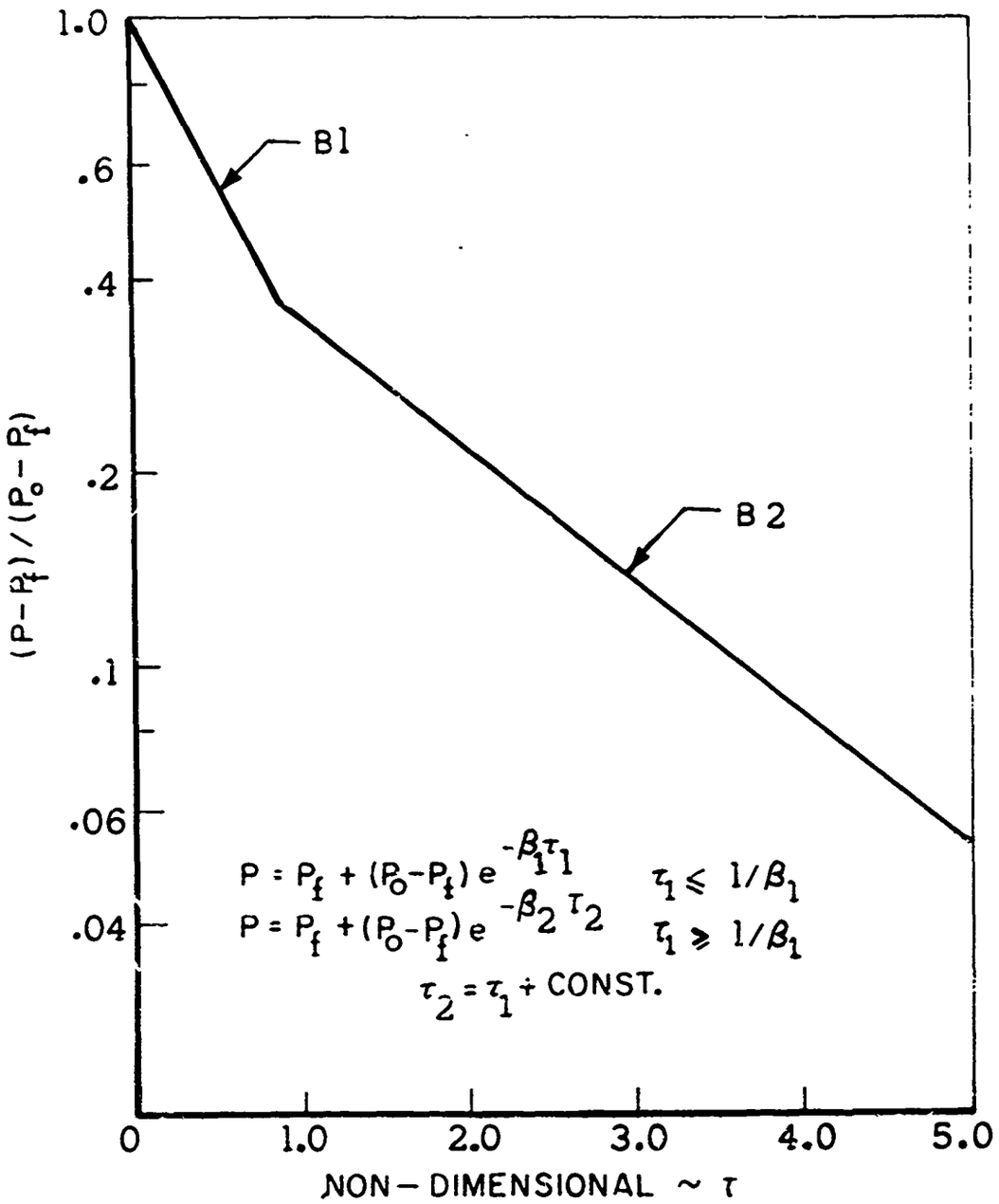

FIGURE 49

JP19 R 4292 69

EFFECT OF CHANGES IN SHAPE OF PRESSURE DECAY CURVE ON PREDICTED EXTINCTION BOUNDARY

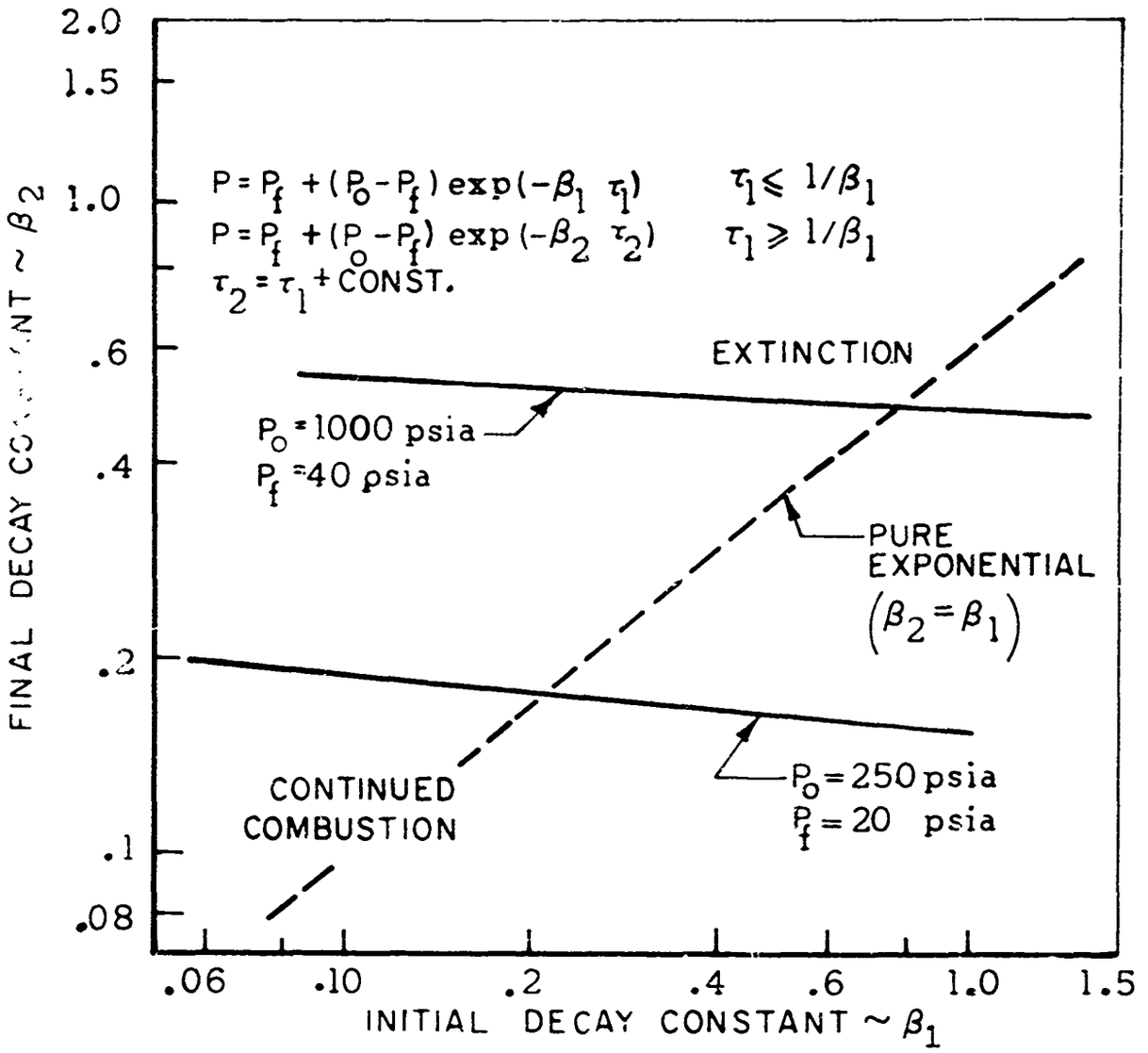

FIGURE 50

STEADY STATE BURNING RATE CURVE
DOUBLE-BASE PROPELLANT

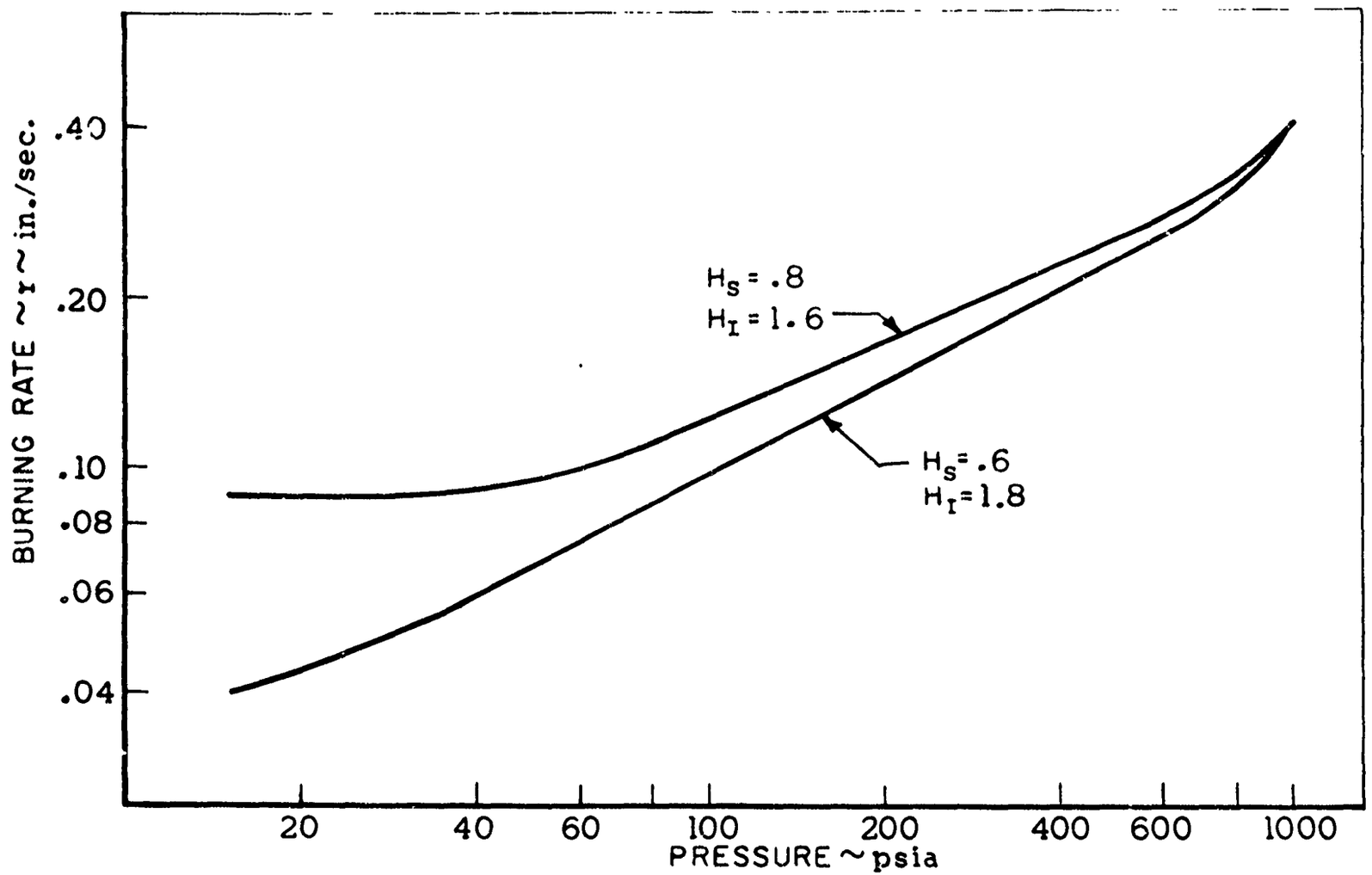

FIGURE 51

JPIG R 4293 G9

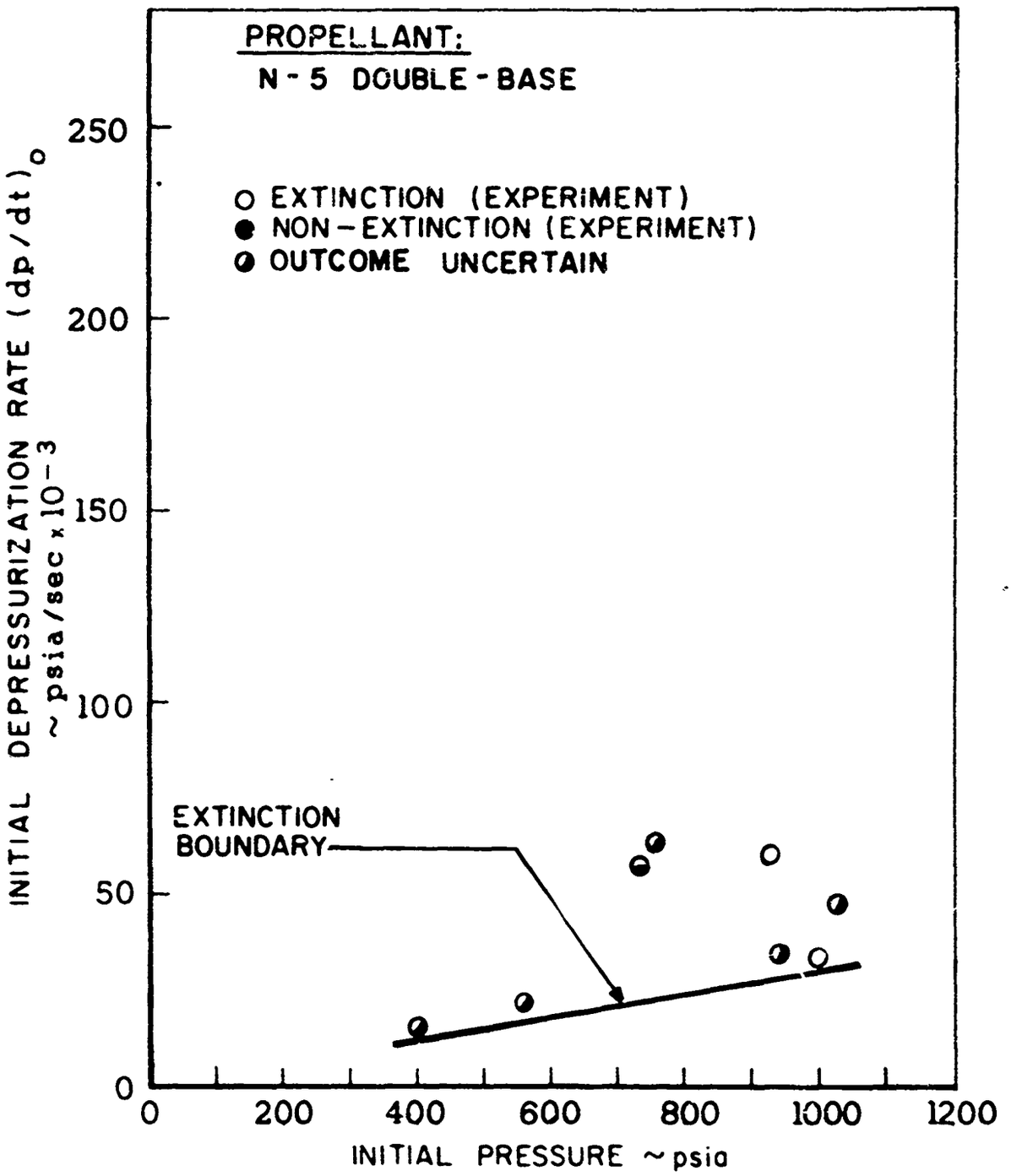

FIGURE 52 REQUIRED DEPRESSURIZATION RATE FOR EXTINCTION
EXPERIMENTAL RESULTS
N-5 DOUBLE-BASE PROPELLANT

JP19 R 4294 69

FIGURE 52

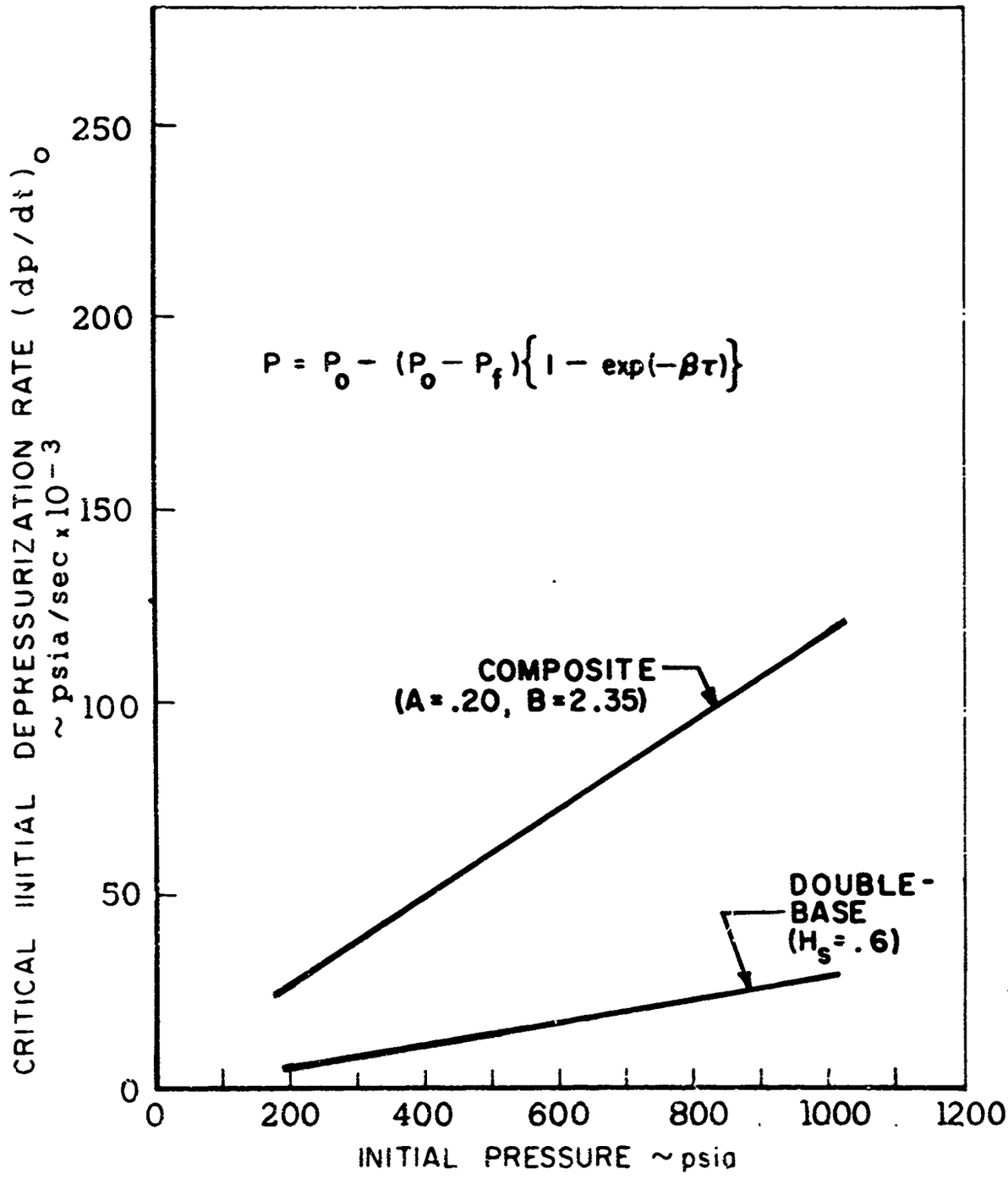

REQUIRED DEPRESSURIZATION RATE FOR EXTINCTION
THEORETICAL RESULTS BASED ON EXPONENTIAL PRESSURE DECAY
COMPARISON BETWEEN DOUBLE-BASE AND COMPOSITE PROPELLANTS

JP 19 R 4295 G9

FIGURE 53

SCHEMATIC SHOWING RELATION BETWEEN THE REGIONS OF PERMANENT, TEMPORARY, AND NON-EXTINCTIONS

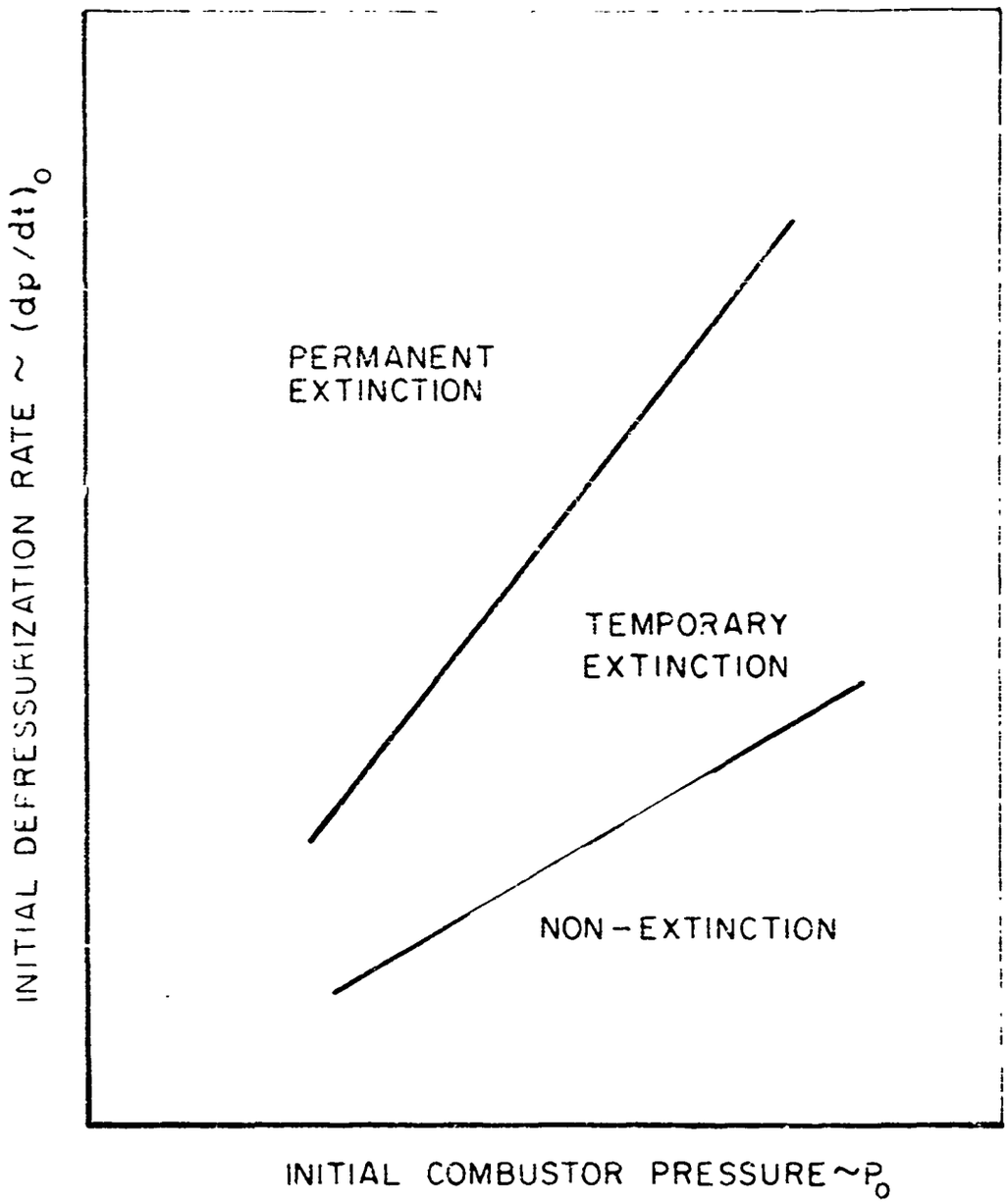

JP19 R 4296 69

FIGURE 54

FIGURE 55

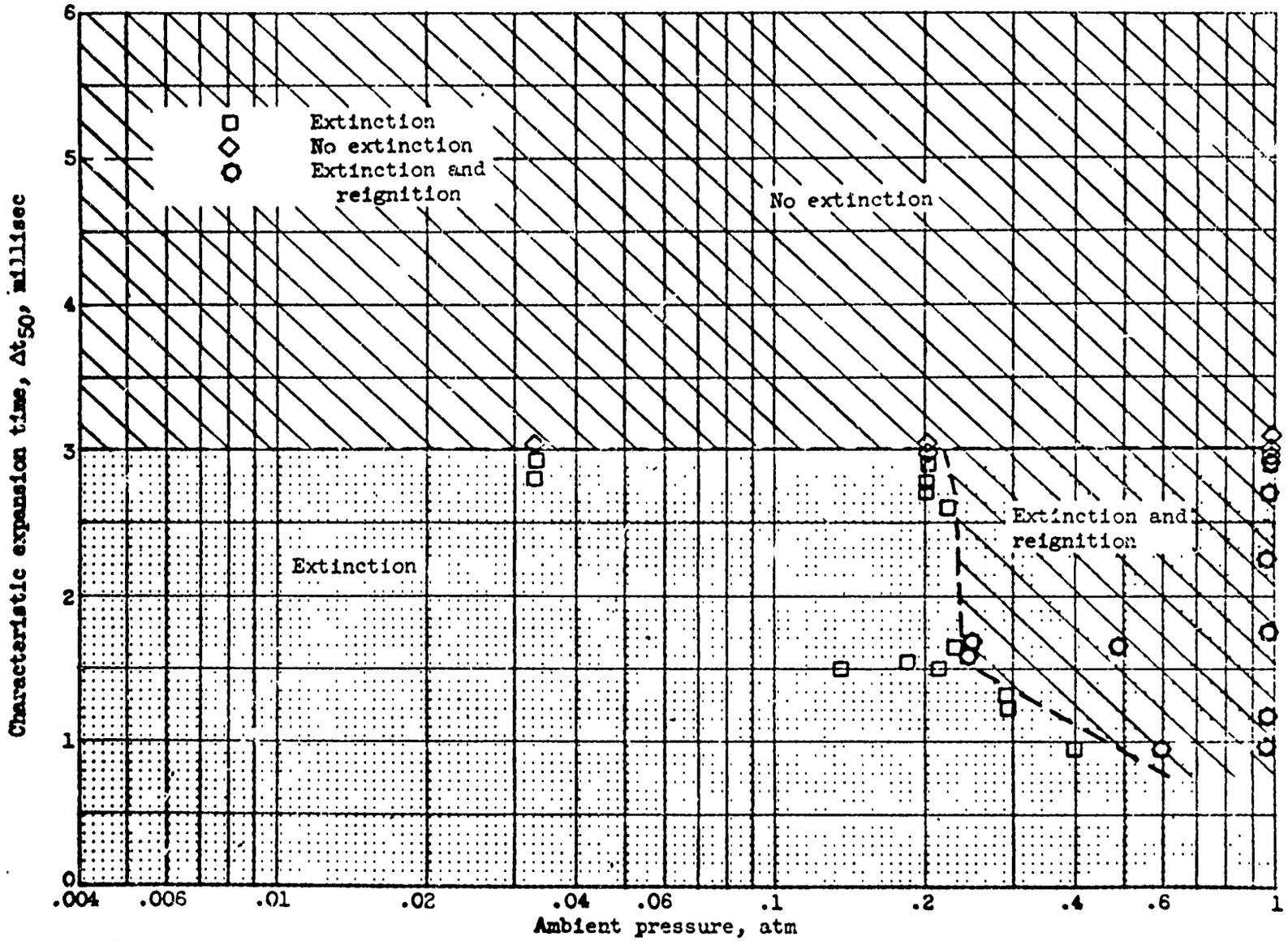

Figure 55. - effect of ambient pressure and expansion time on extinction. Initial chamber pressure, 500 psia. (Taken from Ref. 3) Note: $\Delta t_{50} \sim p_o/(dp/dt)_o$.

JPIB R 4297 69

CALCULATED REDUCTION IN RE-IGNITION TIME DUE TO HEATING BY HOT ENVIRONMENT

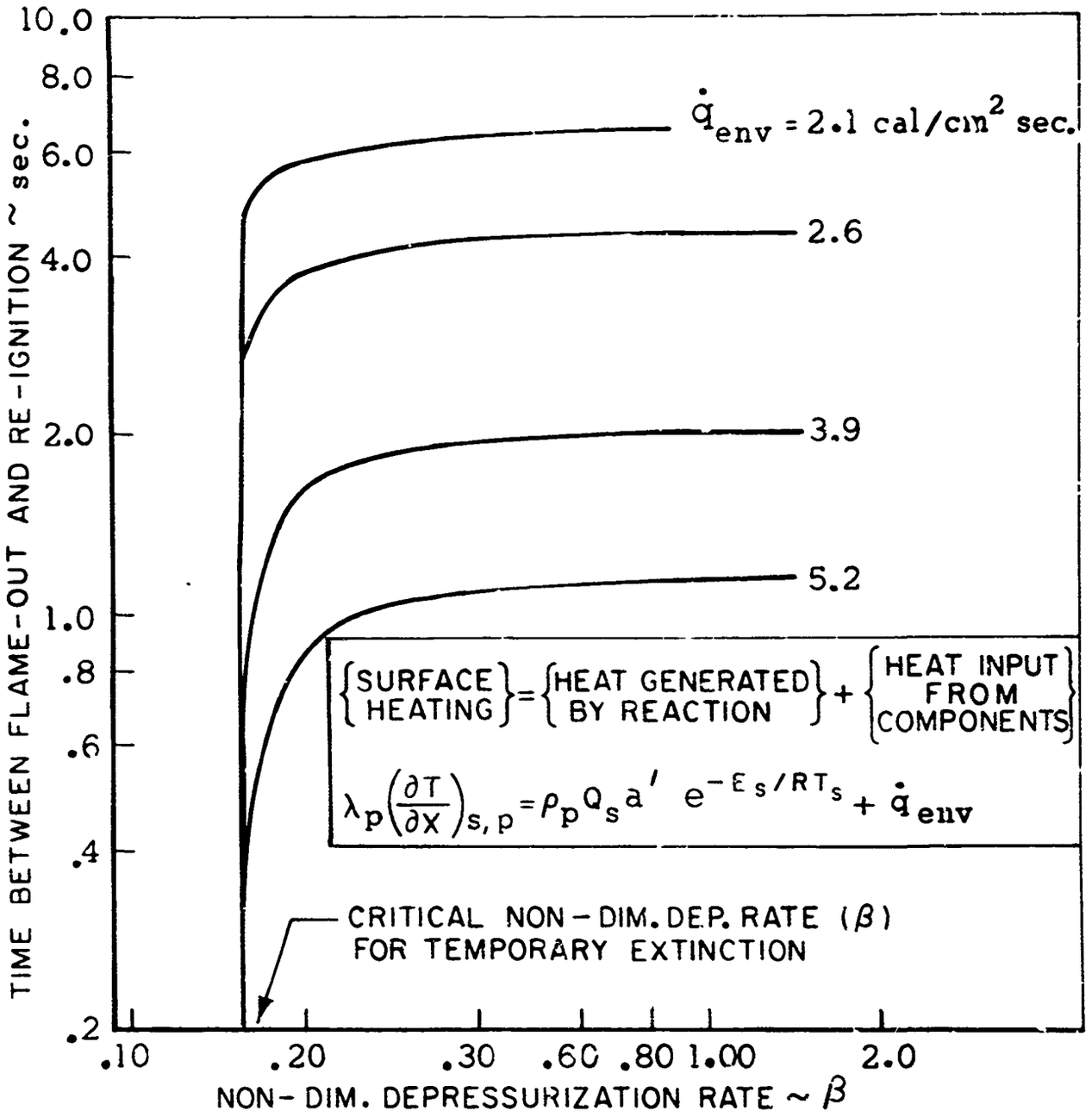

FIGURE 56

COMPARISON OF TRANSIENT PROFILES (OBTAINED BY VARYING THE DEPRESSURIZATION SPEED) AT EXTINCTION WITH VARIOUS STEADY STATE TEMPERATURE PROFILES

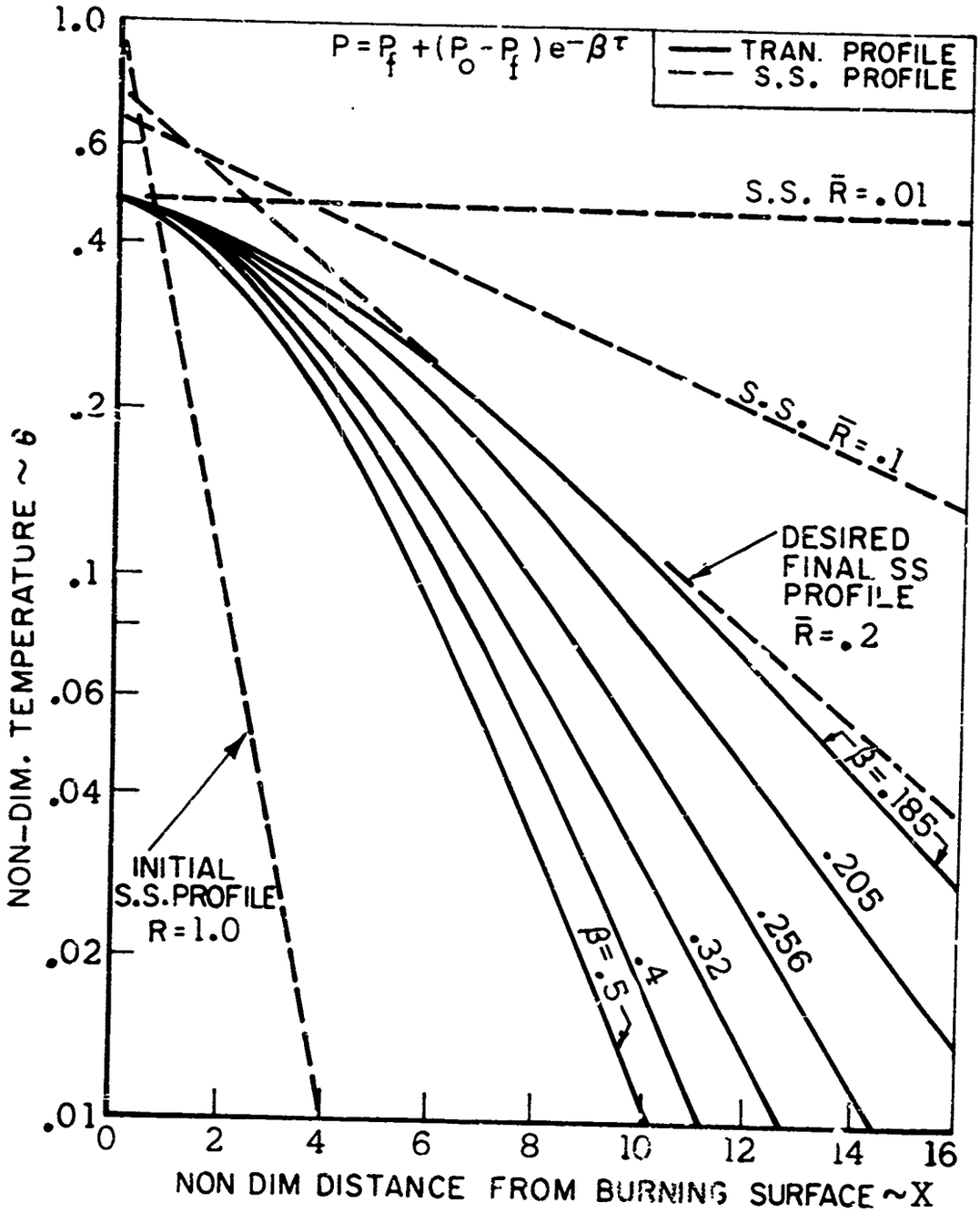

FIGURE 57

JP 19 R 4299 69

TYPICAL EXPERIMENTAL PRESSURE – TIME CURVE

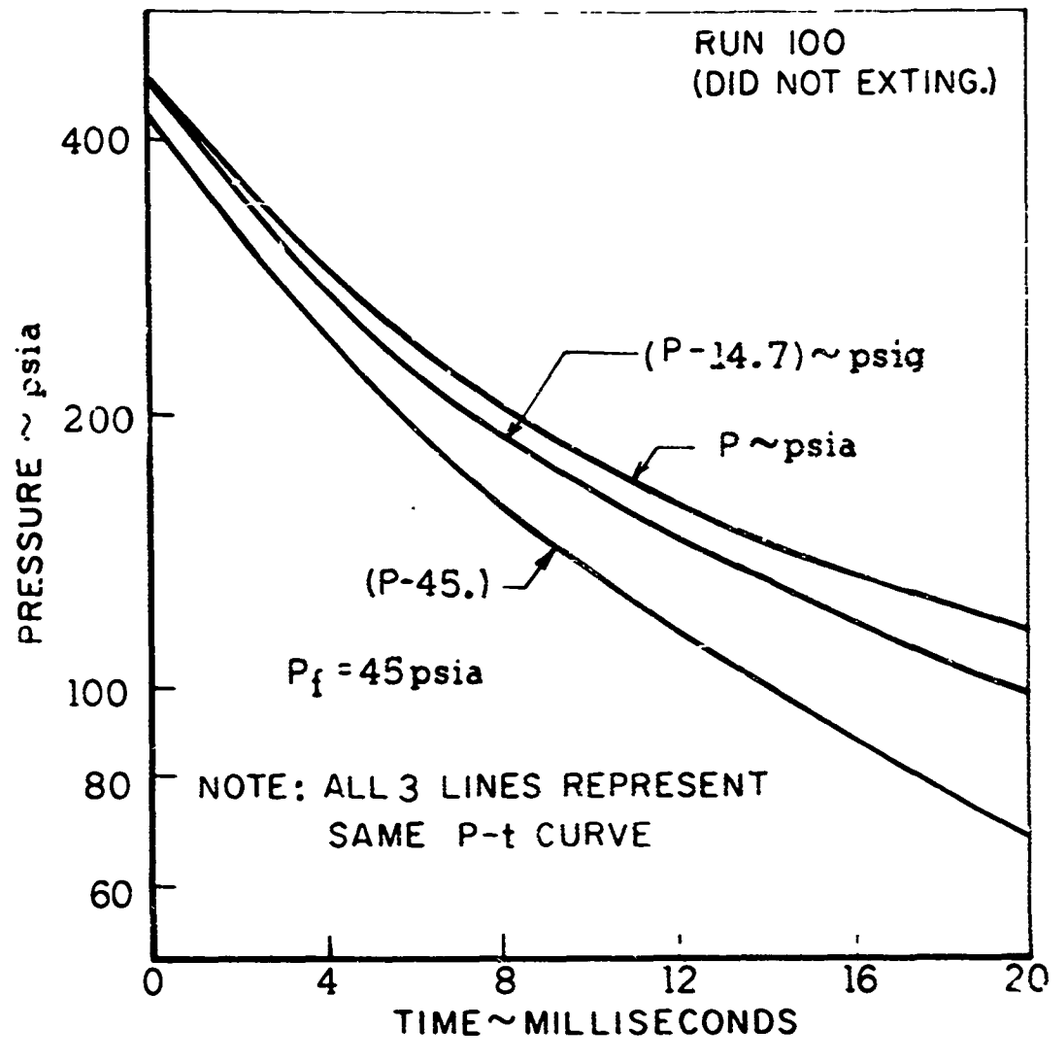

FIGURE 58

APPENDIX I

THE ANALOG COMPUTER AS AN AID IN SOLVING NON-STEADY BURNING PROBLEMS IN SOLID PROPELLANTS

The analog computer has been used extensively in certain fields, however, to date, its use in the field of solid propellants has been rather limited. This appendix describes the feasibility of applying the analog computer to the solution of non-steady combustion problems in solid propellants, and it represents the author's initial results in the research program that eventually led to the study of the extinguishment characteristics of solid propellants.

A. Fundamentals of Analog Computers

The basic element of an electronic analog computer is the operational amplifier. This particular amplifier is so named because of its ability to perform the operations of addition, subtraction, integration, and differentiation. This ability to perform the operation of integration represents the one great advantage that the analogue computer enjoys over the digital computer. A digital computer can perform the operations of addition and subtraction only. Millman[74] gives a good description of the operational amplifier.

The basic operational amplifier consists of a high gain amplifier with a common ground between the input and the output, and with an external feedback loop. The impedance which is placed in this feedback loop serves to determine the computational function of the amplifier, i.e., whether it adds, integrates, or etc. A typical operational amplifier is given in the circuit below

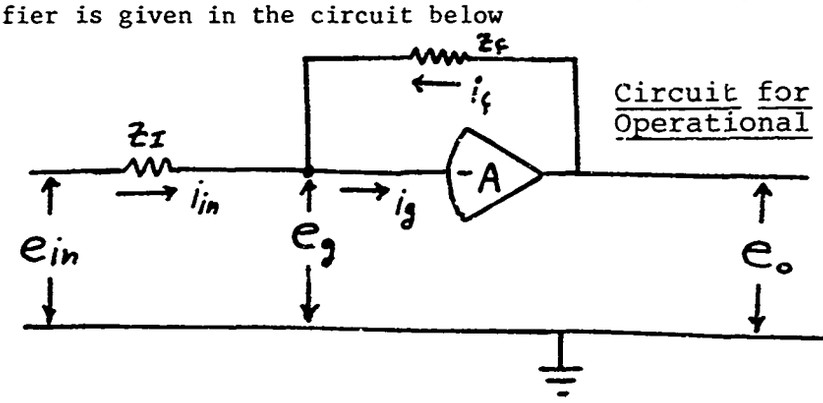

Circuit for Operational Amplifier

In this circuit the amplifier has a gain - A as noted (the negative sign implies that the output is 180° out of phase with the input). Amplifiers which are used in analog computers are chosen to have high open circuit gain, and very small grid (base) currents. Typically, the gain, A, is of the order of 10^8, and the grid (base) current, i_g, is of the order of 10^{-9} amps.

Currents, voltages, and impedances are noted on the above circuit. The input impedance is labeled as Z_I; the feedback impedance is Z_F. These impedances are, in general, complex. Corresponding currents are labeled by i_{in}, i_f and i_g (i_g represents the grid, or base current), while the voltages are labeled by the letter e (e_o represents the

output voltage). Voltages are measured with respect to the common ground.

From Kirchhoff's laws, we find the relation between the three currents,

$$i_{in} + i_f = i_g \tag{I-1}$$

and using Ohm's law,

$$i_g = \frac{e_{in} - e_g}{Z_I} + \frac{e_o - e_g}{Z_f} \simeq 0 \tag{I-2}$$

where we have used the fact that the grid current, i_g , is negligibly small. From the definition of the amplifier gain, we have $e_o = -Ae_g$ so equation I-2 becomes

$$\frac{e_{in} + e_o/A}{Z_I} + \frac{e_o + e_o/A}{Z_f} \simeq 0 \tag{I-3}$$

or,

$$\frac{e_o}{e_{in}} = -\left[\left(1 + 1/A\right)\frac{Z_I}{Z_f} + \frac{1}{A}\right]^{-1} \tag{I-4}$$

and for $A \gg 1$ (as it is for typical operational amplifiers) we have

$$e_o = -\frac{Z_f}{Z_I}\, e_{in} \tag{I-5}$$

This is the basic equation for the operational amplifier. It states that the relation between the input voltage and the output voltage is determined solely by the ratio of the feedback impedance to the input impedance.

Let us now consider some special cases of the operational amplifier. All of these special cases are obtained by using different feedback impedances, or different input impedances. First, consider the case where both the input impedance and the feedback impedance are purely real and are equal in magnitude, i.e., consider the case where they are equal resistors. Then

$$Z_I = R_I \; ; \qquad Z_f = R_f$$

and, taking

$$R_I = R_f$$

we have

$$e_{out} = -\frac{R_I}{R_f}\, e_{in} = -e_{in} \tag{I-6}$$

Thus when the input impedance and the feedback impendance are resistors of equal magnitudes, the operational amplifier performs a sign change only. Such an amplifier is very useful and is given the name, "inverter". The circuit and programming notation is given below

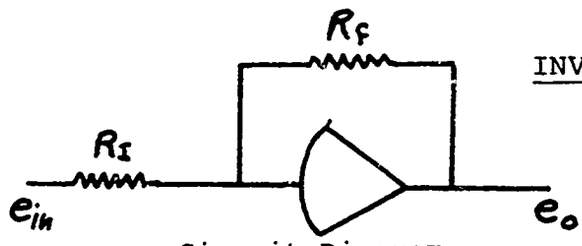

INVERTER

Circuit Diagram

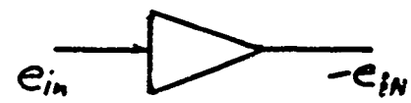

Programming Symbol

(Note that for simplicity, the common ground has been left out of this cuit as it will be for all later circuits.)

As a second case, let us return to our original circuit and modify it so that it has several input impedances. Thus consider the circuit

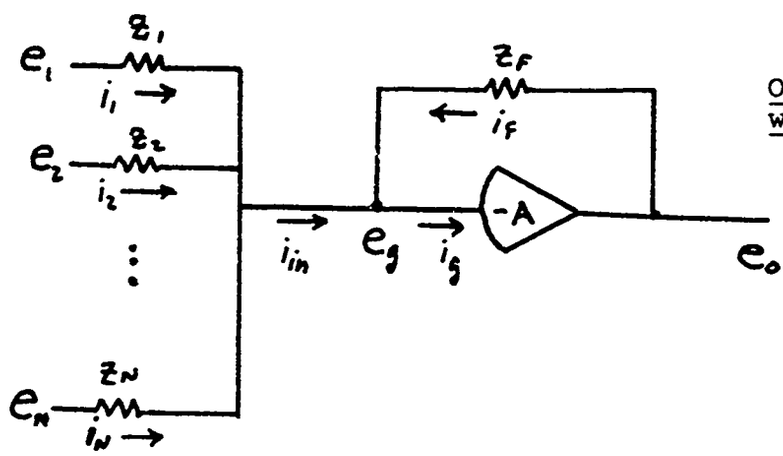

Operational Amplifier with multiple Inputs

As before, Kirchhoff's law gives

$$i_{in} + i_f = i_g \tag{I-7}$$

but we also have

$$i_1 + i_2 + \cdots + i_n = i_{in} \tag{I-8}$$

so

$$i_1 + i_2 + \cdots + i_n + i_f = i_g \simeq 0 \tag{I-9}$$

Again using Ohm's law, we have

$$\frac{e_1 - e_g}{Z_1} + \frac{e_2 - e_g}{Z_2} + \frac{e_3 - e_g}{Z_3} + \cdots + \frac{e_n - e_g}{Z_n} + \frac{e_o - e_g}{Z_f} \simeq 0 \tag{I-10}$$

and taking $e_g = -e_o/A$, we find, after some algebraic manipulation

$$e_o \simeq -\left[\frac{Z_f}{Z_1}e_1 + \frac{Z_f}{Z_2}e_2 + \frac{Z_f}{Z_3}e_3 + \cdots + \frac{Z_f}{Z_n}e_n\right] \qquad \text{(I-11)}$$

If we now choose $Z_1 = Z_2 = Z_3 = \cdots = Z_n = Z_f = R$ (i.e. choose all input impedances and the feedback impedance to be resistors of equal magnitude), then we have

$$e_o = -\left[e_1 + e_2 + e_3 + \cdots + e_n\right] \qquad \text{(I-12)}$$

This then gives us the operation of addition. Such an amplifier with multiple inputs is referred to as a summer. Its circuit and programming symbol are

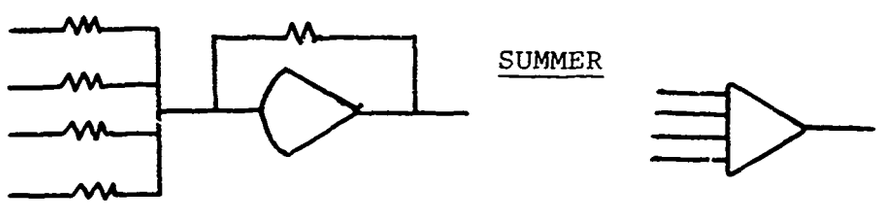

Circuit Diagram Programming Symbol

Subtraction can obviously be performed by combining a summer and an inverter.

Returning again to our single input impedance, and its governing equation I-5, we now consider the third case where both the input impedance and the feedback impedance are purely resistive, but where they are not equal in magnitude. Specifically, we take the case where the ratio of their resistances is given by $R_f/R_I = K$, where K is a constant. Then from equation I-5, we have

$$e_o = -K e_{in} \qquad \text{(I-13)}$$

Thus, this combination of input and feedback impedances gives, not only a sign change, but also a multiplication by a constant. The programming symbol for this is

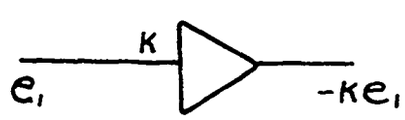

In commercial analog computers, this constant K generally has the value of 10, or 0.1, i.e., generally, it scales by a factor of 10 (either up or down). The extension of this to multiple inputs is obvious.

The multiplication of a variable by a constant can also be accomplished by means of a potentiometer. A potentiometer is a simple voltage divider. Because of its passive nature (no energy source is included in a potentiometer) a potentiometer can only multiply by a factor, K, which is less than 1.0. The circuit and programming symbol for a potentiometer are

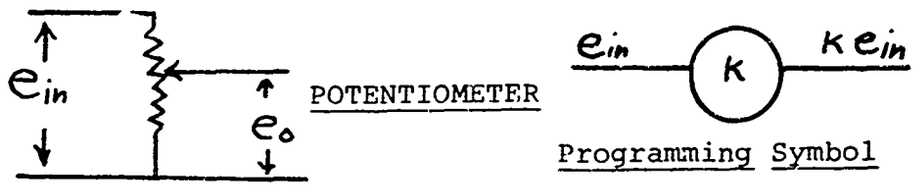

Thus, to multiply a voltage by a number greater than unity, an operational amplifier must be used. Potentiometers are used for multiplication by constants less than 1.0. However, to multiply a voltage by a specific constant, say 2.36, the normal procedure is to use both a potentiometer and an amplifier. The potentiometer first multiplies the voltage by .236; the amplifier then multiplies this result by 10.0 to get the desired 2.36 multiplication.

In order to obtain an integrator, we must use a reactive component in our operational amplifier. The current through a capacitor of capacitance C, is given by

$$i_f = C \frac{de_c}{dt} \tag{I-14}$$

Where C is the capacitance of the capacitor in farads, and e_c is the voltage drop across the capacitor. We have labeled the current through the capacitor as i_f, in anticipation of placing the capacitor in the feedback loop as shown in the following circuit.

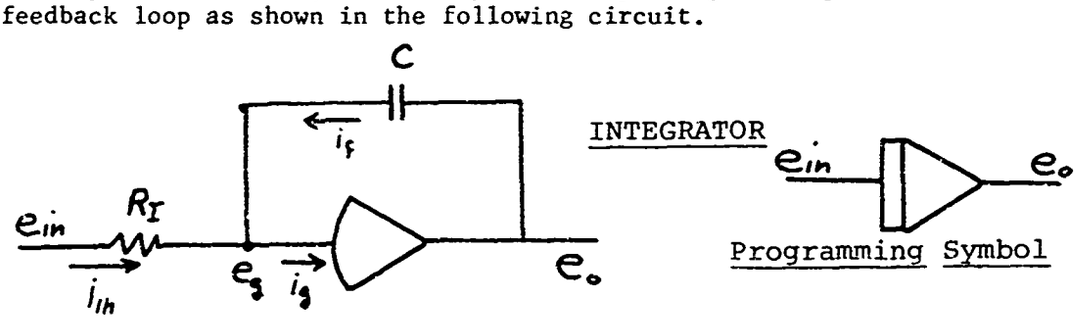

Again, Kirchhoff's law gives

$$i_{in} + i_f = i_g \simeq 0$$

or

$$\frac{e_{in} - e_g}{R_I} + C\frac{d(e_o - e_g)}{dt} \simeq 0 \tag{I-15}$$

Taking $e_o = -Ae_g$, $A >> 1$, we have

$$e_{in} = R_I C \frac{de_o}{dt} \tag{I-16}$$

or

$$e_o = \frac{1}{R_I C} \int_0^t e_{in}\, dt + V_o \qquad \text{(I-17)}$$

where V_o is the voltage (i.e., stored charge) on the capacitor at time zero. Consequently, we see that the output of an integrator is indeed the integral of the input.

This result can also be obtained directly from equation I-5. Expressing the capacitor in terms of its complex impedance, $Z_C = 1/\omega C$, we have

$$e_o = -e_{in}/(\omega R_I C) \qquad \text{(I-18)}$$

where $Z_I = R_I$. This relation is obviously the Fourier transform for the integral of the input voltage.

As indicated above, the initial condition in the integration is represented by the charge which is stored on the capacitor at zero time. Integrators on commercial analog computers commonly have a special circuit which allows the operator to pre-set the initial condition for each integrator by charging each integrating capacitor to a selected initial voltage. This initial condition is denoted in the programming symbol for an integrator as shown below

Integrator with Multiple inputs

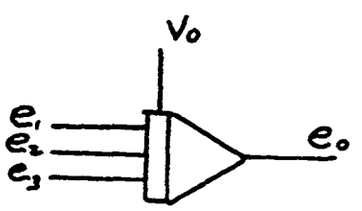

For generality, we have shown multiple inputs on this symbol. It is easy to show that an integrator can act as both a summer and an integrator in one step. For the programming symbol shown, the output voltage, e_o, is related to the input voltages by

$$e_o = -\int_0^t (e_1 + e_2 + e_3)\, dt + V_o \qquad \text{(I-19)}$$

One further interesting and useful characteristic of integrators, is their ability to "time-scale" the problem. For instance, consider a problem in which the actual process time is of the order of milliseconds (as is the case in our depressurizations). If the solution to this problem is computed on so short a time scale, the operator will have no time to observe events that occur during the transient. Consequently it is advantageous to time-scale the problem so that the solution is computed at a "convenient" speed. (Note that in analog computing, the programmer operates the computer and observes the computer "solutions" as they are computed, by means of a cathode ray oscilloscope

or a mechanical X-Y plotter. Consequently, he generally picks a time-scale which is suitable for obtaining the information he is currently seeking.) To visualize how the integrators time scale, we define a new time variable τ which is related to the real time, t, as

$$t = K_1 \tau$$

where X_1 is a constant. Then the integral in equation I-17 becomes

$$e_o = \frac{1}{R_I C} \int_0^{K_1 \tau} e_{in} \, d(K_1 \tau) + V_o$$

or

$$e_o = \frac{K_1}{R_I C} \int_0^{\tau} e_{in} \, d\tau + V_o \qquad \text{(I-20)}$$

Thus time scaling is accomplished by changing either the input resistor, R_I, or the feedback capacitor, C. For instance if we use a new capacitor C' such that $C' = C/K_1$, then we have time-scaled the problem by a factor, K_1.

The differentiating circuit is seldom used in analog computing, and will not be discussed here. Let it suffice to say that a differentiator can be obtained by using a resistor as a feedback impedance, and a capacitor as the input impedance.

Thus far, our discussion of analog computers has concerned only linear elements. Non-linear operations are achieved by resorting to approximations. One of the most useful approximation methods is by means of variable diode function generators (VDFG). These devices can be used to represent a general function of the independent variable x by a series of straight lines. For example, the representation of the general function, $f(x)$, is accomplished by the series of connected line segments as shown below.

Representation of a General Function by Straight Line Segments

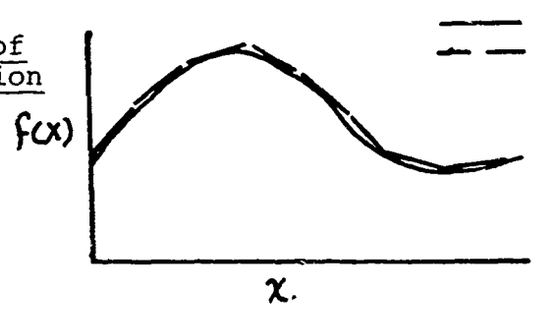

Generally speaking, the VDFG's have a capability of about 20 line segments. The slope of each of the segments is chosen by the operator, by setting the output voltage at each break-point. The programming symbol for these function generators is

Variable Diode Function Generator

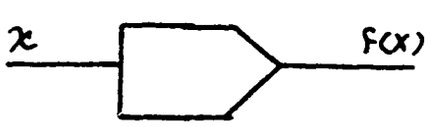

One very important use of the diode function generator is for multiplication of two variables. The break-points on the diode function generators are pre-set by the manufacturer. Each multiplier consists of two function generators, both of which square the input that they receive. Thus, to multiply the two variables, x and y, the sum, x + y, is fed into one function generator, while the difference, x-y, is fed into the second function generator. The outputs of the two function generators are $(x+y)^2$ and $(x-y)^2$, respectively. The desired product is obtained by subtracting these two results.

$$xy = (1/4)\left[(x+y)^2 - (x-y)^2\right] \tag{I-21}$$

This particular type of multiplier is known as the quarter-scale multiplier. Various other means have been devised for multiplication on an analog computer, but the quarter-scale multiplier is probably the most widely used. (Karplus and Soroka[75] devote their entire Chapter 3 to the subject of multipliers).

The programming symbol for a multiplier is

Multiplier

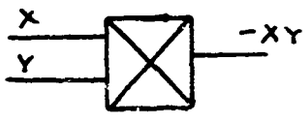

Other pre-set function generators which are generally included on analog computers is a function generator whose output is the logarithm of its input. (Note that some variable diode function generators are also generally available on a commercial analog computer. The variable diode function generators are set by the operator to approximate any function as desired by the operator.)

Several good textbooks are available on the general theory of analog computers. Among them are references 75 to 79. All these references include developments similar to the one given above (which most closely follows reference 78).

B. Magnitude and Source of Errors in Analog Computing

Typical errors in an analog computer solution of a problem generally run around 2 to 5%. For many situations, this accuracy is sufficient, for other applications, it rules out the analog computer. Frequently a problem can be split into two separate parts, for example, if y is the solution to be found, let $y(t) = \xi(t) + \eta(t)$ where $\xi(t)$ is an algebraic function of a certain type which may closely approximate the solution. Frequently physical systems suggest such a function. Thus from the original equations and the boundary conditions a new equation for the unknown function, $\eta(t)$, can be determined. Thus if (for example) $\eta(t)$, is about one-half as large as $\xi(t)$ in magnitude, an error of 3% in $\eta(t)$ will cause an error of only 1% in the final solution.

The sources of the errors in analogue computing are varied. The approximations which are used for non-linear functions are one source of error Normally these can be kept to 0.1% of full-scale, or to an effective level of about 0.5%. Most components have tolerances on the order of 0.1% of full scale. Note that if the feedback resistor and the input resistor in an inverting amplifier are not precisely identical, the amplifier will multiply the input signal by a constant percentage (equal to the percentage difference in the two resistors) as well as change its sign. Amplifier drift can also be a problem, although it can generally be reduced to levels much lower than the other sources of errors by proper use of chopper-stabilized amplifiers. Finally, noise and hum also add their small bit to computing errors.

C. Solution of Simple Ordinary Differential Equations on the Analog Computer

Ordinary differential equations can be solved directly on the analog computer by exploiting its integration capabilities. When solving differential equations, computer time corresponds to the independent variable in the problem, and the voltages in the analog computer represent the dependent variables. By using the time-scaling property (discussed previously), solutions can be obtained very rapidly once the "program" has been checked out. Time scaling is generally chosen so that a typical solution takes about one minute on the analog. Because the operator is actually at the console during the computation, "turnaround" time is inherently fast (when the machine is available). Because the operator is at the console during the time of computation, he is able to observe the effects of variations in parameters in rapid order, and can often adjust his computer runs accordingly. Many computers include the capability of "repetitive operation" which makes it even easier to observe the effects of various parameters on the solution. During repetitive operation, the problem solution time is speeded up by a factor of from 100-1000 (by introducing new feedback capacitors into the integrator feedback loops by means of an internal circuit) and is calculated repeatedly many times per minute. By portraying these repetitive solutions on an oscilloscope, the operator can get a quick qualitative feel for the effect of changes in certain parameters (see reference 78, pp. 241-247).

Because, as noted above, the analog computer is limited to inetrations in one independent variable--machine time (which can be given a one-to-one correspondence with any other independent variable, e.g., distance) -- the analog computer can solve only ordinary differential equations, or systems of ordinary differential equations in a single independent variable. Solution of partial differential equations on the analog computer can only be accomplished after all but one independent variable has been broken down into a network of discontinuous intervals by means of some sort of discretization technique. Such an operation converts the partial differential equation into a coupled system of ordinary differential equations which can then be solved directly on the analogue. (Note that to obtain a solution on a digital computer, all independent variables must be discretized so that only purely algebraic equations remain.)

Before going into the solution of partial differential equations, let us first consider the solution of a relatively simple ordinary differential

equation. Consider, for example, the solution of the ordinary differential equation

$$\frac{d^2y}{dt^2} + .35\frac{dy}{dt} + 1.57\,y = \sin \omega t \qquad \text{(I-22)}$$

where the forcing function, $\sin \omega t$, is available from a function generator external to the analog computer.

We begin by drawing the programming circuit for this equation. In so doing, we will use a very simple-minded approach, but the aim is to illustrate the method for those who are not familiar with it. In drawing the programming circuit, we first start by assuming that the highest derivative, d^2y/dt^2 is available, and then proceed to determine the first derivative, dy/dt, and the function itself. In such a process, one must be careful to remember that a sign change occurs as in every amplifier. We re-write equation I-22 as

$$-\frac{d^2y}{dt^2} = .35\frac{dy}{dt} + 1.57\,y - \sin \omega t \qquad \text{(I-23)}$$

Then we have

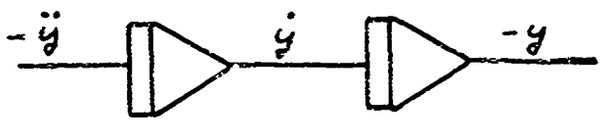

so that the three values $\ddot{y}$, $\dot{y}$, and y are now "available". We now proceed to add the three functions together to give the second derivative (see equation I-23).

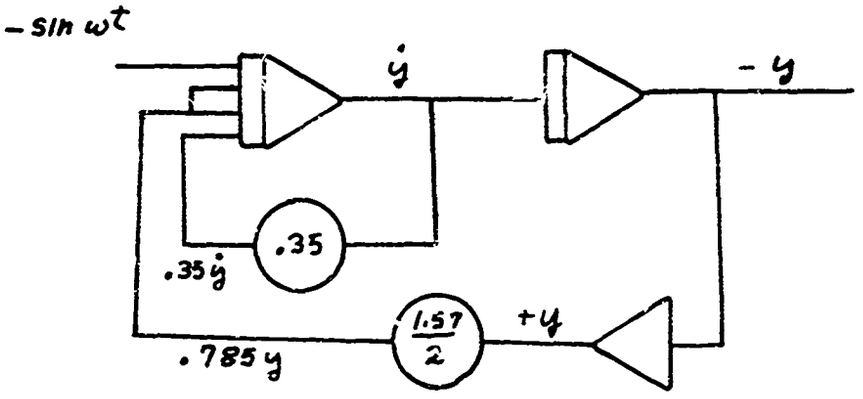

Important facts to note are that we must use an inverter to obtain "+y". Also, to obtain a multiplication of 1.57, we have scaled down by 1.57/2 in a potentiometer (note 1.57/2. is less than unity as is required in a potentiometer) and then we have fed the same input into the first integrator twice using two separate input resistors. This gives the required gain. To obtain ".35 $\dot{y}$" we simply use a potentiometer set at .35. The

forcing function, $-\sin wt$, is assumed to be available externally.

Finally we specify initial conditions and include them in our program circuit. For example, take

$$y(0) = 5.0 \qquad \dot{y}(0) = 0$$

Then we have

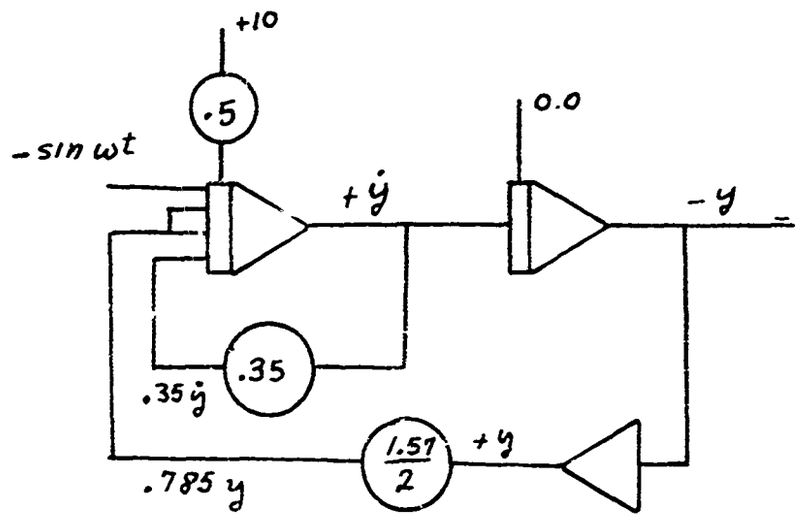

Note for a zero initial condition, the lead-wire can be left out. The capacitor needn't be shunted to ground.

In actual practice, simple forcing functions such as sinusoidal functions need not be obtained from external sources. They can be obtained from solutions of appropriate differential equations. For example the equation

$$\ddot{y} + \omega^2 y = 0 \qquad \begin{cases} y(0) = 0 \\ \dot{y}(0) = 1 \end{cases} \tag{I-24}$$

has the solution

$$y(t) = \sin \omega t \tag{I-25}$$

Hence this simple forcing function can be generated by the circuit

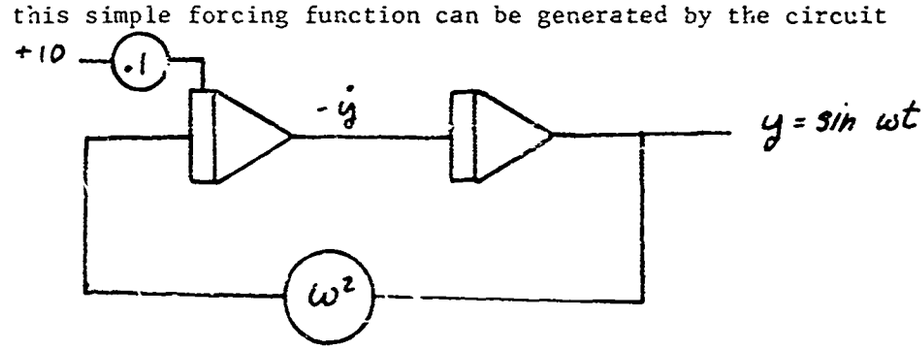

It is similarly easy to generate exponential functions, error functions, etc. Power series in time can be generated by successively integrating a constant voltage, for instance,

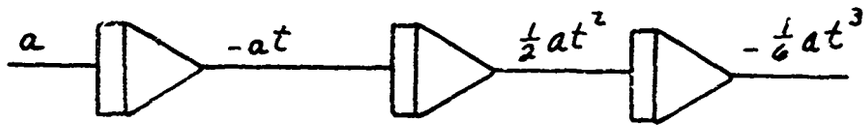

Finally, a transformation of variables is frequently helpful in programming. To evaluate the integral below, we can use a transformation

$$\int y\, dx = \int y \frac{dx}{dt}\, dt \tag{I-26}$$

(Recall an analogue computer can only integrate in one independent variable.)

D. Solution of the KTSS Model on the Analog Computer

The KTSS model, which is presented in reference 43, was programmed for the analog computer by the author as the beginning part of his research program. A considerable number of analog computer solutions were obtained for sinusoidally varying pressures, and for exponentially increasing pressures. In general these results agreed quite well with digital computer results of the same problem (within 5%).

The particular analog computer that was used, was an Electronics Associates, Inc. PACE TR-48 Model computer. This is a small computer as analog computers go. The TR-48 included the following components; 42 amplifiers plus 16 integrators, 6 multiplier, 4 variable diode function generators, and 4 logarithmic function generators. This computer has repetitive operation capabilities.

The equations in the KTSS model which were solved on the analog are

$$\frac{\partial^2 \theta}{\partial x^2} + R\frac{\partial \theta}{\partial x} = \frac{\partial \theta}{\partial \tau} \qquad 0 \le x < \infty \tag{I-27}$$

$$\theta(x,0) = \theta_s e^{-R_0 x}$$

$$\theta(\infty, t) = 0$$

$$\frac{\partial \theta}{\partial x}(0,t) = -\frac{(p^{n/m} - H)p^{2n}}{R} - HR \tag{I-28}$$

The auxiliary pyrolysis realtion is

$$R = \theta_s^{m} \tag{I-29}$$

where m is a constant. Because the number of components was the most stringent restriction on the TR-48, the pyrolysis relation was replaced by

$$R = A\, e^{a\theta_s} \tag{I-30}$$

where A and a are two constants which were chosen so as to most closely represent equation I-29. By using equation I-30 as a pyrolysis relation, the logarithmic function generators could be used directly. An alternative approach would have been to use the variable diode function generators, but this would have required carefully setting the VDFG's each time the analog was operated.

The first step which must be taken before programming equation I-27 on the analog is to discretize the partial differential equation into a series of coupled ordinary differential equations. However, my initial programming efforts indicated that only a very small number of "slabs" in the solid phase could be accomodated on the small TR-48 analog. Consequently a transformation of variables was used so as to make the temperature profile in the solid as nearly linear as possible in the transformed coordinates. With a nearly linear profile, a small number of space increments could still give relatively accurate approximations for the spatial derivatives. The particular transformation that was chosen, was to define the new spatial coordinate, Z, as

$$Z = e^{-x} \tag{I-31}$$

under this transformation, equation I-27 becomes

$$Z^2 \frac{\partial^2\theta}{\partial Z^2} + (1-R)Z\frac{\partial\theta}{\partial Z} = \frac{\partial\theta}{\partial\tau} \qquad 0 \le Z \le 1 \tag{I-32}$$

This is the equation that was eventually programmed for the analog computer. The boundary conditions I-28 become, under this transformation

$$\begin{aligned} \theta(Z,0) &= \theta_s Z^{R_0} \\ \theta(0,t) &= 0 \\ \frac{\partial\theta}{\partial Z}(1,t) &= \frac{(P^{n/m}-H)P^{zh}}{R} + HR \end{aligned} \tag{I-33}$$

To reduce the partial differential equation, I-32 into a series of coupled ordinary differential equations, a discretization technique was applied to the spatial derivatives. The resulting ordinary differential equations are of first order in the independent variable, time. Each of these ordinary differential equations describes the time history of the propellant temperature at a particular point in space. The coupling between the equations at each point in space brings the spatial effects into the problem. The resulting differential equations are of the

form

$$z_i^2 \frac{\theta_{i+1} - 2\theta_i + \theta_{i-1}}{(\Delta z)^2} + (1-R)\, z_i \frac{\theta_{i+1} - \theta_{i-1}}{2\Delta z} = \frac{d\theta_i}{dt} \qquad \text{(I-34)}$$

and in general there are N such equations. As can be seen, each equation is coupled to the one on either side of it. The cold end boundary condition specifies the temperature at Z=0 for all time (see boundary condition, equation I-33). Thus the first equation would be for the first interior point (starting from the cold end). If we designate $\theta(0) = \theta_0$ and $\theta(\Delta z) = \theta_1$, we have

$$\frac{d\theta_1}{dt} = (\theta_2 - 2\theta_1 + \theta_0) + (1-R)\tfrac{1}{2}(\theta_2 - \theta_0) \qquad \text{(I-35)}$$

where $z_1 = \Delta z$. . Since $\theta_0 = 0$, this becomes

$$\frac{d\theta_1}{dt} = (\theta_2 - 2\theta_1) + (1-R)\,\theta_2/2$$

Thus, the cold boundary condition is very simple to include.

At the hot end, the equation had to be treated somewhat differently. We denote the surface temperature $\theta(1) = \theta_N$. The equation for the surface temperature is

$$z\left(\frac{\partial^2\theta}{\partial z^2}\right)_{z=1} + (1-R)\, z\left(\frac{\partial\theta}{\partial z}\right)_{z=1} = \left(\frac{\partial\theta}{\partial \tau}\right)_{z=1} \qquad \text{(I-36)}$$

The first derivative term is simply our boundary condition, equation I-33, so there is no need to use finite difference methods on this term. We simply replace it by the required boundary condition. The second derivative still poses trouble. If we apply the centered finite differences to it, we introduce the new unknown, θ_{N+1} (which represents the temperature one space-step <u>outside</u> the solid phase, i.e., in the gas phase). Consequently we use a non-centered difference approximation for this derivative, but since all our other spatial difference approximations are of order $(\Delta z)^2$ in accuracy, we must take care to use a difference formula for this end condition which has similar accuracy. Reference 79 gives such a formula, on page 324,

$$\frac{d^2\theta_N}{dz^2} = \frac{2\theta_N - 5\theta_{N-1} + 4\theta_{N-2} - \theta_{N-3}}{(\Delta z)^2} \qquad \text{(I-37)}$$

Combining these two special features, and noting that $z_N = N\Delta z = 1$, the differential equation for the Nth temperature (the surface temperature) is

$$\frac{d\theta_N}{dt} = N^2(2\theta_N - 5\theta_{N-1} + 4\theta_{N-2} - \theta_{N-3}) + (1-R)N\left[\frac{P^{2n}(P^{n/m} - H)}{R} + HR\right] \qquad \text{(I-38)}$$

After the spatial coordinate is broken up into N lattice points, with an ordinary differential equation describing the time history of the temperature of each lattice point, the equations are programmed on the computer and are solved in parallel. That is to say, all N equations are solved simultaneously by the computer. The solution for the N equations then marches forward in time, in a process very similar to the physical process. In the physical process, the "solution" (i.e., the actual experiment) "marches forward" in time for each "slab" in the propellant, except that in nature, the slabs are infinite in number and infinitesimal in thickness (i.e., nature really deals with the distributed parameter problem, not the lumped parameter approximation). This physically justifies our reasons for discretizing the spatial coordinate.

If the time variable were discretized, the resulting equations would be second order ordinary differential equations in Z. This would give equations of the form

$$Z^2 \frac{d^2\theta^j}{dZ^2} + (1-R^j) Z \frac{d\theta^j}{dZ} - \frac{\theta^j}{\Delta\tau} = -\frac{\theta^{j-1}}{\Delta\tau} \qquad \text{(I-39)}$$

which is analogous to the equations which were used for the digital computer solution. However, the solution of this set of equations, I-37 must be obtained by serial means. Specifically, given the initial conditions, $\theta^0(Z)$, the solution for $\theta^1(Z)$ can be found, etc. This procedure does not lend itself to an analog computer which is basically a parallel machine. A complete discussion of this problem is given in a very readable form in Chapter 16 of reference 77. From a stability viewpoint, the parallel integration procedure of equation I-34 is always computationally stable.

The circuit diagram for the parallel method of integration of the nonsteady burning equation (equation I-34) is given in figure I-1 for one lattice point in the spatial coordinate. Each lattice point in the solid requires a circuit similar to the one in this figure, i.e., each point requires one multiplier and one integrator plus several amplifiers and potentiometers. But the TR-48 analog contains only 6 multipliers as was stated previously. This sets an upper limit on the number of lattice points that can be accomodated in the simulation of the solid propellant equations. The boundary condition between the solid phase and the gas phase, equation I-38, also requires a multiplier. The circuit for this particular lattice point, the point on the burning surface of the propellant, is shown in figure I-2. Thus, because of the limitation of the number of multipliers which is available on the TR-48, only five lattice points could be programmed. This is really not sufficient to obtain an accurate solution of a partial differential equation, but some suprisingly accurate results were obtained as is shown in the next section.

This points out the most severe limitations of the analog computer. Because it solves equations in a parallel fashion, the maximum number of equations which can be simultaneously solved, is limited by the size of the analog computer. The actual size limitation imposed here is somewhat artificial in that the TR-48 is a small analog computer. A more typical analog (in terms of number of components) is the Model 680 which is also manufactured by Electronics Associates, Inc. This computer is classed as a "middle-size" analog and contains 156 amplifiers and 24

multipliers. Electronics Associates' "large" analog, the Model 8800 contains 224 amplifiers and 46 multipliers. Our non-steady burning problem would, therefore, easily fit on the middle-sized computer, however, there was none available at Princeton at the time the analog computer work was done.

E. Typical Analog Computer Results for the KTSS Analysis

Some typical results which were obtained on the analog computer are shown on figure I-3. The pressure forcing function which was used for this data is an increasing exponential,

$$P = 1 + \Delta P \left(1 - e^{-\tau} \right) \tag{I-40}$$

where τ is the non-dimensional time, and P is the non-dimensional pressure. The pyrolysis expression that was used was of the form

$$R = \theta_s^{M} \tag{I-41}$$

with M=6 as indicated on the figure. The value of ΔP which was used was 2.5; the non-dimensional pressure increased exponentially from P=1.0 to P=3.5. Various values of the surface heat release parameter were used as indicated on the figure. The steady state burning rate was given by

$$R = P^{n} \tag{I-42}$$

with the index n=.5.

A comparison of some of these results with digital computer solutions of the same equation are shown on figure I-4. As can be seen, the analog results are qualitatively correct but larger errors appear as the surface heat release parameter, H, is increased. The most probable source of these errors arises because only five spatial lattice points could be programmed on the analog for the solution of the partial differential equation. This probably overshadowed the normal computing errors in an analog computer in the solution of this particular problem. The digital computer solutions were obtained by using 40 lattice points in the spatial coordinate. The numerical calculation procedure that was used for these digital computer results (and the results themselves) are taken from Krier's work[69].

A series of analog computer solutions were also obtained for an oscillatory pressure forcing function. In general, these solutions were about as accurate (as compared with the digital results) as the comparisons on figure I-4.

F. Hybrid Computers

A third general family of computers in addition to analog computers and digital computers, is hybrid computers. Hybrids (hopefully) combine the best features of both analog and digital computers. The analog

computer lacks the ability to store information; it has no memory or logic. By contrast, this is the digital computer's strongest asset. The hybrid computer consists of both an analog computer and a digital computer, joined together. The digital portion of a hybrid is used for memory and logic; the analog portion is used for integration of differential equations. Through its logic capabilities, the hybrid can function as a sequential machine. This destroys some of the attractiveness of the analog, because parallel solutions are inherently more similar to the natural process than are serial solutions, and so pose less problems of error propagation in the computation (i.e., computational stability is not a problem). However, by functioning as a sequential machine, the hybrid greatly reduces the number of analog computer components that are required for the solution of a particular problem.

As an example of a particular application of hybrid computers, we consider the analog circuit which is necessary for the solution of the non-steady burning problem which was discussed above. The proper finite differencing method to apply this problem to a hybrid computer is to finite difference the time coordinate, giving equation I-39. For reference, we re-write equation I-39 here.

$$z^2 \frac{d^2\theta^j}{dz^2} + (1-R^j)\, z \frac{d\theta^j}{dz} - \frac{\theta^j}{\Delta\tau} = -\frac{\theta^{j-1}}{\Delta\tau} \qquad \text{(I-43)}$$

The circuit diagram for this equation is shown on figure 1-5.

The computational scheme for equation I-43, goes as follows. At the beginning of the computation, the initial condition, $\theta^0(z)$ is stored in the digital portion of the hybrid computer. This stored function is then converted to an analog signal and fed to the analog computer while the analog computer integrates across the spatial domain (note that in this problem, the analog computer "time" corresponds to the spatial coordinate, Z) As the solution, $\theta^1(z)$, is computed, it is stored in the memory banks of the digital. Thus after the analog has integrated across the spatial coordinate, Z, a new function, $\theta^1(z)$ has been stored in the digital portion of the hybrid. Consequently the integration for $\theta^2(z)$ can now be accomplished in the same manner, using the <u>same</u> analog components. Thus the components shown in figure I-5 are the <u>only</u> analog computer components needed for the hybrid computer solution of this problem. The only functions the digital has to perform are the storage of the function $\theta^{j-1}(z)$, and the logical control of the analog, i.e., the digital computer has to tell the analog computer when to integrate, how far, etc.

As can be seen, the hybrid computer is very attractive for the solution of partial differential equations. It still includes the time-scaling abilities of an analog, which enable the operator, to a large extent, to specify the computation time required for a solution. It includes the digital computer advantages of stored memory and logic.

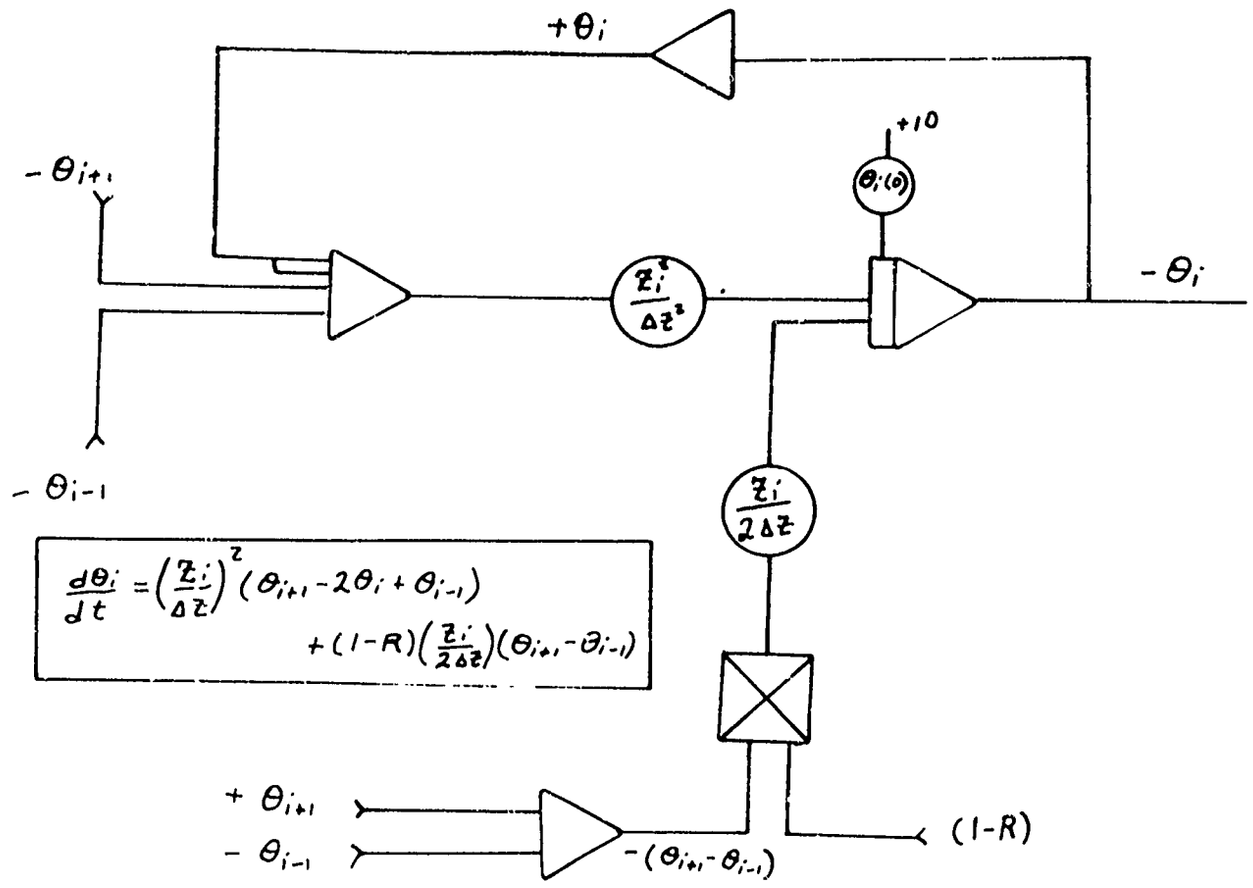

FIGURE I-1 ANALOG COMPUTER CIRCUIT DIAGRAM FOR SOLUTION OF NON-STEADY BURNING EQUATION (EQ. I-34) FOR A GENERAL LATTICE POINT IN SPACE

FIGURE I-1

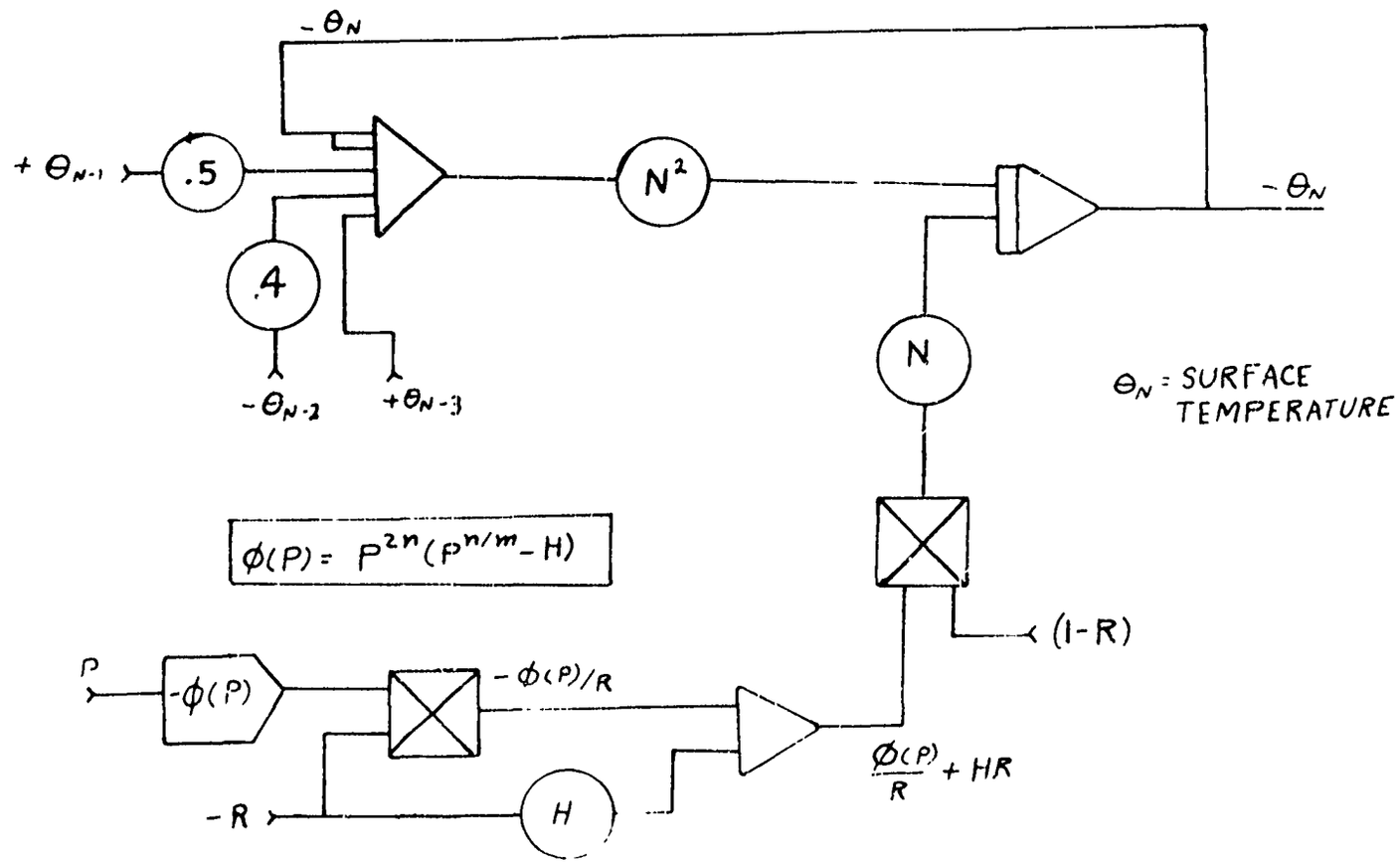

FIGURE I 2 ANALOG COMPUTER CIRCUIT DIAGRAM FOR LATTICE POINT REPRESENTING BURNING SURFACE OF PROPELLANT (see Eq. I-38)

FIGURE I-2

TYPICAL ANALOG COMPUTER RESULTS

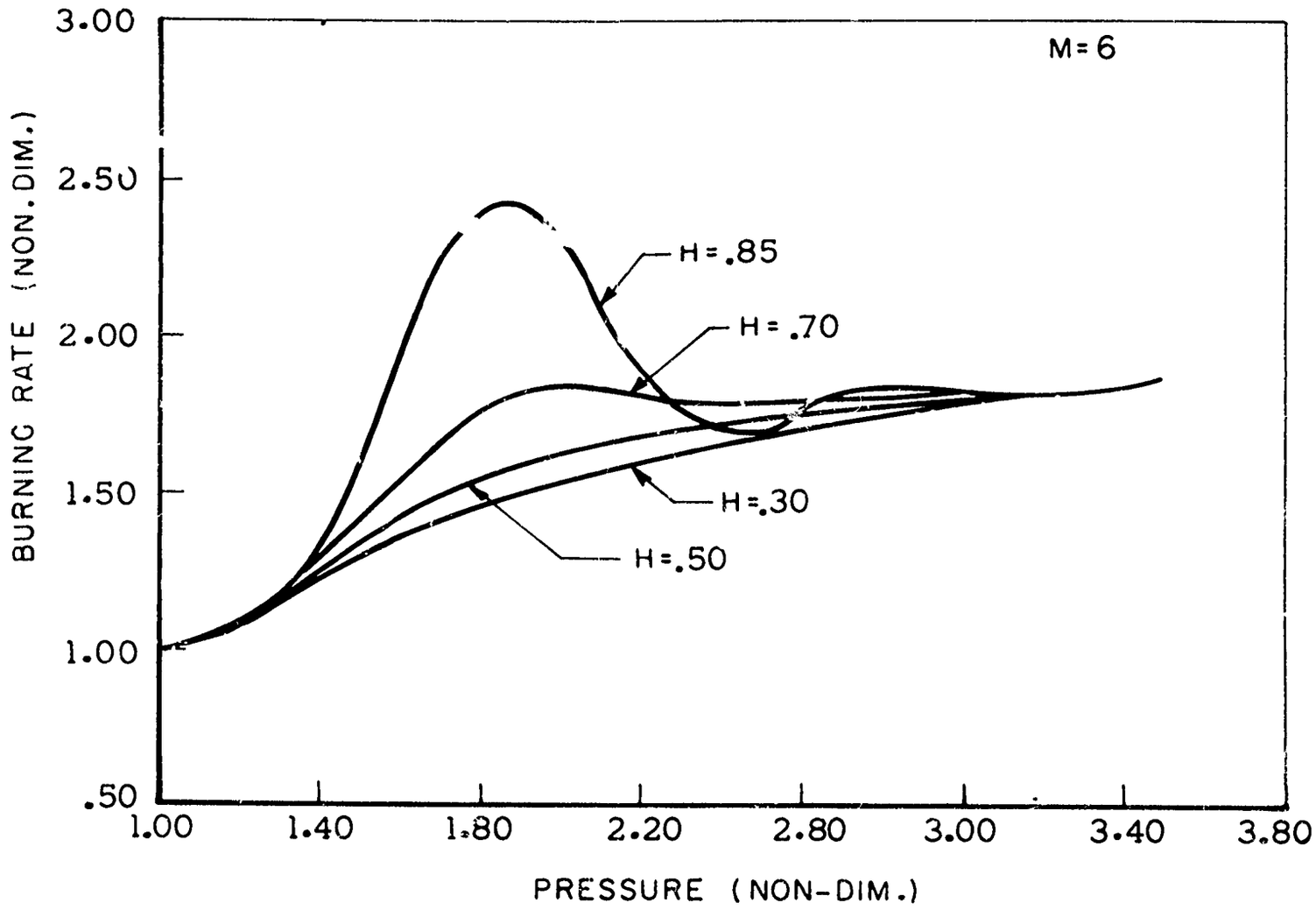

FIGURE I-3

JP 19R430.1 6.9

JP 19 R 4305 69

COMPARISON BETWEEN ANALOG AND DIGITAL COMPUTER RESULTS

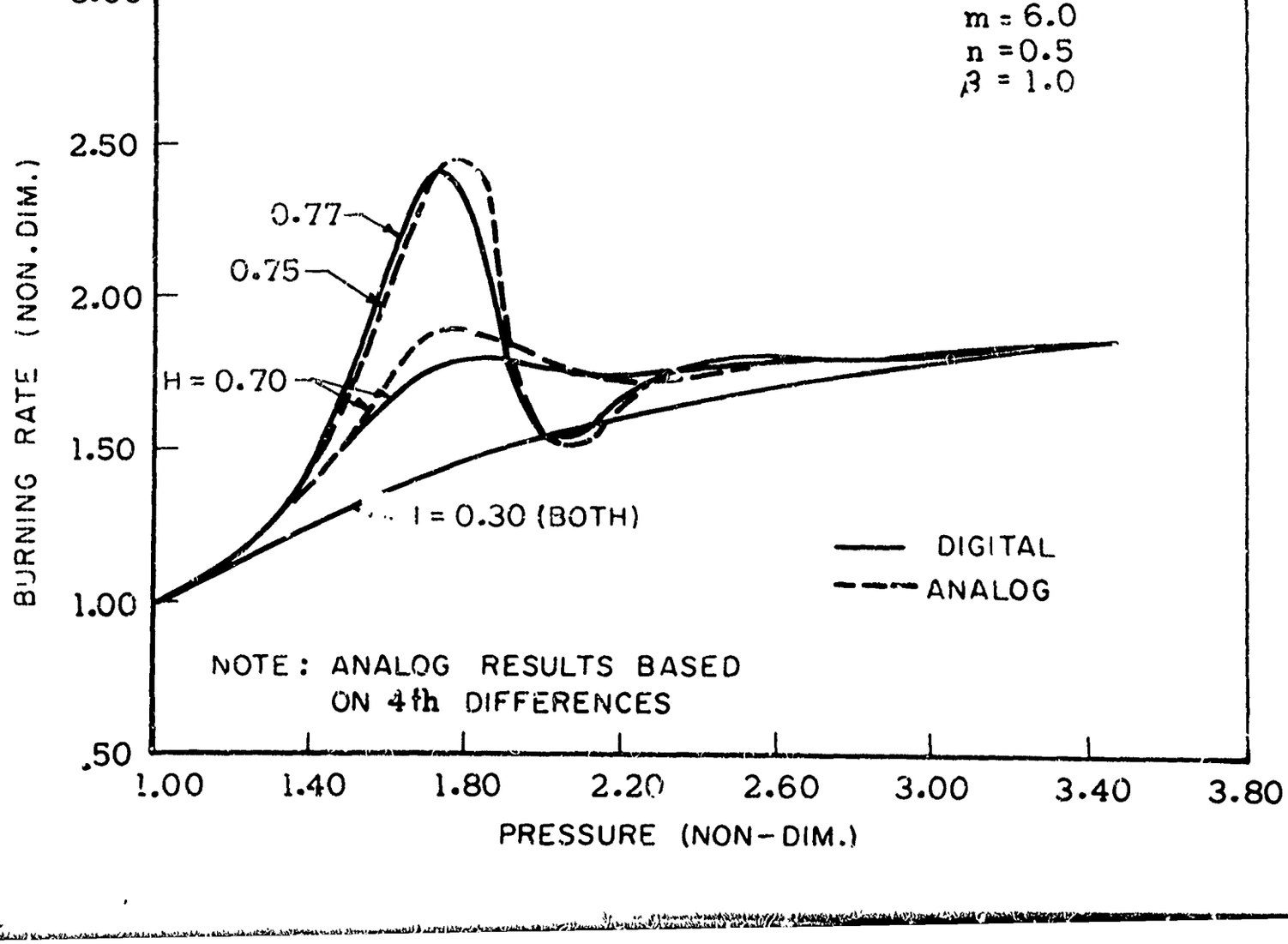

FIGURE I-4

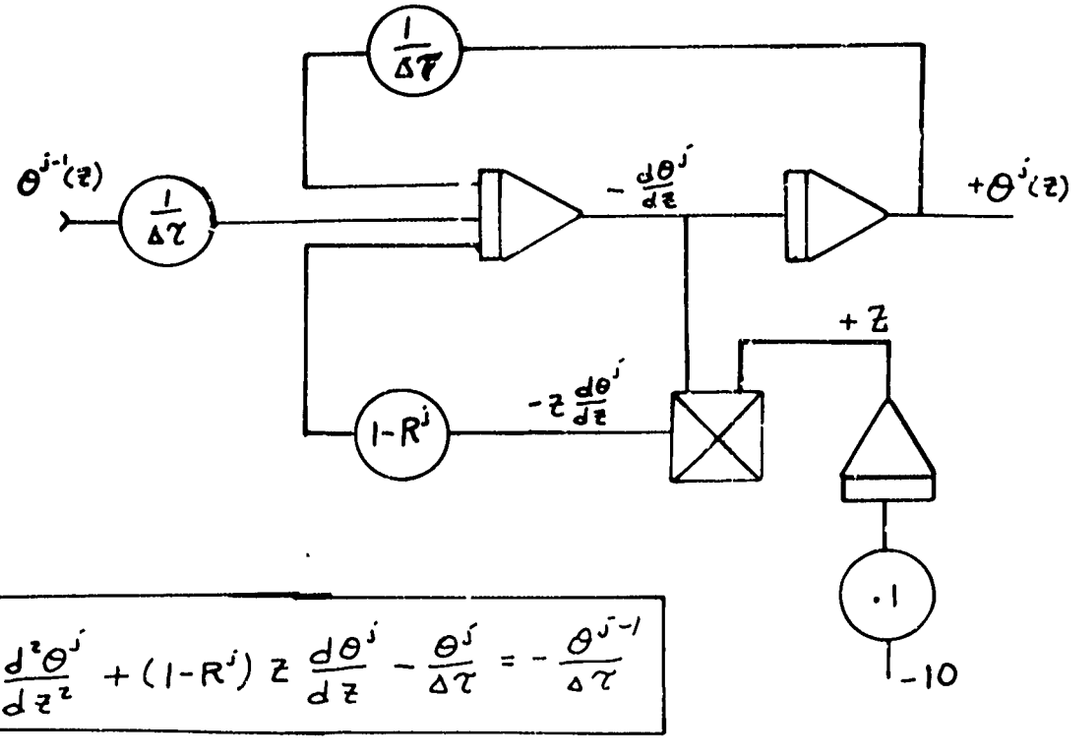

$$z^2\frac{d^2\theta^j}{dz^2} + (1-R^j)\,z\,\frac{d\theta^j}{dz} - \frac{\theta^j}{\Delta\tau} = -\frac{\theta^{j-1}}{\Delta\tau}$$

FIGURE I-5 ANALOG COMPUTER CIRCUIT DIAGRAM FOR SOLUTION OF NON-STEADY BURNING EQUATION BY SERIAL METHOD (see Eq. I-43)

APPENDIX II*

ADIABATIC FLAME TEMPERATURES OF VARIOUS PROPELLANTS AND HEATS OF FORMATION OF VARIOUS FUEL BINDERS

The adiabatic flame temperature calculations which were used in the theoretical depressurization analysis were obtained with the aid of a NASA computer program which is described in reference 82. In order to calculate flame temperatures, the computer program must be supplied with the percentages of each propellant ingredient, the compositions of each propellant ingredient, and the heat of formation of each propellant ingredient. The numerical results for the adiabatic flame temperatures are shown on figures II-1 to II-4. Figures II-1 to II-3 show the adiabatic flame temperature as a function of the percent of ammonium perchlorate in the propellant for three different fuel binders, PBAA, PBCT, and polyurethane, respectively. The flame temperatures are shown at each of several pressure levels. For the three binders, the PU propellant shows the largest dependence of flame temperature on pressure. Note also that the flame temperature becomes more highly dependent on pressure as the per cent oxidizer (AP) is increased. The effect of aluminum addition is shown in figure II-4. Here the flame temperature is plotted against the per cent of aluminum in the propellant, and again several different pressure levels are considered. For these calculations of the adiabatic flame temperatures of aluminized propellants, the ratio of fuel binder to ammonium perchlorate was held constant while the aluminum was added.

When a computer program is available, the calculation of adiabatic flame temperatures is quite easy, however, the determination of the properties of the propellant ingredients is not always as easy. The composition of ammonium perchlorate is well-known, and its heat of formation is readily determined from JANAF Tables (83). The various fuel binder systems are much more complicated. Heats of formation for the fuel binders were obtained by using bond energies (84). (The structures of many solid propellant binder systems are given in reference 85.) To simplify the determination of the heats of formation, and to improve the accuracy of the results, the heats of formation of various "back-bone" polymers (such as polybutadiene) were taken from Flory (86). The accuracy of the heats of formation of the binders which were determined by bond energies is not known exactly. However, such calculations generally lead to errors of several per cent. These are nevertheless the best results which were available and I have tabulated them in order that they may serve as a guide to future students. The heats of formation are tabulated on the next page.

---

* The author acknowledges the extensive help and the many suggestions given to him in determining fuel binder structures and heats of formation by both Mr. P. L. Stang, Member of the Technical Staff, and by Dr. J. A. Steinz, former Post-Doctoral Research Assoicate.

TABLE II

CHEMICAL PROPERTIES OF PROPELLANT INGREDIENTS

Propellant Ingredient	Chemical Formula	Molecular Weight	Heat of Formation	Source
Ammonium Perchlorate	NH_4ClO_4	117.5	- 70.7 kcal/mole	JANAF Tables (Ref. 83)
PBAA/EPON*	$C_{7.092}H_{10.289}O_{.2771}$	100	+ 1.19 kcal/mole	Bond Energies
PU	$C_{5.116}H_{9.611}O_{1.697}N_{.121}$	100	-94,400 kcal/mole	Bond Energies
PBCT/MAPO**	$C_{7.153}H_{10.8}O_{.096}N_{.048}P_{.016}$	100	+ 2.4 kcal/mole	Bond Energies

* EPON is an Epoxy (Diglycidyl ether of bisphenol A) (Shell Chemical Company).

** MAPO is Tris-[1-(2-methyl) aziridinyl] phosphine oxide (Interchemical Corp.).

ADIABATIC FLAME TEMPERATURE OF
PBAA PROPELLANTS

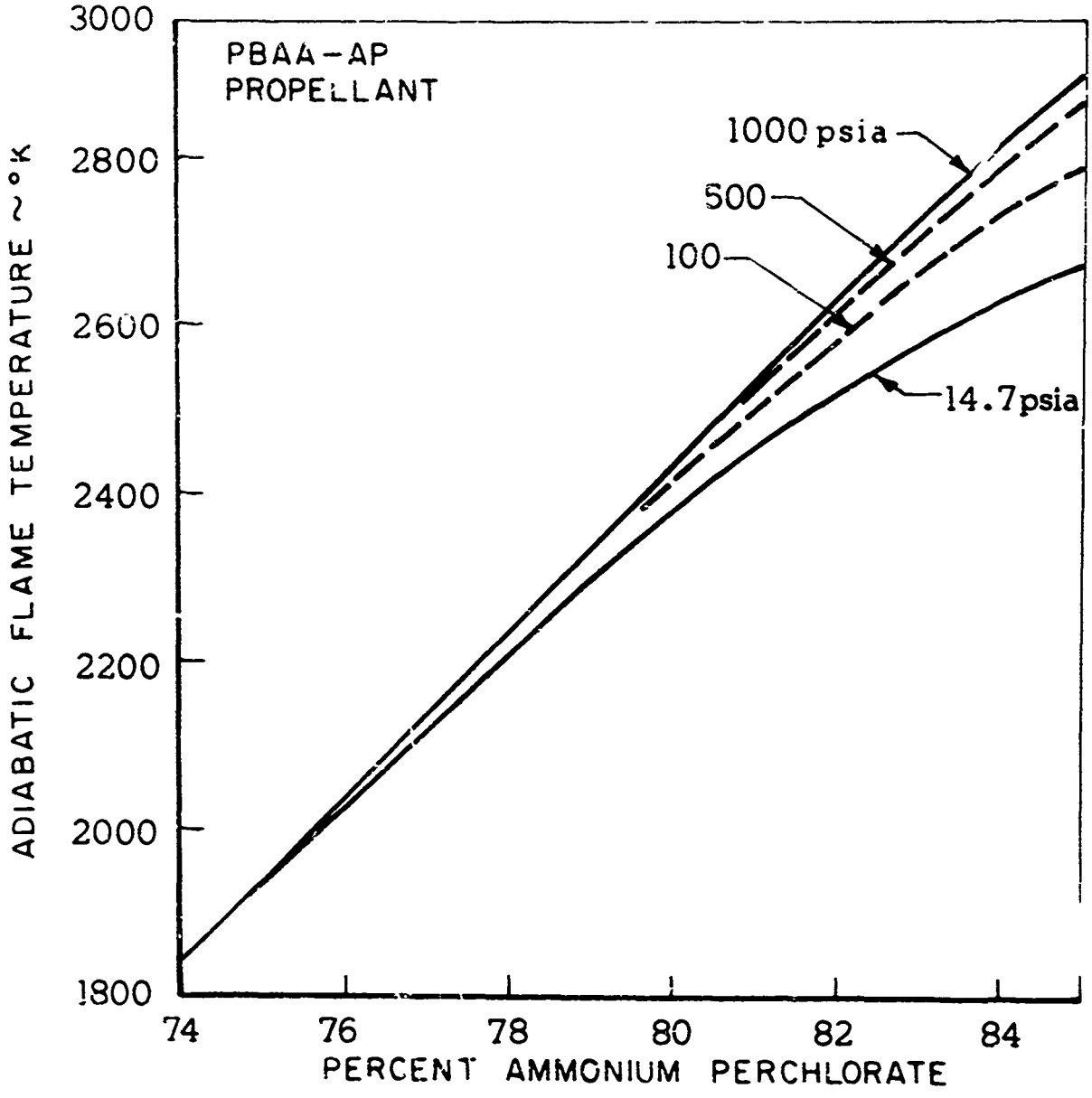

FIGURE II-1

ADIABATIC FLAME TEMPERATURE OF
PBCT PROPELLANTS

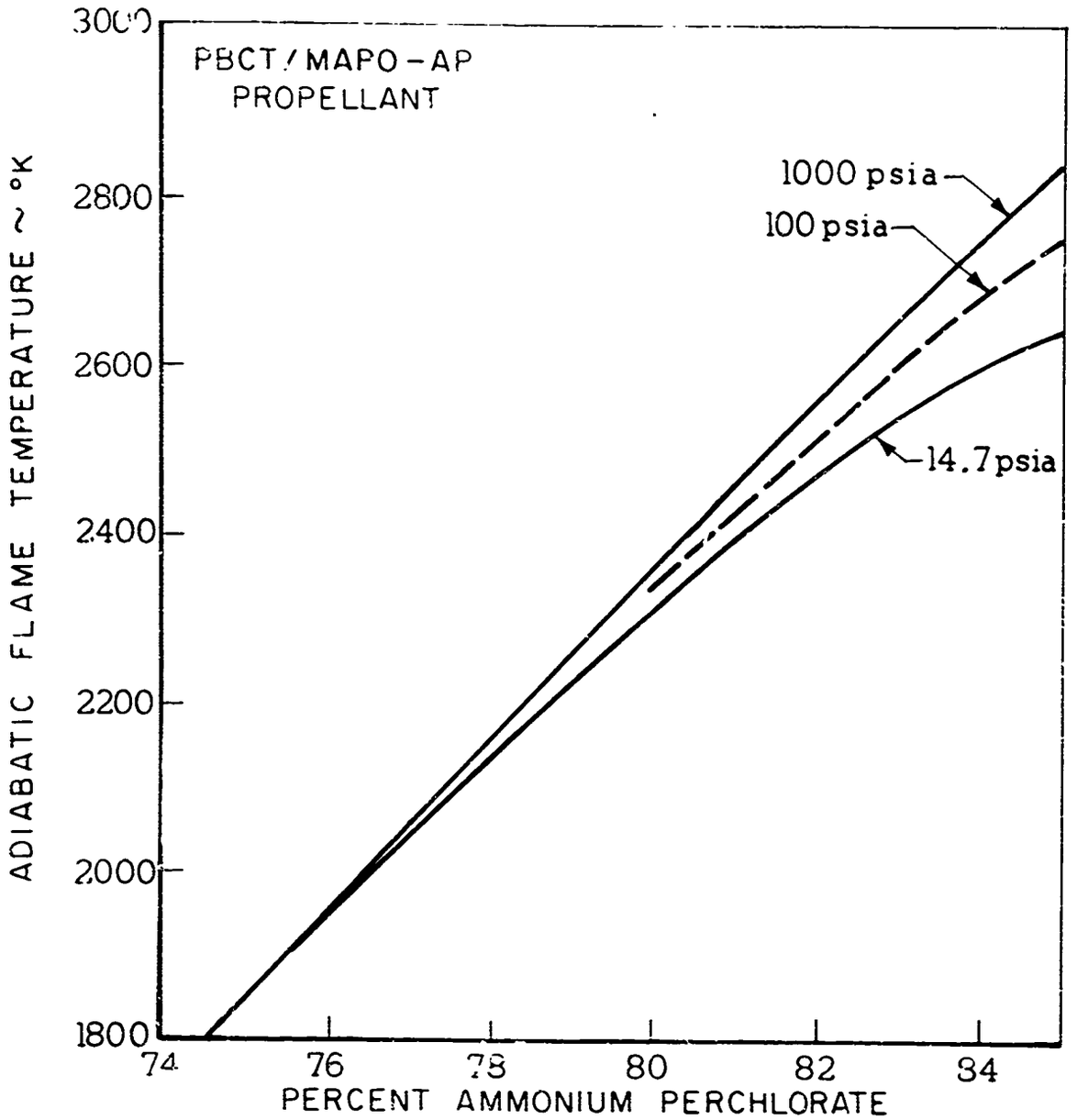

FIGURE II-2

ADIABATIC FLAME TEMPERATURE OF
POLYURETHANE PROPELLANTS

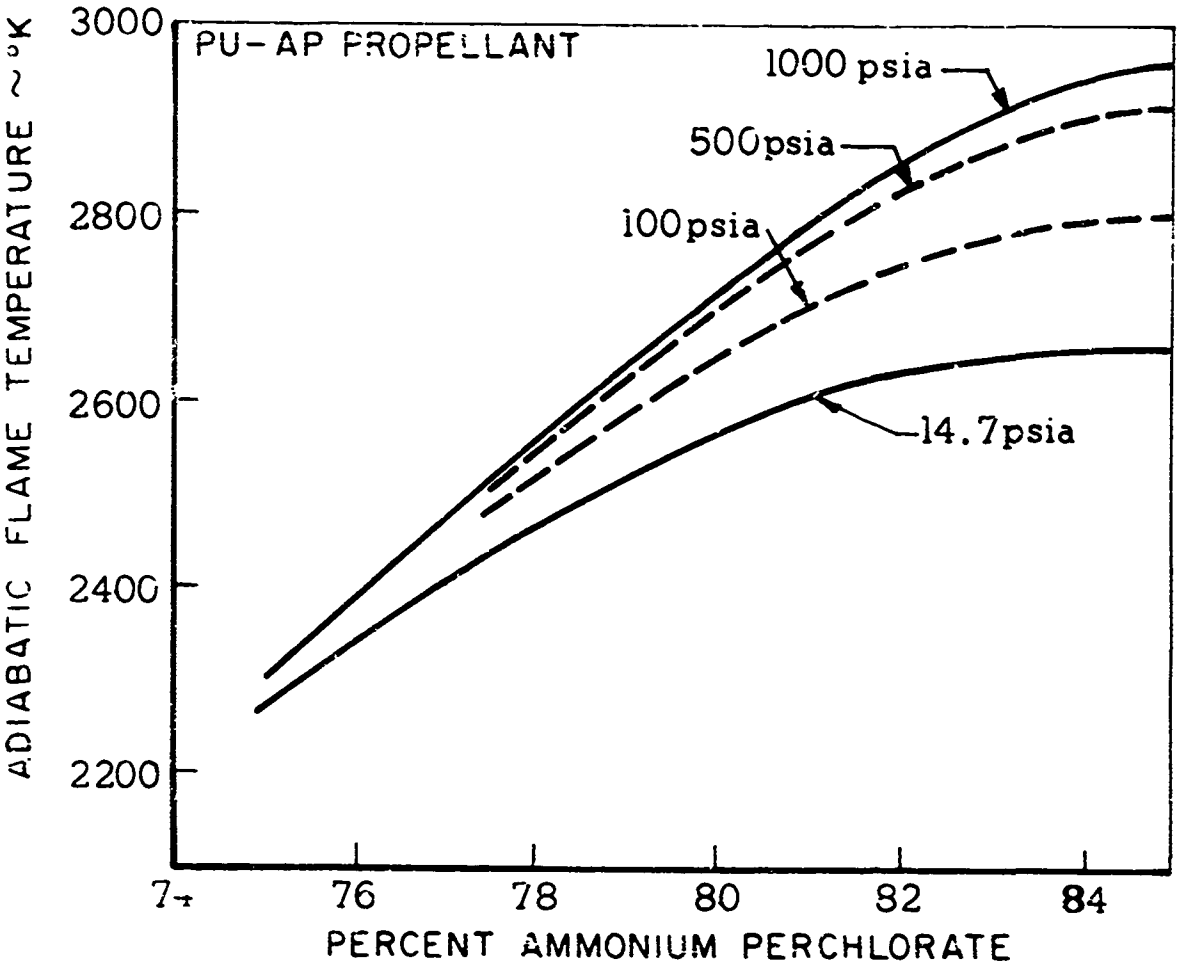

FIGURE II-3

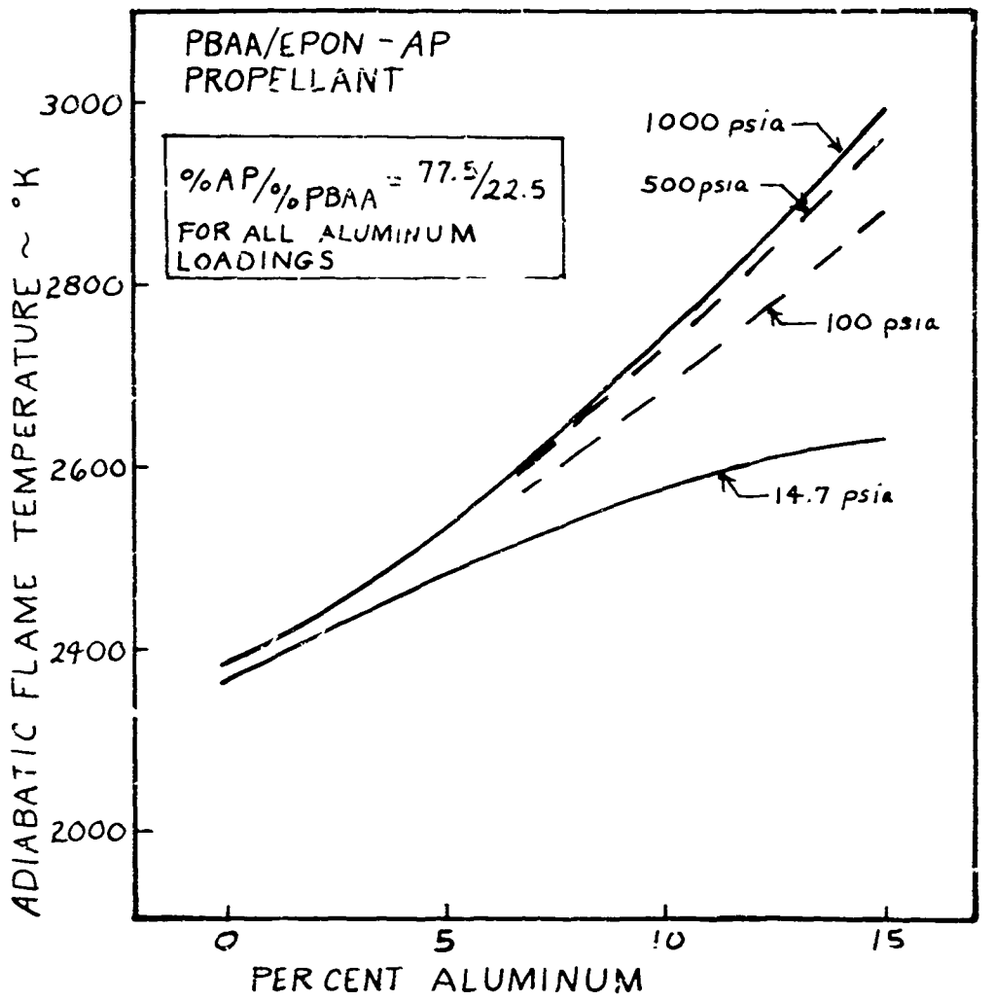

ADIABATIC FLAME TEMPERATURE OF ALUMINIZED PROPELLANTS

FIGURE II-4

APPENDIX III

EXPERIMENTAL PROCEDURES

This appendix summarizes some of the procedures which were used in the experimental part of the program.

A. Procedure Used in Depressurization Experiments

The combustor that was used for the depressurization testing, had a circular cross-section which was nominally 2 inches in diameter, and a height of 1 1/2 inches. The combustor was made from stainless steel and had a wall thickness of 1 1/2 inches. The walls of the combustor contained quartz windows, through which the flame radiation could be monitored. The windows were also used for the temperature measurement attempts which are discussed later in this appendix. The propellant was situated in the bottom of the combustor (see Figure 4) and had a circular burning area which was just slightly less than the cross-sectional area of the combustor. As indicated in the main body of the thesis, the sides of the propellant sample were inhibited by casting the propellant into steel cups.

Ignition of the propellant sample was achieved by means of a bag of propellant shavings. Although uniformity of ignition from run to run was not of great importance in this experiment (because the depressurization did not start until after a steady state operating pressure had been reached), the weight of propellant in each igniter was carefully measured; one gram of shavings were used in each ignit r. This size ignit r was large enough to give fast, positive ignition for all the propellants tested, and it gave a minimum of pressure overshoot. The igniter bags were made of very thin plastic. Ignition of the igniter itself was achieved by threading a thin wire through the igniter bag, and heating the wire by an electrical impulse.

The aluminum which was used for the burst diaphragms was obtained in 2 x 6 foot sheets from the David Smith Steel Company. Aluminum type 3003- 0 was used for diaphragms of thickness .040, .032, and .025 inches. 1100-H14 aluminum was used for the .020 inch diaphragms (the softer aluminum is not sold in sheets thinner than .025 inches). For the burst diaphragms, the sheets of aluminum were cut into 3 1/2 inch squares. Calibrations of the burst pressure for these diaphragms are shown on figure III-1. This calibration is for a diaphragm with an area (subjected to pressure) of about 2 3/4 inches in diameter. There was a fair amount of scatter in the burst pressure from diaphragm to diaphragm, but the double diaphragm apparatus made the experiment insensitive to this variation. Generally speaking, the top diaphragm was chosen as one size thinner than the bottom diaphragm. This appeared to give a better "break" of both the diaphragms. As indicated in the main text, the underside of the lower diaphragm (which was directly exposed to the hot exhaust gases) was protected by a thin coating of RTV (room temperature vulcanizing) silicone rubber.

The primary (large) nozzles used in the experiment (to determin-

the rate of depressurization) varied between .117 and .750 inches in diameter. The nozzles were made of copper and were 3/4 inch thick.

In conducting the experiment, the propellant and igniter were placed in the motor, the motor was assembled, and the desired primary nozzle, secondary nozzle, and burst diaphragms were installed. The area between the two diaphragms was then pressurized manually to within about 75% of the burst pressure of the weaker diaphragm. (The diaphragms were chosen so that the differential between the expected steady state operating pressure and the pressure in the diaphragm cavity would be as near the burst pressure of the lower diaphragm as possible. This ensured that the diaphragms would burst rapidly and cleanly upon venting the cavity between the diaphragms. That is to say, the diaphragms that were used were chosen to be the weakest ones which would contain the expected operating pressure.) From this point on, the sequencing of events was done by a pre-set electrical timer. In the automatic sequencing, the igniter was fired first, and a nominal time of 100 ms was allowed for the burning to reach its steady state operating condition. At this time, the cavity between the burst diaphragms was vented causing the diaphragms to burst, creating the depressurization which was to be observed.

During the depressurizations, the flame radiation was monitored by a photomultiplier tube. However, because of the combustion products, the motor windows, through which the flame radiation was monitored, became progressively more fouled as the burning time increased. Since only a qualitative measure of radiation was desired, this "dirty window" problem did not affect the measurement so long as some radiation could get through the partially obscured window. For the more highly oxidized propellants, the windows never became completely obscured. However for the very under-oxidized propellants, the windows frequently became so dirty that it was impossible to see the flame. For such cases, it was determined, by trial and error, that a plexiglass insert between the flame and the quartz window, would apparently ablate sufficiently to keep the window clean enough to see through, during the entire run. The window remained cleanest when it was long enough to protrude from the wall into the burning zone. When the plexiglass insert became even slightly recessed below the wall, the plexiglass surface would become so covered with carbon, that the flame would become obscured before the 100 ms steady state operating time had elapsed.

B. Thermal Conductivity Measurements*

One important parameter in the theoretical analysis of the depressurization process, is the thermal conductivity of the solid. In fact, the theoretical predictions scale linearly with the thermal conductivity of the solid phase. In an attempt to eliminate this variable, we obtained a thermal conductivity measuring apparatus from the Central Scientific Company. A schematic of this instrument is given in figure III-2. In

* The thermal conductivity measurements were done in their entirety by Mr. S. L. Turk, Undergraduate Junior. A description of the method used is included here for the sake of completeness.

using this apparatus, a thin slab of solid propellant is placed between the upper vessel and the lower insulated copper block. A thermal compound was used on both faces of the solid propellant slab in order to ensure good thermal contact. During the experiment, the upper vessel is kept at a constant temperature of 100°C by boiling water. Heat passes from the upper vessel through the solid propellant sample to the copper block. The temperature difference between the upper vessel and the lower copper block is monitored as a function of time by means of thermocouples. Knowing the mass of the copper (and its thermal capacitance), the amount of heat which was transferred through the solid propellant can be determined (assuming there is no heat loss from the copper block to the surroundings, and assuming that all the heat which is delivered to the copper block comes through the solid propellant sample). The thermal conductivity of the sample can then be obtained from a knowledge of its thickness and its surface area.

This particular instrument is designed for use in demonstration experiments in undergraduate physics, and its accuracy is limited. However, the results obtained with this apparatus were quite repeatable (about 2.5%). Hence it could serve as an efficient comparative device as described in the last paragraph of this section. (Unfortunately, there were no thermal conductivity "standards" available to us, so we could not use it in a comparative manner.)

Because of the inaccuracies of the instrument, we did not attempt to measure absolute thermal conductivities of all our propellants. Instead, we merely attempted to determine the ratio between the thermal conductivities of the aluminized and unaluminized propellants. It was expected that the various unaluminized propellants would have similar thermal conductivities (within a few percent of each other), but that the addition of aluminum would cause a fairly large change in the thermal conductivity. The experimental measurements confirmed this. The difference between the measured thermal conductivities of the unaluminized propellants was within the repeatability of the instrument. However, the measurements showed about a 35% increase in the thermal conductivity of the propellant when 15% aluminum was added. The approximation was made that the product was the same for the unaluminized and aluminized propellants, and that, therefore, the thermal diffusivity is also increased 35% by the addition of 15% aluminum. In the theoretical predictions of extinction, the thermal diffusivity of aluminized propellants was taken to be 35% larger than that of unaluminized propellants.

One of the best commercial sources of high-accuracy thermal conductivity apparatus is the Dynatech Corporation of Cambridge, Massachusetts. Their cheapest models sell for about $3,000. These instruments are supplied with a series of some one-half dozen "standards" whose thermal conductivities are known accurately. In operating these instruments, one first obtains the signal output from the instrument for each of the standards, and then plots this output as a function of the known thermal conductivity of the standards. This serves to calibrate the thermal conductivity instrument, and hence, it will measure the thermal conductivity of unknowns by comparison with the thermal conductivities of knowns. Instruments which measure the absolute thermal conductivities of substances are more expensive than this. For example, Dynatech also

manufactures a complete line of guarded hot plate instruments at higher prices.

C. Attempts at Measuring the Flame Temperature During the Depressurization*

The main text of the thesis presents a theory for the prediction of extinguishment of solid propellants. The predictions of the theory were checked by comparing the experimentally determined boundaries between extinction and non-extinction with the theoretically predicted boundaries. If some parameter could have been measured continuously during the depressurization, it would have provided a much more sensitive check of the theory than is presently available. With this idea in mind, a considerable amount of time was spent in trying to measure the transient flame temperature during depressurizations by an optical technique. These efforts were not successful, and the reason is simply that the windows became dirty during the depressurization, thus destroying the accuracy of any optical temperature measurement system.

The particular type of temperature measurement that was attempted was the so-called "brightness-emissivity" method. Krier[69] has discussed this method in detail in his Appendix V, and shows that this is one of the most promising methods of measuring flame temperature with fast time response. Because of this recent and thorough description, only an outline of the method will be given here, the interested reader is referred to reference 69 for details of the method. The description given here will indicate a minor modification to the brightness-emissivity method which we developed, and will attempt to categorize the "dirty window" problem

In the most concise form, the brightness-emissivity method measures both the brightness and the emissivity of the flame, and then uses some comparison standard to determine the absolute temperature of the flame. The brightness of the flame is measured by a simple observation of the flame by a light-sensitive receiver. The sensitivity of this receiver is calibrated by allowing the receiver to first view a radiating source whose brightness temperature is known. The emissivity of the flame is determined by measuring the percent of the radiation from some external source that can be transmitted through the flame (see Krier's discussion). In the usual brightness-emissivity method, the combuster is placed in the line of sight between a tungsten strip lamp (or other equivalent source) and a light-sensitive receiver. Two windows on opposite sides of the sides of the combustor are placed so that light from the lamp can shine through the combustor and to the receiver. Before an experimental run is to be made, the brightness temperature of the lamp is measured by means of an optical pyrometer, so that the brightness temperature of the lamp filament is known. Then, before the combustion process, the lamp is turned on and is used to calibrate the receiver. During combustion, the lamp is alternately turned "off" and "on" (by a mechanical chopper between

---

* The author acknowledges the considerable contribution to the work described in this section that was made by Dr. David Fleischer, former Member of the Technical Staff. During the course of this work, the author was engaged in many interesting and stimulating discussions with Dr. Fleischer and his contributions, suggestions and advice are greatly appreciated.

the lamp and the combustor). Thus when the lamp is turned "on", the receiver sees the radiation from the flame plus the fraction of the lamp radiation that is transmitted through the flame. When the flame is turned "off," the receiver sees only the output from the flame. Thus the receiver signal is of the form designated "chopper output" on figure III-3.

A modification of the chopper setup was used in the work done in this research program. This modification was to use a polarized light source and two receivers. A crossed polarizer (with respect to the lamp) is placed in front of one of the receivers so that this receiver can not see the lamp radiation; it can only see the radiation from the flame, but it receives the flame radiation continuously (in time). Similarly, the second receiver sees the continuous output of the flame plus the transmitted (polarized) lamp (see schematic on figure III-4). The output signal for this modification of the brightness-emissivity method is thus the envelope of the chopper output, as is shown on figure III-3, and labeled "polarizer output." In a real situation, with an inevitably noisy flame signal, and without completely "square" square-waves, this offers an advantage in data reduction.

The flame temperature and emissivity can be determined from the measurements of either of these set-ups. The same analysis applies to both of them, except for the method in which the signal is recorded.

As indicated above, the problem in this temperature measurement was that the windows in the combustor became dirty during the burning process. It must be emphasized that the brightness emissivity method is independent of the transmissivity of the optical path, so long as the transmissivity remains constant during the experiment (or more accurately, so long as the manner in which the transmissivity varies during the experiment is known). However, when carbon is deposited on the combustor windows, the transmissivity changes by undetermined amounts.

The most obvious way to overcome this "dirty window" problem is to keep the windows clean. The first observation along this line is that the amount of carbon deposited on the windows is a very strong function of the type of propellant binder used. Polyurethane is, far and away, the optimum binder to use for temperature measurement attempts (of the binders tested in this research work). PBAA is much worse. The reason for this is probably that the polyurethane contains a relatively large amount of oxygen (in the polyurethane, itself) as compared to the amount in the PBAA binder. PBCT proved to have similar burning characteristics, in this respect, to the PBAA. Of course, increasing the oxidizer loading to as high a level as possible (for example, using tri-modal ammonium perchlorate particle sizes allows a slightly higher AP loading), greatly decreases the amount of carbon that is deposited on the windows.

As far as placing the windows, it appears that a window that is flush mounted in the wall, or even protruding into the combustion chamber is optimum. If the window surface was recessed into the wall by even the slightest amount, a decided increase in the residue deposition rate was noted.

Another possibility for keeping the windows clean, is to purge them with an inert gas during the experimental firing. The sight glass assembly shown in figure III-5 was designed for this purpose. This sight glass was designed so that a constant mass flow rate of nitrogen entered a manifold and escaped through a narrow annular slot around the entire perimeter of the face of the window. Unfortunately, it appeared that the "recessed" effect (above) very nearly balanced the purging effect of the nitrogen so that nothing was gained by using these windows (in fact, the flush mounted windows might have been slightly superior to the purged windows). Variations in nitrogen mass flow rate, and in the height of the slot through which the nitrogen entered seemed to offer no improvement. There was evidence that during ignition (when the chamber pressurized very rapidly), reverse flow occurred in the sight glass so that combustion products actually flowed through the annular slot designed for the entrance of the nitrogen. (The volume between the choked orifice which supplied the constant mass flow rate of nitrogen and the annular slot entrance to the motor was kept as small as possible.)

One final method of surmounting this problem with the windows, but which was not tested completely, is to keep the windows as clean as possible, and measure the transmissivity of the windows as a function of time. One potential method for calibrating how "dirty" the windows are at a given time, is to use a second light source (besides the one used for temperature measurement) which radiates in a region of the flame where the flame is dark, i.e., in a region in which the flame does not emit. Spectroscopic work, accomplished in this research program, indicated that such a dark region of the flame occurs around 5100 Å for a PU propellant. (Note that the brightness-emissivity measurement must be conducted over a very small wavelength region, ideally in a monochromatic manner. Normally the wavelength chosen is 890 Å, the sodium D lines. Light filters of less than 100 Å in width are normally used for the temperature measurement. Frequently they are as narrow as 5 Å.) If a radiation source were used at this wavelength, and if it were very bright in comparison to the flame emission (or absorption, if in equilibrium in this spectral region, then a separate detector could record the rate of decrease of this lamp signal due to the decreased transmissivity of the windows. Then knowing the transmissivity of the optical path as a function of time, and assuming that it was the same function at 4890 as a 5100 Å, one could calculate the flame temperature and emissivity as the windows got dirty. It must be noted that this method has never been attempted (to the author's knowledge) and that at best, it would require very careful, precise calibrations and experimental procedures.

D. Availability of Experimental Pressure Versus Time Curves for Tested Propellants.

The experimental pressure versus time depressurization curves recorded in this research program are available in tabular form as well as in the form of coefficients of a polynomial equation. The polynominal coefficients were determined by the method of least squares error analysis. The curves are published in a supplement, designated AMS Report No. 880-S, which is available upon request.

APPROXIMATE DIAPHRAGM THICKNESS VS.
BURST PRESSURE (2 3/4 inch diameter)

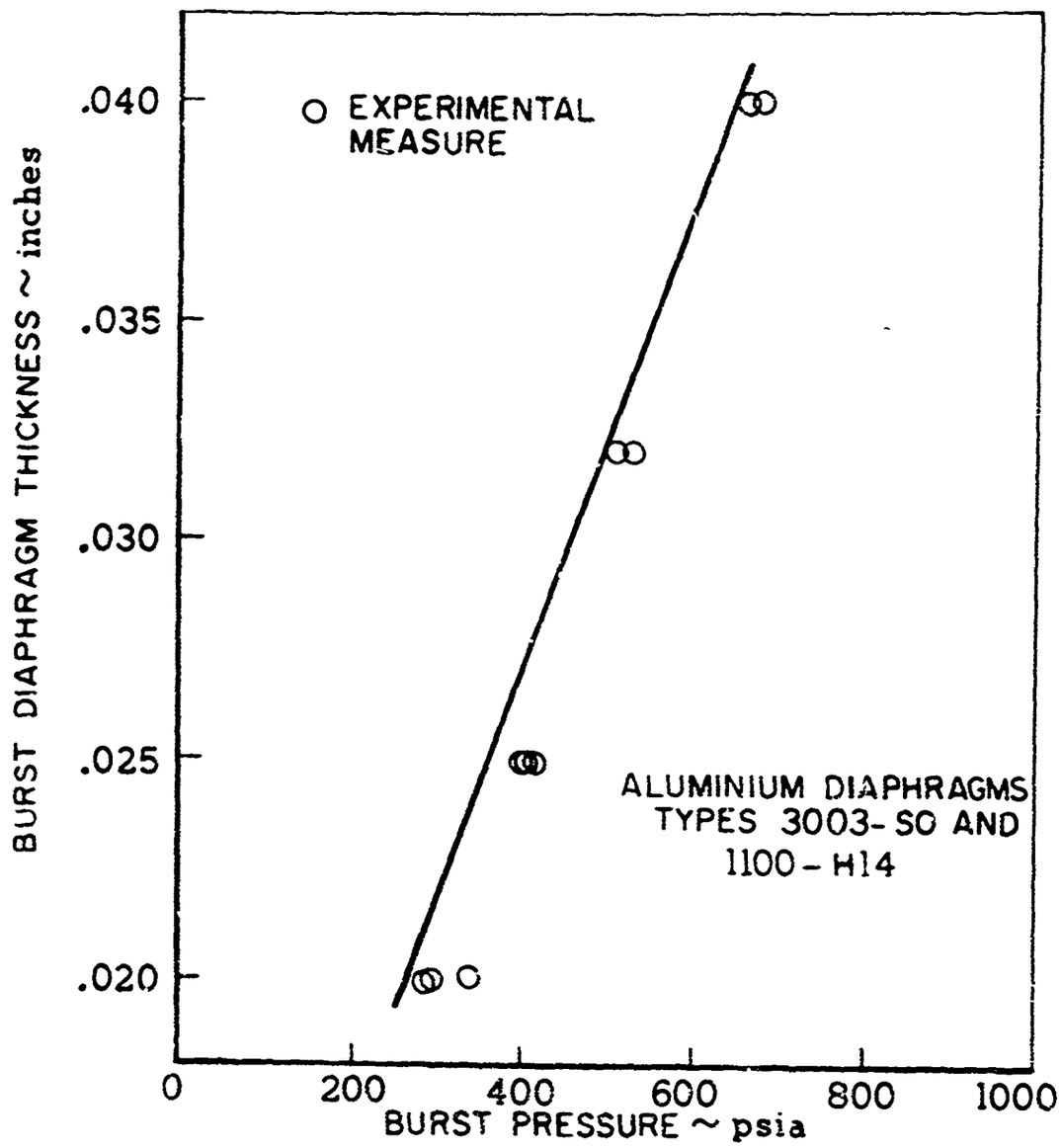

FIGURE III-1

THERMAL CONDUCTIVITY APPARATUS

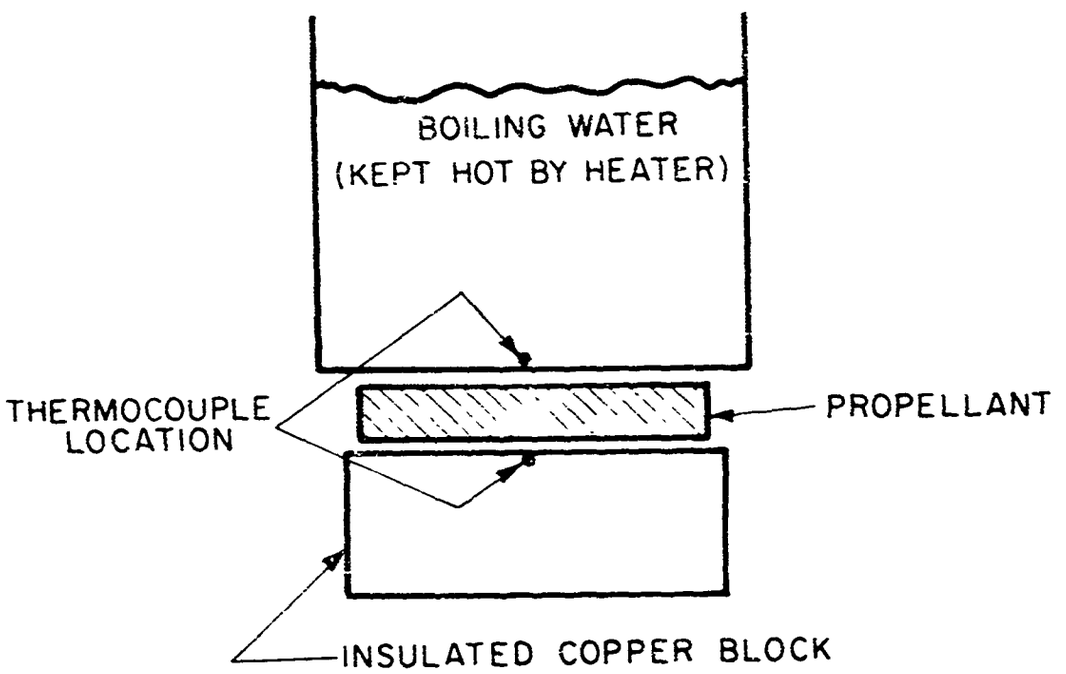

FIGURE III-2

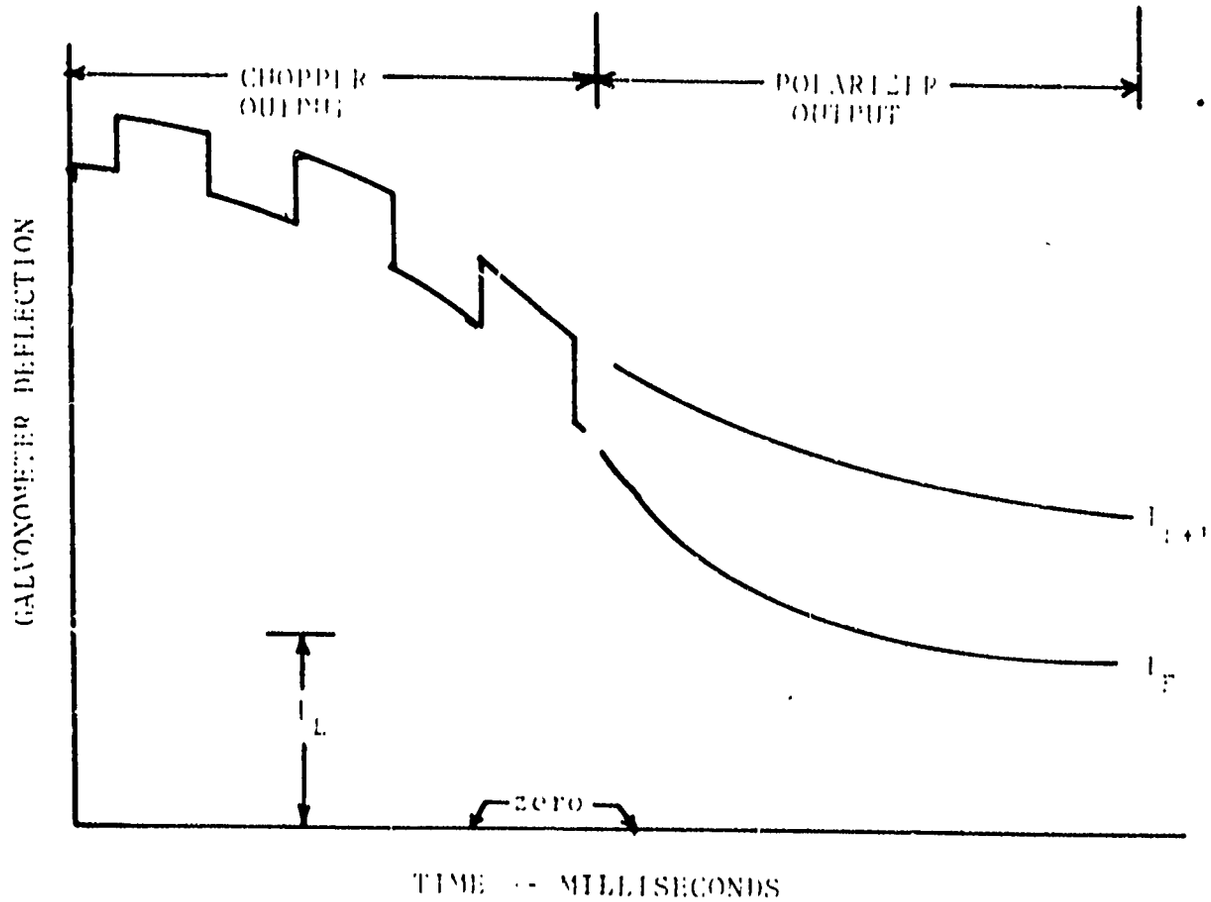

FIGURE III-3 COMPARISON OF DETECTOR OUTPUT WITH CHOPPER AND POLARIZER IN BRIGHTNESS EMISSIVITY-MEASUREMENT

NOT REPRODUCIBLE

FIGURE III-3

FIGURE III - 4

SCHEMATIC REPRESENTATION OF TEMPERATURE MEASURING APPARATUS

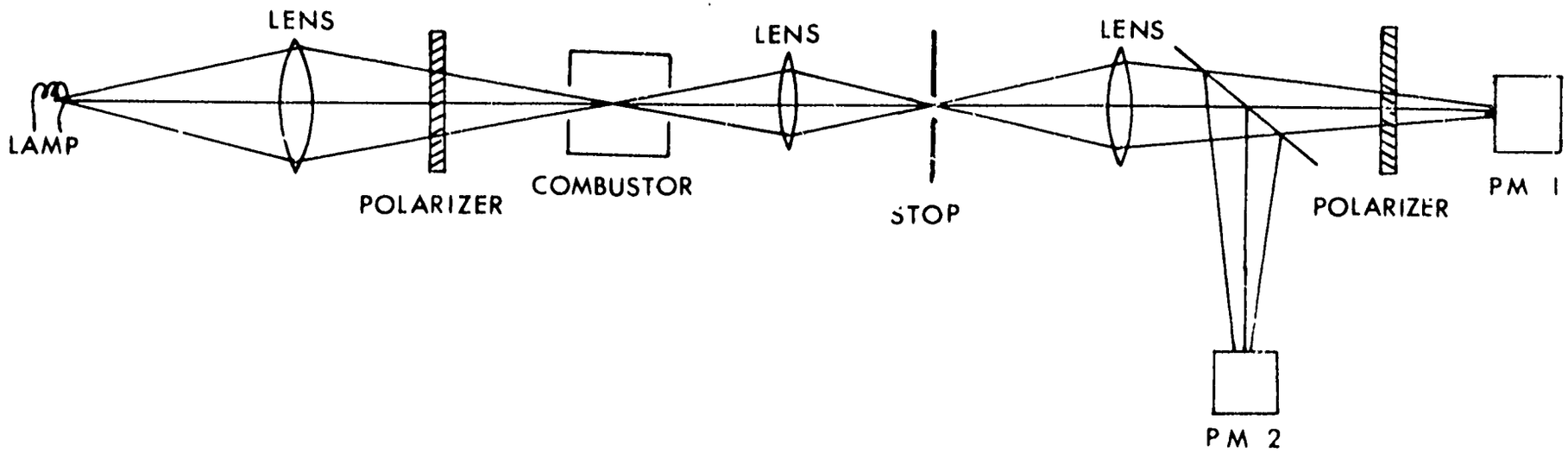

NOTE PM 1 MEASURES FLAME RADIATION ONLY
PM 2 MEASURES FLAME PLUS TRANSMITTED LAMP

JP 19 R 4314 69

SIGHT GLASS ASSEMBLY

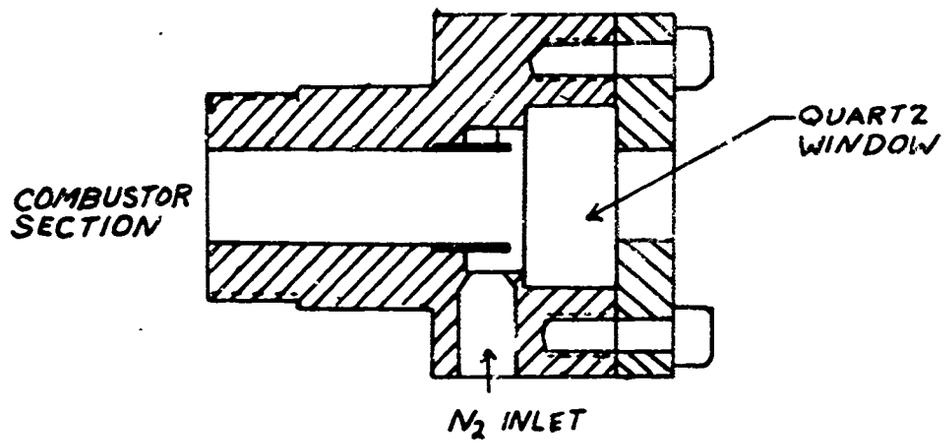

FIGURE III-5 SIGHT GLASS ASSEMBLY

JP 19 R 4315 69

FIGURE III-5

APPENDIX V

Unclassified
Security Classification

DOCUMENT CONTROL DATA - R & D

(Security classification of title, body of abstract and indexing annotation must be entered when the overall report is classified)

1. ORIGINATING ACTIVITY (Corporate author) Princeton University Department of Aerospace & Mechanical Sciences	2a. REPORT SECURITY CLASSIFICATION Unclassified 2b. GROUP

3. REPORT TITLE

EXTINGUISHMENT OF SOLID PROPELLANTS BY RAPID DEPRESSURIZATION

4. DESCRIPTIVE NOTES (Type of report and inclusive dates)

Scientific Interim

5. AUTHOR(S) (First name, middle initial, last name)

C. L. Merkle, S. L. Turk, and M. Summerfield

6. REPORT DATE July, 1969	7a. TOTAL NO. OF PAGES 201	7b. NO. OF REFS 86
8a. CONTRACT OR GRANT NO Nonr 1858(32) b. PROJECT NO. c. d.	9a. ORIGINATOR'S REPORT NUMBER(S) AMS Report No. 880 9b. OTHER REPORT NO(S) (Any other numbers that may be assigned this report)	

10. DISTRIBUTION STATEMENT

1. Distribution of this document is unlimited

11. SUPPLEMENTARY NOTES Tech., Other	12. SPONSORING MILITARY ACTIVITY Power Program, Code 473 Office of Naval Research Dept. of the Navy, Washington, D.C.

13. ABSTRACT A new theory for extinction by depressurization of AP composite propellants is employed to predict the rate of pressure decrease required to achieve flame-out and to rationalize the effects of various composition parameters on the ease of extinguishment. The research is concentrated mainly on the "temporary" extinguishment behavior of solid propellants, but a re-ignition theory is also presented. Attention is given in this theory to the proper derivation of the nonsteady heat feedback from the gaseous flame zone to the burning surface. Included in the model are the essential physical and chemical rate processes of the granular diffusion flame model, as deduced from the steady state burning characteristics. It is predicted theoretically that: (a) whether extinction occurs depends on the entire shape of the pressure transient, not just on the initial slope; (b) extinction depends upon the pressure dependence of the steady state burning rate all the way down to the final pressure; (c) increasing the AP fraction, reducing the AP particle size, or adding fine aluminum powder makes a propellant more difficult to extinguish. These predictions are confirmed by experimental tests with AP composite propellants with PBAA, PB(CT), and PU binders. A brief study of double-base propellants which indicates that they are considerably easier to extinguish than composite propellants concludes this report. A rough model for the burning of double-base propellants is presented which further indicates the importance of the flame structure in determining the extinguishment characteristics of solid propellants.

DD FORM 1 NOV 65 1473

Unclassified
Security Classification

Unclassified
Security Classification

14 KEY WORDS	LINK A ROLE	LINK A WT	LINK B ROLE	LINK B WT	LINK C ROLE	LINK C WT
Aluminum powder						
AP composite propellants						
AP particle size						
Depressurization						
Double-base propellants						
Extinguishment						
Fuel binders: PBAA, PB(CT). PU						
Granular diffusion flame model						
Nonsteady heat feedback						
Pressure transient						
Re-ignition						
Temporary extinction						
Solid Propellants						

Unclassified
Security Classification